UNIVERSITY of LIEGE
FACULTY of SCIENCES

Taking advantage of multicomponent reactions for the synthesis of advanced polymers and porous materials

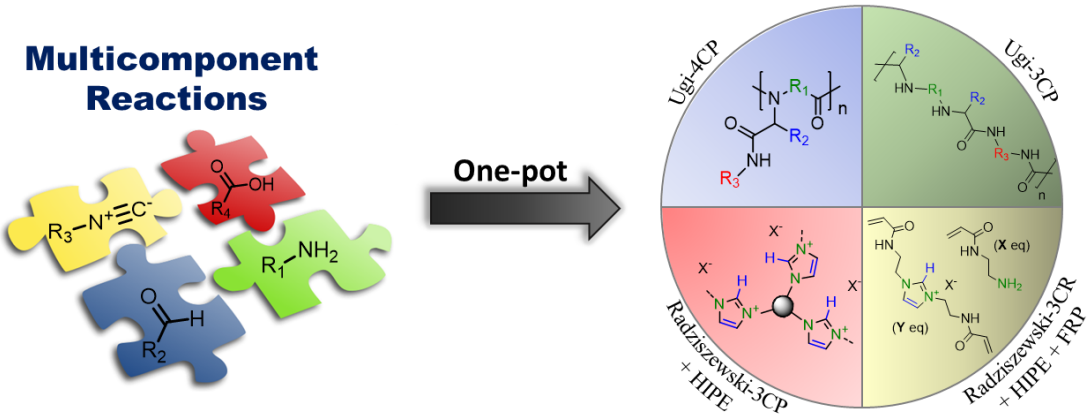

A dissertation submitted by
Pierre STIERNET

For the degree of
Doctor in Sciences

Academic year 2020-2021

CERM Laboratory
CESAM Research Unit
Promoter: Dr. Antoine Debuigne

Thesis defended on October 4th before a jury composed of

Prof. Jean-Christophe Monbaliu……..University of Liège (President)
Prof. Dr. Christine Jérôme……University of Liège (Secretary)
Dr. Antoine Debuigne…….…….University of Liège (Promoter)
Prof. Dr. Filip Du Prez……...…University of Ghent
Dr. Sebastijan Kovačič……National Institute of chemistry, Ljubljana
Prof. Dr. Michael A. R. Meier……...…Institut für Technologie, Karlsruher

SUMMARY

Multicomponent reactions (MCRs) are highly efficient reactions involving more than two compounds which react together and form complex chemical structures containing essentially all atoms of the starting reagents. Applying MCRs in macromolecular science brings new functionalities to polymer structures in a straightforward way with high atom economy, especially when considering step-growth polymerization (MCP). The present thesis aims to further explore the potential of MCRs, in particular of the imine-based Ugi and Radziszewski reactions, for the design of novel functional polymers and structured materials. First, the combinatorial character of the Ugi four-component polymerization (U-4CP) of amino acid derivatives was exploited for the synthesis of a library of peptoid analogues. Some of the latter showed pH- and thermo-responsiveness as well as biocompatibility toward human cells making them candidates for stimuli-responsive biomaterials. Another Ugi-type reaction was adapted for step-growth polymerization, *i.e.* the Ugi three-component reaction (Ugi-3CR), allowing the incorporation of α-amino amide moieties in polymer structures. A series of aromatic and semiaromatic polymers was obtained accordingly which notably revealed pH-responsiveness. Eventually, the modified Radziszewski MCR (MR-3CR), a water-mediated reaction leading to imidazolium ionic liquids, was applied to triamine derivatives under emulsion-templating conditions for the first time to afford macroporous poly(ionic liquid)s networks. The resulting imidazolium acetate materials exhibited excellent catalytic activity for transesterification and decarboxylation reactions as well as easy recyclability. To further extend the scope of functional macroporous networks, the MR-3CR was combined in one-pot with emulsion-templating radical polymerization. This led to pure imidazolium and unprecedented bi-functional imidazolium/amine porous networks with tunable CO_2 uptake capacity and CO_2/N_2 selectivity depending on the imidazolium content and the nature of its counterion. This synergistic effect makes them candidates for post-combustion and direct-air CO_2 capture applications. Overall, this work contributes to the quest for increasingly complex functional polymer structures while respecting a simpler and more efficient chemistry.

RÉSUMÉ

Les réactions multicomposants (RMC) sont des réactions hautement efficaces impliquant plus de deux composés qui réagissent ensemble et forment des structures chimiques complexes contenant essentiellement tous les atomes des réactifs de départ. L'utilisation des RMCs en chimie macromoléculaire, et en particulier la polymérisation multicomposants (PMC), permet d'incorporer de nouvelles fonctionnalités dans des polymères d'une manière simple et efficace en termes d'économie d'atomes. Cette thèse a pour but d'explorer davantage le potentiel des réactions d'Ugi et de Radziszewski, pour la conception de nouveaux polymères fonctionnels et de matériaux structurés. Premièrement, le caractère combinatoire de la polymérisation de dérivés d'acides aminés par la réaction d'Ugi à quatre composants (U-4CP) a été exploité pour la synthèse d'une librairie de polymères d'analogues de peptoïdes. Certains d'entre eux ont montré une sensibilité au pH et à la température ainsi qu'une bonne biocompatibilité envers des cellules humaines (HeLa), ce qui en fait de bons candidats pour des applications impliquant des biomatériaux sensibles aux stimuli. La réaction d'Ugi à trois composants (Ugi-3CR), a ensuite été adaptée pour la polymérisation par étapes, permettant l'incorporation de motifs α-amino amide dans des polymères. Une série de polymères aromatiques et semi-aromatiques a été obtenue et a notamment révélé une certaine sensibilité au pH. Finalement, la réaction de Radziszewski modifiée (RM-3CR), une réaction en phase aqueuse et conduisant à des liquides ioniques à base d'imidazoliums, a été appliquée pour la première fois en émulsion à des dérivés de triamines afin de produire des réseaux macroporeux de poly(liquide ionique)s. Les matériaux à base d'acétate d'imidazolium résultants présentaient une excellente activité catalytique pour les réactions de transestérification et de décarboxylation ainsi qu'une recyclabilité aisée. Pour étendre davantage le panel de réseaux macroporeux fonctionnels, la RM-3CR a été combinée avec une polymérisation radicalaire en émulsion. Les réseaux poreux à base d'imidazolium ou associant des imidazoliums et des amines ainsi obtenus ont montré des capacités d'absorption de CO_2 et des sélectivités du CO_2/N_2 prometteuses. De plus, ces propriétés ont pu être modulées en fonction de la teneur en imidazoliums et de la nature de leurs contre-ions. Cet effet synergique en fait des candidats pour des applications de post-combustion et de capture directe du CO_2 dans l'air. Globalement, ce travail contribue à l'élaboration de structures polymères fonctionnelles de plus en plus complexes tout en respectant une chimie plus simple et plus efficace.

Acknowledgements

About four years ago, I have taken over this journey which was enriching both scientifically and humanly. There have been successes of course but this journey has been strewn with many failures and doubts which in my opinion are the best teachers if we manage to overcome them. I think I grew up thanks to many individuals who took part in this work directly or indirectly and allowed me to go on despite these difficulties. For their support, I would like to thank them.

Je tiens à adresser mes remerciements et ma gratitude envers mon promoteur de thèse, Dr. Antoine Debuigne, pour m'avoir permis d'entamer ce parcours et l'avoir encadré tout du long. Sur ces quatre ans et quelques mois, il y eu de nombreuses discussions enrichissantes et je tiens à te remercier pour les nombreuses heures que tu m'as consacrées. Sans oublier le voyage à Singapour qui fût un vrai plaisir.

J'exprime également toute ma reconnaissance au Prof. Christine Jérôme pour m'avoir accueilli de son laboratoire durant mon mémoire ainsi que pour mon doctorat.

I would like to thank Dr. Jean-Christophe Monbaliu for chairing my thesis jury, Prof. Christine Jérôme for her work as thesis defense secretary as well as Prof. Filip Du Prez, Prof. Michael A.R. Meier and Dr. Sebastijan Kovačič for doing me the honour of being part of my thesis jury. I would especially like to thank Dr. Sebastijan Kovačič with whom I collaborate on CO_2 capture for the fourth chapter. This collaboration allowed me to extend my knowledge in the field of polyHIPEs and their usefulness.

Cette thèse n'aurait pas eu lieu sans les membres du CERM qui m'ont accueilli chaleureusement au laboratoire. Je tiens donc à leur exprimer ma reconnaissance. Tout d'abord à Grégory Cartigny qui consacre beaucoup de son temps à aider les étudiants au laboratoire que ce soit à la paillasse ou pour les nombreuses analyses que tu réalises pour nous. Tu es indispensable au bon déroulement de la vie au laboratoire et tu t'es toujours montré très patient avec moi même quand tu revenais du squash avec des bleus sur le corps ! Merci à toi Greg ! Ensuite, je tiens à remercier chaleureusement Valérie Collard qui veillait sur nous au laboratoire. Tu ne m'as jamais dit non pour quoique ce soit. Des analyses, ton aide ou bien un dinosaurus (sauf s'il avait des points). On a passé pas mal d'heures au SEM ensemble mais aussi en dehors du travail qui sont je pense mémorables. Merci VACO ! Je tiens également à remercier Martine Dejeneffe qui m'a beaucoup soutenu au laboratoire et avec qui nous avons eu des discussions très agréables au travail mais aussi en dehors, qui permettent de garder les pieds sur terre et de garder la pêche au quotidien. Pour nos échanges d'apprentis jardinier et cuisinier. Merci Martine ! Merci également à Sophie Boulanger pour sa bonne humeur, ses

blagues, ses danses originales. Sophie, tu es un élément essentiel au laboratoire, tu es toujours disponible pour les membres du CERM que ce soit en tant que secrétaire mais aussi pour nous remonter le moral avec beaucoup de gentillesse. Tu es une personne très généreuse et attentive. Merci pour tous ces bons moments ! Charlotte Danemark pour ton humeur joviale et nos discussions un peu perchées. Merci Cha !

Durant ma thèse, j'ai également pu compter sur l'aide de nombreux post-doctorants, notamment Jean-Mi, Farid, Raph, Bruno et Abdel. Merci à tous ! Un remerciement tout spécial à Abdel avec qui j'ai pas mal collaboré et même co-publié. Il y a également nos discussions sur d'innombrables sujets et ce fût très instructif, nous provenons de cultures différentes mais nous avons démontré qu'il était possible d'en discuter de façon constructive ce qui est le meilleur moyen pour établir des relations solides. Merci à toi Abdel !

Le travail au laboratoire peut parfois être assez dur car la chimie sur papier fonctionne très bien mais il en va différemment en pratique. Parfois ces échecs entament le moral. Cependant, j'ai eu la chance de travailler avec des collègues géniaux qui m'ont permis de surmonter ces difficultés. Des liens se sont tissés assez rapidement et nous sommes devenus un groupe d'amis. Un merci tout particulier à Jérémie et Philip avec qui nous formions un trio de choc. Nous avons passé de très bon moments ensembles et bien trop nombreux pour les citer tous et je suis persuadés qu'il y en aura encore. Je tiens également à remercier Maxime avec qui, selon certains, nous formions un duo maléfique (surement dû à notre impitoyable duo de beloteur, je ne vois que ça). Nous avons eu d'innombrables discussions et même parfois sur de la chimie. Merci à Charlène qui m'accompagne depuis quelques années déjà. J'ai pu découvrir la richesse de la culture africaine et notamment la nourriture qui est excellente. Nous avons passé de très bons moments ensembles et même partagé quelques temps « mon » bureau. J'ai toujours apprécié ta franchise sans aucune édulcoration. Merci Cha. Enfin merci à Antoine, un doctorant pas comme les autres avec qui une discussion de chimie pouvait dériver sur des questions existentielles. Nous avons passé de bons moments et j'espère avoir l'occasion de te rendre visite en France. Enfin merci à tous les autres doctorants qui ont partagé une partie de mon parcours : Thomas, Fabi, Alvaro, Danil, Muhammad, Florent, Sofia, François, Zoé, Anna, Oscar, Maxime, Rahmet, Kevin, Jérémie, Walid, Sandro, ….

J'aimerais également remercier tous les collaborateurs qui ont contribué à l'aboutissement de ce manuscrit via différentes collaborations. Tout d'abord, je remercie le Dr. Philippe Lecomte, le Prof. Gauthier Eppe de l'Université de Liège ainsi que le Dr. Virginie Bertrand de l'Université de Liège pour ses mesures de viabilité cellulaire. Je remercie également le Dr. Julien De Winter de l'UMons pour m'avoir fourni des analyses MALDI de qualité. Je voudrais

remercier le Dr. Benoît Couturaud de l'Université de Paris Est pour ses analyses GPC et sa collaboration sur la Ugi-4CP. Matjaž Mazaj from National Institute of Chemistry, Ljubljana for the measures of CO_2 sorption.

Je tiens également à remercier les personnes qui ont contribué de façon importante durant mes études supérieures et notamment le laboratoire de chimie analytique et d'électrochimie de l'ULg et plus particulièrement le Prof. Bernard Gilbert, malheureusement décédé en février 2018, ainsi que le Dr. Cédric Malherbe qui ont éveillé ma curiosité scientifique durant des stages de recherches.

Mes anciens camarades de classe et plus particulièrement Alexandre Verdin avec qui une complicité s'est installée, nous permettant tous deux de repousser nos limites. Je le remercie également pour les discussions scientifiques et les analyses qu'il a faites pour moi. Mon seul regret est le fait qu'on n'ait jamais réussi à co-publier même si notre duo a mis au point quelques avancées non créditées. Tu es un des scientifiques les plus curieux que je connaisse mais aussi un des plus compétents (tu ne le verras qu'une seule fois écrit). Il y a pas mal de soirées mémorables également.

Je remercie le Fonds National pour la Recherche Scientifique (FNRS) pour m'avoir octroyé la bourse de doctorat intitulée Fonds pour la Recherche dans l'Industrie et l'Agriculture (FRIA) pour 1 an ainsi qu'un mandat d'aspirant pour 3 ans.

Je finirai en remerciant tout particulièrement ma famille, et plus particulièrement mes parents qui m'ont garanti un soutien indéfectible dans tout ce que j'ai pu entreprendre depuis le début et ce avec beaucoup de patience durant les moments les plus difficiles.

Enfin, je tiens à remercier Elisabeth, ma compagne, pour ses encouragements quotidiens, pour tout son amour, sa patience et le soutien qu'elle m'a procuré plus particulièrement au cours des derniers mois. Lili sans toi, cette thèse n'aurait jamais abouti. Grâce à elle, j'ai pu réaliser ce projet mais également une multitude d'autres. Merci!

MERCI Á TOUS!

LIST OF ABBREVIATIONS

Abbreviation	Name	Abbreviation	Name
General			
3D	Three-dimensional	MOF	metal-organic framework
ADMET	acyclic diene metathesis polymerization	NP	nanoparticle
AIE	aggregation-induced emission	O/W	oil-in-water emulsion
ANOVA	analysis of variance	PH	polymerized high internal phase emulsion
BET	Brunauer–Emmett–Teller theory	PIL	poly(ionic liquid)
CMC	critical micelle concentration	polyHIPE	polymerized high internal phase emulsion
CO_2/IL	CO_2-in-ionic liquid emulsion	PPF	post-polymerization functionalization
CO_2/W	CO_2-in-water emulsion	ROP	ring-opening polymerization
$Đ$	dispersity	RT	Room temperature
DP	degree of polymerization	SSL	single-site Langmuir model
equiv.	equivalent	W/O	water-in-oil emulsion
FRP	free radical polymerization	WU	water uptake
HBP	hyperbranched polymer	m/z	the mass-to-charge ratio of ions.
HeLa	immortal cell line from Henrietta Lacks	M_n	number average molar mass
HIPE	high internal phase emulsion	M_p	molar mass at the peak
IAST	ideal adsorption solution theory	M_w	weight average molar mass
IL	ionic liquid	T_{CP}	cloud point temperature
IMCR	Isocyanide-based multicomponent reaction	T_g	glass transition temperature
LDF	Linear driving force model	T_{OD}	onset degradation temperature
MALI	mercaptoacetic acid locking imine	T_m	melting temperature
MCP	multicomponent step-growth polymerization	v	Charton value
MCR	multicomponent reaction		

Abbreviation	Name	Abbreviation	Name
Characterization techniques			
ATR	Attenuated Total Reflectance	HSQC	heteronuclear single quantum coherence spectroscopy
COSY	correlation spectroscopy	IR	infrared spectroscopy
CP MAS ssNMR	cross polarisation under magic-angle spinning solid state nucleus magnetic resonance	MALDI-ToF	matrix assisted laser desorption ionisation - time of flight
DSC	differential scanning calorimetry	MALS	multi-angle light scattering
EA	elemental analysis	MS	mass spectrometry
ESI-MS	electrospray-ionization mass spectrometry	NMR	nucleus magnetic resonance
FESEM	Field emission scanning electron microscopy	SEC	size-exclusion chromatography
FTIR	Fourier transform infrared spectroscopy	SEM	scanning electron microscopy
HMBC	heteronuclear multiple bond correlation	TGA	thermogravimetric analysis
Chemicals and polymers			
AA	acrylic acid	NNCA	*N*-carboxyanhydrides
aba	γ-aminobutyric acid	OAc	acetate
AEAm	aminoethyl acrylamide	OPA	octylphosphonic acid
AEAm-HCl	aminoethyl acrylamide acidified with hydrochloric acid	o-tol	*ortho*-tolyl
AEP	aminoethylpiperazine	PA	polyamide
BenzOAc	benzyl acetate	PAMAM	poly(amidoamine)s
BenzOH	benzyl alcohol	PEF-68	Pluronic® Flakes-68
Boc-AEAm	*N*-boc-aminoethyl acrylamide	PEG	Poly(ethylene glycol)
DAA	deprotonated acrylic acid	PEHMA	poly(2-ethylhexyl methacrylate)
DCTB	*trans*-2-(3-(4-*tert*-Butyl-phenyl)-2-methyl-2-propenylidene)malononitrile	PEI	poly(ethylenimine)s
DHPM	3,4-dihydropyrimidin-2(1H)-ones	PEO	poly(ethylene oxide)
DMAc	*N*,*N*-dimethylacetamide	PGMA	poly(glycidyl methacrylate);
DMEM	Dulbecco's Modified Eagle Medium	Ph	phenyl
DMF	dimethylformamide	PMF	poly(melamine-formaldehyde) resin
DMSO	dimethyl sulfoxide	PPA	phenylphosphinic acid

Abbreviation	Name	Abbreviation	Name
DVIm	divinyl imidazolium	PPO	poly(propylene oxide)
Et2O	diethyl ether	PS	Poly(styrene)
EtOAc	ethyl acetate	PVA	poly(vinyl alcohol)
glygly	glycylglycine	PVBC	poly(vinylbenzyl chloride)
GMA	glycidyl methacrylate	PVDF-HFP	poly(vinylidenefluoride-co-hexafluoropropylene)
GSH	intracellular glutathione	*t*Bu	tert-butyl
haba	4-amino-3-hydroxybutyric acid	*t*BuNC	tert-butyl isocyanide
HBTC	1,3,5-benzenetricarboxylic acid	TFSI	bis(trifluoromethanesulfonyl)imide
HOAc	acetic acid	THF	tetrahydrofuran
IBAm	imidazolium bis-acrylamide	TPE	tetraphenylethene
Im RMCP	imidazolium synthesized by Radziszewski MCP.	TREN	tris(2-aminoethyl)amine
JEFF	Jeffamine-T403®	TZL	triazole
MeOH	methanol	VA-044	2,2'-Azobis[2-(2-imidazolin-2-yl)propane]dihydrochloride
MTS	3-(4,5-dimethylthiazol-2-yl)-2,5-diphenyltetrazolium bromide	VAc	vinyl acetate
MTT	3-(4,5-dimethylthiazol-2-yl)-5-(3-carboxymethoxyphenyl)-2-(4-sulfophenyl)-2H-tetrazolium	VBC	vinylbenzyl chloride
*N*HC	*N*-heterocyclic carbene	Vim	vinyl imidazolium
NMP	*N*-methyl-2-pyrrolidone		

TABLE OF CONTENT

Chapter I.

Overview of Imine-Based Multicomponent Polymerizations

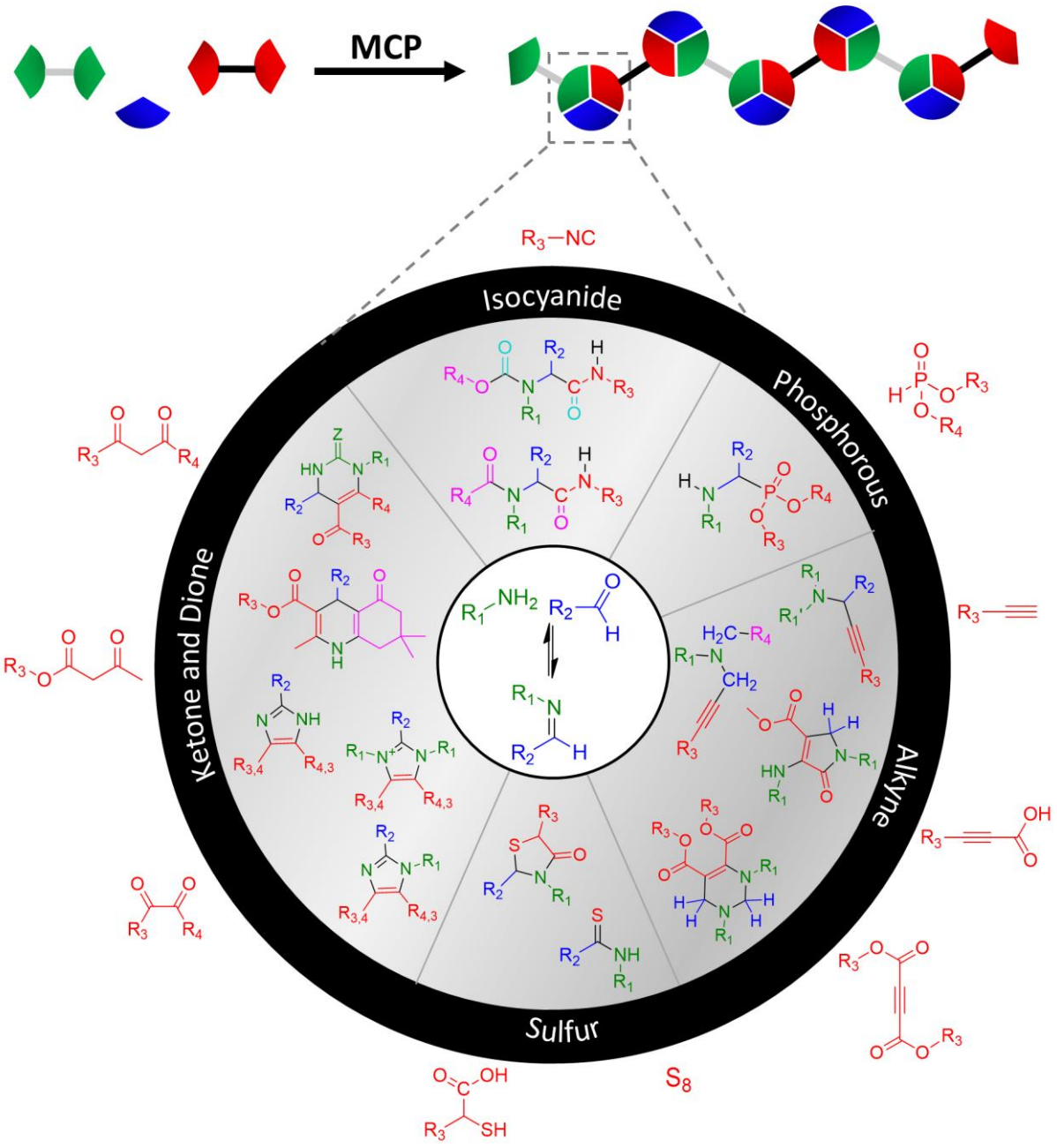

Chapter I. Overview of Imine-Based Multicomponent Polymerizations

I.1. Introduction

I.1.1 Multicomponent reactions: basics and definitions.

Multicomponent reactions (MCR) are commonly described as one-pot reactions involving at least three components reacting to form a product in which almost all atoms of the starting reagents are incorporated.[1,2] MCRs are powerful and straightforward synthetic methods that exhibit key features such as high atom efficiency and ease of implementation. Moreover, these convergent reactions involve the formation of several covalent bonds leading to rather complex structures which can be easily diversified by varying each component of the reaction. For this reason, they are considered as synthetic tools of choice in combinatorial approaches. Although it is generally accepted that MCRs are highly efficient,[3] this aspect needs to be nuanced. Indeed, the conversion depends on the type of MCRs which can be sorted in three categories based on their mechanism (Figure 1).[4]

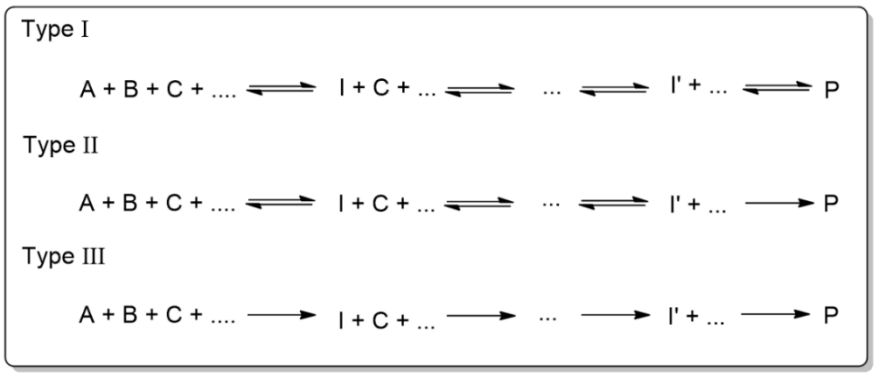

Figure 1. Main classes of MCRs as described elsewhere.[4] Each step represents an elementary reaction. I and P stand for intermediate and product, respectively.

In type I MCR, all steps (elementary reaction) are reversible which can lead to low yields. Nonetheless, it is possible to displace the equilibrium by trapping a byproduct which consists of small molecules like water, nitrogen and low molecular weight acids.[5,6] In type II, the last step is irreversible and drives the overall reaction towards the final product leading to higher conversion. The irreversible step often corresponds to strongly exothermic reactions such as ring-closure, aromatization, rearrangement or formation of a new carbon-carbon bond.[4] Eventually, the most attractive MCRs belong to type III in which each step is irreversible. Although very effective, examples of such MCRs are scarce in preparative chemistry but commonly encountered in biochemical reactions.[4]

In order to clarify the scope of MCRs, it is important to precise the terms of their definition, *i.e.* "one-pot reactions involving at least three components leading to a product containing most of the atoms of the reactants". First, the term "component" needs to be specified since it could designate a chemical compound or a chemical function (functional center). In this review, "component" will refer to an individual compound regardless the number of functional groups it contains. For the sake of clarity, throughout this review, reactions will be designated as follows: name (or abbreviation) of the reaction – number of functional centers - number of components. On the other hand, the term "one-pot reaction" describes a set of chemical reactions, whereby a reagent undergoes successive (or concomitant) chemical reactions in a single vessel or reactor.[7] It does not preclude subsequent addition of reagents, mediators or catalysts nor imply that all reactions steps are carried out under the same conditions. Eventually, it does not exclude manipulation (work-up) or isolation of an intermediate. Indeed, a solution containing the intermediate can be extracted or filtered as long as the product remains in the filtrate, the solvent can be exchanged or concentrated to dryness. Such cases are considered as one-pot processes as long as the intermediate stays in the same reactor.[7]

In the light of these considerations, we will encompass under the term multicomponent reactions "all reactions taking place in a single vessel, involving more than two reagents, whether introduced together at the start or sequentially, whether or not conditions are changed during the reaction, provided that almost all atoms are incorporated into the final product". Importantly, the function generated at each step must be the reaction centre of the next one. This criterion excludes cases where a reagent bearing two orthogonal chemical functions[8] reacts independently with two other compounds.[9]

The first MCR was reported in 1837 by Laurent and Gerhardt who reacted ammonia with bitter almond oil, a source of benzaldehyde and hydrogen cyanide (Figure 2).[10] Few years later (1850), Strecker published the synthesis of α-amino acids derived from α-aminonitriles obtained by one-pot reaction between aldehyde, amine and hydrogen cyanide (Figure 2).[11] Since these pioneering works, multicomponent reactions have flourished giving rise to a multitude of MCRs notably the well-known Hantzsch, Biginelli, Mannich, Passerini and Ugi reactions to name a few. In the last years, they became very popular tools in combinatorial chemistry for the synthesis of complex products notably in drug discovery and development of biological compounds.[5,12]

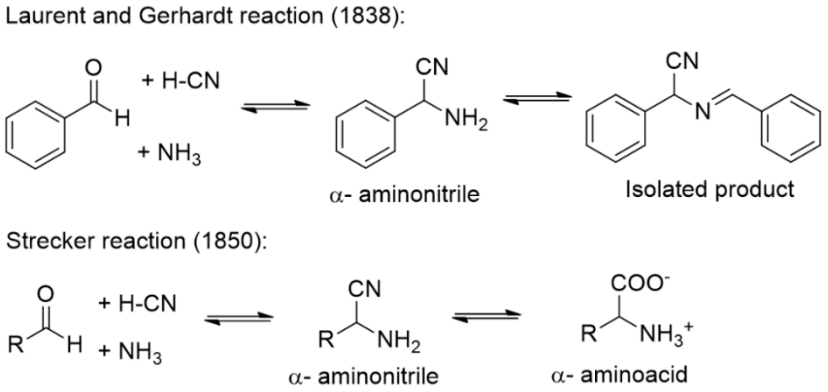

Figure 2. Pioneering multicomponent reactions were reported by Laurent and Gerhardt in 1838 and Strecker in 1850.

I.1.2. Multicomponent reactions in polymer science

Nowadays, the development of advanced macromolecular synthetic methods is essential to satisfy the demand for more and more complex polymer materials and fulfil the requirements of today's highly valued applications. In this context, due to their combinatorial character, ease of implementation and atom economy, multicomponent reactions (MCRs) recently emerged as promising and powerful tools for the design of structurally complex macromolecules. MCRs can be exploited *via* three different approaches for the synthesis of macromolecules, namely monomer synthesis, post-polymerization modification and step-growth polymerization (Figure 3). Briefly, some monomers prepared by MCRs were polymerized by various techniques including ring-opening metathesis polymerization,[13] radical polymerization[14] or acyclic diene metathesis (ADMET) polymerization,[15–17] amongst others (Figure 3A). Multicomponent reactions were also successfully applied onto preformed polymers in order to modify their side chains functions (Figure 3B).[18] Finally, step-growth polymerization can be achieved by applying MCRs onto multifunctional reagents (Figure 3C). The latter approach was introduced in the second half of the 20th century, with few examples involving notably the well-known Mannich reaction.[19] Nevertheless, the use of MCRs in direct polymerization underwent an impressive expansion following the work of Meier *et al.* in 2011 consisting of the polymerization of dicarboxylic acids and dialdehydes in the presence of an isocyanide *via* the Passerini reaction.[15] Since then, examples of polymer synthesis involving MCRs have flourished the literature.[20–28]

In contrast to the two first approaches, the step-growth process requires very efficient MCRs in order to reach decent molar masses since these latter depend on the conversion and follow the Carother's law. Two different systems are possible for the synthesis of linear macromolecules

by step-growth polymerization, *i.e*. the use of homo-functional monomers (A_2 + B_2 system) or hetero-functional monomers (AB system). While homo-functional monomers are generally stable, a chemical function being often orthogonal with itself, it is sometimes more difficult to get hetero-functional monomers due to reactions between the different chemical functions. Nevertheless, AB monomers allow better control on stoichiometry, an important parameter to aim for high molecular weights. Using MCRs instead of classical reactions broadens the structural diversity of the polymers. Indeed, as illustrated in Figure 3C, if we consider a three-component reaction involving the chemical functions A, B and C, two polymerization systems are possible, *i.e.* A_2 + B_2 + C and AB + C for homo- and hetero-difunctional monomers, respectively. In both cases, the structure of the polymer backbone is determined by the difunctional monomers and contains the pattern resulting from the multicomponent reaction. On the other hand, the nature of the side chains of the macromolecules is ruled by the monofunctional monomer(s) (Figure 3). The properties of the polymers can be modulated by varying the linkers or the substituents bearing the chemical functions but also by changing the nature of the difunctional reagents and the monofunctional ones (*e.g.* A_2 + B + C_2 system).

MCRs have been used for the synthesis of hyperbranched polymers (HBPs) and networks as well. A wide variety of combinations is possible to design these architectures (Figure 3). Indeed, MCRs applied to monomers bearing three functions (A_3 or AB_2) with difunctional and monofunctional monomers lead to three-dimensional macromolecules (Figure 3). Networks are obtained when functions are close to the stoichiometry whereas an excess of a function favours the formation of HBPs. Moreover, compared to classical step-growth polymerization, multicomponent polymerization (MCP) allows the use of more available difunctional monomers to get HBPs and networks (A_2 + B_2 + C_2 and AB + C_2).

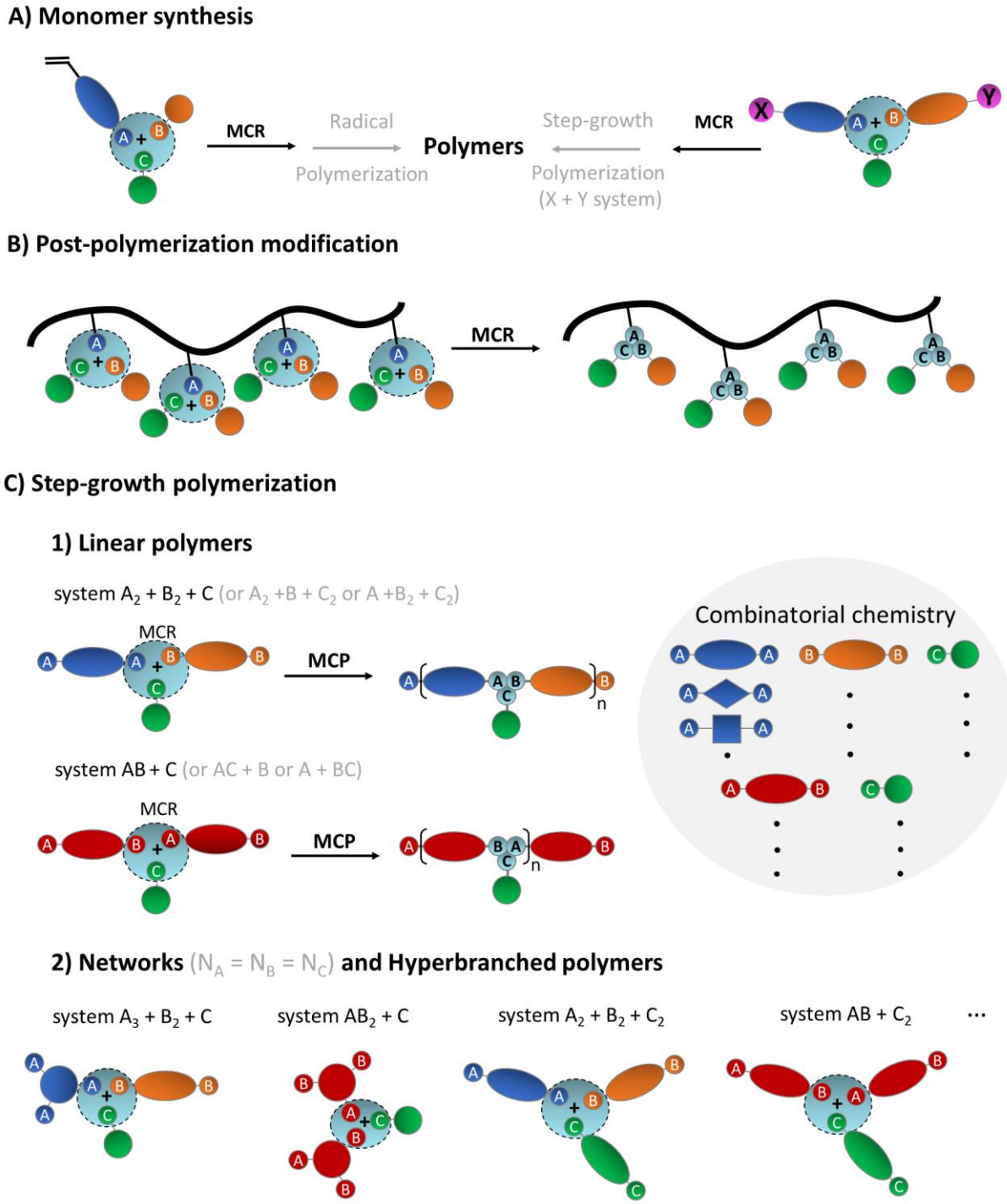

Figure 3: A) Monomer synthesis and B) post-polymerization modification using MCRs. C) Step-growth polymerization of macromolecular architectures using different systems of MCPs.

I.1.3. This review

The present review gives an overview of the recent progress in the design of polymers *via* MCRs. In particular, it focuses on multicomponent polymerization methods for the preparation of linear but also branched and crosslinked polymers. Moreover, we decided to concentrate on imine-based MCPs since the aldehyde/amine condensation is a very common step of numerous MCRs used in organic and polymer synthesis. Also called Schiff base, imines are very interesting MCRs' intermediates leading to iminiums upon protonation which ultimately facilitates a nucleophilic attack on the sp2 carbon similarly to carbonyl compounds. In addition, the nitrogen atom is able to perform nucleophilic attack allowing a great variety of reactions as will be illustrated. Note that the condensation reaction forming the imine is reversible and often leads to incomplete conversion. Consequently, for an imine-based MCR to be efficient, the following steps must displace the equilibrium by consumption of the formed imine through irreversible reaction steps or at least by subsequent reactions largely displaced towards the formation of products.

This introductory chapter aims to depict the great potential of the imine-based MCRs in step-growth polymerizations for the design of linear macromolecules and networks. Special care will be devoted to emphasizing the limits of these imine-based MCP approaches in terms of molar masses and substrates versatility. Although the field of MCPs is still in its infancy, this research area already contributed to the development of cutting-edge applications in biomedical, energy, electronic, CO_2 capture, catalysis, heavy metal recycling sectors and so on.

I.2. Imine-based Multicomponent Polymerizations

I.2.1. Isocyanide-based MCP

An important class of MCPs relies on isocyanide multicomponent reactions (IMCRs). Isocyanides exhibit unusual reactivity coming from their relatively stable divalent carbon. First synthesized by Lieke in 1859,[29] their electronic structure is still under debate today. They can either be represented under a zwitterionic form (Lindemann, 1930) or as a carbene (Nef, 1892).[30] Nevertheless, a recent theoretical study suggests a dominant contribution of the carbene form although the linear geometry is imposed by the zwitterionic contribution.[30] The carbene form explains why isocyanides can act both as a nucleophile or an electrophile on the carbon atom (α-addition). Due to the aforementioned characteristics, the isocyanides became important chemicals in MCRs where they often first react as nucleophiles, to form α-adducts that can subsequently react with other nucleophiles.[31,32] In most IMCRs, the isocyanide divalent carbon is converted into a tetravalent one through the formation of at least one carbon-carbon bond, an exothermic transformation which constitutes the driving force of the reaction and contributes to its efficiency. The use of isocyanides as building blocks in polymer science is increasingly popular,[22–25,33,34] especially upon reactions with imines as described below.

I.2.1.a. Ugi-4C

The Ugi four-component reaction (U-4CR) usually refers to the reaction between a primary amine, an aldehyde (or a ketone), an isocyanide and a carboxylic acid leading to an α-amido amide (Figure 4). The U-4CR is an extension of the first reported isocyanide-based MCR, namely the Passerini three-component reaction (P-3CR) which involves only three components, *i.e.* a carboxylic acid, an aldehyde or a ketone and an isocyanide, and produces α-acyloxycarboxylamides. The introduction of a fourth component, that is, the amine, increased the diversity of the possible products and the U-4CR rapidly became one of the most important MCRs in combinatorial and medicinal chemistries.[4] The most plausible and generally accepted mechanism involves the condensation of the amine and the aldehyde to form a Schiff base that is subsequently protonated by the acid to generate an iminium and a carboxylate. The key step consists of the nucleophilic attack of the isocyanide onto the iminium to form a nitrilium intermediate that undergoes the addition of the carboxylate. Eventually an α-amido amide is generated through acyl group migration (Mumm rearrangement) with water as the sole byproduct (Figure 4).[35] ESI-MS experiments using charge-tagged reagents allowed the

detection of the iminium and the nitrilium intermediates and therefore pointed out the accuracy of the above-mentioned mechanism.[36]

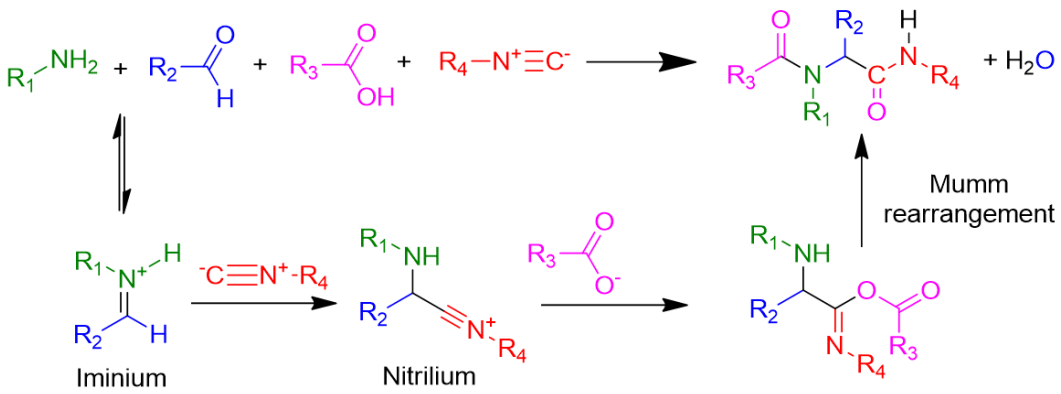

Figure 4. Ugi four-component reaction and plausible mechanism.

In 2014, Meier and coworkers reported the Ugi four-center four-component polymerization (U-4C-4CP) of difunctional reagents bearing the same function (A_2 + B_2 + 2C + 2D system) towards the synthesis of polyamides.[37] Compared to conventional secondary polyamides (PA 6, PA 6.6 and PA 11) synthesized by ring opening or polycondensation, the U-4C-4CP affords polymers bearing both secondary and tertiary amides. It probably disturbs the formation of hydrogen bonds and changes the overall thermal properties and the solubility of the resulting polyamides. The authors investigated the polymerization of different A_2- and B_2-type reagents with monofunctional compounds. This approach enables six combinations leading to diversely substituted polyamides (Figure 5).[37] Interestingly, the chemical structure of the backbone and the side groups could be tune by variating the nature of the difunctional monomers. As a rule, the polymer backbone is composed by the difunctional compounds while the monofunctional reagents constitute the pendant groups. The polymerizations were carried without any catalyst and took place at room temperature under air for at least 37 hours. An excess of monofunctional reagents was used to ensure their availability at high conversion. The U-4CR is usually performed in methanol (MeOH)[38] but when considering polymerization, the solvent was adapted to ensure the solubility of the polymer generated during the reaction. In this case, tetrahydrofuran (THF), known as a good solvent for polyamides, was used as cosolvent with MeOH. Although MCRs are usually favoured by high concentration,[38] elevated viscosity was detrimental for the polymerization. On the other hand, the formation of macrocycles was observed when U-4CP was carried out under diluted medium. The concentration was therefore optimized to get the highest possible M_n. Overall, a wide range of aliphatic bifunctional and monofunctional reagents was considered (Figure 5, Meier 2014) and molar masses (M_n) ranging

from 7 to 21 kg/mol were obtained. Note that the molar masses were determined by size exclusion chromatography (SEC) as will be the case for all the M_n discussed in this review except if stated otherwise. The resulting polyamides displayed glass-transition temperatures (T_g) from 1 to 65 °C but no detectable melting temperature (T_m).[37] This behaviour proves the low capability of the chains to form intermolecular hydrogen bonds due to the steric hindrance of the substituents but also due to the presence of tertiary amides at the side of secondary ones. It is noteworthy that the choice of the aldehyde is crucial for the success of the U-4CP. Indeed, aldehydes with blocked α-position prevent the aldol condensation which hampered the polymerization. The orthogonality of the U-4CP towards alkynes was demonstrated with the introduction alkyne-functionalised monomer, which opened the door for post-polymerization modifications (Figure 5, Meier 2014).[37]

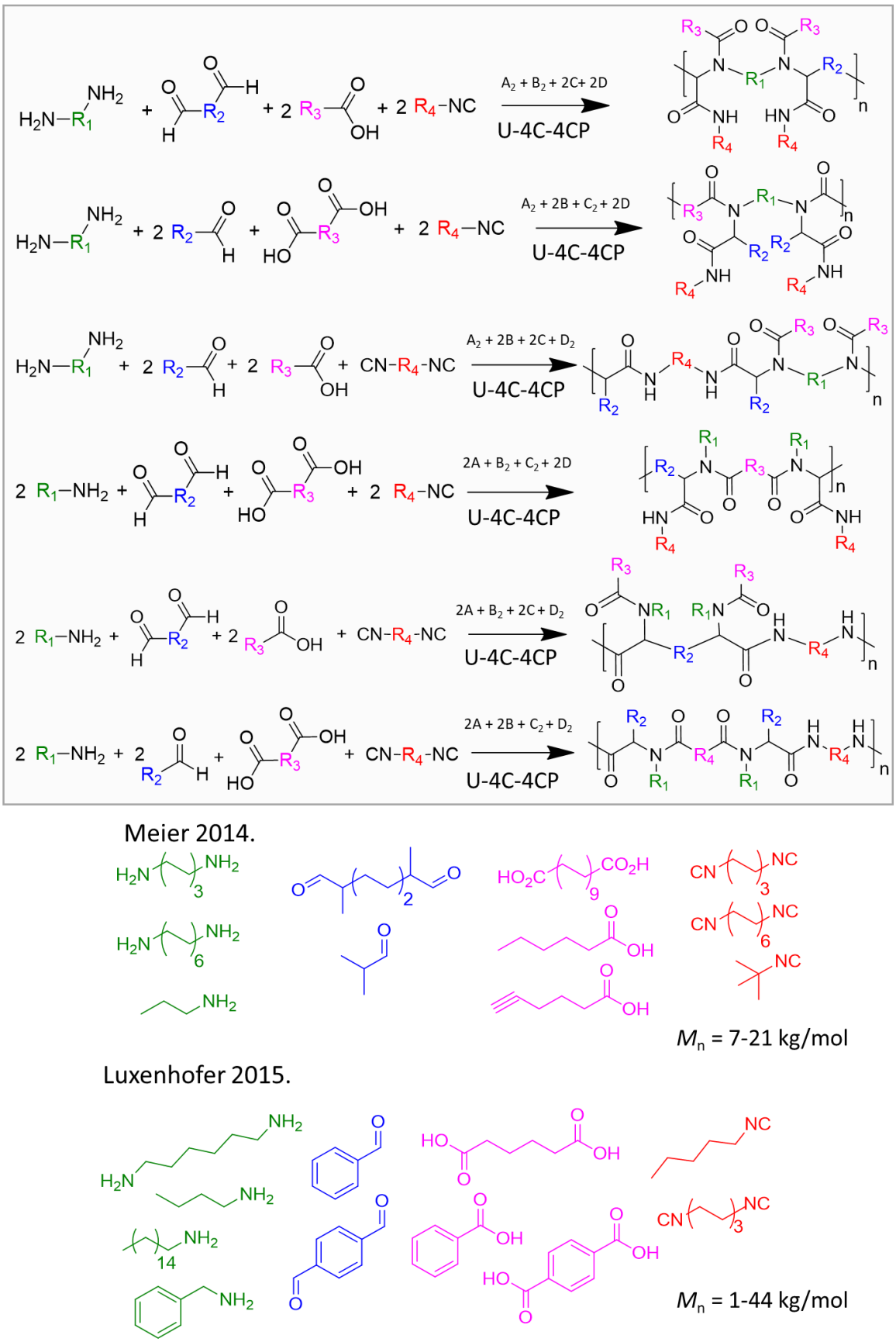

Figure 5. The six different combinations for the Ugi four-center four-component polymerization and the corresponding polymer structures and substrates.

Since this pioneering work, the scope of possible monomers for the U-4CP has been extended leading to a large library of interesting and functional polymers. Luxenhofer and coworkers considered the six possible combinations to polymerize aromatic monomers such as aromatic aldehydes (mono and difunctional), aromatic and aliphatic carboxylic acids with aliphatic isocyanides and amines (Figure 5, Luxenhofer 2015).[39] Interestingly, molar masses above 3.5 kg/mol were only achieved for two combinations, *i.e.* the reactions involving either an aromatic dialdehyde (terephthalaldehyde) and an aromatic dicarboxylic acid or an aliphatic diisocyanide, all other combinations led to oligomers.[39] Encouraged by these results, they further optimized the conditions and finally reached molar masses up to 44 kg/mol. For this purpose, polymerizations were performed under inert atmosphere for prolonged periods (few days). The authors pointed out that the use of aromatic aldehydes and carboxylic acids did not favour the reaction due to their steric hindrance but they ruled out a reduced reactivity coming from the conjugated system.[39]

The U-4CP becoming more mature, various functional polymers and potential applications emerged. In this context, the synthesis of polyampholytes using amino acids as bifunctional compounds was achieved.[40] Protected lysine and protected glutamic acid were reacted with aliphatic and aromatic aldehydes and isocyanides, *i.e.* the *tert*-butyl isocyanide or an oligomer of poly(ethylene glycol) (PEG) functionalized isocyanides (Figure 6A, Wang 2018). Polymers with molar masses above 10 kg/mol were obtained. These results further confirmed the good reactivity of aromatic aldehydes in U-4CP.[40] Interestingly, the resulting PEG-containing polymers displayed thermoresponsiveness in aqueous solution. Moreover, deprotection of the lysine and the glutamic acid afforded protein repelling polyampholytes. Eventually, the authors proved the good cytocompatibility of their polymers towards HeLa cells.[40]

Recently, an aromatic dicarboxylic acid, namely the 2,5-furandicarboxylic acid, was used in U-4CP with aliphatic monomers (Figure 6A, Grunwaldt 2019). In this work, the polymerization conditions of one set of monomers were extensively optimized.[41] Depending on the reaction conditions, the M_n ranged from 0.8 to 11 kg/mol highlighting the huge effects of concentration, solvent choice and purity of the bifunctional reagent on the course of MCPs.

In 2020, Deng *et al.* synthesized oligomers by reacting a diamine linked by a piperazine function with several PEG-diacids of different lengths, various aldehydes and *tert*-butyl isocyanide (Figure 6A, Deng 2020).[42] High molar masses were obtained (M_n up to 46 kg/mol) which is not surprising given the use of PEG macromonomers. The polymers exhibited thermoresponsive behaviour that could be tuned by changing the lengths of the PEG segment or by changing the hydrophobicity of the aldehyde which constituted the pendant group.

Finally, once protonated, the tertiary amines of the piperazine derivative brought antimicrobial activity to the polymers. Interestingly, based on the same PEG-diacids monomers but using dialdehydes and aromatic amines, the same group developed temperature/photo dual sensitive polymers (Figure 6B, Deng 2020).[43] Although aromatic amines are known to be detrimental to the U-4CR[38] and the use of aldehydes with acidic α protons can lead to aldol condensation, they obtained quite high molecular weights, up to 33 kg/mol. The introduction of azobenzene moieties endowed the polymers with some photosensitivity and their properties (cloud point temperature, contact angles and particle sizes) could be tuned upon irradiation (at 365 nm).[43]
Eventually, Chen *et al.* developed some cationic redox-responsive polymers for intracellular protein delivery application. In this case, two different disulphide-containing dicarboxylic acids were reacted with a diisocyanide in the presence of isobutyraldehyde and primary amine derivatives linked to a tertiary amine or a morpholino moiety (Figure 6C, Chen 2020).[44] This strategy gave access to polymers with M_n up to 9 kg/mol which contains disulfide bonds in their backbones and protonable tertiary amines as pendant groups. These macromolecules were used to form polyplexes with proteins that facilitate their introduction in the cells where the intracellular glutathione (GSH) rapidly triggers the cleavage of disulfide bonds and thus the release of proteins.[44]

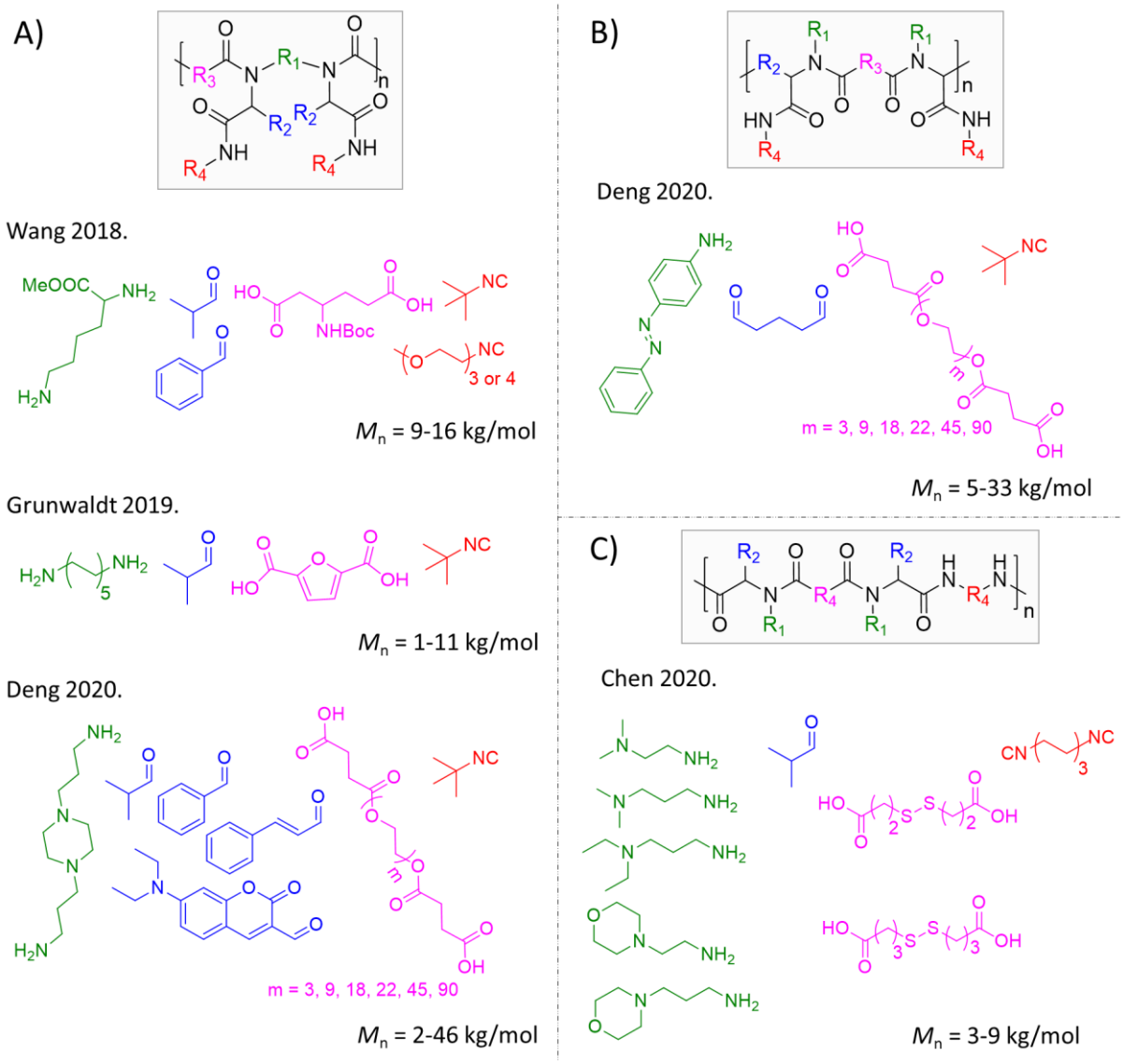

Figure 6. Scope of reagents used in the Ugi four-center four-component for A) A_2 + 2B + C_2 + 2D, B) 2A + B_2 + C_2 +2D and C) 2A + 2B + C_2 + D_2 systems.

Besides the above-mentioned U-4C-4CP, examples of Ugi four-center three-component polymerizations (U-4C-3CP) involving difunctional monomers bearing different chemical functions (AB system) were reported. This strategy allows a better control over the stoichiometry compared to a $A_2 + B_2$ system which strongly relies on the precision of the operator. It should be noted, however, that all combinations of chemical functions are not possible in the U-4C-3CP approach and that the use of AB monomers also reduces the number of components in the reaction and thus the variability of the products.

Amino acids, containing both an amine and a carboxylic acid, quickly drew attention as reactants for the U-4C-3CP due to their availability and their potential to create peptidomimetic materials. Several natural α-amino acids were first reacted with benzaldehyde and *tert*-butyl isocyanide.[45] Unfortunately, only oligomers were obtained and the molar masses were limited to 3.4 kg/mol. The polymerization was hampered by a side-reaction consisting of intramolecular cyclisation and subsequent opening *via* the solvent (MeOH).[45] To tackle this issue, Wang *et al* increased the distance between the amine and the carboxylic acid functions to disfavour the cyclisation reaction. As an example, they used N_{α}-Boc-L-lysine with different aromatic aldehydes and *tert*-butyl isocyanide and obtained molar masses ranging from 7 to 11 kg/mol (Figure 7, Wang 2016). After the amine deprotection of the lysine, the resulting polycations showed antibacterial properties, good biocompatibility and were able to deliver encapsulated curcumin inside the cytoplasm.[45,46] Decreasing the number of carbons between the amine and the carboxylic acid, from five to four or three, decreased the M_n around 5 kg/mol (Figure 7, Wang 2016). Overall, γ-, δ- and ε-peptoids were synthesized *via* the U-4C-3CP of amino acids.[45]

Similarly, Debuigne *et al*. took advantage of natural dipeptides composed of glycine and alanine to move away the acid and amine functions and avoid intramolecular cyclization.[47] They carried out the polymerization in water with formaldehyde and *tert*-butyl isocyanide (Figure 7, Debuigne 2017). A series of thermoresponsive alternating peptide-peptoid polymers was produced accordingly. Interestingly, when repeated in the presence of additional monofunctional carboxylic acids, such as acrylic acid or acid-terminated PEG, the U-4C-3CP of dipeptides led to acrylamide-terminated peptide-peptoid macromonomers and thermoresponsive PEG-*b*-poly(peptide-peptoid) block copolymers, respectively.

Another hetero difunctional monomer used in U-4C-3CP combines an isocyanide moiety and a carboxylate group. Developed by Koyama and coworkers, this monomer was polymerized in isopropanol for a few days with fluorinated ammonium salts and monofunctional aldehydes such as isobutyraldehyde and aromatic aldehydes (Figure 7, Koyama 2018).[48] Note that, the

procedure involves several steps and work-ups but the reaction mixture stays in one-pot. The resulting polymers were notably valued as surface active agents for the chloroform-air interface. In addition, the polymer with biphenyl and perfluoroheptyl pendant groups showed a critical micellar concentration (CMC) below 1 wt%. In a similar way, difunctional isocyanide/carboxylate-bearing monomers were also reacted with preformed imines leading to a Ugi three-center two-component polymerization (U-3C-2CP, A' + BC system).[49,50] Since the isocyanide/carboxylate compounds derived from α-amino acids (glycine and phenylalanine), the resulting polymers presented alternating poly(peptide-peptoid) structures (Figure 7, Koyama 2017 and 2020).[49,50] Except for a few polymers, relatively low molecular weights were obtained but the polymers exhibited good adhesive properties.[50]

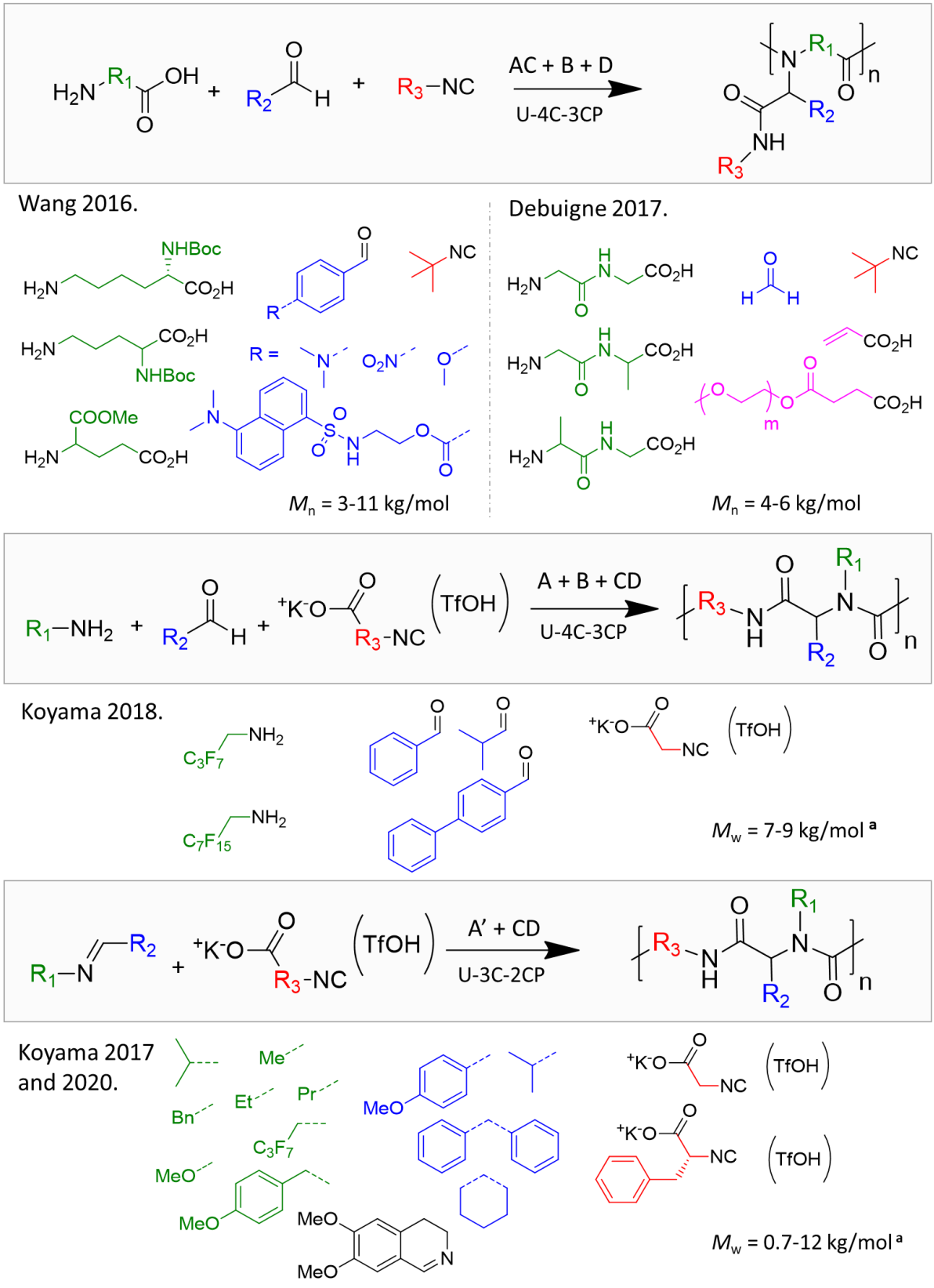

Figure 7. Ugi polymerizations involving hetero difunctional monomers. [a] The M_w were determined by NMR.

The last example of the U-4CP involved levulinic acid, an oxo acids derived from renewable lignocellulosic biomass.[51] Interestingly, when combined with an amine and an isocyanide, oxo acids are known to form lactam *via* an intramolecular Ugi four-center three-component reaction.[52] Therefore, reacting a diisocyanide, a diamine and the levulinic acid did not produce a network but a linear polyamide containing five membered lactams.[51] Indeed, the reaction of 1,6-diisocyanohexane, ethylenediamine and levulinic acid carried out in MeOH at 100 °C for 30 minutes in a microwave reactor afforded a polymer with an M_n of 9.5 kg/mol. As a variation, the authors increased the size of the diamine linker and obtained higher molecular masses around 12 kg/mol (Figure 8). When an aromatic amine, *i.e.* the aniline was used, mainly oligomers or macrocycles were formed while the PEG-diamine led to chain extension but the resulting polymer was contaminated with unreacted PEG.[51] Eventually, the use of a triamine, namely the tris(2-aminoethyl)amine (TREN), resulted in a crosslinked material (Figure 8). To the best of our knowledge, this is the sole example of direct Ugi polymerization of multifunctional monomers towards the synthesis of networks. Note, however, that the Ugi reaction has largely been applied to crosslink pre-existing polymer chains.[53–62]

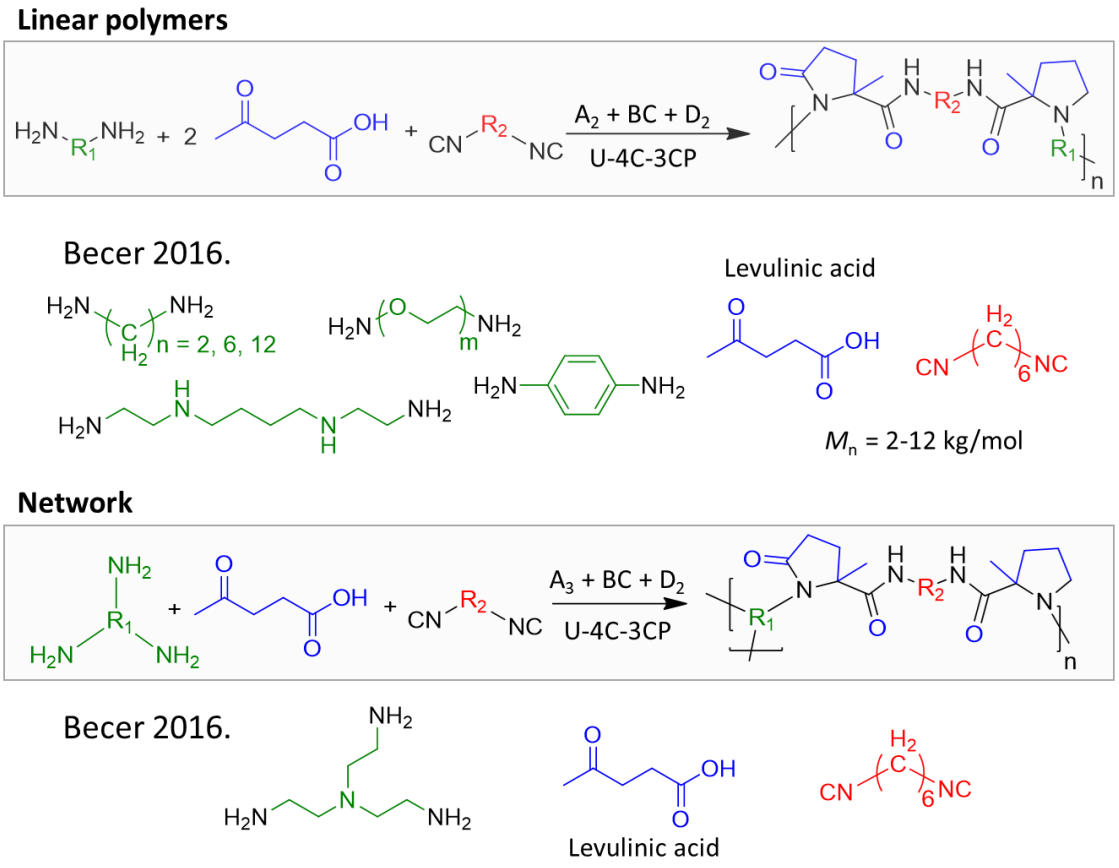

Figure 8. U four-center three-component polymerization of levulinic acid toward linear polymers and network.

I.2.1.b. Ugi-5C

Shortly after its discovery, the Ugi-4CR reaction was extended to a multitude of reagents. The carboxylic acids can be substituted by a variety of other acidic compounds such as carbonic acid monoester, water, activated phenol and hydrogen sulfide to name a few, while the amine can be substituted by hydrazine, urea, sulphonamide, hydroxylamine, etc.[38] A Ugi five-component version (U-5CR) was also reported.[63] The latter implies an alcohol, carbon dioxide, an aldehyde, an isocyanide and a primary amine (Figure 9). In this case, the alcohol and the carbon dioxide produce a carbonate which reacts with the nitrilium intermediate before rearrangement yielding *N*-(alkoxycarbonyl)amino amides. Some years ago, this reaction was adapted for polymerization (U-5C-5CP) (Figure 9).[64] The latter involved a difunctional amine and isocyanide (1,12-diaminododecane and 1,6-diisocyanohexane), isobutyraldehyde and methanol in large excess under 10 bar of carbon dioxide. The polymerization was carried out in a mixture of MeOH/THF and the best yield was obtained in concentrated media (up to 56 %) with M_n of 21 kg/mol. The resulting poly(urethane-amide) possessed a methyl carbamate in α-position of an amide. Due to this peculiar disposition, additional treatment with aqueous potassium hydroxide solution converted the polymer into the corresponding poly(hydantoin)s, which further broadened the scope of the macromolecular engineering *via* Ugi-type reaction.[63]

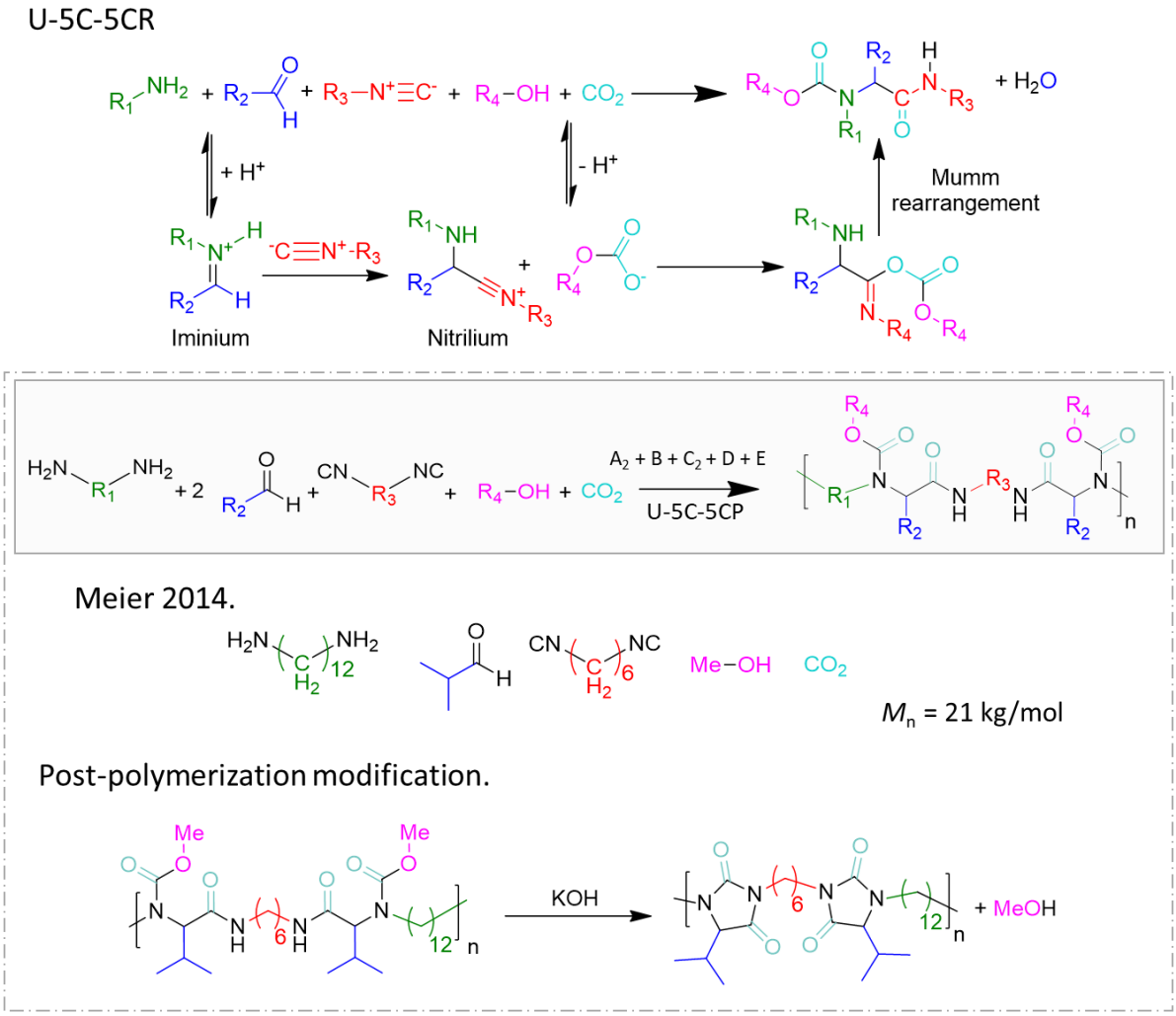

Figure 9. Ugi five-center five-component reaction and polymerization as well as post-polymerization modification.

I.2.2. Phosphorous-based MCP

2.2.a. Kabachnik–Fields

The Kabachnik-Fields three-component reaction (KF-3CR) provides a green procedure for the synthesis of α-amino phosphonates or α-amino phosphonic acids after a further deprotection. These compounds are phosphorous analogues of α-amino acids and exhibit low toxicity towards mammalian cells[65] making them important chemicals for drug research.[66,67] The three-component KF reaction is a one-pot and single step reaction between an aldehyde (sometimes a ketone), an amine and a dialkyl phosphonate (Figure 10). It can be seen as an upgrade of the Pudovik reaction involving a preformed imine and a dialkyl phosphonate.[68] The mechanism is still debated but a plausible hypothesis consists of an aldehyde/amine condensation followed by the addition of the phosphonate onto the imine.[69,70] The reaction proceeds without any catalyst but is accelerated with various Lewis acids and the assistance of microwaves.[70]

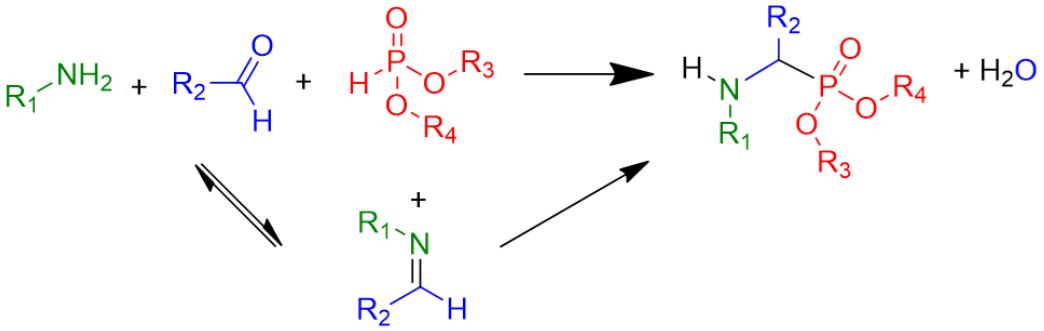

Figure 10. Kabachnik-Fields three-component reaction and plausible mechanism.

The use of KF-3CR in direct polymerization was first reported by Liu and coworkers to produce halogen-free flame retardants and macromolecular crosslinkers for epoxy resins.[71] They selected terephthalic aldehyde and diethylenetriamine as difunctional monomers while diethyl phosphonate was used in large excess playing the role of both the monofunctional monomer and the solvent (Figure 11, Liu 2014).[71] The polymerization was performed at 120°C for 24 h under inert atmosphere yielding a moderate molecular weight of 3 kg/mol. Increasing the reaction time from 1 to 6 days resulted in slightly higher M_n (4.5 kg/mol) and a broader dispersity. Eventually, when the polymer was incorporated in epoxy resins with a weight ratio equal or higher than 20%, the resulting materials showed good flame retardancy.[71]

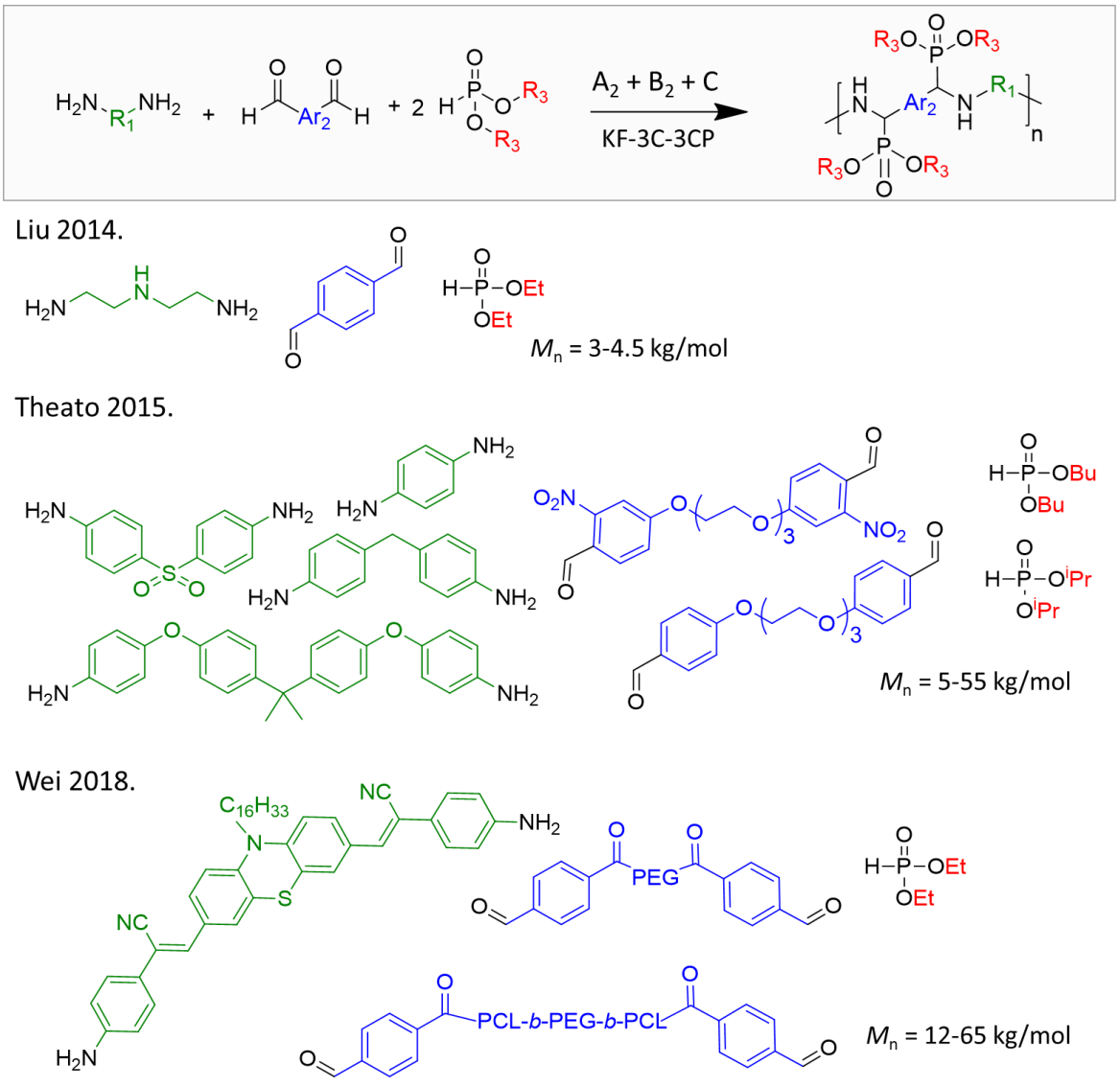

Figure 11. scope of monomers polymerized *via* the Kabachnik-Fields three-component polymerization.

Few months later, the higher efficiency of aromatic diamines over aliphatic ones for the KF-3CP was highlighted.[72] According to the authors, it was due to the faster formation of imine. The polymerizations were carried out at lower temperature (80 °C) during 20 hours. The aromatic dialdehyde, namely the 1,10-bis(4-formylphenyl)-1,4,7,10-tetraoxadecane, was polymerized with various aromatic diamines and diisopropyl or dibutylphosphite (Figure 11, Theato 2015).[72] The choice of the amine and the alkyl group of the phosphonate had a huge impact on the molecular weight (M_n from 5 to 55 kg/mol). Interestingly, after polymerization, the pendant phosphonate moieties could be deprotected upon addition of bromotrimethylsilane to give the corresponding zwitterionic poly(α-amino phosphonic acid). In addition, the authors

demonstrated the possible photocleavage of the polymers containing o-nitrobenzyl groups to retrieve the diamines monomers.[72]

More recently, an aromatic diamine dye (Figure 11, Wei 2018) was used in combination with diethyl phosphonate for chain extension of poly(ethylene glycol) and poly(ethylene glycol)-*co*-poly(caprolactone) α,ω-functionalized with aromatic aldehydes.[73,74] These solvent-free polymerizations were accelerated with microwaves to shorten the reaction time to only 5 minutes. The resulting polymers exhibit low cytotoxicity and photoluminescence upon aggregation (aggregation-induced emission (AIE)) making them good candidates for cell imaging applications.

It is noteworthy that the KF reaction has also been widely used in the modification of pre-existing polymers[75–83] and in one-pot combination with radical polymerization.[84–86] To the best of our knowledge, however, no synthesis of 3D structured materials was reported for the KF-3CR.

I.2.3. Alkyne-based MCP

Alkyne-based MCPs have largely contributed to the development of novel polymeric structures during the past decade. Here, we will describe the combination between an aldehyde, an amine and an alkyne through a condensation reaction named the A^3-coupling. However, one must be aware that there are other alkyne-based MCPs that do not involve an imine. Indeed, as reviewed elsewhere,[20–22,87] alkynes are precursors of ketenimine or alkynone when reacted with sulfonyl azides and acyl chloride, respectively. These intermediates are subsequently reacted with various nucleophiles to afford a wide diversity of chemical structures that can be incorporated in a polymer.

2.3.a. A^3-coupling

Discovered in 2002, the A^3-coupling three-component reaction (A-3CR) was reported as a very efficient green synthesis of propargyl amines *via* the C-H activation of a terminal alkyne with a Cu-Ru catalyst.[88] The accepted mechanism involves the formation of an imine or an iminium depending on the substitution of the amine. The metal activates the alkyne through the formation of a metal acetylide and promotes the nucleophilic addition onto the imine (or iminium) with water as the sole byproduct (Figure 12). Note that for primary amines, a subsequent A-3CR could occur on the newly formed secondary amines depending on its bulkiness. Various transition metals were tested for this reaction extending the scope of reagents to aromatic or aliphatic compounds. Amongst them, indium chloride ($InCl_3$) was reported as a highly efficient catalyst to promote the reaction of aromatic aldehydes and alkynes with aliphatic secondary amines, especially dibenzylamine.[89]

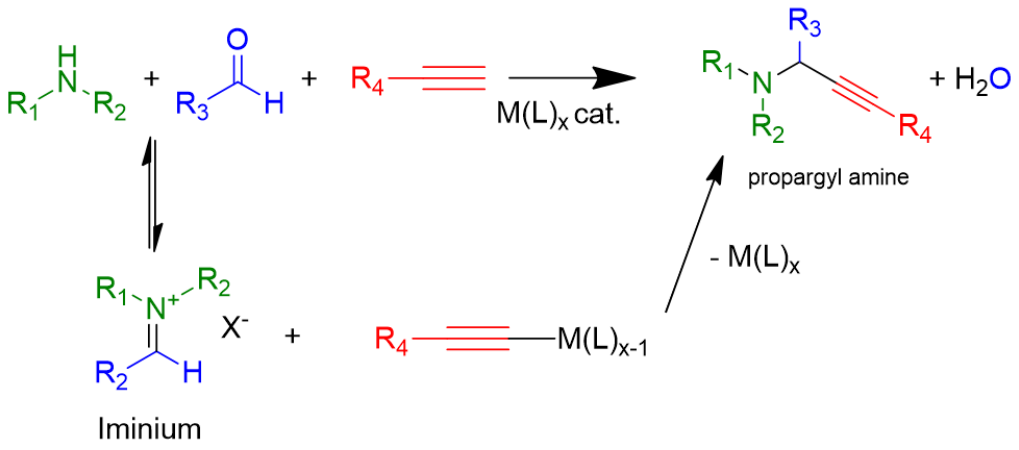

Figure 12. A^3-coupling three-component reaction and plausible mechanism.

Based on this research, Tang *et al*. have developed the A^3-coupling three-center three-component polymerization (A-3C-3CP) using dibenzylamine, terephthalaldehyde and a series of aromatic diynes (Figure 13, Tang 2013).[90] The optimized polymerizations were carried out in o-xylene at 140 °C for 20 hours under inert atmosphere. Molecular sieves were used to trap water and displace the reaction towards the product. Polymers with M_n up to 16 kg/mol were prepared accordingly. They showed a high refractive index due to the presence of polarizable aromatic rings, acetylene units and heteroatoms making them potential candidates for photonic applications (wavelength guide, lenses, etc.).[90] In addition, these polymers readily coordinated cobalt *via* their triple bonds and a subsequent pyrolysis led to nanostructured magnetic ceramics.[90] Eventually, the polymers synthesized with tetraphenylethene (TPE) or silole-containing monomers (Figure 13, Tang 2013) exhibited relatively high fluorescence quantum yields in the aggregate state due to aggregation-induced emission phenomenon (AIE).[90]

The same A-3C-3CP was applied with fluorene-like dialdehyde and diynes with dibenzylamine (Figure 13, Cao 2017) but only oligomers were obtained accordingly.[91] This issue was tackled by using microwaves that ultimately afforded high molecular weights and shorter reaction times (around 1 hour). All the polymers were photoluminescent and the soluble ones were used as cathode interlayers for solar cells improving their efficiency.[91]

Interestingly, primary amines were also used as difunctional monomers in the A-3C-3CP process in combination with diynes and monofunctional aldehydes (Figure 13, Tang 2014).[92] Although, copper iodide was reported as a good catalyst with primary amine,[93] the degrees of polymerization were significantly lower than those achieved through the A-3C-3CPs involving secondary amines. Indeed, moderate to low yields and molecular weights were obtained except for a few polymers exhibiting M_n above 5 kg/mol.[92] The polymers containing a TPE or a silole structure were photoluminescent upon aggregation and their potential for photopatterning was demonstrated. Furthermore, they were used as highly sensitive chemo sensors for detecting explosives, especially picric acid that quenched the fluorescence.[92]

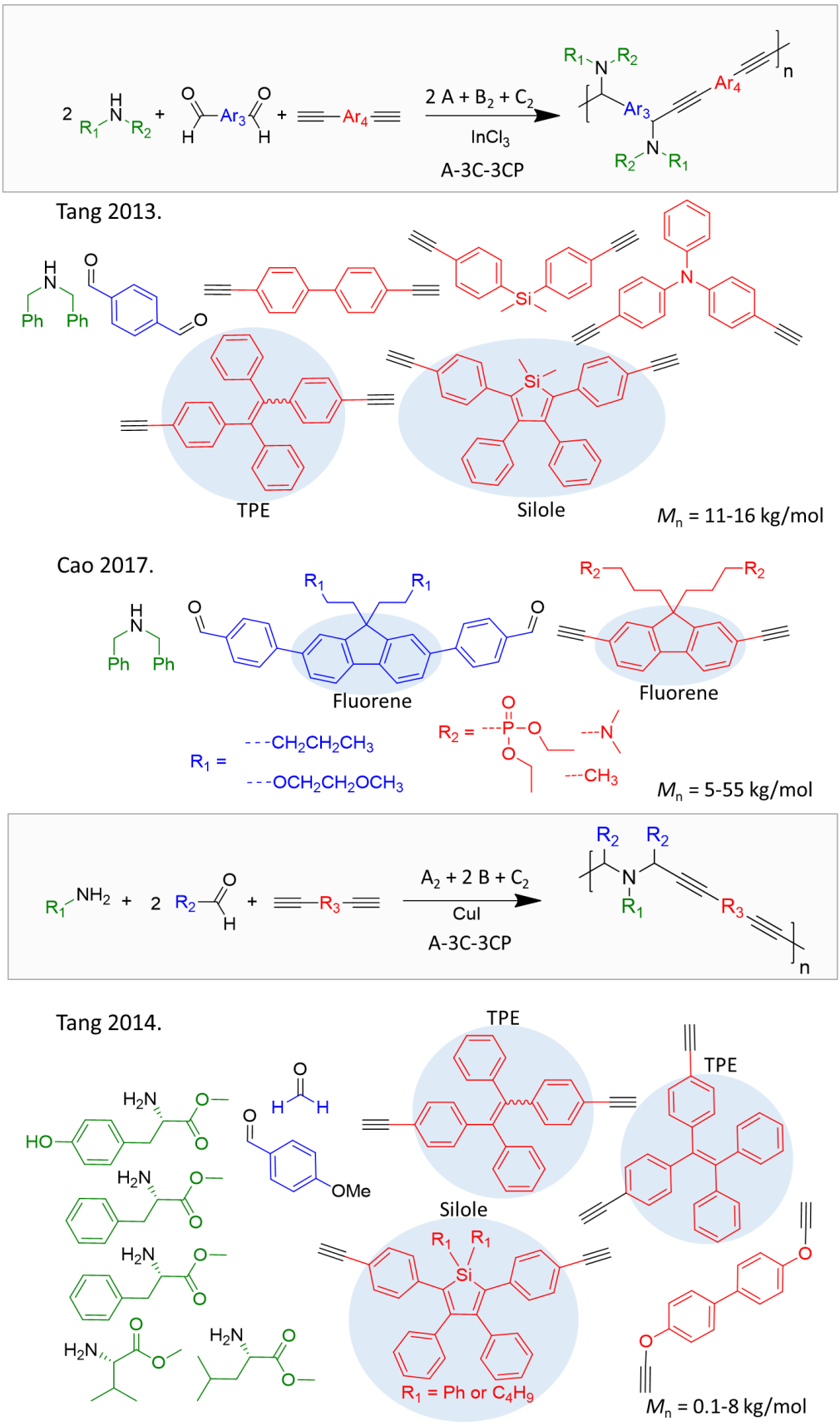

Figure 13. A^3-coupling three-component polymerization with primary and secondary amines. The highlighted monomers correspond to the photoluminescent moieties.

2.3.b. A^3-coupling/Petasis

The A^3-coupling and the Petasis-Borono Mannich reactions are very complementary MCRs. Indeed, in the Petasis-Borono Mannich reaction, a primary amine (or a secondary amine) is condensed with an aldehyde and the resulting imine or iminium further reacts with boronic acid derivative to yield a secondary (or tertiary) amine. When a secondary amine is formed, the latter can be further used in a A^3-coupling reaction (Figure 14).[94] Additionally, to avoid the use of metal catalyst, a decarboxylative version of the A^3-coupling[95] has been successfully combined with the Petasis reaction (Figure 14).[96]

Very recently, this combination of MCRs was exploited for the synthesis of functional poly(propargylamine)s (Figure 14).[97] The A^3-coupling-Petasis five-center four-component polymerization (AP-5C-4CP) was carried out without catalyst under mild conditions (45°C) in dichloroethane for 10 hours. Formaldehyde and aromatic alkynyl carboxylic acids were used as monofunctional reagents whereas dibenzylamines and diboronic acids compounds containing aromatic fluorene or TPE served as difunctional monomers (Figure 14). Polymers with molar masses as high as 12 kg/mol were collected with good yields. Dispersities (Đ ~ 1.02-1.22) were surprisingly low for a polycondensation process but this point was not discussed by the authors. While the fluorene-based polymers did not show photoluminescence in solution, the polymers containing the TPE moieties exhibited a high quantum yield due to aggregation-emission properties. Moreover, the photoluminescence was enhanced upon addition of citric acid.[97] This phenomenon was attributed either to the protonation of the amines or a further ionic crosslinking that induced aggregations.

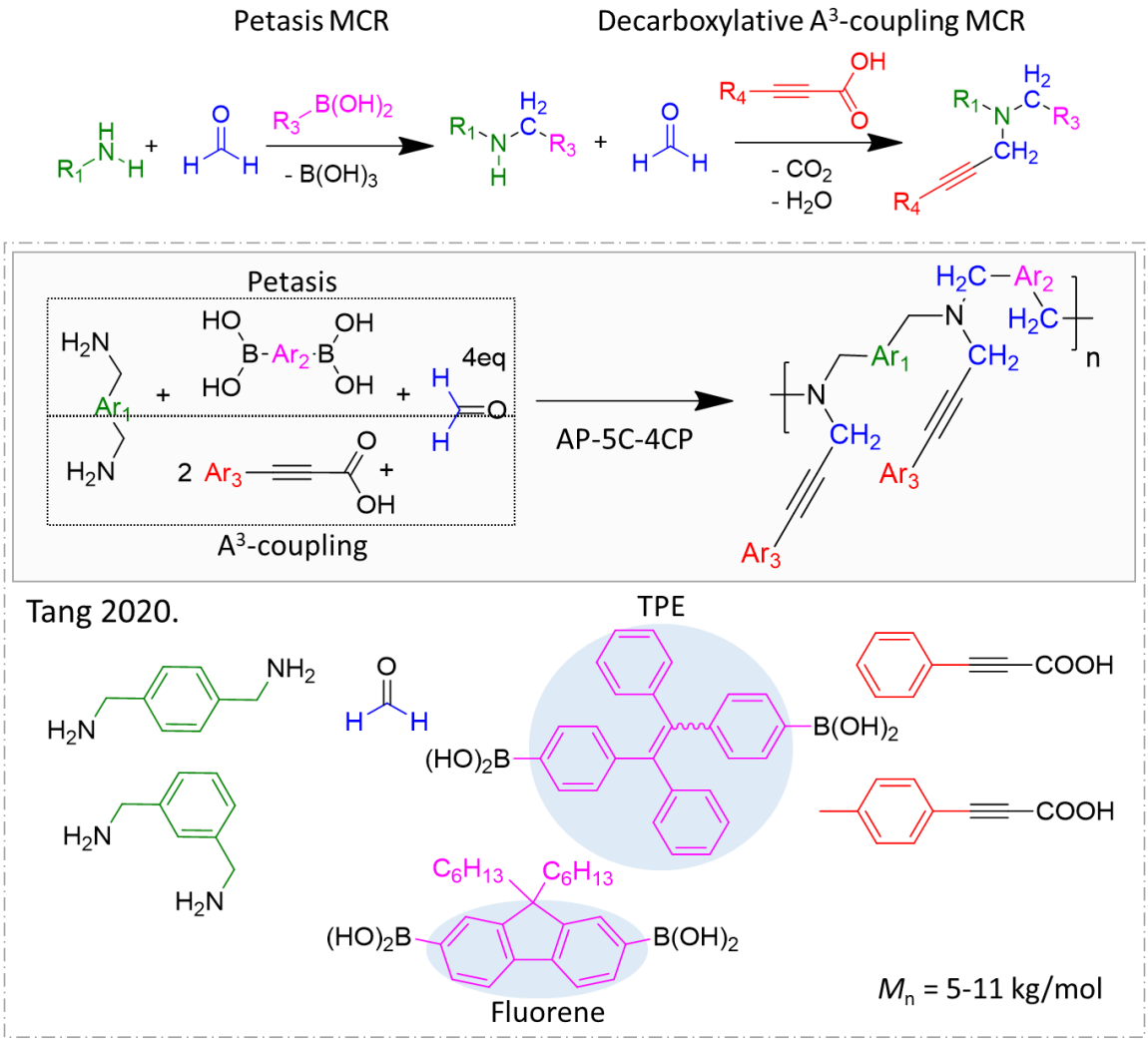

Figure 14. A^3-coupling / Petasis five-center four-component reaction and polymerization. The highlighted monomers correspond to the photoluminescent moieties.

2.3.c A^3-coupling/cycloisomerization/oxidation

Concomitantly to the discovery of the A^3-coupling, it was found that the reaction of aniline derivatives with aldehydes and alkynes in the presence of copper chloride as catalyst produced propargylic amine but also quinoline as side-product (Figure 15).[98] Depending on the substitution of both the aniline and the alkyne, it was possible to favour one product over another. From a mechanistic point of view, the propargylic amine obtained by the A^3-coupling is converted into quinoline *via* subsequent cyclisation and oxidation reactions (ACO-3C-3CR; Figure 15). Since then, the reaction conditions have been optimized to favour the formation of quinoline, *i.e.* up to 90 % when $B(C_6F_5)_3$ was used as the catalyst.[99]

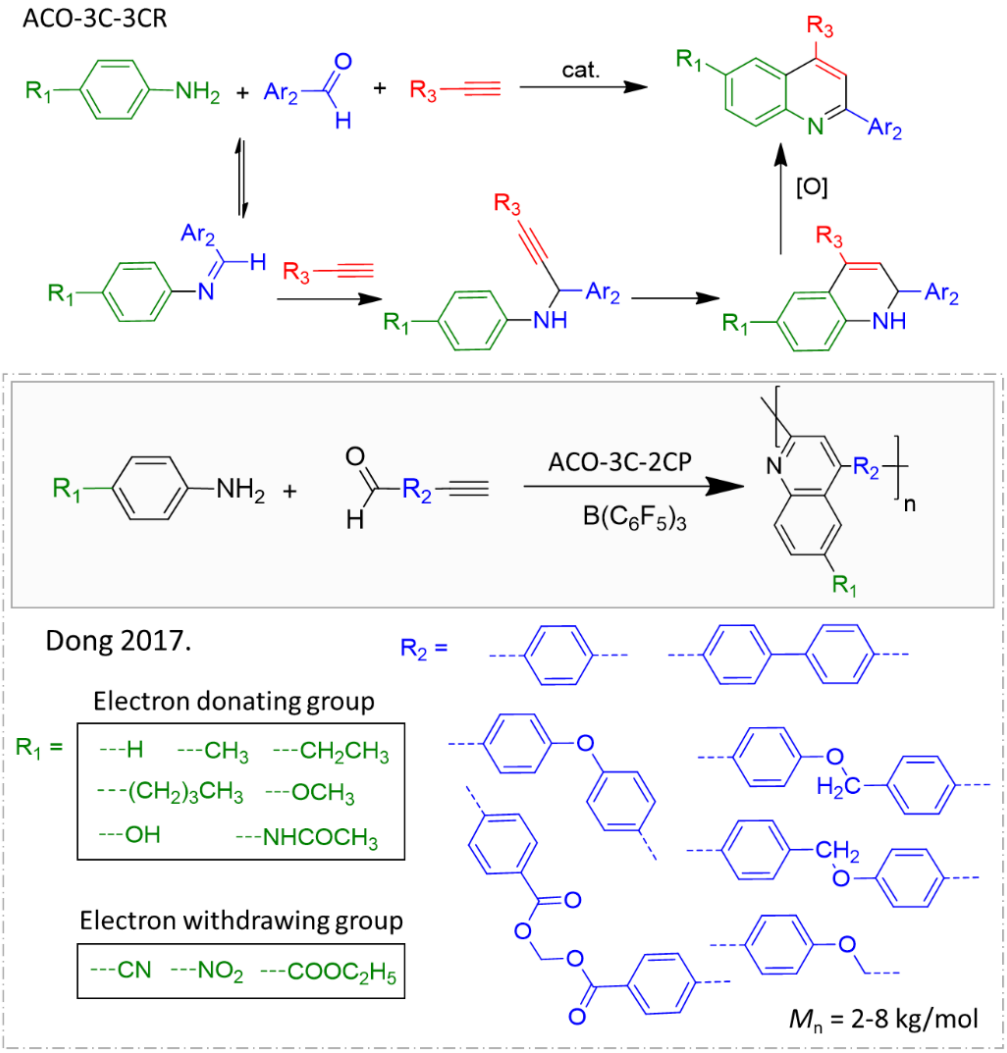

Figure 15. A^3-coupling/cycloisomerization/oxidation multicomponent reaction and polymerization and the substrate scope.

Inspired by these results, Dong *et al* reported an efficient synthesis of poly(quinoline)s *via* the ACO-3C-2CP polymerization of aniline derivatives with monomers bearing both the aldehyde and the alkyne (Figure 15).[100] In brief, different substituted anilines were reacted with various alkyne−aldehyde monomers. It turned out that using aniline compounds with electron-withdrawing groups was detrimental for the polymerization and the yield. Concerning the alkyne−aldehyde monomer, both functions needed to be directly attached to an aromatic ring or no polymer was observed. High yields were obtained when electron-donating groups, such as ether, separate the phenyl rings bearing the functions (Figure 15). The quinoline moiety endowed the resulting polymers with photoluminescence in solution but the phenomenon was quenched upon aggregation.[100]

2.3.d Acetylenedicarboxylate-based consecutive MCP

Imines are well-known precursors of nitrogen heterocyclic rings. When they are combined with acetylenedicarboxylate, they efficiently lead to hydrogenated derivatives of pyrimidine and pyrrole depending on the conditions used (Figure 16).[101,102] Briefly, one equivalent of aniline is reacted with the activated internal alkyne through hydroamination and another equivalent combines with formaldehyde to yield the corresponding imine. These two products react together to form a five-membered ring dihydropyrrole when heated[101] (D-4C-3CR) but it can also produce a six-membered ring tetrahydropyrimidine when a second equivalent of formaldehyde is present under milder conditions (T-5C-3CR) (Figure 16).[102]

Few years ago, inspired by this chemistry, Tang and coworkers presented an efficient multicomponent polymerization leading to polyheterocycles.[103] The polymerization was conducted with various aromatic diamines, formaldehyde and two different acetylenedicarboxylates in methanol. When the polymerizations were carried out with an excess of formaldehyde, pure poly(tetrahydropyrimidine)s were obtained (Figure 16, strategy 1) whereas a stoichiometric amount of formaldehyde led to copolymers of tetrahydropyrimidine and dihydropyrrole (Figure 16, strategy 3).[103] The content of tetrahydropyrimidine in the copolymer could be varied from 100 to 8 %. Note that the process used was not strictly speaking a domino reaction like the MCPs discussed above. In other words, the overall reaction occurred *via* consecutive steps. The first steps consisted of the reaction of one equivalent of amine with the alkyne during 30 minutes at 25 °C. Next, formaldehyde was added in the mixture as well as acetic acid as catalyst and the reaction was proceeded for 16 hours. The temperature stayed unchanged when pure poly(tetrahydropyrimidine)s were aimed and changed to 70 °C for copolymers. Interestingly, this consecutive approach enables the preparation of sequence-controlled polymers. Indeed, alternating poly(tetrahydropyrimidine)s were formed by the reaction ofacetylenedicarboxylate with 0.5 equivalent of a first diamine followed by the reaction with a second diamine (0.5 equiv.) in the presence of formaldehyde and acetic acid (Figure 16, strategy 2).[103] Concerning the monomers reactivity, acetylenedicarboxylate with methyl substituent (R_2) led to oligomers (M_n = 2.5 kg/mol) because of the poor solubility of the corresponding polymer in methanol. Replacing the methyl group by the more polar 2-(2-methoxyethoxy)ethyl increased the M_n up to 30 kg/mol.[103] Moreover, the electron-rich aromatic diamines were more efficient than electron-deficient aromatic diamines or diamines with high steric hindrance.[103] These observations were rationalized by authors based on a reactivity difference in the hydroamination reaction and Schiff base formation. The

poly(tetrahydropyrimidine)s (co)polymers showed photoluminescence provided by the newly formed heterocycles as well as aggregation-induced emission properties.[103]

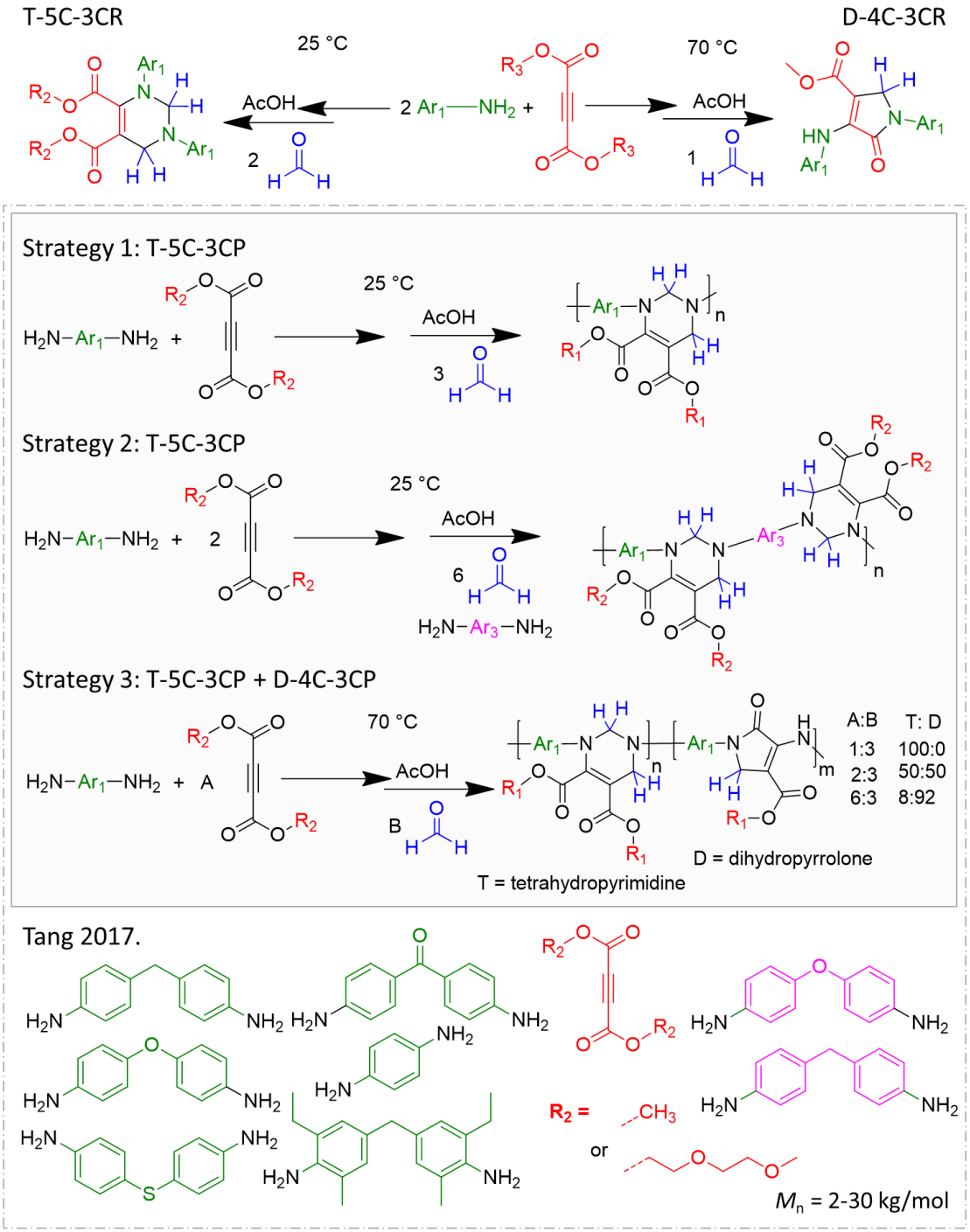

Figure 16. MCR and MCP toward substituted tetrahydropyrimidines (T-5C-3CR/P) and dihydropyrroles (D-4C-3CR/P) and the corresponding polymers.

I.2.4. Sulfur-based MCP

Sulfur appears in many different functional groups making its chemistry incredibly versatile. Moreover, sulfur-containing polymers are attractive materials exhibiting various properties. They are used as stimuli-responsive polymers, for metal coordination, in applications requiring high refractive indexes or semiconducting properties as well as lithium-sulfur batteries, to name a few.[104–106] This section highlights the synthesis of sulfur-containing polymers *via* MCPs using sulfur atoms under the form of elemental sulfur or thiol in combination with an aldhehyde/amine condensation.

2.4.a. Willgerodt-Kindler

Elemental sulfur is one of the most abundant elements on Earth and represents a huge byproduct of petroleum industry. Except for sulfuric acid production, other routes for its valorisation have been unsuccessful due to elevated costs of production and operating issues.[105] Consuming the amounts of produced elemental sulfur thus requires the development of high value materials with facile production methods. It can be converted into high sulfur-content polymers with valuable properties.[105] Several MCPs valorising the elemental sulfur enable the synthesis of poly(thiourea)s,[107] poly(O-thiocarbamate)s[108] and poly(thioamide)s.[109] The latter can be obtained *via* the Willgerodt-Kindler three-center three component reaction (WK-3C-3CR). This reaction involves an aromatic aldehyde with an aliphatic amine and elemental sulfur. The reaction mechanism is still under debate but the first step is widely accepted as the cleavage of the octasulfur ring by the amine with the reversible formation polysulfide anions. This intermediate product then reacts onto the imine formed by condensation of the aldehyde and the amine to yield a thioamide (Figure 17).[110] It should be noted that the third component of the Willgerodt-Kindler reaction, namely the elemental sulfur, cannot be varied which somewhat reduces the combinatorial character of this MCR to a classical two-component reaction although complex structures can be achieved.

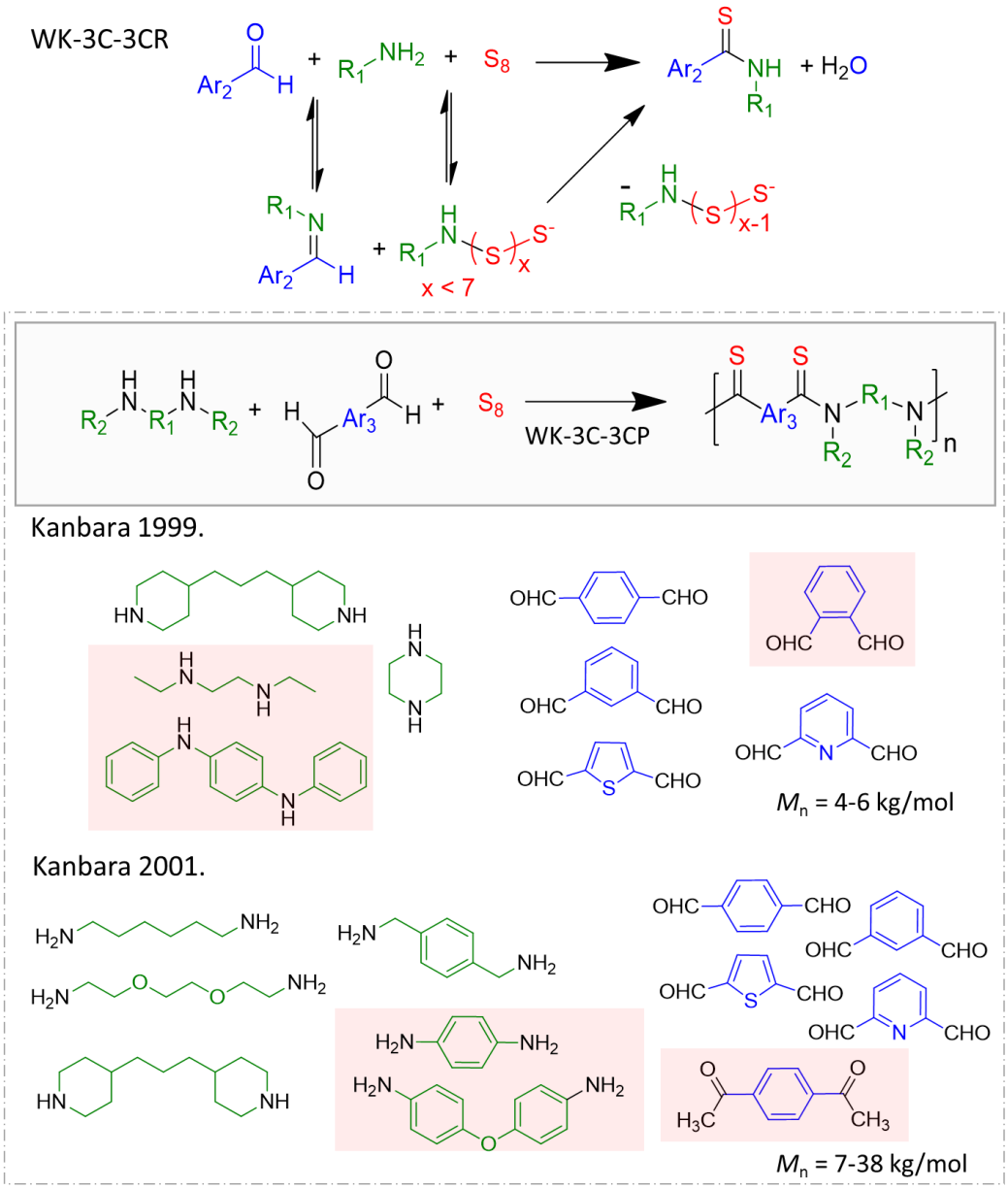

Figure 17. Willgerodt-Kindler multicomponent reaction and polymerization. The monomers highlighted in red failed to give polymers.

The Willgerodt-Kindler reaction was adapted to MCP by the group of Kanbara who identified conditions for the polymerization of various aromatic dialdehydes with aliphatic and aromatic secondary diamines in the presence of elemental sulfur S_8.[111] They used *N*,*N*-dimethylacetamide (DMAc) as solvent, a temperature of 115 °C and performed the polymerization under inert atmosphere with an excess of sulfur. Three isomers of phthalaldehyde were notably considered with 4,4'-trimethylenedipiperidine and S_8 (Figure 17, Kanbara 1999). M_n around 6 Kg/mol and yields above 90% were obtained with *para* and *meta*-isomers contrary to the *ortho*-isomer that failed to produce polymers due to steric hindrance. Heteroaromatic dialdehydes were also tested. For example, electron-poor aromatic dialdehydes

such as 2,6-pyridinedicarbaldehyde led to polymers with similar M_n (~6 kg/mol) and good yields while both lower yield and M_n (4 kg/mol) were obtained with the electron-rich thiophene dicarbaldehyde.[111] Concerning the diamine monomers, the polycondensation of *m*-phthalaldehyde with piperazine afforded insoluble polymer presumably due to its rigid backbone while acyclic and aromatic secondary diamines (*N,N'*-diethylethylenediamine and *N,N'*-diphenyl-p-phenylenediamine) did not lead to the formation of polymer materials (Figure 17, Kanbara 1999).[111] The same group extended the scope of diamines to aliphatic primary amines such as *p*-xylylenediamine, 1,6-hexamethylenediamine and 2,2'-(ethylenedioxy)bis(ethylamine) (Figure 17, Kanbara 2001).[110] In that work, they obtained higher molar masses (>19 kg/mol) and improved the polymerization conditions, notably by changing the order of monomers addition.[111] In the original procedure, the aldehyde and the amine were reacted together to form the Schiff base before addition of the sulfur. However, the limited solubility of some Schiff bases led to the precipitation of poly(Schiff base-thioamide) copolymers. In order to avoid these solubility issues, aldehyde was added as the last component affording pure poly(thioamide)s in better yields. [111] The poor solubility of some Schiff bases also explained the impossibility to use aromatic diamines even with the modified approach. [110] Eventually, the poly(thioamide)s demonstrated their ability to recover valuable metals like gold and platinum from aqueous and organic solutions.[112] Interestingly, the selectivity towards the different metals could be tuned with respect to the pH of the solution.[112] Selective separation of palladium from solution containing nickel and platinum was done based on the same principle.[113] Finally, quantitative removal of mercury was achieved in wastewater with pH ranging from 1 to 8.[114] The strong affinity of poly(thioamide)s for Hg allowed its selective removal from water contaminated with Mn(II), Fe(III), Cu(II), Zn(II), and Pb(II).[114]

2.4.b. MALI

As mentioned earlier, the imine is a precursor of several heterocycles *via* MCRs. Among them, the mercaptoacetic acid locking imine (MALI) reaction affords the formation of 4-thiazolidinone, a compound of interest in the biological and medical fields.[115] In this catalyst-free MALI three-center three-component reaction (M-3C-3CR), a primary amine and an aromatic aldehyde are condensed into the corresponding Schiff base that undergoes a nucleophilic attack from the thiol function of mercaptoacetic acid (or derivative). The resulting intermediate then generates the 4-thiazolidinone group by subsequent cyclization *via* the addition of the amine onto the carboxylic acid (Figure 18). The reaction is accelerated by addition of a desiccant or a molecular sieve that removes the produced water.[116]

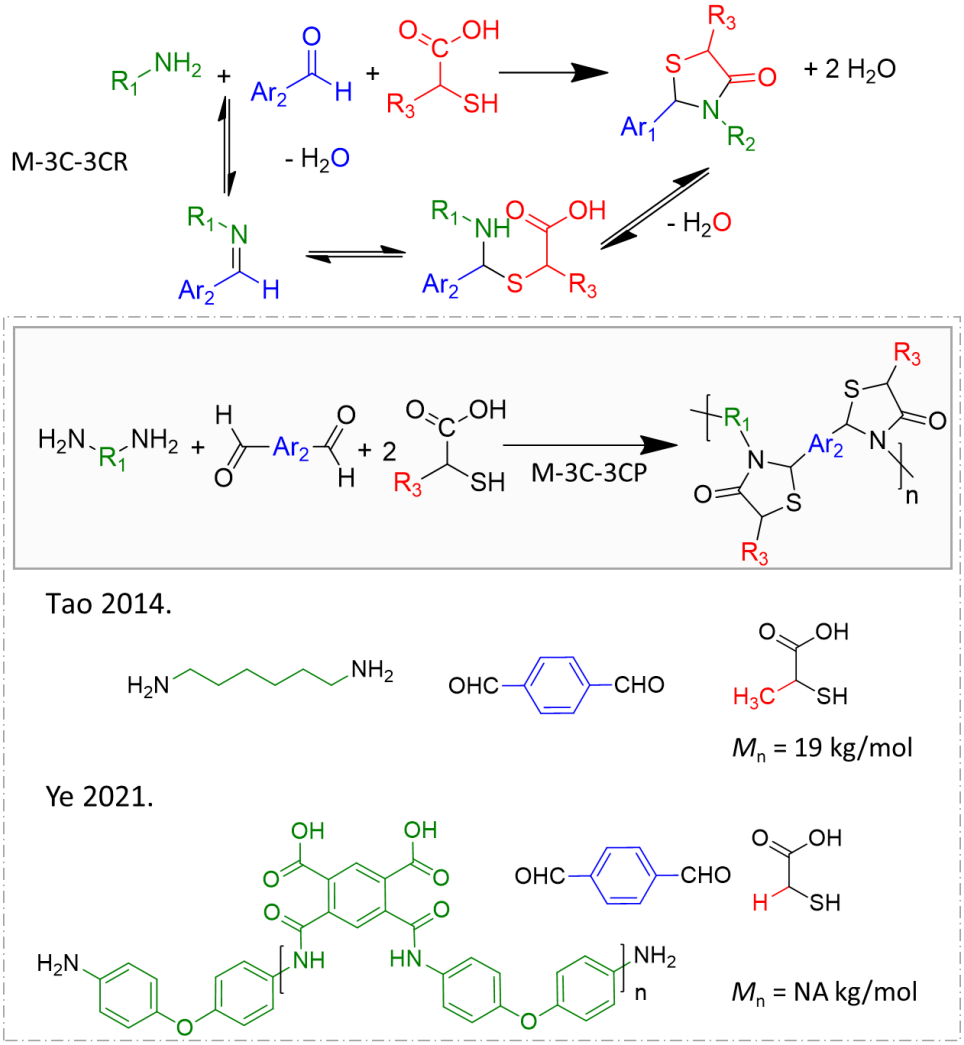

Figure 18. Mercaptoacetic acid locking imine multicomponent reaction and polymerization. NA stands for not available.

MALI three-center three-component (M-3C-3CP) polymerization was introduced by Tao and coworkers.[116] They performed direct polymerization of hexamethylenediamine, terephthalaldehyde with an excess of 2-mercaptopropionic acid under mild conditions (room temperature and catalyst-free) for two days leading to complete conversion and polymers with high molar masses (19 kg/mol) (Figure 18, Tao 2014).

Very recently, the M-3C-3CP was applied to a telechelic amine-terminated polyamide acid preformed *in situ* from pyromellitic dianhydride and an excess of 4,4'-oxydianiline (Figure 18, Ye 2021).[117] This reaction was conducted in *N*-methyl-2-pyrrolidone (NMP) in the presence of molecular sieve (4 A°) to capture the produced water. The polymerization was followed by annealing at 400 °C to promote the ring closure and, ultimately, the formation of the corresponding poly(imide-thiazolidinone)s. The latter exhibited exceptional thermal stability with degradation temperature close to 600 °C. In addition, they were casted onto a glass plate as uniform films and showed good adhesion properties with copper, aluminium and stainless-steel plates.[117] Note that the MALI reaction was also used for the modification of pre-formed polymers[118,119] or in combination with radical polymerization.[120–122] However, we found no example of direct MALI polymerization for the synthesis of networks or hyperbranched polymers. The sole example of 3D structures synthesized by MALI concerns photoluminescent nanoparticles obtained by crosslinking of pre-existing polymer chains.[123,124]

I.2.5. Dione-based MCP

2.5.a. Biginelli

The Biginelli three-component reaction was discovered by Pietro Biginelli in 1891.[125] Unlike the above-mentioned MCRs, it does not involve an amine but urea (or thiourea). The reaction of the latter with an aldehyde and a 1,3-dicarbonyl compound gives access to pyrimidine derivatives, namely 3,4-dihydropyrimidin-2(1H)-ones (or thiones) often abbreviated DHPMs, that are of great interest in medicinal chemistry.[126] The generally accepted mechanism implies the formation of an iminium by addition of urea onto the aldehyde (Figure 19). This rate-determining step is catalysed by Brønsted acids and followed by a nucleophilic attack of the 1,3-dicarbonyl, generally an alkyl acetoacetate under its enol form. Finally, the nucleophilic attack of the second nitrogen of urea onto the carbonyl and dehydration leads to the final product (Figure 19).[127] This mechanism is supported both by experiments and theoretical calculations.[35] Note that the reaction can also be catalysed by Lewis acids but the mechanism becomes far more complex.[35] As illustrated by previous reviews,[128,129] the Biginelli MCR has been used for a few years in polymer chemistry. The following section consists of an update with a special focus on the Biginelli step-growth polymerization.

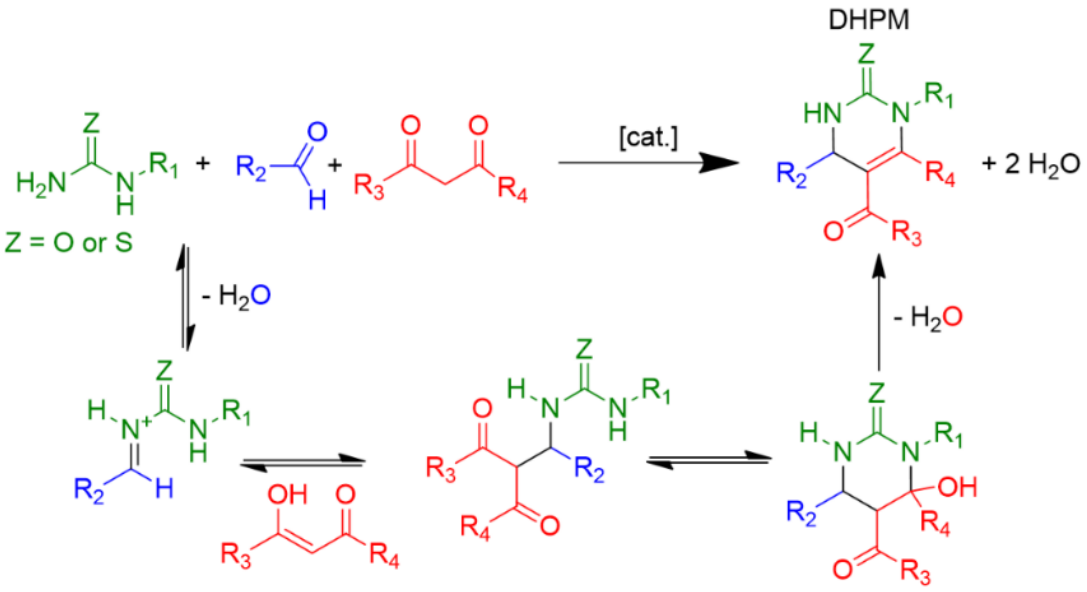

Figure 19. Biginelli three-component reaction and plausible mechanism.

The Biginelli three-center three-component polymerization (B-3C-3CP) of homo-functional monomers ($A_2 + B_2 + C$ system) was reported by Tao *et al.*[130] By reacting 8 different bis(β-keto ester) derivatives with 5 aromatic dialdehydes in the presence of urea or thiourea, they synthesized 80 novel polymers highlighting the combinatorial feature of MCPs (Figure 20, Tao 2016). The difunctional monomers differed by the length of the linker between their reactive groups. The bis(β-keto ester)s possessed alkyl linkers while the aromatic dialdehydes were separated by oligomers of PEG linkers (Figure 20, Tao 2016). Typical polymerizations were carried out using an excess of urea or thiourea components (1.5 equiv.) in acetic acid at 100 °C for 24 hours with 20 mol% of $MgCl_2$ as a Lewis acid catalyst. Poly(DHPM)s with molar masses ranging from 7 to 30 Kg/mol were obtained accordingly. The systematic variation of the linker allowed to tune the T_g of the polyDHPMs from 50 to 159 °C with small increments.[130] Interestingly, the poly(3,4-dihydropyrimidin-2(1H)-thiones) synthesized with thiourea instead of urea showed lower T_g. Finally, thiourea was successfully replaced by *N*-methylthiourea broadening the scope of this polymerization method (Figure 20, Tao 2016).[130]

In 2016, Meier and coworkers applied the B-3C-3CP to difunctional monomers that can be derived from renewable feedstock.[131] A series of bis-acetoacetate derivatives with saturated and unsaturated hydrocarbon linkers was prepared and reacted with aromatic dialdehydes such as terephthalaldehyde or divanillin in the presence of urea (Figure 20, Meier 2016). These polymerizations were performed under microwave and catalysed by a Brønsted acid, namely the *para*-toluenesulfonic acid, allowing a reaction time of maximum 4 hours. The obtained poly(DHPM)s had molar masses between 3 and 15 Kg/mol.[131] The T_g were quite high (141-203 °C) and tunable by varying the aliphatic chain length of the diacetoacetate monomer.[131]

Recently, the same group extended the scope of the polymerization and considered other renewable monomers. They notably polymerized terephthalaldehyde with a series of bis-acetoacetates and bis-acetoacetamides containing alkyl and isosorbide linkers in presence of urea and methyl-urea (Figure 20, Meier 2021). [132] Overall, M_n ranging from 4 to 15 Kg/mol and broad dispersities (2.8 to 4.2) were obtained especially with the isosorbide-based monomers (Đ up to 8.71). These results indicate aggregation issues presumably due to hydrogen bonding. Eventually, the polymers exhibited T_g from 160 to 308 °C.[132]

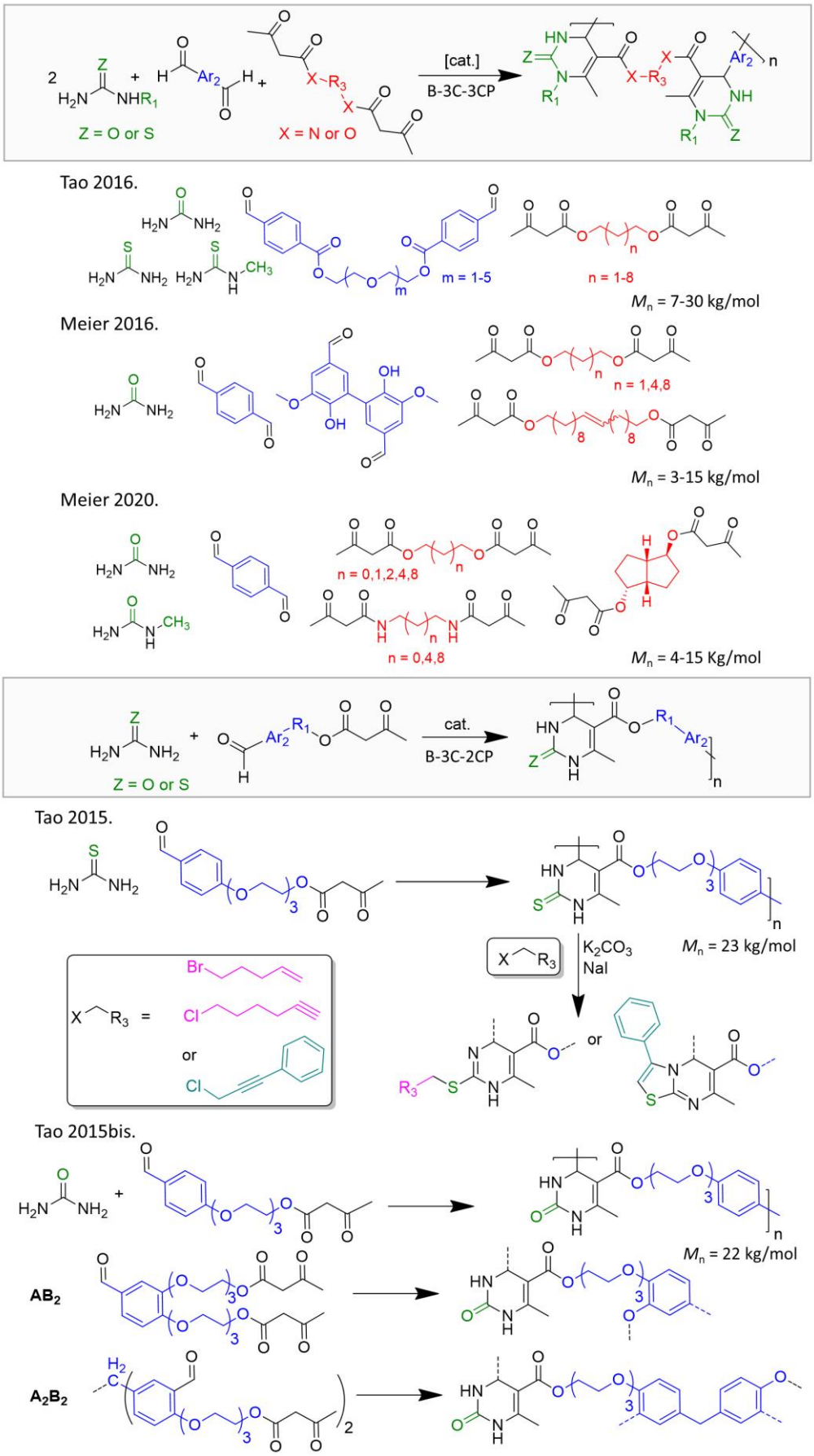

Figure 20. Biginelli multicomponent polymerization of homo (B-3C-3CP) and hetero-functional (B-3C-2CP) monomers toward linear and hyperbranched polymers and networks.

The Biginelli polycondensation of hetero-functional monomers was made possible by the synthesis of monomers containing benzaldehyde and β-keto ester groups. This "AB" monomer was reacted with thiourea through the Biginelli three-center two-component polymerization (B-3C-2CP) at 100 °C with an excess of thiourea (2 equiv.) in acetic acid with $MgCl_2$ as catalyst (Figure 20, Tao 2015).[133] Under these conditions, the reaction was fast and reached almost full conversion after 1 hour. Nevertheless, the reaction time was extended to 9 hours to afford the corresponding poly(dihydropyrimidin-2(1H)-thione) with M_n up to 23 kg/mol. Under basic conditions, the thiourea moiety could be tautomerized into the isothiourea which promoted nucleophilic substitution reactions and ultimately allowed the post-polymerization modifications with haloalkanes.[133] The modification was demonstrated with haloalkane bearing alkene as well as terminal or internal alkynes which served as functions for further modifications (Figure 20, Tao 2015).[133] The polymer properties such as glass transition temperatures and fluorescence were consequently modified.[133]

Tao's group also performed the B-3C-2CP with the same AB monomer using urea instead of thiourea.[134] A poly(dihydropyrimidin-2(1H)-one) with a molar mass of 22 kg/mol was obtained after 4 hours (Figure 20, Tao 2015bis).[134] The resulting poly(DHPM) exhibited interesting metal adhesive properties especially with brass. For the ease of the application, the polymerization of the AB monomer with urea was performed directly between the metal brass sheets without solvent and catalyst. After heating at 130 °C for 20 minutes, the tensile shear strength reached a plateau at 2.8 MPa.[134] Further improvement consisted of the synthesis of hyperbranched polymers and networks from AB_2 and A_2B_2 monomers which increased the tensile shear strength to 3.6 and 5.9 MPa, respectively (Figure 20, Tao 2015bis).[134] To the best of our knowledge, it is the sole example of direct Biginelli polycondensation leading to 3D structures.

2.5.b. Hantzsch

The original Hantzsch MCR consists of a four-center three-component reaction (H-4C-3CR) involving ammonia or ammonium salt, an aldehyde and two equivalents of a β-keto ester with water as the sole byproduct.[135] The Hantzsch adduct is a 1,4-dihydropyridine derivative well-known in pharmacology.[12] Another version, namely the Hantzsch four-center four-component reaction (H-4C-4CR), in which one equivalent of β-keto ester is replaced by the dimedone, leads to asymmetric 1,4-dihydropyridine (Figure 21).[136] H-3CR and H-4CR share one of the most complex mechanism amongst MCRs. As detailed elsewhere, the latter depends on several parameters like solvent, catalyst, substituent of the reagents, etc.[35] H-4CR has been used in

polymer chemistry for monomers synthesis, post-polymerization modifications and in one-pot combination with radical polymerization.[137138] Hereafter, we describe its use as direct polymerization tool.

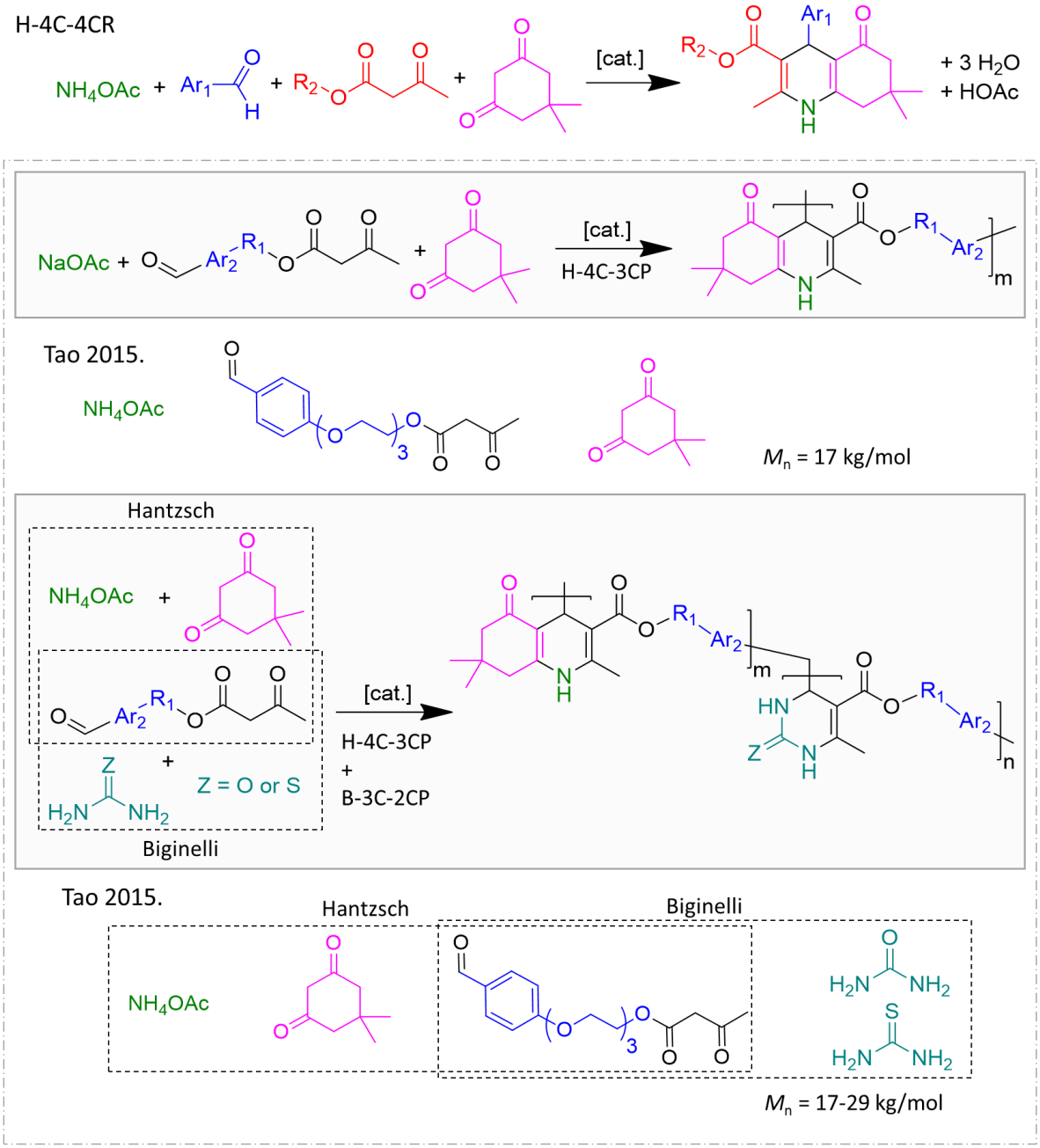

Figure 21. Hantzsch four-center four-component reaction and Hantzsch four-center three-component polymerization as well as its combination with Biginelli three-center two-component polymerization.

The sole example of synthesis of poly(1,4-dihydropyridine)s by Hantzsch polymerization was reported by Tao *et al.*[139] In this case, an AB monomer containing benzaldehyde and the β-keto ester group was polymerized with ammonium acetate and dimedone by Hantzsch four-center-three component polymerization (H-4C-3CP) (Figure 21). The H-4C-3CP was almost complete after 40 minutes in acetic acid at 100 °C with $MgCl_2$ as catalyst. Polycondensates with a molar mass of 17 kg/mol were obtained in these conditions.[139]

Because the Hantzsch and the Biginelli reactions share some common reagents, *i.e.* an aldehyde and a β-ketone ester, their corresponding MCPs, *i.e.* the H-4C-3CP and B-3C-2CP, were combined for the preparation of copolymers.[139] In practice, the AB monomer containing the benzaldehyde and the β-keto ester group was reacted with urea and NH_4OAc/dimedone yielding copolymers of 1,4-dihydropyridine (Hantzsch adduct) and dihydropyrimidin-2(1H)-one (Biginelli adduct) (Figure 21).[139] By varying the monofunctional monomers concentration, the ratio of Hantzsch/Biginelli adducts in the main chain was tuned.[139] In comparison to the comonomer feed, the copolymers were slightly enriched in the Hantzsch adduct probably due to the higher rate of the latter reaction compared to the Biginelli one in the selected copolymerization conditions. To extend the scope of polymers, urea was replaced with thiourea giving access to poly(1,4-dihydropyridine-*co*-dihydropyrimidin-2(1H)-thione)s.[139] Varying the Hantzsch/Biginelli adduct ratio in these copolymers allowed to tune their T_g (~ 80-105 °C) which increases with the content of the Biginelli adduct. [139]

Finally, no report was found in the literature concerning the synthesis of HBPs or networks *via* the Hantzsch polycondensation. Nonetheless, polymers and networks were respectively cross-linked[140] and modified[141] *via* Hantzsch reaction in order to endow them with fluorescent properties coming from the 1,4-dihydropyridine moiety.

2.5.c. Radziszewski

One of the oldest MCR is the Debus-Radziszewski reaction, so named in reference to its first two contributors. It is still nowadays the most employed method to synthesize imidazole compounds. This reaction was discovered by Debus in 1852 who reacted ammonia with glyoxal yielding the simplest imidazole named glyoxaline.[142] Later on, Radziszewski contributed to this field by adding an aldehyde (formaldehyde or substituted aldehyde) to glyoxal and ammonia in mild acidic conditions affording higher yields and broadening the scope of imidazole products.[143] He also extended the reaction to substituted 1,2-diketones affording 2,4,5-trisubstituted imidazoles (Figure 22, type I) for which harsher conditions were required.[144] The original Debus-Radziszewski reaction, often simply called the Radziszewski reaction, is a three-components reaction with four centers since it requires two equivalents of ammonia considered here as a single component (R-4C-3CR). More than 100 years later, Arduengo introduced a fourth component by replacing one equivalent of ammonia by a primary amine (Figure 22, type II).[145] The resulting Radziszewski four-center four-component reaction (R-4C-4CR) gives access to tetra-substituted imidazoles. In the last version of this reaction, ammonia is replaced by two equivalents of primary amine (Figure 22, type III).[146] This reaction, also known as the "modified Radziszewski" reaction, involved four centers and three components (MR-4C-3CR). The final product is not a neutral imidazole but an imidazolium salt which is of great interest in the field of ionic liquid (IL)[147] and medical science.[148] Very few articles deal with the mechanism of each type of Radziszewski reaction, possibly due to the complexity of the subject.[149] All we can say is that condensation reactions take place between the ammonia (or primary amine) and the carbonyl compounds, namely the 1,2-dicarbonyl and the aldehyde, and water is released as byproduct. Moreover, Radziszewski MCRs are generally carried out in acidic media and their driving force is the formation of an aromatic heterocycle. Under appropriate conditions, high conversion can be reached making these reactions interesting candidates for polymer synthesis. All the approaches, *i.e.* monomers synthesis, modification or crosslinking of preformed polymers and step-growth polymerization, have been reviewed by Dupuy and coworkers.[150] In the following section, we focus on the direct Radziszewski MCP and establish the state-of-the-art of this topic.

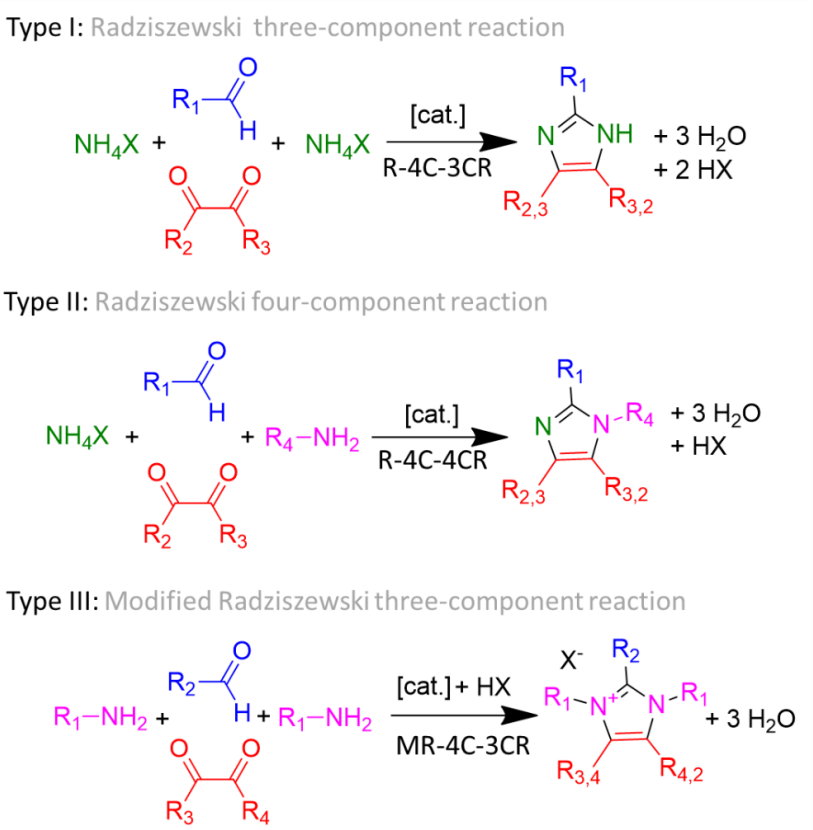

Figure 22: The different types of Radziszewski reactions toward imidazoles and imidazoliums.

The first attempt to synthesize poly(imidazole) *via* the Radziszewski type I reaction is one of the oldest examples of MCP and dates from 1967.[151] In this work, an aryl bis(1,2-diketone), named bisbenzyl, was reacted with various aromatic dialdehydes in the presence of ammonium acetate in acetic acid at the boil for 240 h under nitrogen (Figure 23, Manecke 1967). Only oligomers were collected accordingly, with great uncertainty on their molar masses measured by infrared spectroscopy (IR), but they showed good thermal and semi-conductive properties with low activation energy (below 1.12 eV).[151]

Forty years later, Mercier *et al*. enhanced the polymerization efficiency and extended its scope to various dialdehyde monomers (Figure 23, Mercier 2008).[152] The monomers were solubilized in acetic acid with additional NMP to ensure the polymer solubility during the polymerization. In addition, the authors used a ten-fold excess of ammonium acetate and irradiated the mixture for 15 minutes with microwaves in a high-pressure reactor. Only two polymers were sufficiently soluble in SEC solvent (DMF) to determine their molar masses of 10 and 17 kg/mol. All poly(arylimidazole)s exhibited high thermal stability with degradation temperatures above 400 °C and were casted into films after dissolution in NMP suggesting quite high molar masses.[152]

Finally, a poly(arylene-imidazole) was synthesized *via* the type I R-4C-3CP with the bisbenzyl and a hexamethyl-terphenyl dialdehyde as bifunctional monomers (Figure 23, Holdcroft

2017).[153] The authors performed the polymerization in conditions similar to those reported by Mercier[152] using microwaves to enhance the conversion and a ten-fold excess of ammonium acetate. The reaction mixture was heated at 120 °C for 35 minutes. The resulting polymer served as a precursor for high molar mass (50 kg/mol) poly(arylene-imidazolium) upon modification with iodomethane (Figure 23, Holdcroft 2017). The final product exhibited high performance as polyelectrolyte membrane for alkaline fuel-cells.[153] The steric hindrance around the C2-position, that is the carbon between the two nitrogen atoms, prevents its degradation in concentrated hydroxide solution which is usually a severe limitation for the use of poly(imidazolium)s in this application.[154]

So far, there is only one report on the Radziszewski type II polymerization in the litterature.[155] In this work, a series of tetrasubstituted poly(aryl imidazole)s was produced from various

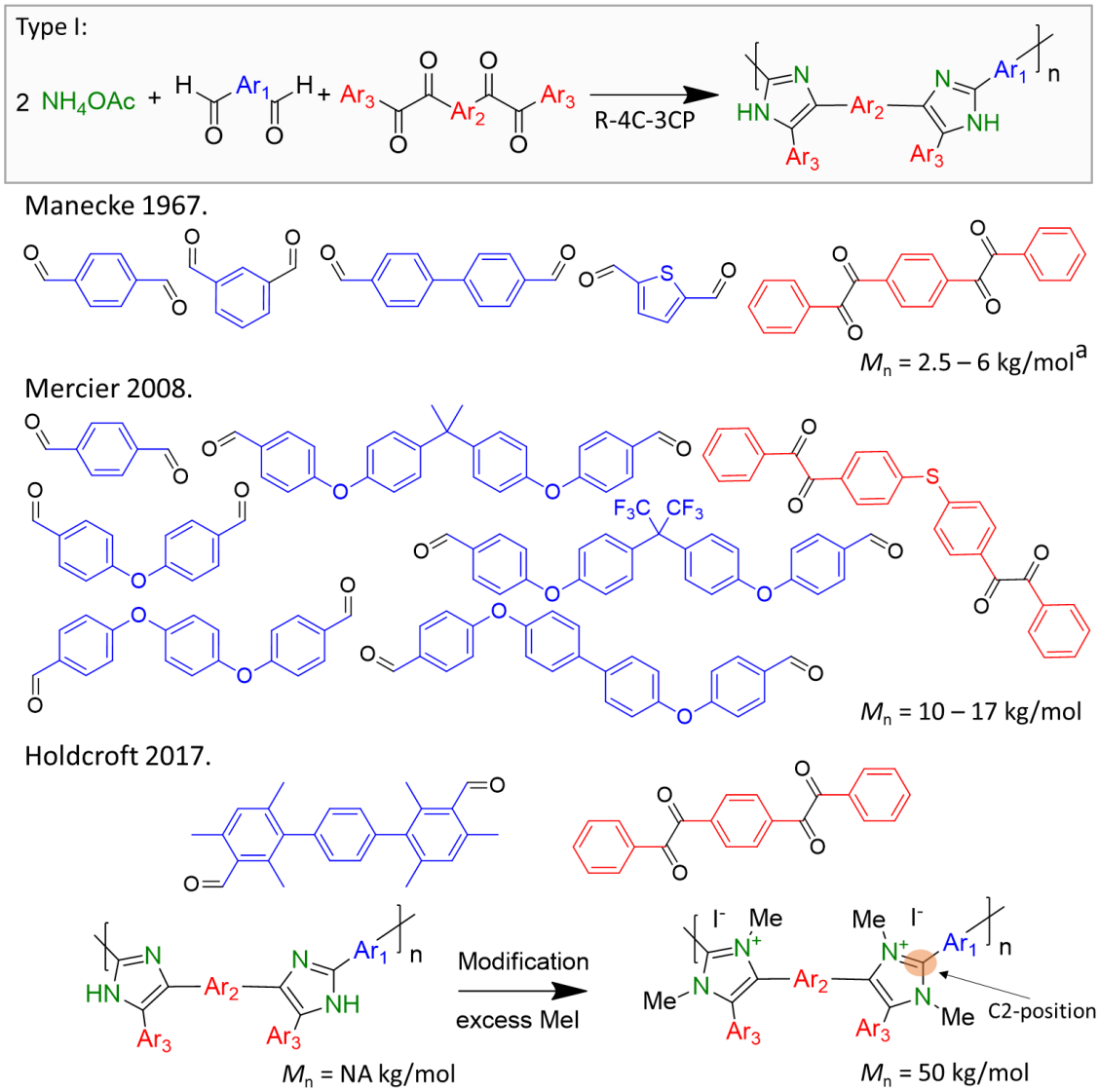

Figure 23. Substrates scope of Radziszewski type I polymerization toward poly(imidazole)s.

[a] Determined by infrared spectroscopy. NA stands for not available.

bis(aryl 1,2-diketone)s, bis(aryl aldehyde)s, mono-aryl amines and ammonium acetate (Figure 24). In addition to the use of microwave, an elevated temperature (140 °C) and a high pressure (25 bar), the reaction required a catalytic amount of trifluoroacetic acid. Poly(aryl imidazole)s with molar masses between 18 and 31 kg/mol were formed accordingly in quantitative yield. They showed very high degradation temperatures (up to 527 °C) and were soluble in common organic solvents (THF, NMP, DMSO, etc.) allowing their casting into films.

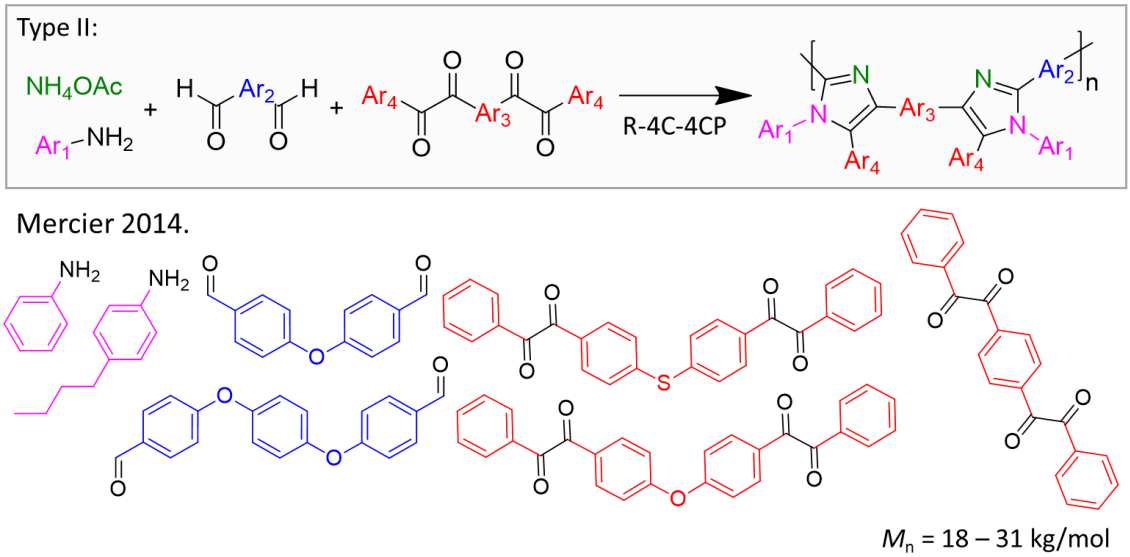

Figure 24. Substrates scope of Radziszewski type II polymerization toward tetrasubstituted poly(imidazole)s.

The modified Radziszewski type III polymerization (MR-4C-3CP) is by far the most common category of Radziszewski MCPs. Instead of neutral poly(imidazole)s, it gives access to poly(imidazolium)s, an important class of poly(ionic liquid)s (PILs). These materials combine some valuable features of ILs with the intrinsic characteristics of polymers and over the years became essential in many areas.[148,156,157] The type III is articulated around the amine component which constitutes the attachment points of the imidazolium moiety in the backbone. Replacing two equivalents of monofunctional amine by one equivalent of diamine allows the step-growth polymerization. In the following examples, diamines monomers are used in combination with mono-1,2-dicarbonyls and monoaldehydes. Unlike types I and II Radziszewski polymerizations, the carbonyl compounds involved in the type III MCP are almost not substituted such as formaldehyde and glyoxal (or sometimes pyruvaldehyde).

The MR-4C-3CP was first reported and patented by BASF in 2010[158] and further improved and applied by Lindner (from BASF) few years later.[159–163] These researches were summarized in his paper published in 2016.[164] First, he performed the polymerization of diaminobutane with glyoxal and formaldehyde in aqueous solution using acetic acid as catalyst (Figure 25, Lindner 2016).[164] In this case, the polymerization was highly accelerated at 100 °C compared to room

temperature which ultimately shortened the reaction time from 24 to 1 hour to reach the same molar mass. Under optimal conditions, including a slight excess of carbonyl compounds, a poly(imidazolium) acetate with a molar mass about 10 kg/mol was obtained.[164] Various aliphatic diamines were tested affording a series of polymers with T_g ranging from -52 to 48 °C depending on the flexibility of their backbone dictated by the diamine compound (Figure 25, Lindner 2016).[164]

Shortly later, Yuan *et al.* considered the same strategy to synthesize a series of poly(imidazolium)s from diamines with different aliphatic chains but they used the biomass-derived pyruvaldehyde (methylglyoxal) instead of glyoxal (Figure 25, Yuan 2017).[165] Polymers with M_n of 20 kg/mol were obtained which is higher than those reported by Lindner. The authors claimed for a better reactivity of methylglyoxal over glyoxal due to electron-donating character of the methyl group. They also successfully exchanged the acetate counterion for bis(trifluoromethane sulfonyl)imide anion (TFSI) in order to tune the polymer properties such as the solubility. Importantly, the polymerization was also successful with an aromatic diamine, namely the *para*-pheylenediamine, leading to poly(imidazolium acetate) with M_n of 20 kg/mol. The acetate counterion was then replaced by a nitrogen-rich dicyanamide followed by carbonization to afford micro/mesoporous nitrogen-doped carbon with almost 70 % of residual weight.[165] This sample was used for CO_2 capture and selective aerobic oxidation of benzyl alcohol.[166]

Interestingly, Qian and coworkers synthesized a poly(imidazolium chloride) from *para*-phenylenediamine, glyoxal and paraformaldehyde (polymeric form of formaldehyde). In addition, they replaced the acetic acid with hydrochloric acid (Figure 25, Qian 2018).[167] The polymerization was carried out in DMSO during 48 h and produced an insoluble powder. The poly(imidazolium chloride) was then converted into the corresponding *N*-heterocyclic carbene-Pd organometallic specie *via* deprotonation of the C2-carbon and subsequent addition of palladium salt. This complex was valued as a catalyst in the Suzuki-Miyaura reaction between various aryl bromides and phenylboronic acid.[167]

Eventually, a poly(imidazolium) prepared *via* MR-4C-3CR of hexamethylenediamine, glyoxal and formaldehyde was anchored onto cellulosic substrate (Figure 25, Lucena 2019).[168] The modified cellulose then served as sorptive phase for anti-inflammatory drugs microextraction form urines.[168]

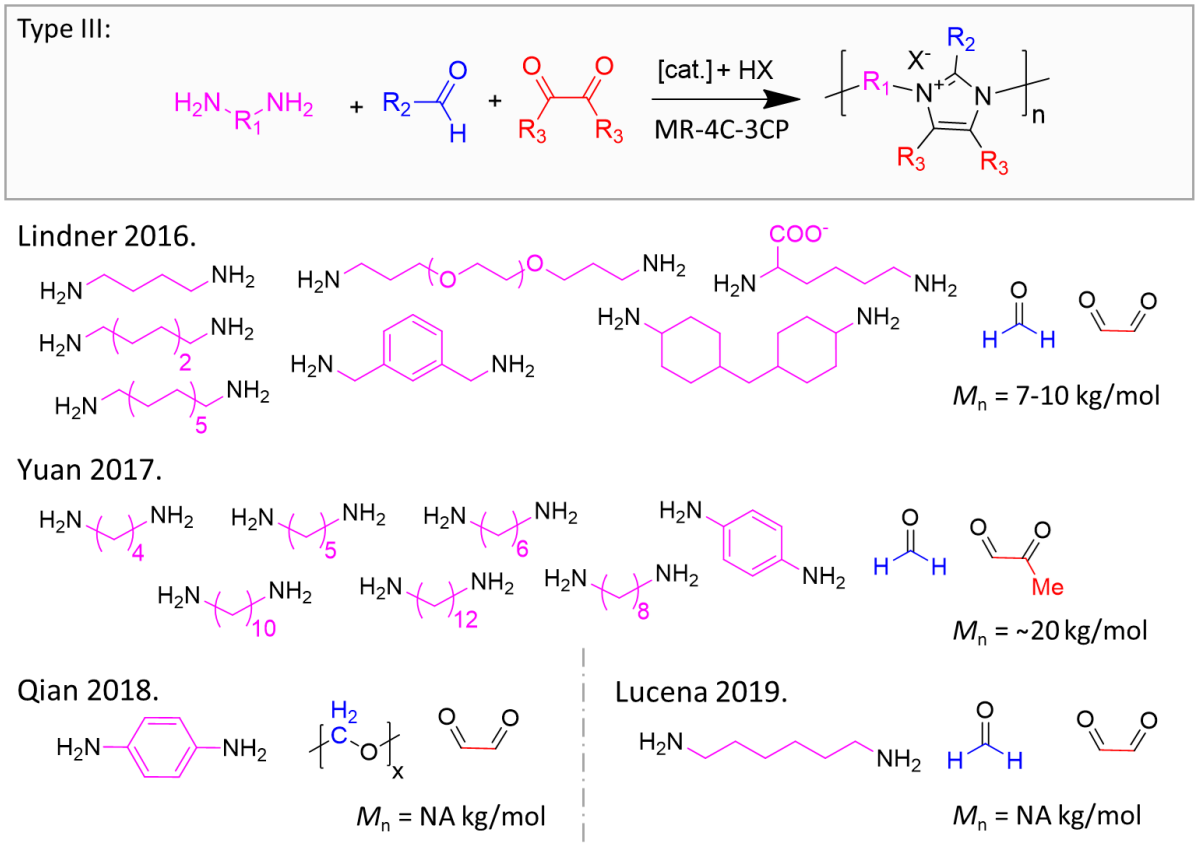

Figure 25. Substrates scope of the Radziszewski type III polymerization toward poly(imidazolium)s. NA stands for not available.

The linear poly(imidazolium)s prepared by MR-4C-3CP have raised peculiar interest for functional membranes synthesis. Due to their charged cationic structures, they can be further crosslinked by physical interactions. In addition, these polymers generally present amino end-groups, as a result of the diamine involved in their synthesis, which allows subsequent chemical crosslinking. Below, we describe the preparation of membranes based on poly(imidazolium)s synthesized *via* the Radziszewski reaction.

Yuan *et al.* prepared reprocessable porous membranes by mixing a poly(imidazolium)-TFSI made of glyoxal, formaldehyde and 1,4-diaminobutane with polyacrylic acid in aqueous ammonia (Figure 26, Yuan 2018).[169] The crosslinking was achieved by ionic interactions between the carboxylates and the imidazolium moieties. Interestingly, the pores size could be tuned by varying the molecular weight of the polyacrylic acid. Moreover, the ionic interactions being reversible, the membrane could be dissolved in LiTFSI solution and reprocessed at will by evaporation.[169]

Feng and coworkers combined imidazolium and siloxane groups into a polymer in one step by MR-4C-3P of 1,3-bis(3-aminopropyl)tetramethyldisiloxane, glyoxal and formaldehyde (Figure 26, Feng 2019).[170] Instead of using pure acetic acid as both the catalyst and the counterion

precursor, oxalic acid was added to promote an ionic crosslinking. The imidazolium moiety endowed the membrane with ionic conductivity while good healing ability was brought by the dynamic ionic crosslinking. Furthermore, the material emitted a yellow-green fluorescence under UV light and showed a stable and reversible stretching sensitivity (variation of the conductivity upon stretching).[170]

Next, Liu *et al.* synthesized a poly(imidazolium TFSI) by reacting 1,2-bis(2-aminoethoxy)ethane, glyoxal and formaldehyde with acetic acid followed by ions-exchange reaction (Figure 26, Liu 2020).[171] Porous membranes were prepared from poly(imidazolium TFSI) and poly(vinylidenefluoride-co-hexafluoropropylene) (PVDF-HFP) by phase inversion method. Physical crosslinking was assumed to occur through ion-dipole interactions between the imidazolium cations and the polar fluorine atoms from PVDF-HFP. The self-supported membrane exhibited good mechanical properties, high liquid-electrolytes uptake, fire-resistance and electrochemical stability making it a high-performance material for Li ion batteries.[171]

Meng's group synthesized poly(imidazolium)s with low and high molecular weights by performing the polymerization at room temperature or 100 °C, respectively. They used their terminal amine functions for further crosslinking reactions with multifunctional epoxides (Figure 26, Meng 2020).[172] A series of networks with different crosslinking densities were shaped into membranes that were tested in CO_2 capture and diffusivity. The solubility of CO_2 was further increased with addition of free ILs in the membrane. As a result, the behaviour of the membranes towards CO_2 could be precisely tuned by playing with the different parameters.[172]

As mentioned previously, except for pyruvaldehyde, the carbonyl compounds used in the MR-4C-3P are usually not substituted. The recent work from Yan *et al.* radically changed this limitation.[173] They synthesized a series of substituted poly(imidazolium)s using *L*-proline as a co-catalyst (Figure 26, Yan 2020), which was already known to efficiently promote the types I and II Radziszewski MCRs.[174] With the alkaline fuel-cell application in mind, the authors anticipated a beneficial effect of the imidazolium group substitution on its stability toward hydroxide-induced ring opening.[153175] In practice, these PILs were physically entangled in a crosslinked glutaraldehyde-poly(vinyl alcohol) network. All the membranes showed good

hydroxide ion conduction but, as expected, only the highly substituted ones retained stable conduction after 120 hours at 80 °C in concentrated alkaline solution.[173]

The MR-4C-3CR was also used to crosslink pre-formed polymers with pendant amine functions such as poly(L-Lysine)[176] and chitosan.[177,178] In addition to the proof of concept, the chitosan-imidazolium gel was used for dye removal.[177] At the frontier between the crosslinking of

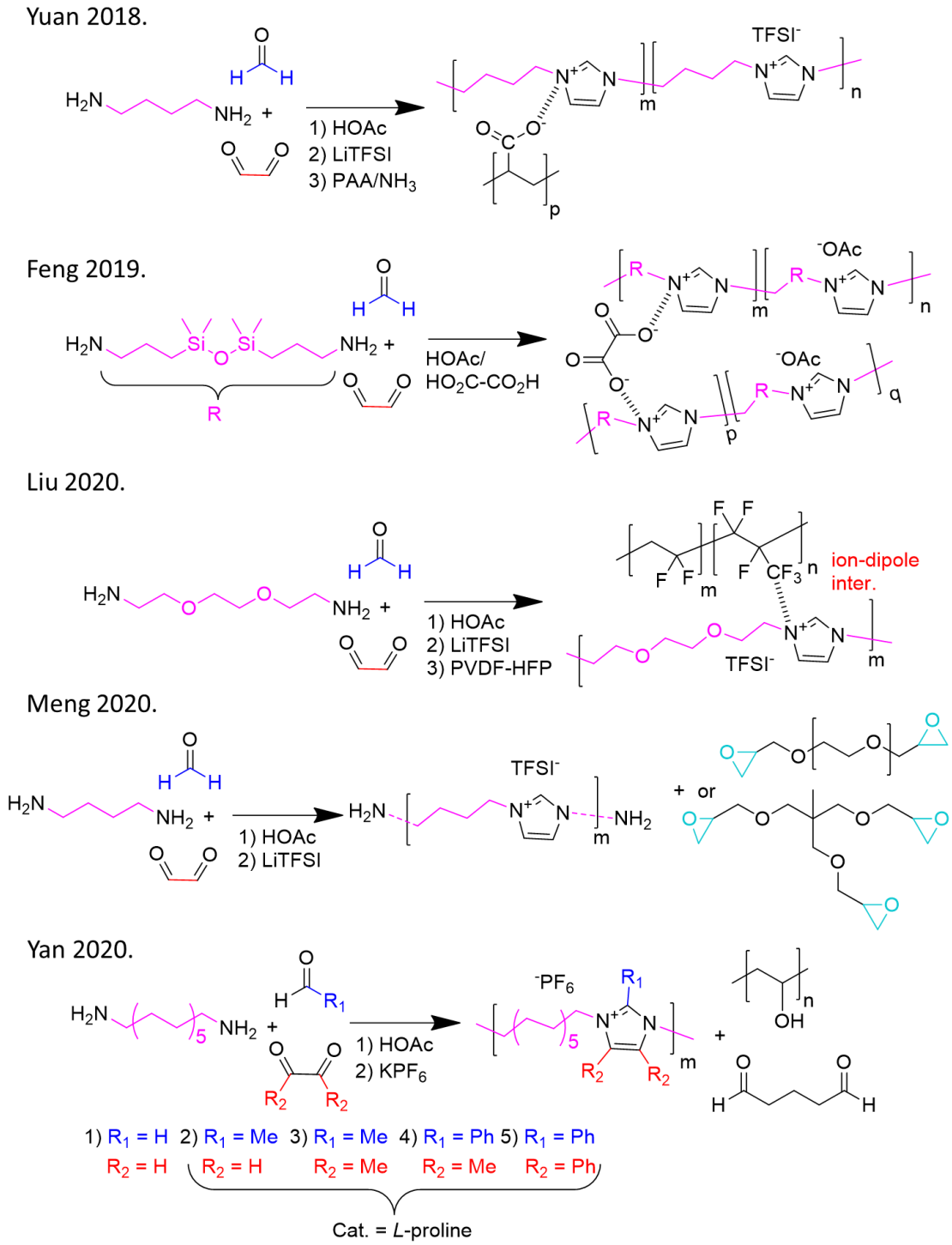

Figure 26. Membranes preparation using linear poly(imidazolium)s synthesized by the modified Radziszewski four-center three-component polymerization.

polymer chains and the polymerization of low molecular weight molecules bearing more than 2 amino groups, Song and coworkers applied the MR-4C-3CP to poly(amidoamine)s (PAMAM) dendrimers (Figure 27, Song 2017).[179] Different generations of PAMAM dendrimers (from 4 to 128 amines) were considered. The reaction was carried out in ionic liquid (1-ethyl-3-methylimidazolium acetate) using methylglyoxal and formaldehyde as monomers but without acetic acid which therefore led to poly(imidazolium) materials with hydroxide as the counterion. The resulting ionogels presented excellent ionic conductivity at room temperature and good mechanical properties.[179]

The MR-4C-3CP of hexamethylenediamine, glyoxal and formaldehyde, was also conducted in the presence of magnetic iron oxide nanoparticles (NPs) covered by amine functions which served as additional "multiamine" (Figure 27, Lucena 2017).[180] The resulting nanocomposite composed of poly(imidazolium) attached to magnetic NPs showed its potential for the removal of anionic drugs from aqueous solutions but also from bioanalytical samples such as saliva.[180]

In the last example, the MR-4C-3CP was applied to an aromatic tetraamine, the tetrakis(4-aminophenyl)methane, in combination with methylglyoxal and formaldehyde in acetic acid leading to a powdery network of imidazolium acetate (Figure 27, Bordiga 2017).[181] Several counterions exchanges were made to tune the properties of the materials and *tert*-butoxide was used to deprotonate the imidazolium yielding the neutral carbene. All these materials showed microporosity that comes from the sterically hindered amine monomer inducing empty spaces inside the networks. These materials demonstrated excellent behaviour in carbon dioxide adsorption.[181]

Although it does not match with our MCP definition, it is noteworthy to mention that imidazolium networks with CO_2 sorption ability were also produced *via* a pseudo-Radziszewski reaction carried out in a two-pot, two-step process with the synthesis of the imine-based network from tetraamine followed by its transformation into imidazolium.[182]

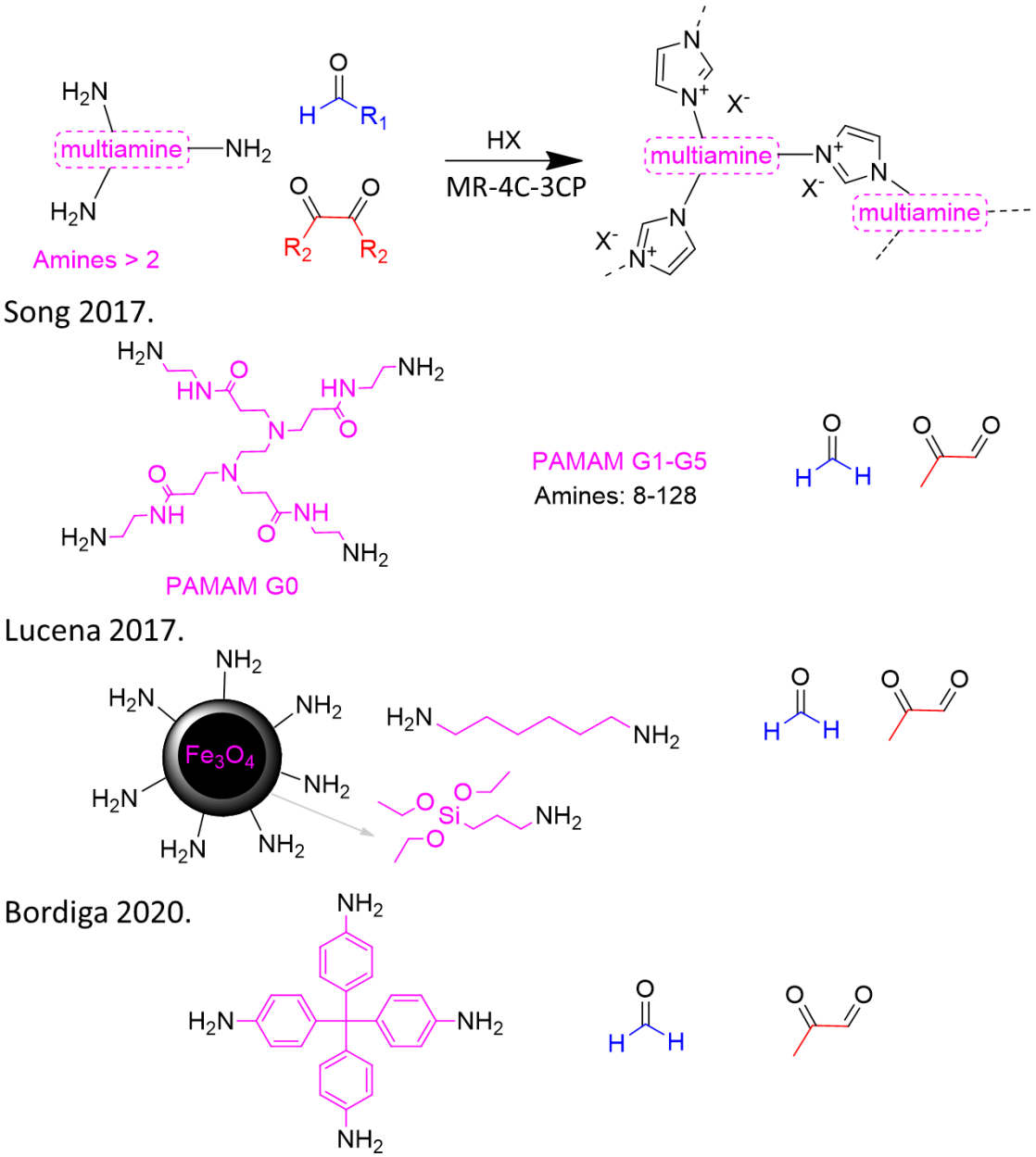

Figure 27. Networks synthesized by the modified Radziszewski four-center three-component polymerization.

In the light of these considerations, the Radziszewski step-growth polymerization appears today as one of the most developed and mature MCPs which gives access to a broad range of linear and crosslinked polymers of practical interest for various applications.

I.2.6. Miscellaneous-MCP

2.6.a. Active hydrogen compound-based MCP

The Mannich three-component reaction is a hundred years old reaction that significantly evolved since its discovery by Carl Mannich in 1912.[183] The reaction starts with the condensation of a secondary amine with formaldehyde followed by a nucleophilic attack by a compound containing a reactive hydrogen. This reaction is catalysed by Brønsted acids and generates Mannich bases which are important pharmacophores.[184] The versatility of the reaction comes from the numerous possibilities for the acidic hydrogen compound (Figure 28). This active hydrogen was initially located in the α-position of a carbonyl but it can also be in α-position of an imine, a nitrile and a nitro functional group, to name a few.[185] Moreover, aromatic protons from phenols, pyrroles, thiophenes and furans, etc., also present acidic features suitable to perform Mannich reaction.[185,186]

The first examples of the Mannich polymerization date back to the seventies as summarized by Ghedini.[19] Such polymerization can be performed with homo-difunctional monomers and formaldehyde *via* a Mannich three-center three-component polymerization (M-3C-3CP).

First, diamines and compounds with activated protons located on two distinct carbons can polymerize in the presence of formaldehyde (Figure 28, strategy 1). A typical example of such M-3C-3CP involves 1,3-di(piperidin-4-yl)propane, cyclohexanone and formaldehyde (Figure 28, strategy 1).[187] The reactive hydrogens can be carried by carbons as it is the case for cyclohexanone, furan, phenol, 2,6-dimethylpyridine but it can also be carried by the nitrogen of an amide or an urea. All these compounds have been considered and reacted with several secondary diamines.[19]

One variant of this MCP consists of using a compound where two reactive hydrogens are on the same carbon, such as acetophenone. The latter could thus react twice with 1,3-di(piperidin-4-yl)propane and formaldehyde (Figure 28, strategy 2).[187]

Nest, a primary amine can undergo two subsequent Mannich reactions and, therefore, can be used as difunctional monomer as illustrated by the M-3C-3CP of methylamine, pyrrole and formaldehyde (Figure 28, strategy 3).[188]

Finally, a Mannich two-component reaction was also considered using arylamine derivatives that behave simultaneously as an amine and an activated hydrogen compound, as exemplified by the M-3C-2CP of *para*-aminobenzoic acid and formaldehyde (Figure 28, strategy 4).[189] Nevertheless, this approach led to branched and crosslinked polymer products since *para*-aminobenzoic acid contains four reaction sites, *i.e.* two acidic protons in *ortho* positions of the

amine and the two protons of the latter which can also react.[189] The Mannich reaction has been extensively employed to synthesize polymer networks.[190–192] These syntheses often involve primary diamines and/or compounds containing multiple carbons bearing two reactive hydrogens.

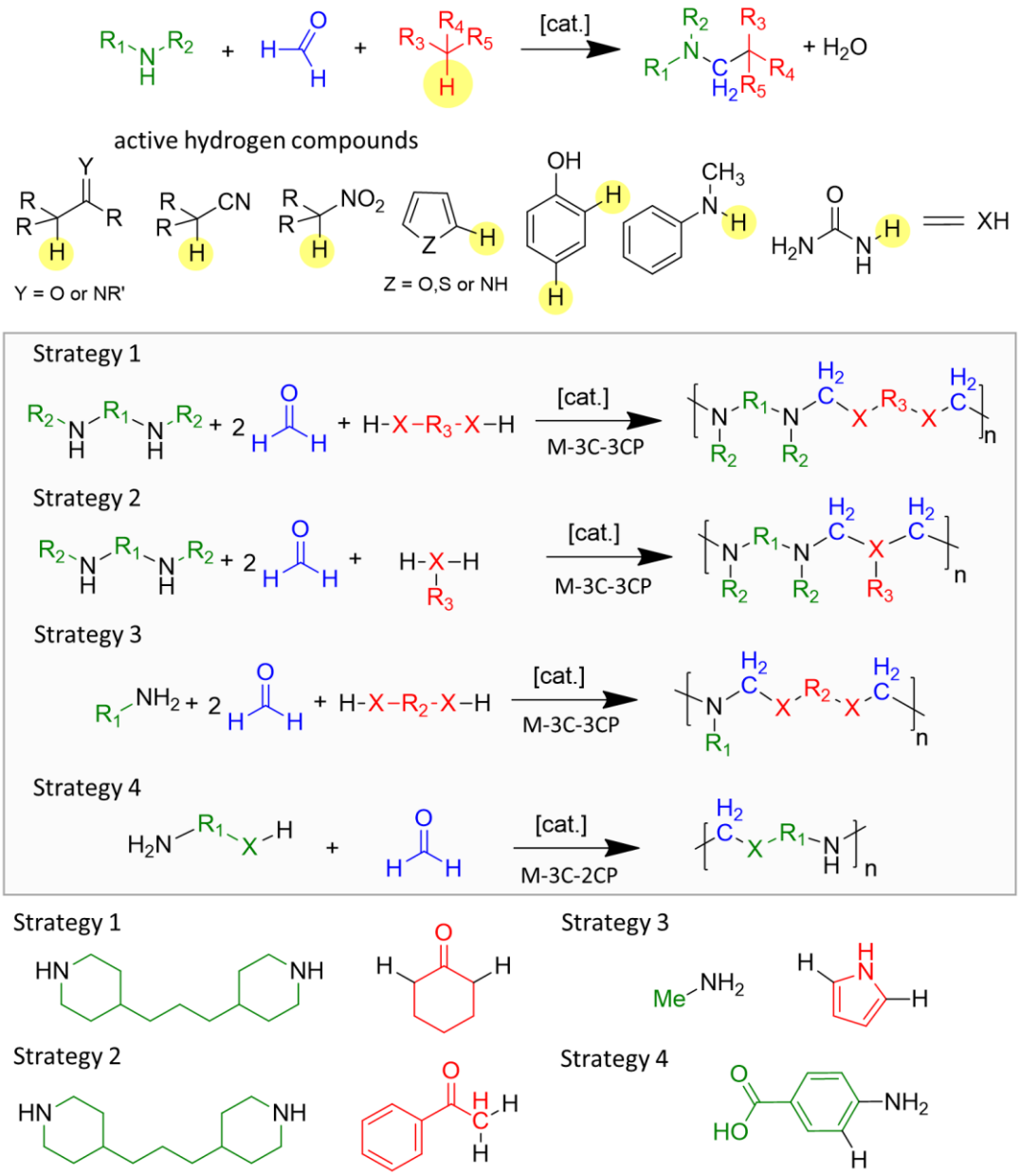

Figure 28. Mannich three-center and both three- and two-component polymerizations with examples illustrating each strategy.

This section cannot be closed without mentioning the synthesis of benzoxazine and poly(benzoxazine)s *via* the Mannich reaction.[193,194] The benzoxazine is a bicyclic compound that consists of a benzene fused with an oxazine. The 1,3-benzoxazine isomer could be formed by reacting a primary amine with formaldehyde and a phenol derivative. In this case, the phenol

reacts at two different sites: the hydroxyl group with a labile hydrogen and the *ortho* position of the hydroxyl *via* its active hydrogen (Figure 29). The resulting 1,3-benzoxazine could be polymerized upon heating leading to the expected classical Mannich product (Figure 29, path 1).[195] On the other hand, a polymer containing benzoxazine groups in its backbone is obtained when using a diphenol and a primary diamine (Figure 29, path 2).[195] Interestingly, further heating this material produces a network.[196] Plethora of poly(benzoxazine)s are reported in the literature and have already been reviewed.[193,194]

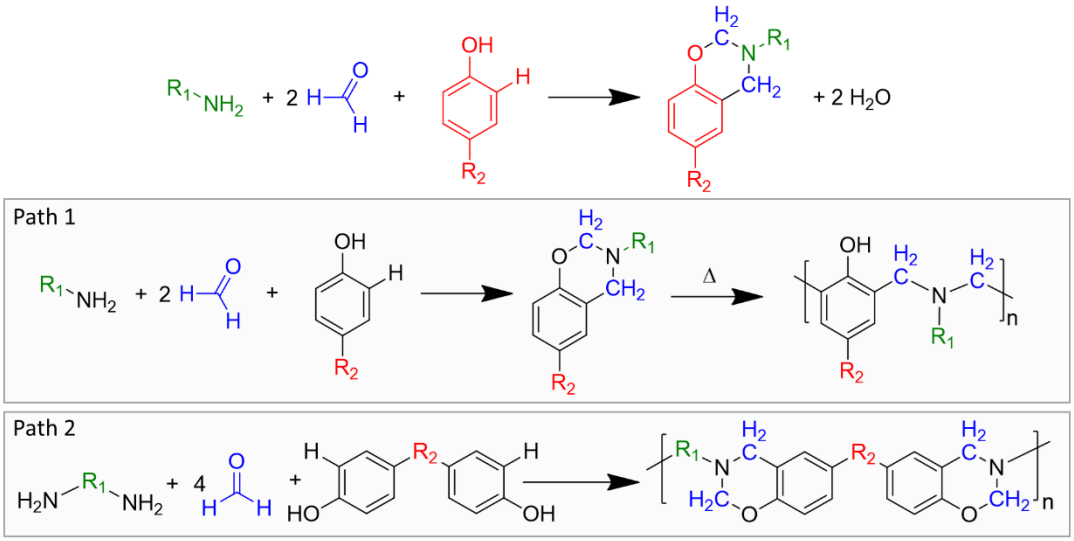

Figure 29. 1,3-Benzoxazines synthesis *via* Mannich reaction and their subsequent polymerization as well as preparation of poly(benzoxazine)s by Mannich polymerization.

2.6.b. Preformed imine-based MCP

The last section of this review is dedicated to multicomponent polymerizations involving preformed imines. Compared to the previous MCRs, the imine is no more synthesized *in situ* by the condensation of an amine and an aldehyde. According to this approach, years ago, Arndtsen and coworkers developed a one-pot synthesis of münchnones by reacting an imine with an acyl chloride and carbon monoxide in the presence of a palladium catalyst and a base to deal with HCl, the sole byproduct (Figure 30).[197] The münchnones are versatile 1,3-dipolar addition substrates and are thus key intermediates for the synthesis of heterocycles. Subsequent cycloadditions with alkynes and alkenes give access to substituted pyrroles while a treatment with tosyl imines leads to imidazoles (Figure 30).[198]

Recently, Arndtsen *et al.* took advantage of this efficient reaction to synthesize poly(münchnone)s.[199] They used various aromatic difunctional monomers, *i.e.* diacyl chlorides and diimines combined with carbon monoxide (20 bar) (Figure 30, Arndtsen 2015).[199] The

polymerizations were carried out at 45 °C for 64 h with $Pd[P(o\text{-}tol)_3]_2$ and *N*,*N*-diisopropylethylamine as the catalyst and the base, respectively. The resulting polymers could be isolated but, due to their moisture sensitivity, they were modified prior to characterization. For the same reason, they were directly transformed into a series of conjugated polymers by one-pot addition of different reagents (alkynes, alkenes and tosyl imines). The final conjugated polymers exhibited fluorescence properties and possessed tunable band gaps which make them good candidates for electronic applications.[199] The munchnone ring could also be opened by addition of an alcohol to produce a poly(amide-ester) (Figure 30).[199] In addition, the authors showed the possibility to perform a four-component reaction by direct addition the alkyne in the reaction medium. Accordingly, CO_2 was released and a poly(pyrrole) derivative was formed in good yield (87 %) with a molar mass of 14 kg/mol (Figure 30, Arndtsen 2015).[199] Note that the same group reported a four-component polymerization based on a diacyl chloride, an imine, carbon monoxide and a difunctional tosyl imine compound, affording oligomers of conjugated poly(imidazole)s.[200] In this case, however, the side-product consisting of *para*-toluenesulfonic acid significantly reduces the atom economy of the reaction.

Phospha-münchnones, analogues to münchnones, were also synthesized by Arndtsen using phosphinite instead of carbon monoxide.[201] Advantageously, no catalyst is required for this reaction but phosphonate is released when the phospha-münchnones is reacted with a dipolarophile which somewhat lowers the atom economy. Recently, this reaction was used for the direct polymerization of a series of aromatic diacyl chlorides and diimines with a phosphinite, *i.e.* the (catechyl)PPh (Figure 30, Arndtsen 2016).[202] The poly(phospha-münchnone)s were subsequently transformed in one-pot into conjugated poly(pyrrole)s by addition of different alkynes.[202] The scope of this reaction was extended to vanillin-based monomers (Figure 30, Arndtsen 2016 bis).[203] To close this section, we would like to emphasize that the syntheses of poly(münchnone)s and poly(phospha-münchnone)s conform to the concept of multicomponent polymerizations but the same cannot always be said for their subsequent transformations. It is especially true for the transformations of phospha-münchnones releasing significant byproducts which affects the atom economy of the process.

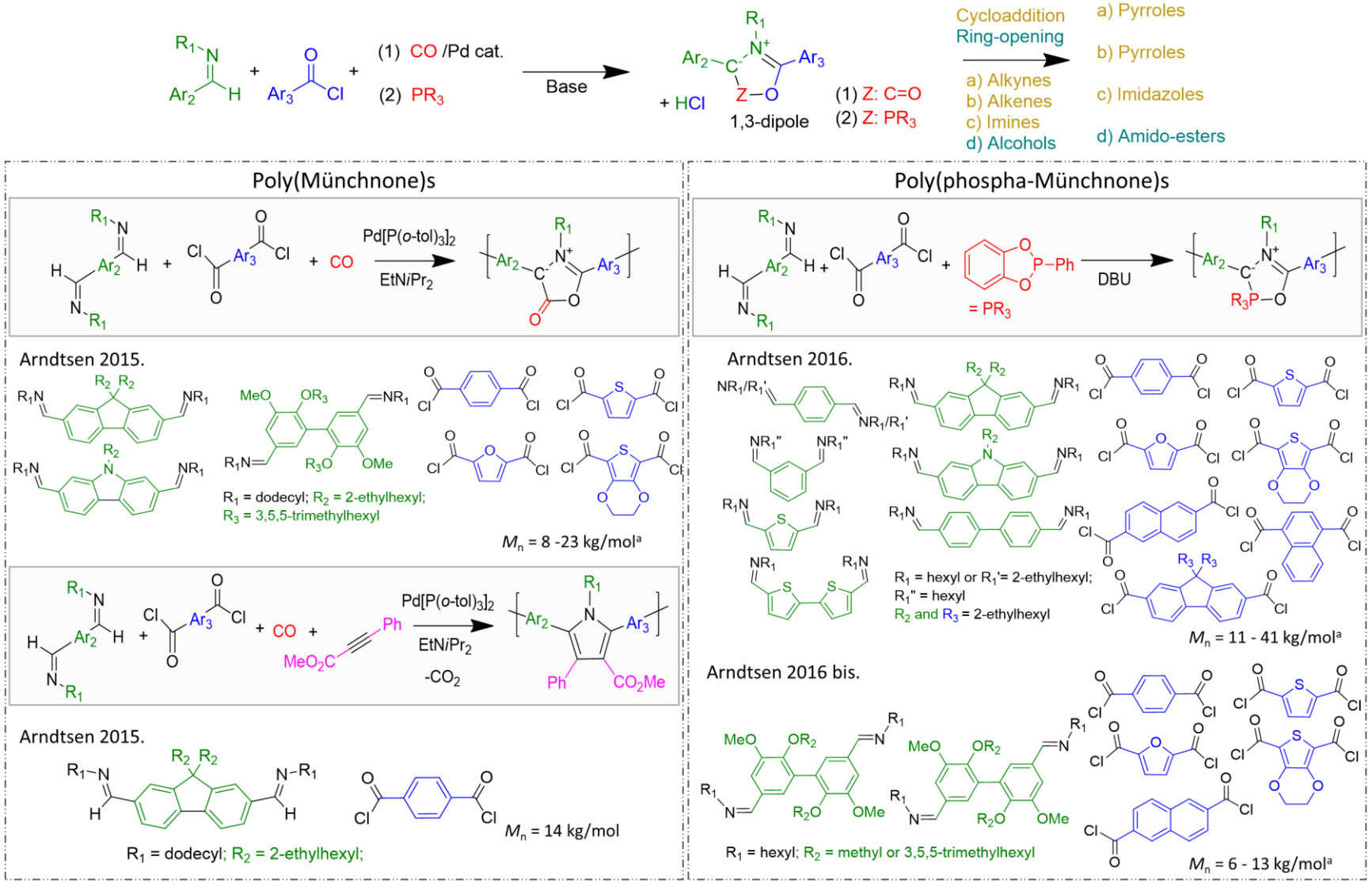

Figure 30. Synthesis of poly(münchnone)s and poly(phospha-münchnone)s by MCPs and their post-polymerization modification. [a] SEC measurement performed onto modified polymers due to the moisture sensitivity of münchnones.

I.3. Conclusion and outlook

For a few decades now, MCRs are employed in polymer chemistry for monomers synthesis, post-polymerization modifications and step-growth polymerizations but this approach has seen a great acceleration in the last years. This general trend is noticeable in the present review dedicated to step-growth multicomponent polymerizations involving an imine as the principal component. The addition of one or more component(s) to the imines generated *in situ* (or sometimes preformed) by amine/aldehyde condensation affords a great diversity of valuable polymer structures. Throughout the document, we highlighted the combinatorial feature and versatility of these imine-based MCPs. Besides the large libraries of linear polymers that can be achieved accordingly, we described the design of hyperbranched polymers and networks *via* these MCPs. Examples of such macromolecular structures prepared by MCPs are still limited but they illustrate the huge potential of these techniques in macromolecular engineering. Of course, the development of MCPs is still in its infancy and deserves improvements notably in terms of conversion and molar masses for some of them. Nevertheless, these polymerization techniques become mature enough to witness the emergence of cutting-edge applications in the biomedical, energy, electronic, gas capture, catalysis, heavy metal recycling sectors and so on. Future prospects of MCPs are vast and promising. Owing their combinatorial feature, countless substrates could be used to enlarge the already consequent scope of functional polymers. Moreover, most of the MCRs described in organic chemistry have not yet been adapted to polymer chemistry and constitute a huge field of unexplored opportunities. As exemplified by the combination of the Hantzsch/Biginelli and the A^3-coupling/Petasis reactions, MCPs can also proceed hand-in-hand towards unique and highly complex polymer structures in one-pot. This strategy is particularly relevant for the imine-based MCPs since they already share two components, i.e. the amine and the aldehyde, and should be pursued. Eventually, the combination of MCRs with other techniques such as radical polymerization and click chemistry also opens up interesting prospects. In conclusion, MCPs will undoubtedly further grow and become essential tools for macromolecular engineering in the future.

I.4. References

(1) Ugi, I.; Dömling, A.; Hörl, W. *Endeavour* **1994**, *18* (3), 115–122.

(2) Zarganes-Tzitzikas, T.; Chandgude, A. L.; Dömling, A. *Chem. Rec.* **2015**, *15* (5), 981–996.

(3) Zhu, J. *European J. Org. Chem.* **2003**, *2003* (7), 1133–1144.

(4) Dömling, A.; Ugi, I. *Angew. Chemie* **2000**, *39* (18), 3168–3210.

(5) Ruijter, E.; Scheffelaar, R.; Orru, R. V. A. *Angew. Chemie Int. Ed.* **2011**, *50* (28), 6234–6246.

(6) Zhi, S.; Ma, X.; Zhang, W. *Org. Biomol. Chem.* **2019**, *17* (33), 7632–7650.

(7) Hayashi, Y. *Chem. Sci.* **2016**, *7* (2), 866–880.

(8) Wong, C.-H.; Zimmerman, S. C. *Chem. Commun.* **2013**, *49* (17), 1679–1695.

(9) Brinkø, A.; Risinger, C.; Lambert, A.; Blixt, O.; Grandjean, C.; Jensen, H. H. *Org. Lett.* **2019**, *21* (18), 7544–7548.

(10) Laurent, A. *Ann. Chim. Phys.* **1837**, *66*, 181–196.

(11) Strecker, A. *Justus Liebigs Ann. Chem.* **1850**, *75* (1), 27–45.

(12) Dömling, A.; Wang, W.; Wang, K. *Chem. Rev.* **2012**, *112* (6), 3083–3135.

(13) Robotham, C. V; Baker, C.; Cuevas, B.; Abboud, K.; Wright, D. L. *Mol. Divers.* **2003**, *6* (3), 237–244.

(14) Sehlinger, A.; Ochsenreither, K.; Bartnick, N.; Meier, M. A. R. *Eur. Polym. J.* **2015**, *65*, 313–324.

(15) Kreye, O.; Tóth, T.; Meier, M. A. R. *J. Am. Chem. Soc.* **2011**, *133* (6), 1790–1792.

(16) Kreye, O.; Türünç, O.; Sehlinger, A.; Rackwitz, J.; Meier, M. A. R. *Chem. - A Eur. J.* **2012**, *18* (18), 5767–5776.

(17) Kreye, O.; Trefzger, C.; Sehlinger, A.; Meier, M. A. R. *Macromol. Chem. Phys.* **2014**, *215* (22), 2207–2220.

(18) Afshari, R.; Shaabani, A. *ACS Comb. Sci.* **2018**, *20* (9), 499–528.

(19) Tramontini, M.; Angiolini, L.; Ghedini, N. *Polymer.* **1988**, *29* (5), 771–788.

(20) Liu, X.; Han, T.; Lam, J. W. Y.; Tang, B. Z. *Macromol. Rapid Commun.* **2021**, *42* (6), 2000386.

(21) Liu, Y.; Qin, A.; Tang, B. Z. *Prog. Polym. Sci.* **2018**, *78*, 92–138.

(22) Llevot, A.; Boukis, A. C.; Oelmann, S.; Wetzel, K.; Meier, M. A. R. *Top. Curr. Chem.* **2017**, *375* (66), 1–29.

(23) Tao, Y.; Wang, Z.; Tao, Y. *Biopolymers* **2019**, *110* (6), e23288.

(24) Kakuchi, R. *Angew. Chemie - Int. Ed.* **2014**, *53* (1), 46–48.
(25) Rudick, J. G. *J. Polym. Sci. Part A Polym. Chem.* **2013**, *51* (19), 3985–3991.
(26) Kakuchi, R. *Polym. J.* **2019**, *51* (10), 945–953.
(27) Zhang, Z.; You, Y.; Hong, C. *Macromol. Rapid Commun.* **2018**, *39* (23), 1800362.
(28) Theato, P., Ed.; Springer International Publishing, 2015.
(29) Lieke, W. *Justus Liebigs Ann. Chem.* **1859**, *112* (3), 316–321.
(30) Ramozzi, R.; Chéron, N.; Braïda, B.; Hiberty, P. C.; Fleurat-Lessard, P. *New J. Chem.* **2012**, *36* (5), 1137.
(31) Mironov, M. A.; Ayaz, M.; De Moliner, F.; Dietrich, J.; Hulme, C. *Isocyanide Chemistry*. August 23, 2012, pp 35–73.
(32) Ayaz, M.; De Moliner, F.; Dietrich, J.; Hulme, C. *Isocyanide Chemistry*. August 23, 2012, pp 335–384.
(33) Yang, B.; Zhao, Y.; Wei, Y.; Fu, C.; Tao, L. *Polym. Chem.* **2015**, *6* (48), 8233–8239.
(34) Wu, H.; Gou, Y.; Wang, J.; Tao, L. *Macromol. Rapid Commun.* **2018**, *39* (13), 1800064.
(35) Alvim, H. G. O.; da Silva Júnior, E. N.; Neto, B. A. D. *RSC Adv.* **2014**, *4* (97), 54282–54299.
(36) Medeiros, G. A.; da Silva, W. A.; Bataglion, G. A.; Ferreira, D. A. C.; de Oliveira, H. C. B.; Eberlin, M. N.; Neto, B. A. D. *Chem. Commun.* **2014**, *50* (3), 338–340.
(37) Sehlinger, A.; Dannecker, P.-K.; Kreye, O.; Meier, M. A. R. *Macromolecules* **2014**, *47* (9), 2774–2783.
(38) Marcaccini, S.; Torroba, T. *Nat. Protoc.* **2007**, *2* (3), 632–639.
(39) Gangloff, N.; Nahm, D.; Döring, L.; Kuckling, D.; Luxenhofer, R. *J. Polym. Sci. Part A Polym. Chem.* **2015**, *53* (14), 1680–1686.
(40) Tao, Y.; Wang, S.; Zhang, X.; Wang, Z.; Tao, Y.; Wang, X. *Biomacromolecules* **2018**, *19* (3), 936–942.
(41) Schade, O. R.; Dannecker, P.-K.; Kalz, K. F.; Steinbach, D.; Meier, M. A. R.; Grunwaldt, J.-D. *ACS Omega* **2019**, *4* (16), 16972–16979.
(42) Liu, N.; Fu, C.; Zhang, Q.; Zhao, R.; Sun, Z.; Zhang, P.; Ding, L.; Deng, K. *ChemistrySelect* **2020**, *5* (9), 2725–2734.
(43) Fu, C.; Ding, L.; Yin, J.; Tian, S.; Ma, L.; Zhang, Q.; Qin, F.; Cao, L.; Deng, K. *J. Polym. Res.* **2020**, *27* (8), 216.
(44) Le, Z.; Xiao, T.; Liu, Z.; Liu, X.; Liu, H.; Liu, L.; Chen, Y. *Sci. China Chem.* **2020**, *63* (11), 1619–1625.

(45) Zhang, X.; Wang, S.; Liu, J.; Xie, Z.; Luan, S.; Xiao, C.; Tao, Y.; Wang, X. *ACS Macro Lett.* **2016**, *5* (9), 1049–1054.

(46) Cai, Q.; Zhu, H.; Zhong, K. *E3S Web Conf.* **2020**, *213*.

(47) Al Samad, A.; De Winter, J.; Gerbaux, P.; Jérôme, C.; Debuigne, A. *Chem. Commun.* **2017**, *53* (90), 12240–12243.

(48) Koyama, Y.; Ihsan, A. B.; Taira, T.; Imura, T. *RSC Adv.* **2018**, *8* (14), 7509–7513.

(49) Koyama, Y.; Gudeangadi, P. G. *Chem. Commun.* **2017**, *53* (27), 3846–3849.

(50) Ihsan, A. Bin; Taniguchi, M.; Koyama, Y. *Macromol. Rapid Commun.* **2020**, *n/a* (n/a), 2000480.

(51) Hartweg, M.; Becer, C. R. *Green Chem.* **2016**, *18* (11), 3272–3277.

(52) Jida, M.; Malaquin, S.; Deprez-Poulain, R.; Laconde, G.; Deprez, B. *Tetrahedron Lett.* **2010**, *51* (39), 5109–5111.

(53) König, S.; Ugi, I. *Z. Naturforsch.* **1991**, *46b*, 1261–1265.

(54) Bu, H.; Kjøniksen, A.-L.; Nyström, B. *Eur. Polym. J.* **2005**, *41* (8), 1708–1717.

(55) Crescenzi, V.; Francescangeli, A.; Capitani, D.; Mannina, L.; Renier, D.; Bellini, D. *Carbohydr. Polym.* **2003**, *53* (3), 311–316.

(56) de Nooy, A. E. J.; Capitani, D.; Masci, G.; Crescenzi, V. *Biomacromolecules* **2000**, *1* (2), 259–267.

(57) Shulepov, I. D.; Kozhikhova, K. V; Panfilova, Y. S.; Ivantsova, M. N.; Mironov, M. A. *Cellulose* **2016**, *23* (4), 2549–2559.

(58) Bu, H.; Kjøniksen, A.-L.; Knudsen, K. D.; Nyström, B. *Biomacromolecules* **2004**, *5* (4), 1470–1479.

(59) Cole, J. P.; Lessard, J. J.; Rodriguez, K. J.; Hanlon, A. M.; Reville, E. K.; Mancinelli, J. P.; Berda, E. B. *Polym. Chem.* **2017**, *8* (38), 5829–5835.

(60) Chen, K.; Li, J.; Feng, Y.; He, F.; Zhou, Q.; Xiao, D.; Tang, Y. *Mater. Sci. Eng. C* **2017**, *70*, 617–627.

(61) de Nooy, A. E. J.; Rori, V.; Masci, G.; Dentini, M.; Crescenzi, V. *Carbohydr. Res.* **2000**, *324* (2), 116–126.

(62) de Nooy, A. E. J.; Masci, G.; Crescenzi, V. *Macromolecules* **1999**, *32* (4), 1318–1320.

(63) Hulme, C.; Ma, L.; Romano, J. J.; Morton, G.; Tang, S.-Y.; Cherrier, M.-P.; Choi, S.; Salvino, J.; Labaudiniere, R. *Tetrahedron Lett.* **2000**, *41* (12), 1889–1893.

(64) Sehlinger, A.; Schneider, R.; Meier, M. A. R. *Macromol. Rapid Commun.* **2014**, *35* (21), 1866–1871.

(65) Lejczak, P. K. and B. *Current Medicinal Chemistry - Anti-Cancer Agents*. 2001, pp

301–312.

(66) Danila, D. C.; Wang, X.; Hubble, H.; Antipin, I. S.; Pinkhassik, E. *Bioorg. Med. Chem. Lett.* **2008**, *18* (7), 2320–2323.

(67) Xu, Y.; Yan, K.; Song, B.; Xu, G.; Yang, S.; Xue, W.; Hu, D.; Lu, P.; Ouyang, G.; Jin, L.; Chen, Z. *Molecules* **2006**, *11* (9), 666–676.

(68) Pudovik, A. N.; Konovalova, I. V. *Synthesis (Stuttg).* **1979**, *1979* (02), 81–96.

(69) Keglevich, G.; Kiss, N. Z.; Menyhárd, D. K.; Fehérvári, A.; Csontos, I. *Heteroat. Chem.* **2012**, *23* (2), 171–178.

(70) Keglevich, G.; Bálint, E. *Molecules* . 2012.

(71) Qiu, J.-J.; Xue, Q.; Liu, Y.-Y.; Pan, M.; Liu, C.-M. *Phosphorus. Sulfur. Silicon Relat. Elem.* **2014**, *189* (3), 361–373.

(72) Moldenhauer, F.; Kakuchi, R.; Theato, P. *ACS Macro Lett.* **2016**, *5* (1), 10–13.

(73) Jiang, R.; Huang, L.; Liu, M.; Deng, F.; Huang, H.; Tian, J.; Wen, Y.; Cao, Q.; Zhang, X.; Wei, Y. *Mater. Sci. Eng. C* **2018**, *83*, 115–120.

(74) Jiang, R.; Liu, M.; Huang, H.; Huang, L.; Huang, Q.; Wen, Y.; Cao, Q.; Tian, J.; Zhang, X.; Wei, Y. *Dye. Pigment.* **2018**, *149*, 581–587.

(75) Kakuchi, R.; Theato, P. *ACS Macro Lett.* **2014**, *3* (4), 329–332.

(76) Bachler, P. R.; Schulz, M. D.; Sparks, C. A.; Wagener, K. B.; Sumerlin, B. S. *Macromol. Rapid Commun.* **2015**, *36* (9), 828–833.

(77) Wagner, N.; Schneider, L.; Michelswirth, M.; Küpper, K.; Theato, P. *Macromol. Chem. Phys.* **2015**, *216* (7), 783–793.

(78) Guo, L.; Liu, Y.; Dou, J.; Huang, Q.; Lei, Y.; Chen, J.; Wen, Y.; Li, Y.; Zhang, X.; Wei, Y. *J. Mol. Liq.* **2020**, *308*, 112964.

(79) Cao, Q.; Jiang, R.; Liu, M.; Wan, Q.; Xu, D.; Tian, J.; Huang, H.; Wen, Y.; Zhang, X.; Wei, Y. *Mater. Sci. Eng. C* **2017**, *80*, 578–583.

(80) Long, Z.; Liu, M.; Jiang, R.; Zeng, G.; Wan, Q.; Huang, H.; Deng, F.; Wan, Y.; Zhang, X.; Wei, Y. *Ultrason. Sonochem.* **2017**, *35*, 319–325.

(81) Omichi, M.; Yamashita, S.; Okura, Y.; Ikutomo, R.; Ueki, Y.; Seko, N.; Kakuchi, R. *Polymers* . 2019.

(82) Hamada, T.; Yamashita, S.; Omichi, M.; Yoshimura, K.; Ueki, Y.; Seko, N.; Kakuchi, R. *ACS Sustain. Chem. Eng.* **2019**, *7* (8), 7795–7803.

(83) Kakuchi, R.; Yoshida, S.; Sasaki, T.; Kanoh, S.; Maeda, K. *Polym. Chem.* **2018**, *9* (16), 2109–2115.

(84) Zhang, Y.; Zhao, Y.; Yang, B.; Zhu, C.; Wei, Y.; Tao, L. *Polym. Chem.* **2014**, *5* (6),

1857–1862.

(85) He, X.; Liu, G.; Tian, Y.; Mao, T.; Wu, H.; Wei, Y.; Tao, L. *Macromol. Biosci.* **2020**, *20* (12), 1900419.

(86) Tian, Y.; Zeng, Y.; Li, Y.; He, X.; Wu, H.; Wei, Y.; Wu, Y.; Wang, X.; Tao, L. *Eur. Polym. J.* **2020**, 109773.

(87) Hu, R.; Li, W.; Tang, B. Z. *Macromol. Chem. Phys.* **2016**, *217* (2), 213–224.

(88) Li, C.-J.; Wei, C. *Chem. Commun.* **2002**, No. 3, 268–269.

(89) Zhang, Y.; Li, P.; Wang, M.; Wang, L. *J. Org. Chem.* **2009**, *74* (11), 4364–4367.

(90) Chan, C. Y. K.; Tseng, N.-W.; Lam, J. W. Y.; Liu, J.; Kwok, R. T. K.; Tang, B. Z. *Macromolecules* **2013**, *46* (9), 3246–3256.

(91) Jia, T.; Zheng, N.; Cai, W.; Zhang, J.; Ying, L.; Huang, F.; Cao, Y. *Chinese J. Polym. Sci.* **2017**, *35* (2), 269–281.

(92) Liu, Y.; Gao, M.; Lam, J. W. Y.; Hu, R.; Tang, B. Z. *Macromolecules* **2014**, *47* (15), 4908–4919.

(93) Uhlig, N.; Li, C.-J. *Org. Lett.* **2012**, *14* (12), 3000–3003.

(94) Wang, J.; Shen, Q.; Li, P.; Peng, Y.; Song, G. *Org. Biomol. Chem.* **2014**, *12* (30), 5597–5600.

(95) Park, K.; Heo, Y.; Lee, S. *Org. Lett.* **2013**, *15* (13), 3322–3325.

(96) Wang, J.; Shen, Q.; Zhang, J.; Song, G. *Tetrahedron Lett.* **2015**, *56* (7), 903–906.

(97) Wu, X.; Li, W.; Hu, R.; Tang, B. Z. *Macromol. Rapid Commun.* **2020**, *n/a* (n/a), 2000633.

(98) Syeda Huma, H. Z.; Halder, R.; Singh Kalra, S.; Das, J.; Iqbal, J. *Tetrahedron Lett.* **2002**, *43* (36), 6485–6488.

(99) Fasano, V.; Radcliffe, J. E.; Ingleson, M. J. *Organometallics* **2017**, *36* (8), 1623–1629.

(100) Fu, W.; Dong, L.; Shi, J.; Tong, B.; Cai, Z.; Zhi, J.; Dong, Y. *Macromolecules* **2018**, *51* (9), 3254–3263.

(101) Zhu, Q.; Jiang, H.; Li, J.; Liu, S.; Xia, C.; Zhang, M. *J. Comb. Chem.* **2009**, *11* (4), 685–696.

(102) Zhu, Q.; Jiang, H.; Li, J.; Zhang, M.; Wang, X.; Qi, C. *Tetrahedron* **2009**, *65* (23), 4604–4613.

(103) Wei, B.; Li, W.; Zhao, Z.; Qin, A.; Hu, R.; Tang, B. Z. *J. Am. Chem. Soc.* **2017**, *139* (14), 5075–5084.

(104) Kausar, A.; Zulfiqar, S.; Sarwar, M. I. *Polym. Rev.* **2014**, *54* (2), 185–267.

(105) Griebel, J. J.; Glass, R. S.; Char, K.; Pyun, J. *Prog. Polym. Sci.* **2016**, *58*, 90–125.

(106) Mutlu, H.; Ceper, E. B.; Li, X.; Yang, J.; Dong, W.; Ozmen, M. M.; Theato, P. *Macromol. Rapid Commun.* **2019**, *40* (1), 1800650.

(107) Tian, T.; Hu, R.; Tang, B. Z. *J. Am. Chem. Soc.* **2018**, *140* (19), 6156–6163.

(108) Zhang, J.; Zang, Q.; Yang, F.; Zhang, H.; Sun, J. Z.; Tang, B. Z. *J. Am. Chem. Soc.* **2021**, *143* (10), 3944–3950.

(109) Cao, W.; Dai, F.; Hu, R.; Tang, B. Z. *J. Am. Chem. Soc.* **2020**, *142* (2), 978–986.

(110) Kanbara, T.; Kawai, Y.; Hasegawa, K.; Morita, H.; Yamamoto, T. *J. Polym. Sci. Part A Polym. Chem.* **2001**, *39* (21), 3739–3750.

(111) Kawai, Y.; Kanbara, T.; Hasegawa, K. *J. Polym. Sci. Part A Polym. Chem.* **1999**, *37* (12), 1737–1740.

(112) Kagaya, S.; Sato, E.; Masore, I.; Hasegawa, K.; Kanbara, T. *Chem. Lett.* **2003**, *32* (7), 622–623.

(113) Kagaya, S.; Tanaka, E.; Kawai, N.; Masore, I.; Sato, E.; Hasegawa, K.; Kishi, M.; Kanbara, T. *J. Inorg. Organomet. Polym. Mater.* **2009**, *19* (1), 67–73.

(114) Kagaya, S.; Miyazaki, H.; Ito, M.; Tohda, K.; Kanbara, T. *J. Hazard. Mater.* **2010**, *175* (1), 1113–1115.

(115) Verma, A.; Saraf, S. K. *Eur. J. Med. Chem.* **2008**, *43* (5), 897–905.

(116) Schmolka, I. R.; Spoerri, P. E. *J. Am. Chem. Soc.* **1957**, *79* (17), 4716–4720.

(117) Xu, J.; Cao, L.; Wang, Y.; Zhu, D.; Ye, Q. *J. Polym. Sci.* **2021**, *59* (4), 312–320.

(118) Shi, Y.; Jiang, R.; Liu, M.; Fu, L.; Zeng, G.; Wan, Q.; Mao, L.; Deng, F.; Zhang, X.; Wei, Y. *Mater. Sci. Eng. C* **2017**, *77*, 972–977.

(119) Ren, X.; Zhao, Y.; Yang, B.; Wang, X.; Wei, Y.; Tao, L. *RSC Adv.* **2015**, *5* (67), 54133–54137.

(120) Tian, J.; Chen, Z.; Jiang, R.; Mao, L.; Liu, M.; Deng, F.; Huang, H.; Liu, L.; Zhang, X.; Wei, Y. *Dye. Pigment.* **2019**, *171*, 107673.

(121) Wan, Q.; Jiang, R.; Mao, L.; Xu, D.; Zeng, G.; Shi, Y.; Deng, F.; Liu, M.; Zhang, X.; Wei, Y. *Mater. Chem. Front.* **2017**, *1* (6), 1051–1058.

(122) Wan, Q.; Liu, M.; Mao, L.; Jiang, R.; Xu, D.; Huang, H.; Dai, Y.; Deng, F.; Zhang, X.; Wei, Y. *Mater. Sci. Eng. C* **2017**, *72*, 352–358.

(123) Wan, Q.; Liu, M.; Xu, D.; Mao, L.; Tian, J.; Huang, H.; Gao, P.; Deng, F.; Zhang, X.; Wei, Y. *Carbohydr. Polym.* **2016**, *152*, 189–195.

(124) Wan, Q.; Liu, M.; Xu, D.; Mao, L.; Huang, H.; Gao, P.; Deng, F.; Zhang, X.; Wei, Y. *Polym. Chem.* **2016**, *7* (27), 4559–4566.

(125) Biginelli, P. *Berichte der Dtsch. Chem. Gesellschaft* **1891**, *24* (1), 1317–1319.

(126) Kappe, C. O. *Eur. J. Med. Chem.* **2000**, *35* (12), 1043–1052.
(127) Kappe, C. O. *J. Org. Chem.* **1997**, *62* (21), 7201–7204.
(128) Zhu, C.; Yang, B.; Zhao, Y.; Fu, C.; Tao, L.; Wei, Y. *Polym. Chem.* **2013**, *4* (21), 5395–5400.
(129) Zhao, Y.; Wu, H.; Wang, Z.; Wei, Y.; Wang, Z.; Tao, L. *Sci. China Chem.* **2016**, *59* (12), 1541–1547.
(130) Xue, H.; Zhao, Y.; Wu, H.; Wang, Z.; Yang, B.; Wei, Y.; Wang, Z.; Tao, L. *J. Am. Chem. Soc.* **2016**, *138* (28), 8690–8693.
(131) Boukis, A. C.; Llevot, A.; Meier, M. A. R. *Macromol. Rapid Commun.* **2016**, *37* (7), 643–649.
(132) Windbiel, J. T.; Meier, M. A. R. *Polym. Int.* **2021**, *70* (5), 506–513.
(133) Zhao, Y.; Wu, H.; Zhang, Y.; Wang, X.; Yang, B.; Zhang, Q.; Ren, X.; Fu, C.; Wei, Y.; Wang, Z.; Wang, Y.; Tao, L. *ACS Macro Lett.* **2015**, *4* (8), 843–847.
(134) Zhao, Y.; Yu, Y.; Zhang, Y.; Wang, X.; Yang, B.; Zhang, Y.; Zhang, Q.; Fu, C.; Wei, Y.; Tao, L. *Polym. Chem.* **2015**, *6* (27), 4940–4945.
(135) Hantzsch, A. *Justus Liebigs Ann. Chem.* **1882**, *215* (1), 1–82.
(136) Singh, S. K.; Singh, K. N. *J. Heterocycl. Chem.* **2010**, *47* (1), 194–198.
(137) Wu, H.; Wang, Z.; Tao, L. *Polym. Chem.* **2017**, *8* (47), 7290–7296.
(138) Liu, G.; Pan, R.; Wei, Y.; Tao, L. *Macromol. Rapid Commun.* **2020**, *n/a* (n/a), 2000459.
(139) Wu, H.; Fu, C.; Zhao, Y.; Yang, B.; Wei, Y.; Wang, Z.; Tao, L. *ACS Macro Lett.* **2015**, *4* (11), 1189–1193.
(140) Liu, G.; Shegiwal, A.; Zeng, Y.; Wei, Y.; Boyer, C.; Haddleton, D.; Tao, L. *ACS Macro Lett.* **2018**, *7* (11), 1346–1352.
(141) Wang, R.; Sun, S.; Wang, B.; Mao, Z.; Xu, H.; Feng, X.; Sui, X. *Macromol. Rapid Commun.* **2021**, *42* (6), 2000496.
(142) Debus, H. *Justus Liebigs Ann. Chem.* **1858**, *107* (2), 199–208.
(143) Radzisewski, B. *Berichte der Dtsch. Chem. Gesellschaft* **1882**, *15* (2), 2706–2708.
(144) Radziszewski, B. *Berichte der Dtsch. Chem. Gesellschaft* **1882**, *15* (2), 1493–1496.
(145) Arduengo, A. J.; Gentry, F. P.; Taverkere, P. K.; Howard, E. S. US 6,177,575 B1, 2001.
(146) Arduengo, A. J. 5,077,414, 1991.
(147) Lei, Z.; Chen, B.; Koo., Y.-M.; Douglas, R. M. *Chem. Rev.* **2017**, *117* (10), 6633–6635.
(148) Riduan, S. N.; Zhang, Y. *Chem. Soc. Rev.* **2013**, *42* (23), 9055–9070.

(149) Kua, J.; Krizner, H. E.; De Haan, D. O. *J. Phys. Chem. A* **2011**, *115* (9), 1667–1675.
(150) Saxer, S.; Marestin, C.; Mercier, R.; Dupuy, J. *Polym. Chem.* **2018**, *9* (15), 1927–1933.
(151) Krieg, V. B.; Manecke, G. *Die Makromol. Chemie* **1967**, *108* (1), 210–217.
(152) Chauveau, E.; Marestin, C.; Martin, V.; Mercier, R. *Polymer.* **2008**, *49* (24), 5209–5214.
(153) Fan, J.; Wright, A. G.; Britton, B.; Weissbach, T.; Skalski, T. J. G.; Ward, J.; Peckham, T. J.; Holdcroft, S. *ACS Macro Lett.* **2017**, *6* (10), 1089–1093.
(154) Wang, Y.-J.; Qiao, J.; Baker, R.; Zhang, J. *Chem. Soc. Rev.* **2013**, *42* (13), 5768–5787.
(155) Chauveau, E.; Marestin, C.; Mercier, R. *Polymer.* **2014**, *55* (25), 6435–6438.
(156) Qian, W.; Texter, J.; Yan, F. *Chem. Soc. Rev.* **2017**, *46* (4), 1124–1159.
(157) Yuan, J.; Mecerreyes, D.; Antonietti, M. *Prog. Polym. Sci.* **2013**, *38* (7), 1009–1036.
(158) Siemer, M.; Koltzenburg, S.; Klein, M. WO 2010/072571 A1, 2010.
(159) Siemer, M.; Lindner, J.-P. B.; Rimassa, S.; Kaprinidis, N. WO 2016/096502 A1, 2016.
(160) Lindner, J.-P. B.; Konradi, R.; Gruendling, T.; Son, S.; Koltzenburg, S. WO 2016/020214 A1, 2016.
(161) Lindner, J.-P. B.; Koltzenburg, S.; Gruendling, T.; Son, S.; Konradi, R. WO 2016/020216 A1, 2016.
(162) Wiethan, J.; Lindner, J.-P. B. WO 2017/025433 A1, 2017.
(163) Lindner, J.-P. B. WO 2017/121657 A1, 2017.
(164) Lindner, J.-P. *Macromolecules* **2016**, *49* (6), 2046–2053.
(165) Grygiel, K.; Kirchhecker, S.; Gong, J.; Antonietti, M.; Esposito, D.; Yuan, J. *Macromol. Chem. Phys.* **2017**, *218* (18), 1600586.
(166) Gong, J.; Lin, H.; Grygiel, K.; Yuan, J. *Appl. Mater. Today* **2017**, *7*, 159–168.
(167) Zhang, W.; Peng, L.; Deng, C.; Zhang, Y.; Qian, H. *Mol. Catal.* **2018**, *445*, 170–178.
(168) Ríos-Gómez, J.; García-Valverde, M. T.; López-Lorente, Á. I.; Toledo-Neira, C.; Lucena, R.; Cárdenas, S. *Anal. Chim. Acta* **2020**, *1094*, 47–56.
(169) Wu, Y.; Regan, M.; Zhang, W.; Yuan, J. *Eur. Polym. J.* **2018**, *103*, 214–219.
(170) Song, M.; Wang, Y.; Zhang, L.; Lu, H.; Feng, S. *Macromol. Rapid Commun.* **2019**, *40* (23), 1900469.
(171) Hu, Z.; Chen, J.; Guo, Y.; Zhu, J.; Qu, X.; Niu, W.; Liu, X. *J. Memb. Sci.* **2020**, *599*, 117827.
(172) Yin, J.; Zhang, C.; Yu, Y.; Hao, T.; Wang, H.; Ding, X.; Meng, J. *J. Memb. Sci.* **2020**, *593*, 117405.
(173) Pan, J.; Sun, Z.; Zhu, H.; Cao, H.; Wang, B.; Zhao, J.; Yan, F. *J. Memb. Sci.* **2020**, *610*,

118283.

(174) Samai, S.; Nandi, G. C.; Singh, P.; Singh, M. S. *Tetrahedron* **2009**, *65* (49), 10155–10161.

(175) Hugar, K. M.; Kostalik, H. A.; Coates, G. W. *J. Am. Chem. Soc.* **2015**, *137* (27), 8730–8737.

(176) Krannig, K.-S.; Esposito, D.; Antonietti, M. *Macromolecules* **2014**, *47* (7), 2350–2353.

(177) Sirviö, J. A.; Visanko, M.; Liimatainen, H. *RSC Adv.* **2016**, *6* (61), 56544–56548.

(178) Tröger-Müller, S.; Liedel, C. *ACS Appl. Polym. Mater.* **2019**, *1* (10), 2606–2612.

(179) Zhao, X.; Guo, S.; Li, H.; Liu, J.; Liu, X.; Song, H. *Macromol. Rapid Commun.* **2017**, *38* (21), 1700415.

(180) Castro-grijalba, A.; Reyes-gallardo, E. M.; Wuilloud, R. G. *RSC Adv.* **2017**, *7*, 42979–42985.

(181) Dani, A.; Crocellà, V.; Magistris, C.; Santoro, V.; Yuan, J.; Bordiga, S. *J. Mater. Chem. A* **2017**, *5* (1), 372–383.

(182) Talapaneni, S. N.; Buyukcakir, O.; Je, S. H.; Srinivasan, S.; Seo, Y.; Polychronopoulou, K.; Coskun, A. *Chem. Mater.* **2015**, *27* (19), 6818–6826.

(183) Mannich, C.; Krösche, W. *Arch. Pharm. (Weinheim).* **1912**, *250* (1), 647–667.

(184) Bala, S.; Sharma, N.; Kajal, A.; Kamboj, S.; Saini, V. *Int. J. Med. Chem.* **2014**, *2014*, 191072.

(185) Blicke, F. F. *Organic Reactions*. March 15, 2011, pp 303–341.

(186) Roman, G. *Mini-Reviews in Organic Chemistry*. 2013, pp 27–39.

(187) Tomono, T.; Hasegawa, E.; Tsuchida, E. *J. Polym. Sci. Polym. Chem. Ed.* **1974**, *12* (5), 953–965.

(188) Tsuchida, E.; Tomono, T. *J. Polym. Sci. Polym. Chem. Ed.* **1973**, *11* (4), 723–735.

(189) Chaplin, M. F.; Kennedy, J. F. *Carbohydr. Res.* **1976**, *50* (2), 267–274.

(190) Hamouz, O. C. S. Al; K. Estatie, M.; Morsy, M. A.; Saleh, T. A. *J. Taiwan Inst. Chem. Eng.* **2017**, *70*, 345–351.

(191) Al Hamouz, O. C. S.; Akintola, O. S. *Process Saf. Environ. Prot.* **2017**, *106*, 180–190.

(192) Dai, Y.-X.; Lv, F.-N.; Wang, B.; Chen, Y. *Polymer.* **2018**, *145*, 454–462.

(193) Ghosh, N. N.; Kiskan, B.; Yagci, Y. *Prog. Polym. Sci.* **2007**, *32* (11), 1344–1391.

(194) Lyu, Y.; Ishida, H. *Prog. Polym. Sci.* **2019**, *99*, 101168.

(195) Alhassan, S.; Schiraldi, D.; Qutubuddin, S.; Agag, T.; Ishida, H. Ishida, H., Agag, T. B. T.-H. of B. R., Eds.; Elsevier: Amsterdam, 2011; pp 309–318.

(196) Takeichi, T.; Kano, T.; Agag, T. *Polymer.* **2005**, *46* (26), 12172–12180.

(197) Dhawan, R.; Dghaym, R. D.; Arndtsen, B. A. *J. Am. Chem. Soc.* **2003**, *125* (6), 1474–1475.

(198) Morin, M. S. T.; St-Cyr, D. J.; Arndtsen, B. A.; Krenske, E. H.; Houk, K. N. *J. Am. Chem. Soc.* **2013**, *135* (46), 17349–17358.

(199) Leitch, D. C.; Kayser, L. V; Han, Z.-Y.; Siamaki, A. R.; Keyzer, E. N.; Gefen, A.; Arndtsen, B. A. *Nat. Commun.* **2015**, *6* (1), 7411.

(200) Siamaki, A. R.; Sakalauskas, M.; Arndtsen, B. A. *Angew. Chemie Int. Ed.* **2011**, *50* (29), 6552–6556.

(201) St. Cyr, D. J.; Arndtsen, B. A. *J. Am. Chem. Soc.* **2007**, *129* (41), 12366–12367.

(202) Kayser, L. V; Vollmer, M.; Welnhofer, M.; Krikcziokat, H.; Meerholz, K.; Arndtsen, B. A. *J. Am. Chem. Soc.* **2016**, *138* (33), 10516–10521.

(203) Kayser, L. V; Hartigan, E. M.; Arndtsen, B. A. *ACS Sustain. Chem. Eng.* **2016**, *4* (12), 6263–6267.

Aim of the thesis

Aim of the thesis

Nowadays, the demand for advanced functional polymers able to fulfil the requirements of cutting-edge applications is constantly increasing which is a strong incentive to push further the limits of macromolecular synthesis tools and to develop new ones. Another challenge is to achieve this in combination with cleaner and more efficient chemistries. In this perspective, multicomponent reactions (MCRs) are particularly attractive since they are highly efficient reactions involving more than two compounds which react together and form a complex chemical structure containing essentially all atoms of the starting reagents. Besides being atom economic, these reactions are versatile and constitute very powerful methods for combinatorial chemistry. In the last years, some MCRs have been applied in the field of polymer synthesis bringing new functionalities to polymer structures in a straightforward manner *via* monomer synthesis, post-polymerization modification but also step-growth polymerization (MCP). Although very promising, the use of MCRs in polymer design is still in infancy with room for improvement and innovation. For example, in spite of the great availability of the starting reagents, the intrinsic combinatorial character of MCRs remains underused in MCPs. Moreover, only a limited number of MCRs were successfully applied in direct step-growth polymerization which requires high efficiency to produce polymers with decent molecular weights. Nonetheless, other MCRs could certainly meet the necessary criteria for MCP if handled judiciously or performed with the suitable catalyst. In addition, the MCP synthesis of linear polymers is developing intensely but little effort has been dedicated to the design of hyperbranched polymers and networks. Finally, tuning the 3D morphology of polymers from MCP, like creating a porosity within these materials, has essentially been disregarded despite of the potential benefits such as enhanced specific surface area, designable spatial structure and improved flow-through properties, to name a few.

This thesis aims to further develop the use of MCRs for polymer synthesis and address some of the above-mentioned limitations in order to achieve novel functional polymers and structured materials. In particular, we focused on two imine-based MCRs, namely the Ugi-type and Radziszewski reactions.

First, the versatility of the popular Ugi-4C polymerization towards many substrates was investigated in order to generate a library of novel functional polypeptoids, i.e. peptidomimetic polymers of interest in biomedical applications (Chapter II). Next, we explored the potential of the Ugi three-component reaction (Ugi-3C) in step-growth polymerization for the first time with the intent to produce unprecedented polymers containing α-amino amide moieties. The

combination of both functions as well as their spatial proximity could endow the resulting polymers with new properties compared to classical polyamides (Chapter III).

In the second part of the thesis, the modified Radziszewski three-component reaction (MR-3CR) was combined with high internal phase emulsion (HIPE) templating methods to yield interconnected macroporous imidazolium-based networks (Chapter IV and V). Chapter IV presents the Radziszewski MCP of trifunctional monomers carried out under HIPE conditions and the formation of the corresponding porous poly(imidazolium)s networks. The latter were notably tested as heterogenous catalysts for different reactions. Eventually, Chapter V investigates the combination of the Radziszewski MCR with free radical polymerization and HIPE-templating techniques in one-pot for the preparation of poly(imidazolium) and poly(imidazolium-*co*-amine) macroporous networks. Given the known affinity of both amine and imidazolium for CO_2, the pure imidazolium and bifunctional porous networks were considered in CO_2 capture application.

Overall, this work is expected to contribute to the development of multicomponent reactions in polymer science and to the integration of these techniques within the global polymer synthesis toolbox for the design of polymer materials with greater chemical and morphological diversity.

Chapter II.

Ugi Four-Component Polymerization of Amino Acid Derivatives: A Combinatorial Tool for the Design of Polypeptoids.

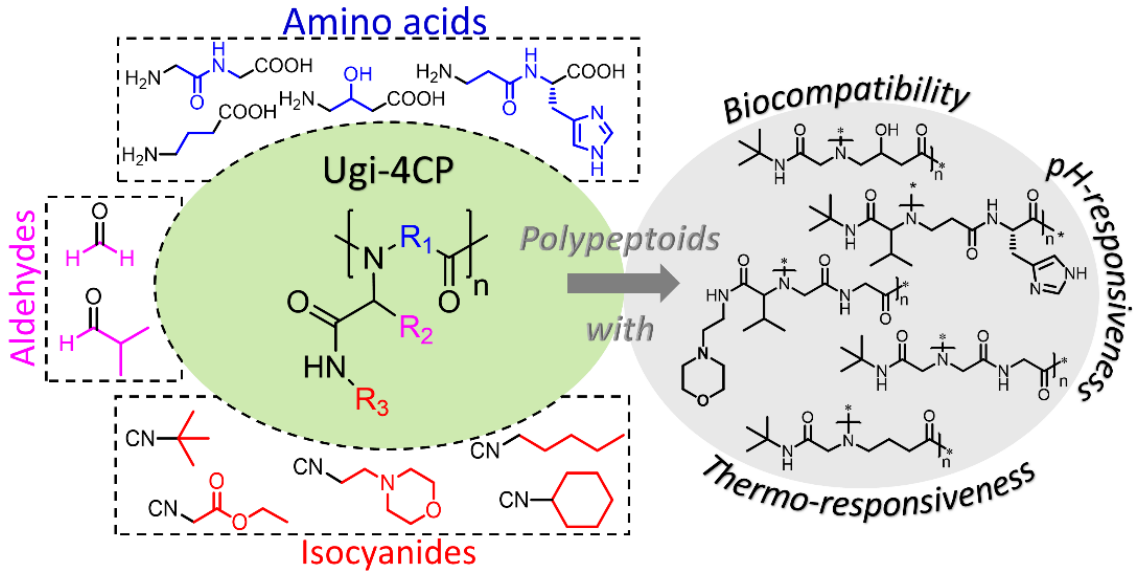

Abstract: Polypeptoids, consisting of nitrogen-substituted analogues of polypeptides, have become a real asset in modern sciences especially in the biomedical field. To address the increasing demand for polypeptoid structures with specific properties, this work explores the combinatorial character of the Ugi-four component polymerization of amino acid derivatives such as dipeptides and aminobutyric acid compounds, with different aldehydes and isocyanides. A library of structurally diverse polypeptoids is prepared accordingly. Thermal and solution properties of the latter are characterized and discussed in a structure-property relationship approach highlighting the impact of both the backbone and side chains. Some materials demonstrate pH-responsiveness, thermo-responsiveness with tunable transition temperatures and biocompatibility. Given the great variety of possible substrates and the promising properties of the obtained polypeptoids, this straightforward and combinatorial strategy is attractive for the future development of polypeptoids and resulting applications.

Inspired from:

Stiernet, P.; Couturaud, B.; Bertrand, V.; Eppe, G.; De Winter, J.; Debuigne, A.; *Polym. Chem.*, **2021**,12, 2141-2151.

Chapter II. Ugi Four-Component Polymerization of Amino Acid Derivatives: A Combinatorial Tool for the Design of Polypeptoids.

II.1. Introduction

Polypeptoids are a class of non-natural biomimetic polymers that have raised huge interest in the last few years especially for biomedical applications.[1–4] They consist of nitrogen-substituted analogues of natural polypeptides. In theory, the term polypeptoid should be restricted to polymers based on *N*-substituted glycine units[5] but it is commonly used to designate indiscriminately all polypeptoid analogues, i.e. the *N*-substituted polyamide backbone, and so will it be throughout the text. The substitution of the nitrogen atom in polypeptoids accounts for major differences in their secondary and tertiary structures compared to polypeptides. While the secondary structures of polypeptides are stabilized by hydrogen bonds between amides present in the backbone, the *N*-substitution prevents such interactions in polypeptoids. However, a wise choice of the *N*-substituted group can generate well-defined secondary structures similar to those of polypeptides by steric and electronic effects. [1,6–14] These specificities generally impart to them a good solubility in common solvents,[15–17] high stability of their 3D structure[18] and improved resistance to hydrolysis and proteolysis,[4,19] phenomena that can be problematic for peptides-assisted drug delivery.[19–22] Like polypeptides, polypeptoids exhibit good biocompatibility, a prerequisite for its applicability in the biomedical field.[1,23,24]

The synthesis of polypeptoids can be achieved by various pathways.[25–27] First, they can be prepared by classical iterative methods (Scheme 1A) involving repeated monomer addition/deprotection steps often carried out onto solid phase material[28,29] or *via* a solid-phase submonomer approach based on primary amines and haloacetic acid building blocks which does not require deprotection reaction.[30,31] The iterative methods allow a perfect sequence control with absolute monodispersity, but at the cost of a yield which decreases and a longer reaction time when the number of monomer units increases.[25] Alternatively, the living ring-opening polymerization (ROP) of *N*-substituted α-amino acid-*N*-carboxyanhydrides (NNCAs) gives access to poly-α-peptoids with high molar masses in good yields (Scheme 1B).[1,2,23,32,33] This ROP has been successfully extended to β-NNCAs (Scheme 1B).[34] Although, the sequence regulation is more limited in this case, valuable polypeptoid structures including statistical and block copolymers can be produced accordingly.[33] As a downside, the synthesis of NNCAs is not trivial especially when the complexity of the side chains increases. Moreover, their ROP

must be carried out under strict anaerobic and anhydrous conditions due to the moisture sensitivity of these monomers. Note that the synthesis of poly-β-peptoids and poly-γ-peptoids can also been achieved by ring opening copolymerization of aziridine and azetidine with carbon monoxide (Scheme 1C).[17,35] Another recent strategy for preparing polypeptoid analogues relies on the Ugi four-component reaction (Ugi-4CR) (Scheme 1D). This efficient, atom-economical, catalyst-free and air-tolerant multicomponent reaction (MCR) occurs under mild conditions and generates α-amido amide derivatives in one-pot from carbonyl, amine, carboxylic acid and isocyanide reactants.[36] The key steps consist of the condensation of the carbonyl and the amine to afford the formation of iminium that undergoes a nucleophilic attack from the isocyanide to form a nitrilium intermediate. Eventually, after the addition of carboxylate onto the nitrilium, an α-amido amide is generated through acyl group migration (Mumm rearrangement) with water as the sole by-product (Figure S1A).[37] Since its introduction in macromolecular chemistry by Meier *et al.*,[38] the Ugi-4CR has been applied to several monomers giving access to a large variety of amide-containing polymers[39–41] including polypeptoid analogues (scheme 1D).[42] Sequence-defined polypeptoids were produced by the Ugi-4CR through an iterative approach[43,44] whereas step-growth process based on the Ugi-4CR paved the way to sequence-undefined polypeptoids.[24,42,45–48] For example, lysine methyl ester and *N*-boc-glutamic acid served as AA and BB type monomers in the Ugi-4C step-growth polymerization leading to alternating polypeptoids and the corresponding polyampholytes upon cleavage of the protecting groups.[24] Some alternating polypeptide-*alt*-peptoids were also produced by the Ugi-4CR involving a carboxylic acid/isocyanide AB monomer and an imine.[47–49] In this context, amino acid derivatives possessing two of the four functions necessary to the Ugi-4CR quickly drew attention as natural AB building blocks. Unfortunately, the use of α-amino acids is hampered by a side-reaction consisting of intramolecular cyclisation *via* the Ugi-4CR leading to oxazepinone (Figure S1B).[45] This can be tackled by increasing the distance between the amine and the carboxylic acid in the building block which limits this side reaction and allows the step-growth polymerization to occur. For example, a modified lysine (N_α-Boc-L-lysine), with the α-amine protected by *tert*-butoxycarbonyl group and a free ε-amine, led to the corresponding poly-ε-peptoids by reaction with an isocyanide and a carbonyl derivative.[45] Poly-γ- and poly-δ-peptoids were prepared following the same strategy.[45] Finally, some alternating poly(peptides-*alt*-peptoides) have also been synthesized by Ugi-4 component polymerization (Ugi-4CP) of simple dipeptides carried out in water in the presence of *tert*-butyl isocyanide and formaldehyde.[46]

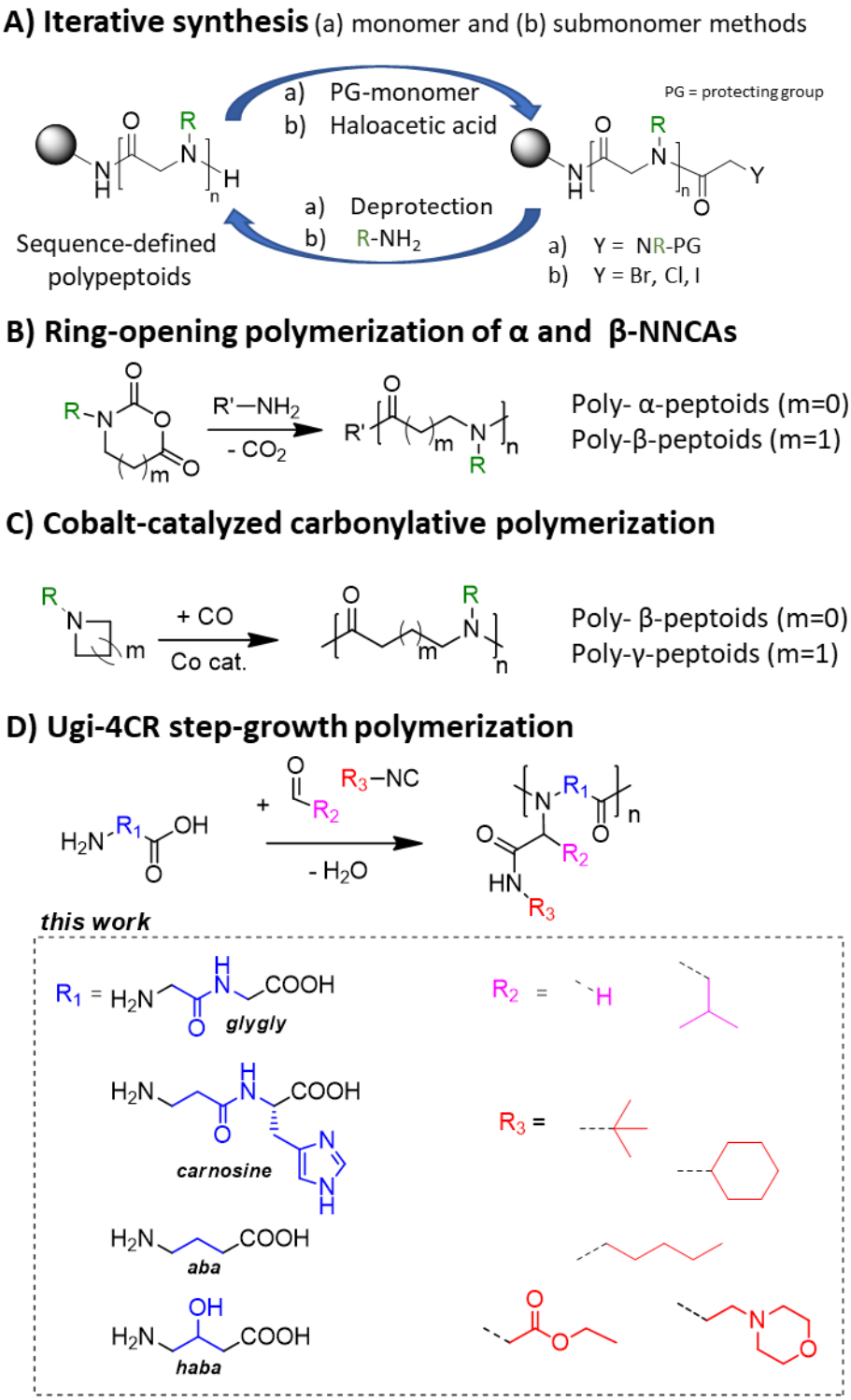

Scheme 1. Synthesis methods of polypeptoids and their analogues.

In this work, we explored the combinatorial character of the Ugi-4CR in the step-growth polymerization of a variety of amino acid derivatives, isocyanides and aldehydes, in order to access structurally diverse polypeptoids with specific properties and fulfil the ever-growing

demand for unique polypeptoid materials (Scheme 1D). In addition to simple dipeptide like glycylglycine, we considered β-alanyl-L-histidine as difunctional substrate as well as some easily available 4-amino-butyric acid compounds with different polarities. These building blocks were reacted with common aldehydes, namely formaldehyde and isobutyraldehyde, in combination with various isocyanides bearing differently substituted aliphatic groups or hydrophilic substituents such as the morpholino function. This systematic study notably emphasized the impact of the solvent choice on the reaction efficiency and thus on the molar mass of the polymers. A library of unprecedented polypeptoids was prepared accordingly. Thermal properties and solution behaviours of the latter were then characterized and discussed in a structure-property relationship approach. Some of them exhibit pH sensitivity but also thermoresponsiveness with tunable transition temperatures. The biocompatibility of novel water-soluble polypeptoid structures was also validated by cell viability tests.

II.2 Results and discussions

II.2.1 Synthesis of polypeptoids

In a combinatorial approach, four amino acid building blocks were reacted with different aldehydes and isocyanides to design structurally diverse polypeptoids *via* Ugi-4C step-growth polymerization (Scheme 1D). In particular, we selected a series of amino acids in which the distance between the amine and the carboxylic acid moiety is sufficient to prevent the 6-membered ring cyclisation *via* the intramolecular side reaction discussed above. In addition to glycylglycine (*glygly*), we considered another natural dipeptide of β-alanine and histidine, namely *carnosine*, notably because of its protonability and potential as precursors of pH-responsive materials. Two aliphatic and commercially available amino acids, *i.e.* the γ-aminobutyric acid (*aba*) and its hydroxylated derivative, the 4-amino-3-hydroxybutyric acid (*haba*), completed the study.

Table 1. Ugi-4C polymerization of amino acid derivatives with *t*BuNC and formaldehyde.

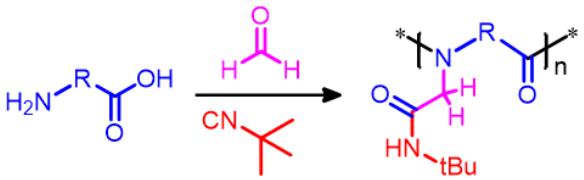

Entry	H_2N-R-CO_2H	Solvent	M_n [a] (g mol^{-1})	M_p [a] (g mol^{-1})	$Đ$ [a]
1	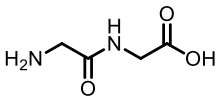	MeOH	3300	4700	1.6
2		H_2O	4600	8100	1.8
3		H_2O /MeOH	5400	11800	2.1
4	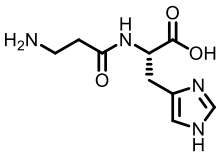	MeOH	1500	1500	1.2
5		H_2O	500	600	1.1
6		H_2O /MeOH	700	1000	1.5
7	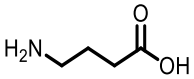	MeOH	2400	3100	1.3
8		H_2O	3400	4300	1.4
9		H_2O /MeOH	5400	8400	1.6
10	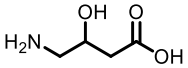	MeOH	2700	3400	1.4
11		H_2O	4200	5400	1.9
12		H_2O /MeOH	4400	6900	1.7

Room temperature polymerization, [H_2N-R-CO_2H]/[formaldehyde]/[*t*BuNC] = 1/1.3/1.3. [a] determined by SEC in DMF using PS calibration.

First, these four amino acid building blocks were reacted with *tert*-butyl isocyanide (*t*BuNC) and formaldehyde (Table 1) in order to vary the structure of the backbone of the polypeptoids while keeping constant the nature of their side chains. Since step-growth polymerization *via* the Ugi-4CR is often carried out in MeOH,[24,38,45] this solvent was selected for our first polymerization assays. All reactions were performed for 24 h at room temperature (RT) under ambient atmosphere using an amino acid concentration of 1.6 M and a slight excess (1.3 equiv.) of monofunctional reagents, *i.e.* *t*BuNC and formaldehyde. As demonstrated elsewhere,[38,46] an excess of monofunctional components guarantees the availability of these reactants even at high

conversions without detrimental effect on the conversion. The four amino acids were insoluble in MeOH, certainly due to the stable zwitterionic form adopted by amino acid (Figure S2) at neutral pH, and the initial polymerization media consisted of a suspension. Along the reaction, the suspension became soluble in the cases of *glygly* and γ-aminobutyric while the products containing *carnosine* and 4-amino-3-hydroxybutyric acid stayed in suspension. At the end of the reactions, products were collected by precipitation in diethyl ether (Et_2O) and analysed by size exclusion chromatography (SEC) in DMF. The macromolecular parameters are presented in Table 1. Under these conditions, the formation of polymers with quite low molar masses was observed in all cases. Concerning the dipeptides, *glygly* gave a polypeptoid with an apparent average molar mass (M_n) of 3300 g mol^{-1} (entry 1, Table 1) whereas oligomers with M_n of about 1500 g mol^{-1} were formed with *carnosine* (entry 4, Table 1). On the other hand, the aliphatic *aba* and *haba* led to polymers with M_n of 2400 and 2700 g mol^{-1} respectively (entries 7 and 10, Table 1).

In order to tackle the solubility issues of the starting materials and to possibly increase the molar mass of the polymers, we carried out the same reactions in water which is known as a suitable solvent for the Ugi-4CR.[50] As anticipated, the four amino acids were soluble in water and polymerizations started in the form of homogeneous solutions. Except for the *carnosine*-based experiment, we observed the precipitation of the polymers during the reaction. Overall, using water as solvent in place of MeOH increased the apparent M_n for all polymerizations of amino acids except *carnosine* (entries 2, 5, 8 and 11, Table 1). Since amino acids are soluble in water and insoluble MeOH and because the opposite trend is observed for the final products, we presumed that a mixture of both solvents (1:1 v:v) would ensure partial solubility of the amino acids while keeping the polymers soluble during the polymerization, which might be helpful to increase the molar masses. Except for *carnosine*, the results confirmed our hypothesis. Indeed, M_n were higher in the MeOH/H_2O mixture than in pure solvents for *glygly*, *aba* and *haba* (entries 3, 9 and 12, Table 1). The improvement is even more striking when comparing the peak molar mass (M_p) which doubled when using a MeOH/H_2O mixture instead of MeOH as the solvent. Water afforded intermediate M_n and M_p for these polymers. However, using a mixture of solvent did not further improve the molar mass of the *carnosine*-based polypeptoid obtained in MeOH (1500 g mol^{-1}).

Besides the solvent, other parameters such as temperature, reaction time and stoichiometry of the reagents were varied in order to optimize the reaction and to possibly increase the molar mass of the polypeptoids (Table S1). As illustrated for the Ugi-4C polymerization of *glygly*, increasing temperature from 20 °C to 50 °C had a detrimental effect on the molar mass (compare

entries 1 and 2 in Table S1). Moreover, prolonging the reaction time from 24 to 120 h did not improve the molecular weight (compare entries 1 and 3 in Table S1). Finally, polypeptoids produced from a stoichiometric amount of reagents had a significantly lower M_n than those synthesized with 1.3 equiv. of *t*BuNC and formaldehyde (1400 and 5400 g mol^{-1} respectively, entries 1 and 4 in Table S1), which emphasized the benefit of using a slight excess of monofunctional reagents in the Ugi-4C polymerization of amino acid derivatives.

In order to gain insight into the reaction and the polymer structure, the *glygly*-based polypeptoid (entry 3, Table 1) was analysed by MALDI-ToF (Figure S3). The MS spectrum showed different populations whose peaks are separated by an interval of 227.13 mass units corresponding to the expected repeating unit. Note that the intensity of the peaks significantly decreased with the molecular weight of the species due to the overestimation of low molecular weight ions.[51] The intense population at low *m/z* (*e.g. m/z* =*n*×227.13 +22.99, *m/z* 704.32 (*n* = 3) *m/z* 931.43 (*n* = 4),…) was attributed to the sodiated macrocyclic compounds. Besides macrocycles, magnification at higher *m/z* values highlighted the presence of linear polymers with a large diversity of chain-ends which emphasizes the great complexity of the termination modes. Unfortunately, at this stage, these populations could not be unambiguously assigned and do not correspond to the most obvious terminal groups such as amine, carboxylic acid, imine, etc.

After this first screening, the synthesis of polymers with decent molar mass, *i.e.* M_p above 3000 g mol^{-1}, was scaled up in order to characterize their structures and properties. For this purpose, the optimized polymerization conditions were used and polypeptoids were purified by dialysis instead of precipitation which was more efficient to remove residual traces of starting materials. Macromolecular parameters of the scaled-up polymers P_1, P_2 and P_3 prepared form *glygly*, *aba* and *haba*, respectively, are presented in Table S2. Their SEC analyses are shown in Figure S4 after purification. ^{1}H NMR analyses performed in DMSO-d_6 confirmed the chemical structures of $P_{1\text{-}3}$ (Figure 1). The three polymers present typical signals of the α-amido amide motif generated by the Ugi-4C reaction, *i.e.* the amidic proton **a** around 7.5 ppm, the methylene protons **b** around 3.9 ppm and the methyl protons **c** of the *tert*-butyl group at 1.3 ppm (Figure 1). 2D NMR experiments (COSY and HSQC) confirmed these assignments and helped to attribute other protons specific to the amino acids (Figure S5). Infrared analyses emphasized the presence of amides with characteristic peaks at 1645 and 1540 cm^{-1} corresponding to the C=O stretching and N−H deformation, respectively, whereas the aliphatic part of the polymers

was evidenced by the CH_3 deformation and CH_2 scissoring peaks between 1460 and 1390 cm^{-1} (Figure S6).

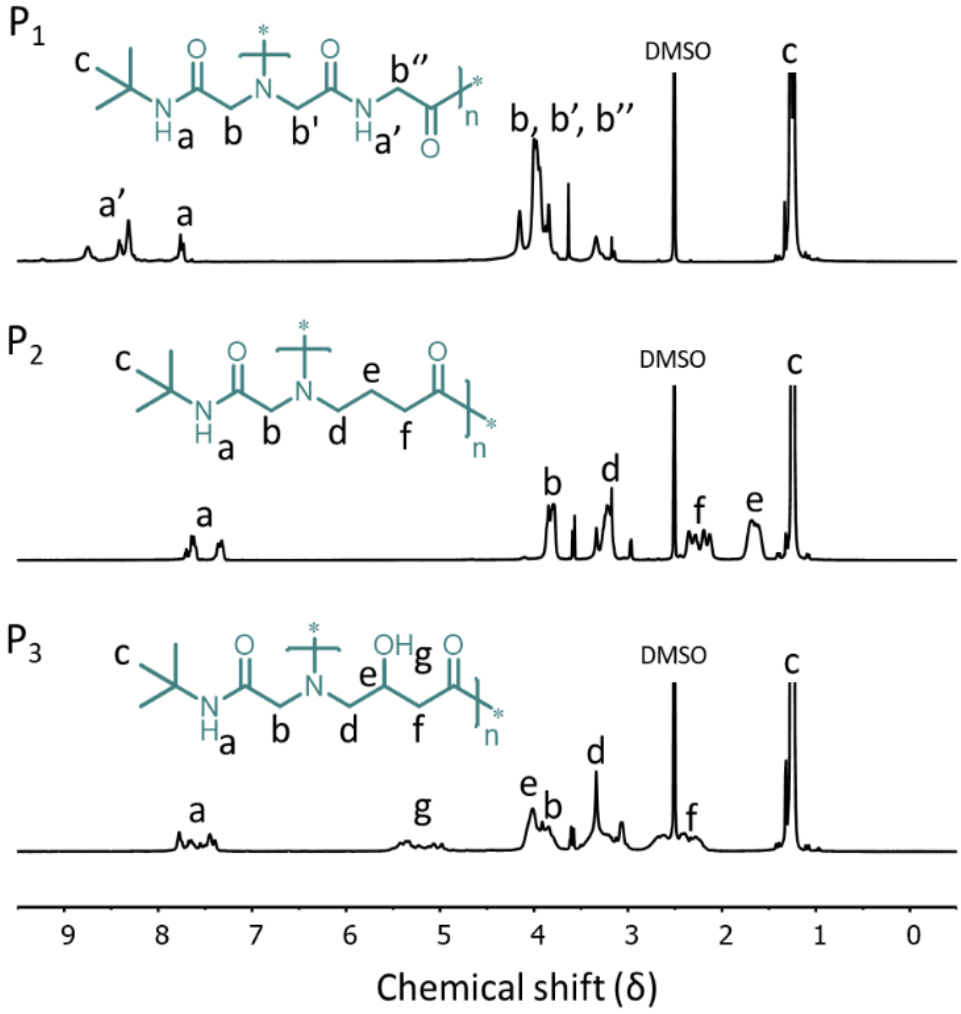

Figure 1. ^1H NMR spectra of P_1, P_2 and P_3 in DMSO-d_6.

Table 2. Ugi-4C polymerization of amino acids with *t*BuNC and isobutyraldehyde.

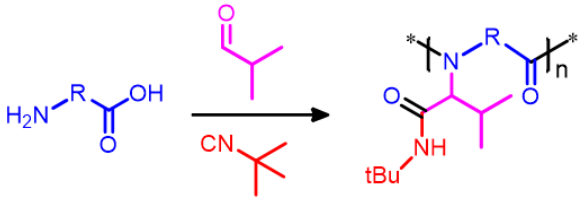

Entry	H_2N-R-CO_2H	Solvent	M_n [a] (g mol^{-1})	M_p [a] (g mol^{-1})	$Đ$ [a]
1	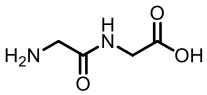	H_2O	2100	5100	1.7
2		H_2O /MeOH	2600	4100	1.6
3		MeOH[b]	5300	12400/1000	2.2
4	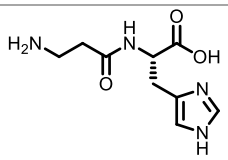	H_2O /MeOH	3300	5300	1.6
5		MeOH	2700	6400/1100	1.9
6	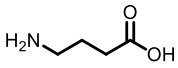	H_2O /MeOH	1700	5200/1000	2.3
7		MeOH[b]	2400	5400	2.0
8	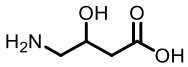	H_2O /MeOH[b]	2100	1900	1.3
9		MeOH[b]	1700	1900	1.2

Room temperature polymerization, [H_2N-R-CO_2H]/[isobutyraldehyde]/[*t*BuCN] = 1/1.3/1.3. [a] Determined by SEC in DMF using PS calibration. [b] Purified by precipitation in H_2O instead of Et_2O.

Next, the polymerization of the four amino acids with *t*BuNC was investigated with another aldehyde, *i.e.* isobutyraldehyde (Table 2). H_2O, MeOH and a mixture of both were considered for the polymerization of *glygly* involving isobutyraldehyde. In spite of a minor secondary peak at 1000 g mol^{-1}, the best results were obtained in MeOH with M_p and M_n equal to 12400 and 5300 g mol^{-1}, respectively (entry 3, Table 2). Trials carried out in water and in water/MeOH gave lower M_n values, *i.e.* 2100 and 2600 g mol^{-1} respectively (entries 1 and 2, Table 2), and the SEC chromatogram showed a broad and multimodal peak for the polymerization in water (Figure S7). The MALDI-TOF analysis of this polypeptoid (entry 3, Table 2) confirmed the nature of the repeating unit (269.17 mass units) and the presence of low molecular weight macrocyclic species (Figure S8). The other three amino acids were reacted with *t*BuNC and isobutyraldehyde in the most promising solvents, *i.e.* MeOH and the MeOH/H_2O mixture. In all the cases, the macromolecular parameters of the polymers were quite similar in both

solvents. Note that *carnosine* gave slightly higher M_n in MeOH/H_2O (3300 g mol^{-1}, entry 4, Table 2) compared to MeOH due to a lower contamination by low molar mass oligomers. *Aba* led to polymers with slightly higher M_n and M_p in MeOH (entry 7, Table 2) while *haba* only produced low molar mass polymers with the M_p below the threshold of 3000 g mol^{-1}. After this second screening, the synthesis of three more polypeptoids (Table 2, entries 3, 4 and 7, respectively) were deemed worthy for the scaling up ($P_{4\text{-}6}$ in Table S2). The structures of $P_{4\text{-}6}$ were corroborated by ^{1}H NMR (Figure 2) and 2D NMR (COSY and HSQC, Figure S9) but also by IR analyses showing characteristic peaks of C=O stretching and N−H deformation of amides at 1645 and 1540 cm^{-1}, respectively (Figure S10).

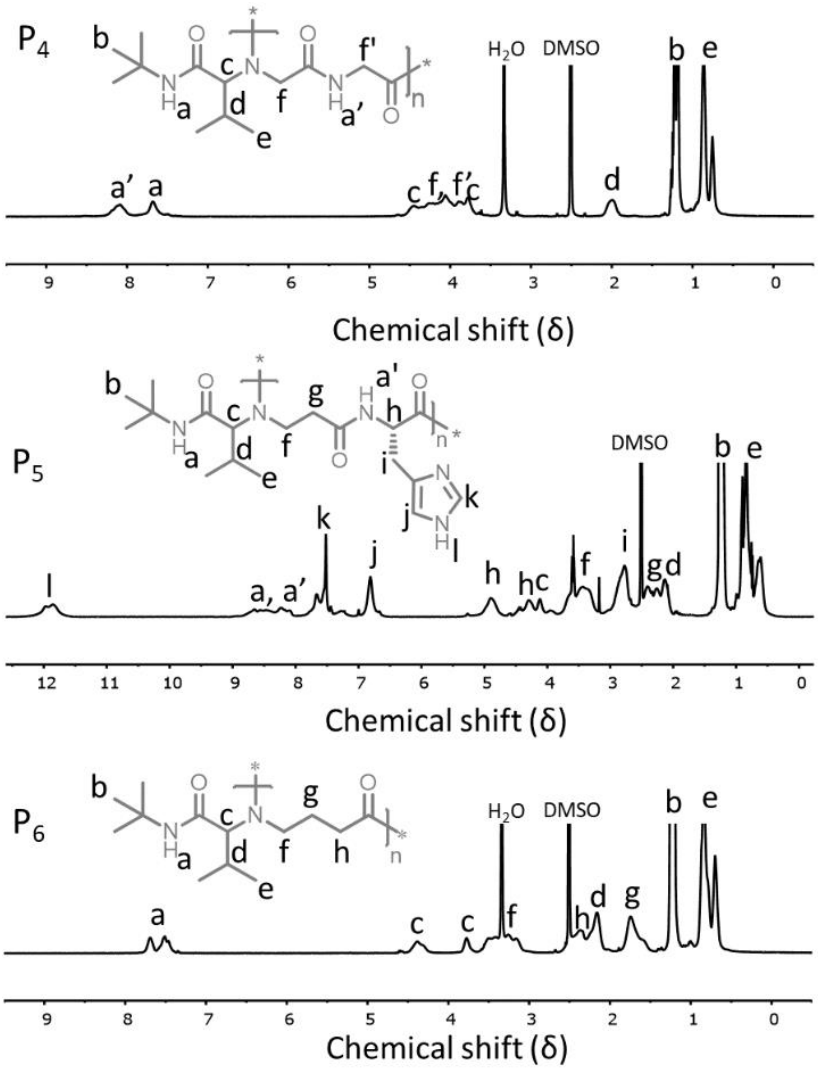

Figure 2. ^{1}H NMR spectra of polypeptoids P_4, P_5 and P_6 in DMSO-d_6 (see Table S2 for details).

Table 3. Ugi-4C polymerization of *glygly* with different aldehydes and isocyanides.

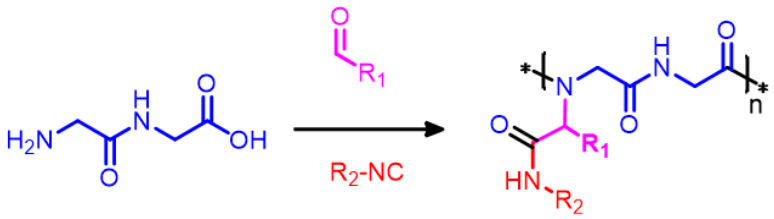

Entry	R_1	R_2	solvent	M_n [a] (g mol^{-1})	M_p [a] (g mol^{-1})	$Đ$ [a]
1	-H	-*t*Bu	H_2O	4600	8100	1.8
2	-H	-cyclohexyl	H_2O	2100	3600	1.8
3	-H	-pentyl	H_2O	1500	2400	2.0
4	-H	$-CH_2CO_2Et$	H_2O	700	700	1.5
5	-H	$-C_2H_4$(*N*-morpholino)	H_2O	600	800	1.3
6	$-CH(CH_3)_2$	-*t*Bu	MeOH[b]	5300	12400 /1000	2.5
7	$-CH(CH_3)_2$	-cyclohexyl	MeOH	3600	5200	1.5
8	$-CH(CH_3)_2$	-pentyl	MeOH[b]	2300	3100	1.5
9	$-CH(CH_3)_2$	$-CH_2CO_2Et$	MeOH[b]	1600	1800	1.2
10	$-CH(CH_3)_2$	$-C_2H_4$(*N*-morpholino)	MeOH	2400	3200	1.5

Room temperature polymerization, [*glygly*]/[R_1CHO]/[R_2NC] = 1/1.3/1.3. [a] determined by SEC in DMF using PS calibration. [b] Purified by precipitation in H_2O instead of Et_2O.

Eventually, a series of isocyanides was tested with both aldehydes in the Ugi-4CP of *glygly*. In addition to *t*BuNC, two aliphatic isocyanides with different lengths and branchings, namely cyclohexyl and *n*-pentyl isocyanide, were reacted for 24 h in water or methanol with *glygly* in the presence of formaldehyde or isobutyraldehyde (entries 1-3 and 6-8, Table 3).

Regardless of the solvent used, we observed a significant decrease of the M_n of the polymer when *t*BuNC was replaced by cyclohexyl (from 5300 g mol^{-1} to 3600 g mol^{-1} in MeOH). The drop in the M_n was even more pronounced for *n*-pentyl isocyanide (2300 g mol^{-1}, entry 6, Table 3). Such a trend suggests that the efficiency of the present Ugi-4CR depends on the bulkiness of the isocyanides. The latter can be estimated by the Charton values (ν) of the substituents ($\nu_{tert\text{-}butyl}$ = 1.24, $\nu_{c\text{-}hexyl}$ = 0.87, $\nu_{n\text{-}pentyl}$ = 0.68) derived from van der Waals radii.[52,53] In these studies, kinetics of various reactions were found to be directly related to the bulkiness of the reagents:

the more bulkier the substituent, the slower the reaction.[52,53] Therefore, the steric hindrance of the isocyanide could have affected the kinetic of concurrent reactions more than the Ugi-4CP itself. This might explain why bulkier isocyanides (*t*Bu > cyclohexyl > *n*-pentyl) led to polypeptoids with higher molecular masses. Finally, two other isocyanides bearing an ester or a morpholino function, namely ethyl isocyanoacetate and 2-morpholinoethyl isocyanide, were tested. Oligomers were obtained (M_n of 700 and 600 g mol^{-1}) when the reaction was performed in water with formaldehyde (entries 4 and 5, Table 3) whereas their polymerization in MeOH with isobutyraldehyde gave higher M_n especially for 2-morpholinoethyl isocyanide (M_n =2400 g mol^{-1}, M_P = 3200 g mol^{-1}) (entry 10, Table 3). Four novel polypeptoids (P_{7-10}, Table S2) were scaled up (entries 2, 7, 8 and 10, Table 3) and characterized by NMR (Figures S11 and S12) and IR (Figure S13). Overall, a library of ten novel polypeptoids differing by the nature of their backbone and/or side chains was produced by Ugi-4CP highlighting the strength of this combinatorial MCR approach. Thereafter, thermal and solution properties of these unique polymers were measured and put in perspective with their structural variations.

II.2.2 Thermal properties of polypeptoids

Polypeptoids P_{1-10} present different backbones formed by the amino acids and various side chains composed of aldehydes and isocyanides, all articulated around a typical α-amido amide moiety generated by Ugi-4CR. Such a systematic variation of the reactants allowed us to study the relationship between the structure of the polypeptoids and their thermal properties. All polymers were submitted to thermal gravimetric analysis (TGA) to determine their onset degradation temperature, that is, the temperature at 5 weight% of loss (T_{OD}) (Figure S14). Differential scanning calorimetry (DSC) analyses were also carried out to measure their glass transition temperatures (T_g) and their melting temperatures (T_m) (Figure S15). Although the thermal properties of polymers depend in a certain extent on their degree of polymerization, in this study, we considered polymers with molar masses in the same range.

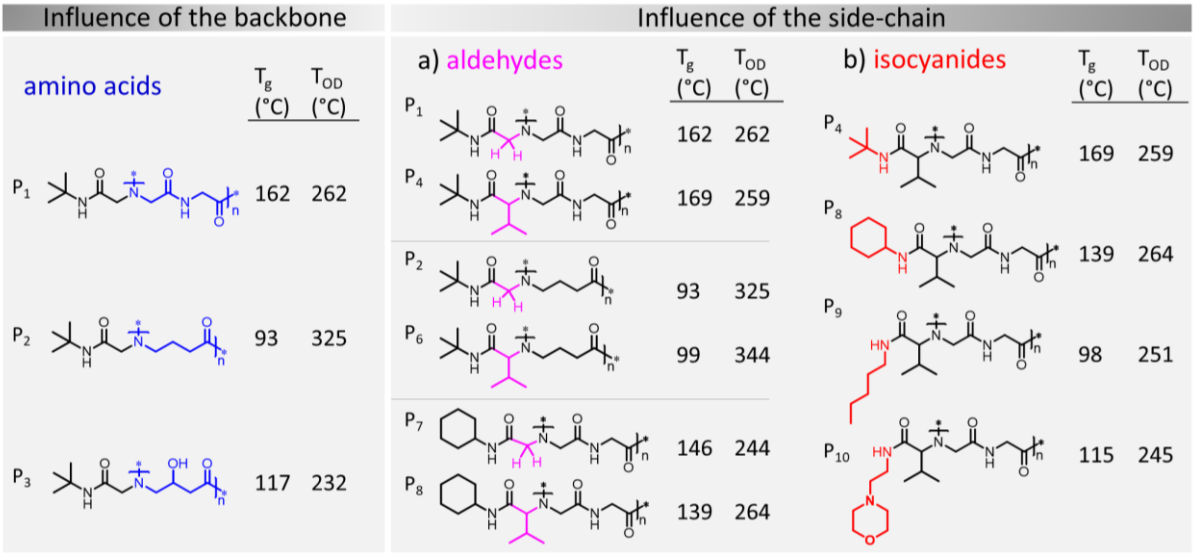

Figure 3. Comparison of the thermal properties of polypeptoids with various backbones and/or side chains.

First, the thermal properties of $P_{1\text{-}3}$ having identical side chains with three different backbones made of *glygly*, *aba* and *haba*, were compared (Figure 3). The *aba*-based polymer P_2 with aliphatic carbons between the peptoid bonds showed the highest thermal stability with a T_{OD} equal to 325 °C. Introduction of an additional peptide bond within the repeating unit of the polypeptoid, *i.e. glygly*-based polymer P_1, decreased the T_{OD} by 63 °C. The decrease of the onset degradation temperature was even greater for the *haba*-based polymer P_3 (T_{OD} = 232 °C) likely due to the elimination of the hydroxyl group similarly to the degradation of poly(vinylalcohol) (PVA).[54] This hypothesis is comforted by the degradation profile of P_3 showing a two-steps degradation like the poly(vinyl alcohol) (Figure S14).[55] On the other hand, no T_m was detected in the DSC analyses of $P_{1\text{-}3}$ (Figure S15). Among them, P_2 presented the lowest T_g (93 °C) as a result of the relatively high flexibility of the aliphatic sections of the main chain. Interestingly, the presence of an alcohol in P_3 increased the T_g to 117 °C. In this case, the alcohol moieties probably induce extra intermolecular hydrogen bond interactions which reduce the chain mobility. Moreover, the formation of a six-membered ring *via* intramolecular H-bond between the alcohol and the adjacent tertiary amide can also rigidify the backbone (Figure S16). As anticipated, P_1 had the highest T_g (162 °C) among the three polymers. Indeed, the peptide bond within repeating unit of P_1 certainly favors interchain interactions *via* H-bonding but also the formation of a five-membered *via* intramolecular hydrogen bond interaction between the secondary and tertiary amides, as shown in Figure S16, which stiffens the main chain.

The influence of the side chains, and thus of the choice of the aldehyde and isocyanide, on the thermal properties of the polypeptoids was then examined (Figure 3). In this perspective, we considered three pairs of polymers (P_1-P_4, P_2-P_6 and P_7-P_8) which differ by the aldehyde used in their synthesis (*i.e.* formaldehyde or isobutyraldehyde). In each couple of polymers, the maximum variations in T_{OD} and T_g were smaller than 20 °C and 10 °C, respectively, highlighting the limited impact of this group on the thermal properties. On the other hand, polypeptoids produced from different isocyanides (P_4, P_8, P_9 and P_{10}) showed no differences regarding their T_{OD} meaning that their degradation mainly depends on the backbone structure. In contrast, the choice of the isocyanide precursor significantly affected the T_g. In the series of aliphatic isocyanides, the glass transition of the resulting polypeptoids decreased in the following order: *tert*-butyl > cyclohexyl > *n*-pentyl ($T_{g\,P4} > T_{g\,P8} > T_{g\,P9}$). In order to rationalize these observations, it is worth considering a recent study by Gomez *et al.*[56] demonstrating that the dynamics of the backbone and the side chain of a polymer, in that case polythiophene, are mutually affected. Briefly, an increase of the side chain mobility led to an increase of the backbone mobility and eventually to a decrease of T_g. The dynamics of an atom of the side chain was shown to increase with its distance from the backbone underlying the dependence of the mobility of the chains on the length of the alkyl side group. When comparing branched and linear alkyl chains with the same number of carbon atoms, the mobility of the former was lower since its carbons are located closer to the main chains. These conclusions were validated for polypeptoids with different side chain lengths.[57] In the light of these considerations, the lower T_g observed for P_9 compared to P_4, bearing a *n*-pentyl and *tert*-butyl group respectively, can be rationalized by the higher mobility of the *n*-pentyl group. The same reasoning applies to the higher T_g of P_8 bearing a cyclohexyl group compared to P_9 (*n*-pentyl) since atoms of cyclohexyl are closer to the main chain and the mobility of this group is restrained by its cyclic structure. A similar trend was reported for poly(methacrylate)s with *n*-pentyl and cyclohexyl pending moieties and supported by the free volume theory.[56] Eventually, the lower T_g of P_8 compared to P_4 can also be explained based on the distance between the atoms of the side chain and the backbone which is higher for the furthest methylene group of cyclohexyl compared to the methyl ends of *tert*-butyl. Note that P_{10} with morpholino lateral groups exhibited a quite similar T_{OD} (251 °C) and intermediate T_g (115 °C) in comparison to their aliphatic counterparts.

II.2.3 Solution behaviour

Polymers that respond to stimuli such as changes of temperature or external pH are steadily gaining increasing interest for advanced applications especially in the biomedical field.[58–60] In

this context, the aqueous solution behaviour of our library of polypeptoids $P_{1\text{-}10}$ was examined under different conditions. A first screening showed that five polypeptoids are soluble in water at a concentration of 2 mg mL^{-1}. These include $P_{1\text{-}3}$, all produced from formaldehyde. In contrast, the corresponding polymers obtained from isobutyraldehyde were insoluble probably due to the higher hydrophobicity and bulkiness of the lateral chain. The sole exceptions were polypeptoids P_{10} and P_5 which possess polar morpholino and imidazole pending groups. Note that P_{10} was soluble in water in the whole range of pH while the solubilization of the *carnosine*-based polymer P_5 required an acidic medium as discussed below.

The polypeptoid P_5 exhibited a pH-responsive behaviour and solubilized in water after protonation of the pendant imidazole of the histidine units. The pK_a of P_5, measured by basic titration of an acidified solution of P_5, was found equal to 5.9 (Figure 4A).
During the titration, the precipitation of P_5 began at pH 5.8, so close to the measured pK_a. This behaviour was very similar to that of poly-*L*-histidine which is soluble below pH 6 near its pK_a. Interestingly, the sudden pH rise suggests that the protonability of the histidine side chain does not depend on neighbouring interactions. It was confirmed by the Henderson-Hasselbalch equation (equation 1).[61]

$$pH = pK_a - m\,log\left(\frac{1-\alpha}{\alpha}\right) \qquad (1)$$

where α corresponds to the degree of neutralization, K_a is the average dissociation constant and the parameter *m* reflects the electrostatic interaction between neighbour ionizable groups.

In practice, the *m* value of P_5 was extracted from the slope of Henderson-Hasselbalch plots in a region where α value ranges between 0.2 and 0.6 (Figure S17). It was equal to 1 showing the absence of neighbouring interactions within P_5. By comparison, the *m* value of poly(vinylamine)s having a high density of amine functions is around 5.3.[62]

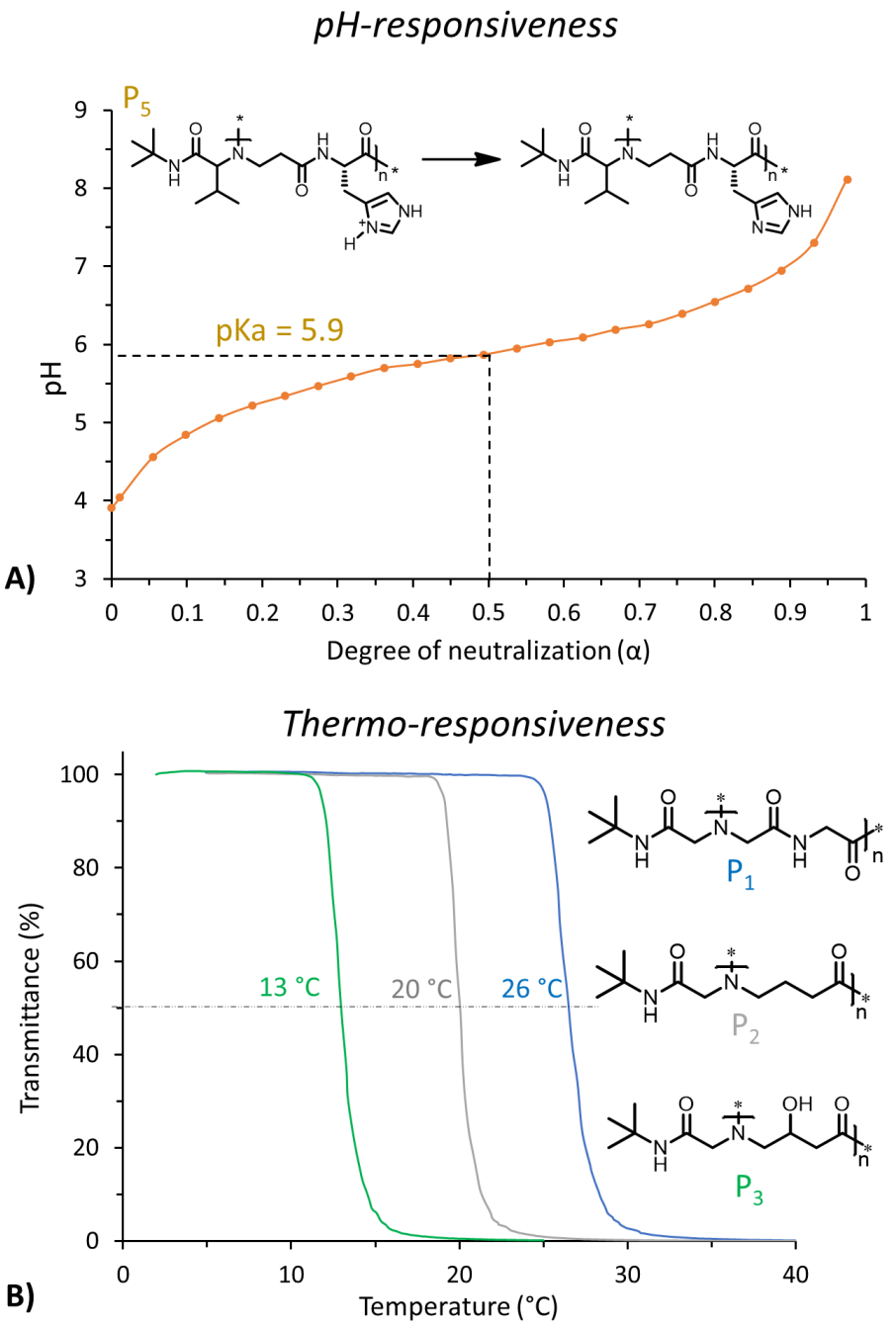

Figure 4. A) pH *vs* the degree of neutralization for titrations of *carnosine* and P_5 with NaOH. B) Transmittance vs temperature for turbidimetry measurements of aqueous solution of P_1, P_2 and P_3 at a concentration of 2 mg mL^{-1}.

The possible thermoresponsiveness of the polypeptoids P_1, P_2, P_3, P_5 and P_{10} was also explored. The starting polymer solutions (2 mg mL^{-1}) were prepared at low temperature (6 °C) and neutral pH, except for P_5 which was dissolved in 60 mM HCl to ensure its solubility. The thermal response of the polypeptoid solutions was studied by monitoring the evolution of their transmittance at 260 nm during heating and cooling cycles. The cloud point temperature (T_{CP}),

that is the temperature above which a demixing of phases occurs, was measured at 50% loss of transmittance. Concerning P_5 and P_{10}, no thermoresponsive behaviour was observed upon heating the polymer solutions (2 mg mL^{-1}) until 90 °C. In these cases, the imidazolium and morpholino group drastically enhanced the solubility of the polypeptoids preventing their solution demixing. As an additional proof of their improved solubility, more than 50 mg of P_5 and P_{10} were dissolved per mL of water. In contrast, the *glygly*-based polypeptoid P_1 exhibited a T_{CP} at 26.5 °C upon heating, in perfect accordance with previous observations (Figure 4B).[46] The reversibility of the transition was attested by monitoring the transmittance during the cooling (Figure S18). In this case, a hysteresis phenomenon of few degrees was observed suggesting the formation of intermolecular hydrogen bonds in the collapsed state *via* the secondary amides, as was the case for poly(*N*-isopropylacrylamide).[63] Expectedly, the corresponding *aba*-based polypeptoids P_2 showed a lower T_{CP} value (20 °C) compared to P_1 due to the increase of the hydrophobicity of the backbone resulting from the substitution of a secondary amide for an aliphatic chain (Figure 4B). More surprisingly, the introduction of a polar hydroxyl group within the aminobutyric acid backbone P_3 further decreased T_{CP} to 13 °C suggesting that the −OH groups are preferentially involved in inter- or intra-chain interactions rather than in the solvation of the polymer. All in all, we identified three thermoresponsive polypeptoids with specific transition temperatures.

II.2.4 Cell viability

As a first evaluation of the potential of these novel polypeptoid sequences in the biomedical field, we assessed their cytotoxicity towards HeLa cells *via* MTS assay. In this study, we considered polymers that are soluble at 37 °C in the cell culture medium at certain concentrations ranging from at 100-1000 µg mL^{-1}, namely P_1, P_2 and P_{10}. More precisely, clear solutions of P_1 and P_2 could be prepared for concentrations of 500 µg mL^{-1} and 100 µg mL^{-1}, respectively, and the morpholino-functional P_{10} was soluble at all concentrations. In addition to our polypeptoids, poly(ethylene glycol) (PEG) (5000 g mol^{-1}) was selected as a common standard.[24,64] In practice, cells were incubated at 37 °C for 72 hours with the polymer and cell viability was expressed as a percentage relative to the controls containing no polymers set at 100%. The data are presented in Figure 5. The PEG standard logically exhibited a low cytotoxicity towards HeLa cells with a minimal viability of 88 % at 1000 µg mL^{-1}. Importantly, the *glygly*-based P_1 and P_{10} as well as the *aba*-containing P_2 showed excellent cell viability levels that were statistically similar to those of PEG. A cell viability slightly higher than 100% was measured for P_1 due to statistical error. Interestingly, for the morpholino-functional P_{10}, we

noticed a slight increase of the toxicity with the increase of its concentration but its intrinsic cell viability remained competitive to PEG even at the highest concentration. This dependence of cell viability on the concentration of P_{10} was confirmed by a one-way ANOVA test (Figure S19). Overall, the data clearly demonstrated the low toxicity of these polypeptoid sequences obtained by this single-step MCP without advanced purification.

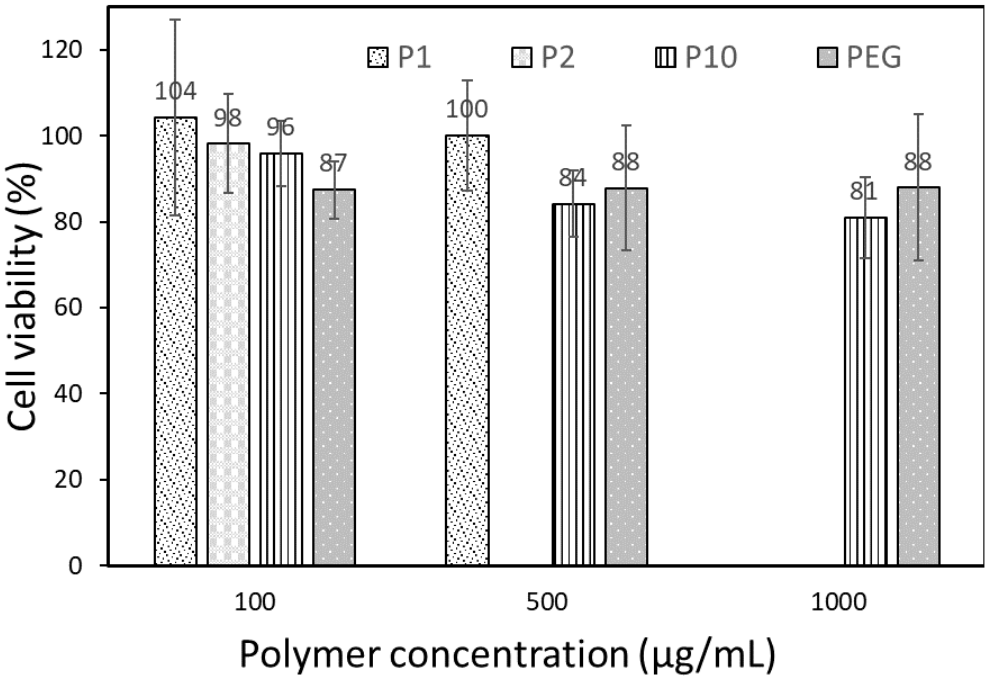

Figure 5. Cell viability of P_1, P_2 and P_{10} compared with PEG_{5K} evaluated by the MTS method after 72 h of incubation with HeLa cells at 37 °C. The error bars represent the standard deviations.

II.3 Conclusions

In summary, we developed a straightforward one-step synthesis of polypeptoid analogues *via* Ugi-4C polymerization of amino acid derivatives. In a combinatorial approach, a wide variety of reactants, namely amino acids, aldehydes and isocyanides, were considered in this multicomponent polymerization with the aim to prepare a library of structurally diversely polypeptoids. The polymerization conditions were optimized and scaled up for ten unprecedented polymers. The systematic variation of the three constituents of the reaction allowed us to study the influence of a change in the backbone or in the side chain on the thermal and solution properties of the polypeptoids. It notably revealed that the T_g of the polypeptoids markedly depends on the choice of the amino acid and of the isocyanide while changing the

aldehyde has little impact on their thermal properties. In contrast, the replacement of formaldehyde for isobutyraldehyde strongly affects the water solubility of the polymer. In this respect, we highlighted the excellent water solubility of the morpholino-functionalized P_{10}, the pH-responsiveness of the *carnosine*-based P_5 and the thermo-responsiveness of a series of polypeptoids $P_{1\text{-}3}$ with various transition temperatures. The low cytotoxicity of some polypeptoid structures was also demonstrated. Considering the ease of this multicomponent polymerization, the great variety of potential substrates and the valuable properties of the polymers prepared accordingly, this approach is attractive to sustain the demand for innovative polypeptoid analogues and the applications resulting therefrom.

II.4 References

(1) Luxenhofer, R.; Fetsch, C.; Grossmann, A. *J. Polym. Sci. Part A Polym. Chem.* **2013**, *51* (13), 2731–2752.

(2) Secker, C.; Brosnan, S. M.; Luxenhofer, R.; Schlaad, H. *Macromol. Biosci.* **2015**, *15* (7), 881–891.

(3) Matharage, J. M.; Minna, J. D.; Brekken, R. A.; Udugamasooriya, D. G. *ACS Chem. Biol.* **2015**, *10* (12), 2891–2899.

(4) Jahnsen, R. D.; Frimodt-Møller, N.; Franzyk, H. *J. Med. Chem.* **2012**, *55* (16), 7253–7261.

(5) Buckle, D. R.; Erhardt, P. W.; Ganellin, C. R.; Kobayashi, T.; Perun, T. J.; Proudfoot, J.; Senn-Bilfinger, J. *Pure Appl. Chem.* **2013**, *85* (8), 1725–1758.

(6) Roy, O.; Caumes, C.; Esvan, Y.; Didierjean, C.; Faure, S.; Taillefumier, C. *Org. Lett.* **2013**, *15* (9), 2246–2249.

(7) Laursen, J. S.; Engel-Andreasen, J.; Olsen, C. A. *Acc. Chem. Res.* **2015**, *48* (10), 2696–2704.

(8) Lee, B.-C.; Zuckermann, R. N.; Dill, K. A. *J. Am. Chem. Soc.* **2005**, *127* (31), 10999–11009.

(9) Rosales, A. M.; Murnen, H. K.; Kline, S. R.; Zuckermann, R. N.; Segalman, R. A. *Soft Matter* **2012**, *8* (13), 3673–3680.

(10) Kirshenbaum, K.; Barron, A. E.; Goldsmith, R. A.; Armand, P.; Bradley, E. K.; Truong, K. T. V.; Dill, K. A.; Cohen, F. E.; Zuckermann, R. N. *Proc. Natl. Acad. Sci. U. S. A.* **1998**, *95* (8), 4303–4308.

(11) Armand, P.; Kirshenbaum, K.; Goldsmith, R. A.; Farr-Jones, S.; Barron, A. E.; Truong, K. T. V; Dill, K. A.; Mierke, D. F.; Cohen, F. E.; Zuckermann, R. N.; Bradley, E. K.

Proc. Natl. Acad. Sci. **1998**, *95* (8), 4309–4314.

(12) Goodman, M.; Chen, F.; Prince, F. R. *Biopolymers* **1973**, *12* (11), 2549–2561.

(13) Shin, S. B. Y.; Yoo, B.; Todaro, L. J.; Kirshenbaum, K. *J. Am. Chem. Soc.* **2007**, *129* (11), 3218–3225.

(14) Pokorski, J. K.; Miller Jenkins, L. M.; Feng, H.; Durell, S. R.; Bai, Y.; Appella, D. H. *Org. Lett.* **2007**, *9* (12), 2381–2383.

(15) Gordon, D. J.; Sciarretta, K. L.; Meredith, S. C. *Biochemistry* **2001**, *40* (28), 8237–8245.

(16) Fetsch, C.; Grossmann, A.; Holz, L.; Nawroth, J. F.; Luxenhofer, R. *Macromolecules* **2011**, *44* (17), 6746–6758.

(17) Lin, S.; Zhang, B.; Skoumal, M. J.; Ramunno, B.; Li, X.; Wesdemiotis, C.; Liu, L.; Jia, L. *Biomacromolecules* **2011**, *12* (7), 2573–2582.

(18) Brown, N. J.; Dohm, M. T.; Bernardino de la Serna, J.; Barron, A. E. *Biophys. J.* **2011**, *101* (5), 1076–1085.

(19) Miller, S. M.; Simon, R. J.; Ng, S.; Zuckermann, R. N.; Kerr, J. M.; Moos, W. H. *Drug Dev. Res.* **1995**, *35* (1), 20–32.

(20) Bruno, B. J.; Miller, G. D.; Lim, C. S. *Ther. Deliv.* **2013**, *4* (11), 1443–1467.

(21) Hamman, J. H.; Enslin, G. M.; Kotzé, A. F. *BioDrugs* **2005**, *19* (3), 165–177.

(22) Frokjaer, S.; Otzen, D. E. *Nat. Rev. Drug Discov.* **2005**, *4* (4), 298–306.

(23) Lahasky, S. H.; Hu, X.; Zhang, D. *ACS Macro Lett.* **2012**, *1* (5), 580–584.

(24) Tao, Y.; Wang, S.; Zhang, X.; Wang, Z.; Tao, Y.; Wang, X. *Biomacromolecules* **2018**, *19* (3), 936–942.

(25) Sun, J.; Zuckermann, R. N. *ACS Nano* **2013**, *7* (6), 4715–4732.

(26) Zhang, D.; Lahasky, S. H.; Guo, L.; Lee, C.-U.; Lavan, M. *Macromolecules* **2012**, *45* (15), 5833–5841.

(27) Knight, A. S.; Zhou, E. Y.; Francis, M. B.; Zuckermann, R. N. *Adv. Mater.* **2015**, *27* (38), 5665–5691.

(28) Kruijtzer, J. A. W.; Hofmeyer, L. J. F.; Heerma, W.; Versluis, C.; Liskamp, R. M. J. *Chem. – A Eur. J.* **1998**, *4* (8), 1570–1580.

(29) Simon, R. J.; Kania, R. S.; Zuckermann, R. N.; Huebner, V. D.; Jewell, D. A.; Banville, S.; Ng, S.; Wang, L.; Rosenberg, S.; Marlowe, C. K. *Proc. Natl. Acad. Sci.* **1992**, *89* (20), 9367 LP – 9371.

(30) Gao, Y.; Kodadek, T. *Chem. Biol.* **2013**, *20* (3), 360–369.

(31) Zuckermann, R. N.; Kerr, J. M.; Kent, S. B. H.; Moos, W. H. *J. Am. Chem. Soc.* **1992**,

114 (26), 10646–10647.

(32) Gangloff, N.; Fetsch, C.; Luxenhofer, R. *Macromol. Rapid Commun.* **2013**, *34* (12), 997–1001.

(33) Gangloff, N.; Ulbricht, J.; Lorson, T.; Schlaad, H.; Luxenhofer, R. *Chem. Rev.* **2016**, *116* (4), 1753–1802.

(34) Grossmann, A.; Luxenhofer, R. *Macromol. Rapid Commun.* **2012**, *33* (19), 1714–1719.

(35) Chai, J.; Liu, G.; Chaicharoen, K.; Wesdemiotis, C.; Jia, L. *Macromolecules* **2008**, *41* (23), 8980–8985.

(36) Marcaccini, S.; Torroba, T. *Nat. Protoc.* **2007**, *2* (3), 632–639.

(37) Medeiros, G. A.; da Silva, W. A.; Bataglion, G. A.; Ferreira, D. A. C.; de Oliveira, H. C. B.; Eberlin, M. N.; Neto, B. A. D. *Chem. Commun.* **2014**, *50* (3), 338–340.

(38) Sehlinger, A.; Dannecker, P. K.; Kreye, O.; Meier, M. A. R. *Macromolecules* **2014**, *47* (9), 2774–2783.

(39) Kakuchi, R. *Angew. Chemie Int. Ed.* **2014**, *53* (1), 46–48.

(40) Gangloff, N.; Nahm, D.; Döring, L.; Kuckling, D.; Luxenhofer, R. *J. Polym. Sci. Part A Polym. Chem.* **2015**, *53* (14), 1680–1686.

(41) Stiernet, P.; Lecomte, P.; De Winter, J.; Debuigne, A. *ACS Macro Lett.* **2019**, *8* (4), 427–434.

(42) Tao, Y.; Wang, Z.; Tao, Y. *Biopolymers* **2019**, *110* (6), e23288.

(43) Wang, S.; Tao, Y.; Wang, J.; Tao, Y.; Wang, X. *Chem. Sci.* **2019**, *10* (5), 1531–1538.

(44) Hartweg, M.; Edwards-Gayle, C. J. C.; Radvar, E.; Collis, D.; Reza, M.; Kaupp, M.; Steinkoenig, J.; Ruokolainen, J.; Rambo, R.; Barner-Kowollik, C.; Hamley, I. W.; Azevedo, H. S.; Becer, C. R. *Polym. Chem.* **2018**, *9* (4), 482–489.

(45) Zhang, X.; Wang, S.; Liu, J.; Xie, Z.; Luan, S.; Xiao, C.; Tao, Y.; Wang, X. *ACS Macro Lett.* **2016**, *5* (9), 1049–1054.

(46) Al Samad, A.; De Winter, J.; Gerbaux, P.; Jérôme, C.; Debuigne, A. *Chem. Commun.* **2017**, *53* (90), 12240–12243.

(47) Koyama, Y.; Gudeangadi, P. G. *Chem. Commun.* **2017**, *53* (27), 3846–3849.

(48) Koyama, Y.; Ihsan, A. B.; Taira, T.; Imura, T. *RSC Adv.* **2018**, *8* (14), 7509–7513.

(49) Ihsan, A. Bin; Taniguchi, M.; Koyama, Y. *Macromol. Rapid Commun.* **2020**, *n/a* (n/a), 2000480.

(50) Pirrung, M. C.; Das Sarma, K. *J. Am. Chem. Soc.* **2004**, *126* (2), 444–445.

(51) Lloyd, P. M.; Suddaby, K. G.; Varney, J. E.; Scrivener, E.; Derrick, P. J.; Haddleton, D. M. *Eur. Mass Spectrom.* **1995**, *1* (3), 293–300.

(52) Charton, M. *J. Am. Chem. Soc.* **1975**, *97* (6), 1552–1556.

(53) Gavin, D. P.; Stephens, J. C. *Arkivoc* **2011**, *2011* (9), 407–421.

(54) Alexy, P.; Bakoš, D.; Crkoňová, G.; Kolomaznik, K.; Kršiak, M. *Macromol. Symp.* **2001**, *170* (1), 41–50.

(55) Peng, Z.; Kong, L. X. *Polym. Degrad. Stab.* **2007**, *92* (6), 1061–1071.

(56) Zhan, P.; Zhang, W.; Jacobs, I. E.; Nisson, D. M.; Xie, R.; Weissen, A. R.; Colby, R. H.; Moulé, A. J.; Milner, S. T.; Maranas, J. K.; Gomez, E. D. *J. Polym. Sci. Part B Polym. Phys.* **2018**, *56* (17), 1193–1202.

(57) Fetsch, C.; Luxenhofer, R. *Polymers*. 2013, pp 112–127.

(58) Sponchioni, M.; Capasso Palmiero, U.; Moscatelli, D. *Mater. Sci. Eng. C* **2019**, *102*, 589–605.

(59) Shen, Y.; Fu, X.; Fu, W.; Li, Z. *Chem. Soc. Rev.* **2015**, *44* (3), 612–622.

(60) Krannig, K.-S.; Schlaad, H. *J. Am. Chem. Soc.* **2012**, *134* (45), 18542–18545.

(61) Lee, E. S.; Shin, H. J.; Na, K.; Bae, Y. H. *J. Control. Release* **2003**, *90* (3), 363–374.

(62) Kobayashi, S.; Suh, K. Do; Shirokura, Y. *Macromolecules* **1989**, *22* (5), 2363–2366.

(63) Cheng, H.; Shen, L.; Wu, C. *Macromolecules* **2006**, *39* (6), 2325–2329.

(64) Zhang, J.; Zhang, M.; Du, F.; Li, Z. *Macromolecules* **2016**, *49* (7), 2592–2600.

II.5 Experimental Section

Materials. *tert*-butyl isocyanide (*t*BuNC) (98 %), cyclohexyl isocyanide (98 %), 1-pentyl isocyanide (97 %), formaldehyde (37 wt % in H_2O) were purchased from Sigma-Aldrich, γ-aminobutyric acid (> 99 %), 2-Morpholinoethyl isocyanide (> 98 %), ethyl isocyanoacetate (95 %), glycylglycine (> 99 %), isobutyraldehyde (> 99 %) were purchased from Acros Organic and 4-amino-3-hydroxybutyric acid (> 98 %) was purchased from Tokyo Chemical Industry Europe (TCI). Beta-alanyl-L-histidine (98 %) was purchased from abcr and dimethylformamide (DMF) and diethylether (Et_2O) were purchased from VWR Chemical. Methanol (MeOH) was purchased from Fisher Chemical. All chemicals and solvents were used without purification. Spectra/Por® dialysis tubings (cut-off, 1 kDa) were purchased from SpectrumLabs. DMEM solution: 89% Dulbecco's Modified Eagle's Medium, high glucose (4,5 g L^{-1} D-glucose, GlutaMAX™ Supplement, pyruvate (Gibco, Grand Island, NY, United States), 10% fetal bovine serum (Gibco, Grand Island, NY, United States), 1% of antibiotics (penicillin/streptomycin 10 000 U/10 000 µg ml^{-1}) (Lonza, Basel, Switzerland). DMEM/F-12 no phenol red (Gibco, Grand Island, NY, United States and CellTiter 96® Aqueous One Solution Cell Proliferation Assay (MTS) (Promega, Leiden, The Netherlands) were obtained.

Characterization. Molar masses (M_n, M_w) and dispersity ($Đ$) of the polymers were characterized by size exclusion chromatography (SEC) at 55 °C in dimethylformamide (DMF) containing LiBr (0.025 M) using a flow rate of 1 mL min^{-1} with polystyrene calibration. SEC curves were recorded with a Waters chromatograph equipped with two columns (Waters Styragel pss gram 100 Å (×2) in an oven at 55 °C and a refractive index detector (Waters 2414) working at 40 °C. ^{1}H NMR, HSQC and COSY spectra were recorded at 298 K with a Bruker Avance III HD spectrometer (B_0=9.04 T) (400 MHz) and treated with MestReNova software. IR spectra were recorded on Thermo Fischer Scientific Nicolet IS5 equipped with an ATR ID5 module using a diamond crystal (650 cm^{-1} −4000 cm^{-1}). Differential scanning calorimetry (DSC) was performed on a TA Instruments Q1000 DSC, using hermetic aluminium pans, indium standard for calibration, nitrogen as the purge gas, and a sample weight of ∼5 mg. The sample was cooled down to −80 °C at 20 °C min^{-1} cooling rate, followed by an isotherm at −80°C for 2 min and heating up to 180 °C at 10 °C min^{-1} heating rate. These cycles were repeated twice. The fourth cycle (last heating from −80 to 180 °C) was analysed. Thermogravimetric analysis (TGA) analyses were carried out with a TGA 2 large furnace from Mettler Toledo under nitrogen at a heating rate of 20°C min^{-1} from ambient temperature to 600 °C with a sample weight of ∼10 mg. Turbidity was determined by measuring the absorbance at

260 nm on a un Jasco v-630 spectrophotometer. The polymers (P_1, P_2, P_3, P_5 and P_{10}) were dissolved in water Milli-Q (2 mg mL^{-1}) and subjected to heating-cooling cycles in a quartz cuvette at a constant rate of 2 °C min^{-1} in a temperature controlled multicell holder. pH measurements were realized on a pH/ORP meter HANNA HI2211. The calibration of the instrument was realized with HANNA buffer solutions at pH of 7.01 and 4.01 before the titrations. Regarding the HeLa cells viability, the CellTiter 96® Aqueous One Solution Cell Proliferation Assay is based on similar principles to the widely used MTT assay. The active component is a tetrazolium compound called MTS (similar to MTT and its derivatives), which is reduced to a coloured formazan product. The amount of the formazan product is directly proportional to the number of living cells; therefore, cell proliferation or death can be quantified by reading the plate at 490 nm. The absorbance was read at 490 nm using the Powerwave X microplate spectrophotometer (BioTek Instrument Inc., Winooski, USA) and the viability was calculated and normalized from the absorbance of control samples taken as 100%.

The Matrix-Assisted Laser Desorption/Ionization Time-of-Flight (MALDI-ToF) mass spectra were recorded using a Waters QToF Premier mass spectrometer equipped with a Nd:YAG laser using the 3rd harmonic with a wave length of 355 nm. In the context of this study, a maximum output of ~65 µJ is delivered to the sample in 2.2 ns pulses at 50 Hz repeating rate. Time-of-flight mass analyses were performed in the reflection mode at a resolution of about 10 000. *trans*-2-(3-(4-*tert*-Butyl-phenyl)-2-methyl-2-propenylidene)malononitrile (DCTB) was used as the matrix and was prepared as a 40 mg ml^{-1} solution in chloroform. The matrix solution (1 µL) was applied to a stainless-steel target and air-dried. Polymer samples were dissolved in adequate solvent to obtain 1 mg mL^{-1} solutions and 20 µL of NaI solution (2 mg mL^{-1} in acetonitrile) were added as source of cationization agent. Then, 1 µL aliquots of these solutions were applied onto the target area (already bearing the matrix crystals) and then air-dried**.**

General procedure for the Ugi-4C polymerization. In a typical experiment, the amino acid (1.0 mmol) was dissolved in 0.62 mL of H_2O Milli-Q, MeOH or a H_2O/MeOH mixture (1:1 v:v). Aldehyde (1.3 mmol) was added to the stirred solution at room temperature followed by addition of isocyanide (1.3 mmol). The polymerization was carried out at room temperature. After 24 h of reaction, the crude mixture was dried under vacuum and the remaining solid was dissolved in MeOH (0.5 mL) then precipitated in 10 mL of Et_2O unless otherwise stated. Centrifugation was applied when necessary to recover the precipitate. The polymers were analysed by NMR in deuterated DMSO and SEC in DMF/LiBr.

Synthesis of poly(peptide-*alt*-peptoids) P_1-P_{10} *via* Ugi-4C polymerization. In all experiments, the corresponding amino acid (4 mmol) was dissolved in 2.48 mL of water Milli-Q water/MeOH (1:1 v:v) or MeOH. Aldehyde (5.2 mmol) was added to the stirred solution at room temperature followed by addition of isocyanide (5.2 mmol). The polymerization carried out at room temperature. After 24 h of reaction, the crude mixture was dried under vacuum and the remaining solid was dissolved in MeOH (10 mL) then dialyzed against MeOH (cut-off 1 kDa) during 24 h except for P_7 and P_8 for which the dialysis was performed in DMF. The collected polymers (see Table S2) were analysed by SEC in DMF/LiBr with polystyrene calibration, by NMR (^{1}H, HSQC, COSY, HMBC) (30 mg mL^{-1} of deuterated DMSO), ATR, TGA and DSC.

Titration of P_5. The polymer solution (0.05 M) was prepared by solubilization of 272.6 mg of P_5 in 15 mL of a HCl solution (0.1 M). A solution of sodium hydroxide was prepared by solubilization of 1 g in 250 mL Milli-Q water and calibrated with oxalic acid dihydrate in presence of phenolphthalein. The NaOH concentration was 0.1019 M. The pH was monitored with pH meter after each addition of 0.5 or 0.2 mL of NaOH solution in 10 mL of the polymer solution.

Cell Viability. Solutions containing the polymers P_1, P_2, P_{10} and PEG_{5K} were prepared at the desired concentrations (1000, 500 and 100 µg mL^{-1} of DMEM) under aseptic conditions by filtration through 0.2 µm filter and kept at 6 °C. HeLa cells were seeded in 96-well plates at a density of 2000 cells per well. The cells were incubated in DMEM at 37 °C and 5% of CO_2. After 24 h, fresh media containing the polymers were added to the corresponding wells after removing the old media. Each condition was replicated in five wells. On the same plate, we prepared 5 controls which contain no polymers as well as 5 blanks that contain no cell nor polymer. After incubation for 72 h at 37 °C under 5% of CO_2, the wells were washed three times with DMEM-F12 and cell viability was measured by the MTS method. Cell viability was expressed as a percentage relative to the controls set at 100%. The experiment was repeated two more times. The final results are given by the averages of each measurement which are normalized for each plate using the average of the controls set at 100%. The standard deviations are represented by error bars after removal of outliers.

II.6 Supporting information

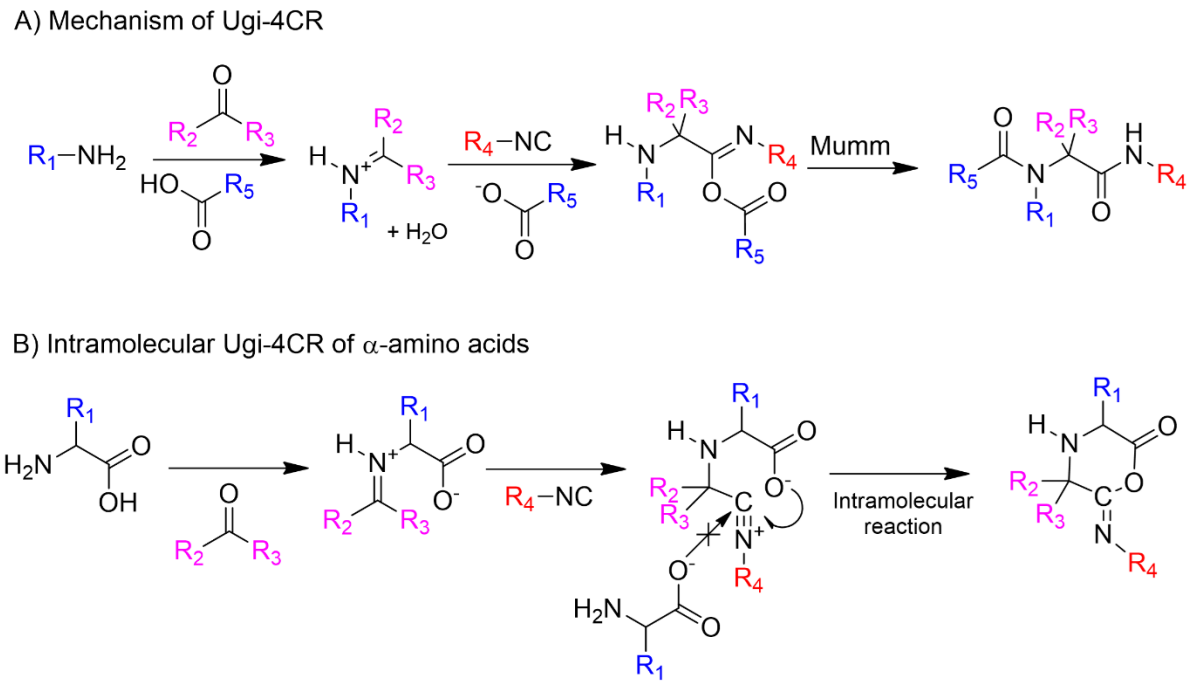

Figure S1. A) Mechanism of Ugi-4CR and B) Intramolecular Ugi-4CR of α-amino acids leading to six-membered ring intermediate.

Figure S2. Displaced equilibrium between neutral and zwitterionic forms of amino acid around neutral pH.

Table S1. Ugi-4C polymerization of glygly : Effect of temperature, time and stoichiometry.

Entry	Temperature (°C)	Time (hours)	[glygly]/ [formaldehyde]/ [*t*BuNC]	M_n (g mol^{-1})[a]	M_p (g mol^{-1})[a]	$Đ$[a]
1	20	24	1/1.3/1.3	5400	11800	2.09
2	50	24	1/1.3/1.3	3100	6100	2.04
3	20	120	1/1.3/1.3	5600	10000	1.77
4	20	24	1/1/1	1400	4200	2.54

Conditions: polymerization in 0.62 mL H_2O/MeOH (1:1 v:v). [a] determined by SEC in DMF using PS calibration.

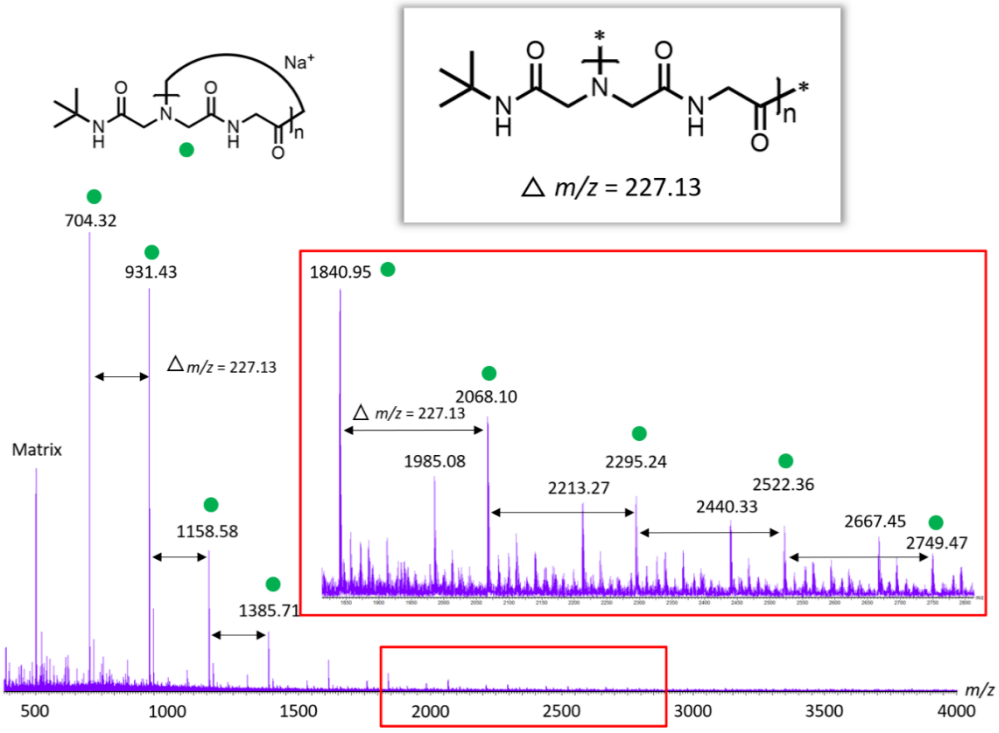

Figure S3. MALDI-ToF spectrum and magnification between *m/z* 1800 – 2800 of the polypeptoid obtained from glygly/tBuNC/formaldehyde (entry 3, Table 1).

Table S2. Synthesis and purification of polymers P_1-P_{10}.

		Before Dialysis		After dialysis		
Entry	Polymer	M_w [a] (g mol^{-1})	M_n [a] (g mol^{-1})	M_w [a] (g mol^{-1})	M_n [a] (g mol^{-1})	Yield [b] (%)
P_1	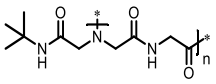	9600	4900	10500	5900	83
P_2	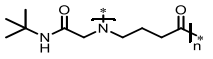	6500	3500	7100	4200	72
P_3	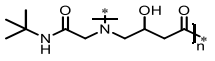	6600	3800	7100	4600	70
P_4	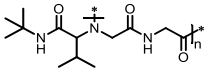	7400	3100	11600	7900	54
P_5	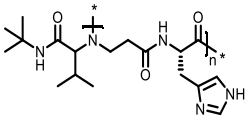	3900	2600	5000	3500	70
P_6	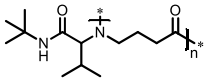	5400	1800	11600	8000	33
P_7	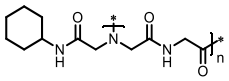	5500	3200	6000	4000	35
P_8	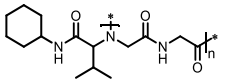	4600	2700	5100	3400	45
P_9	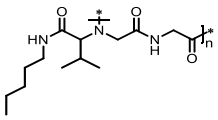	2000	1600	4200	3200	24
P_{10}	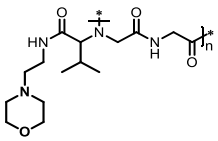	3300	2200	5700	3600	42

The polymerizations were carried out at r.t. in water/MeOH (1:1 v:v) mixture (P_1, P_2, P_3, P_6 and P_7) or in MeOH (P_4, P_5, P_8, P_9 and P_{10}). [H_2N-R-CO_2H]/[aldehyde]/[isocyanide] = 1/1.3/1.3, 24 hours. Purification by dialysis (cut-off of 1kD). **[a]** Determined by SEC in DMF using PS calibration. **[b]** Isolated yields were determined by gravimetry after dialysis.

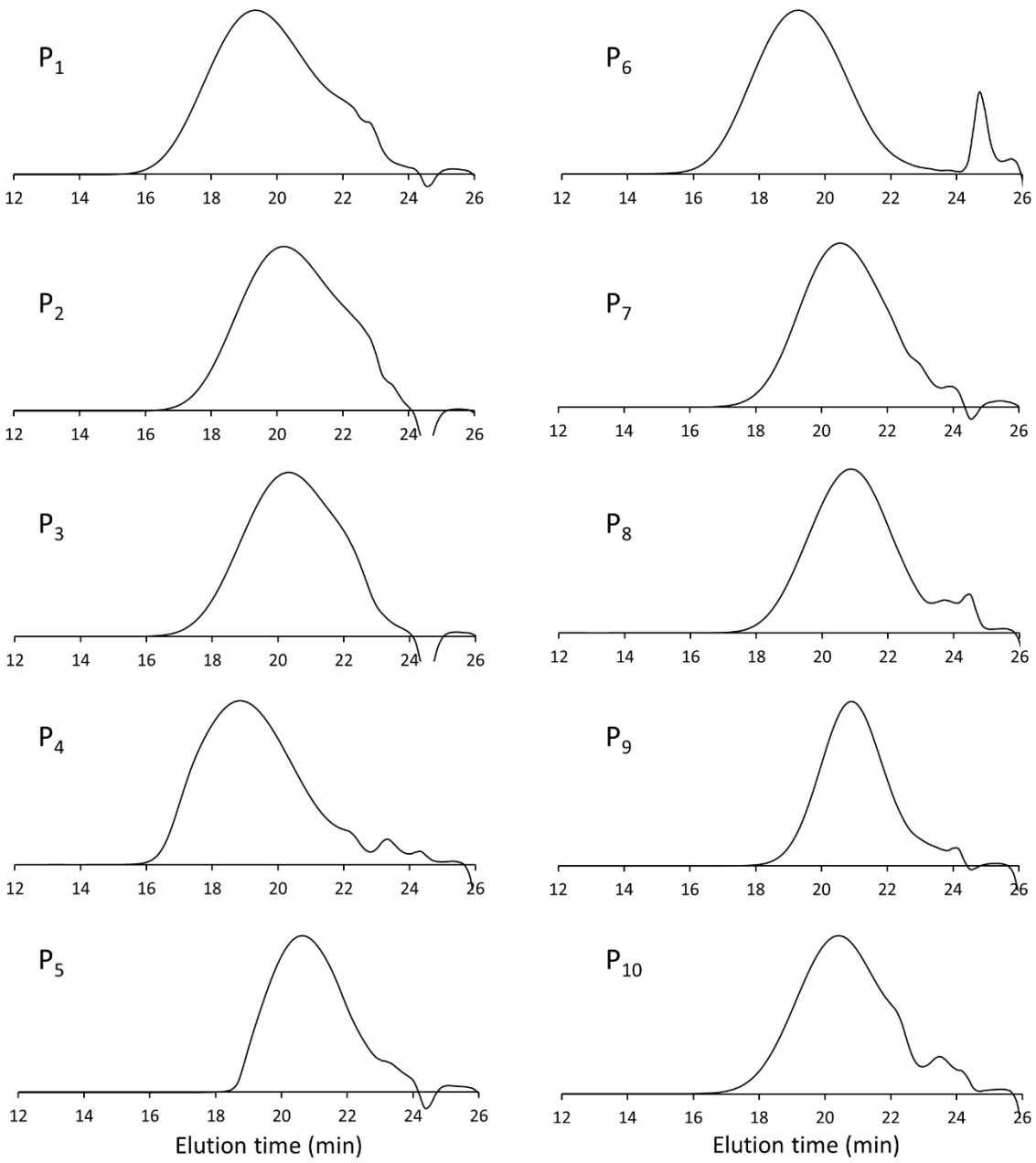

Figure S4. Size exclusion chromatography of polymers P_1-P_{10} after purification by dialysis.

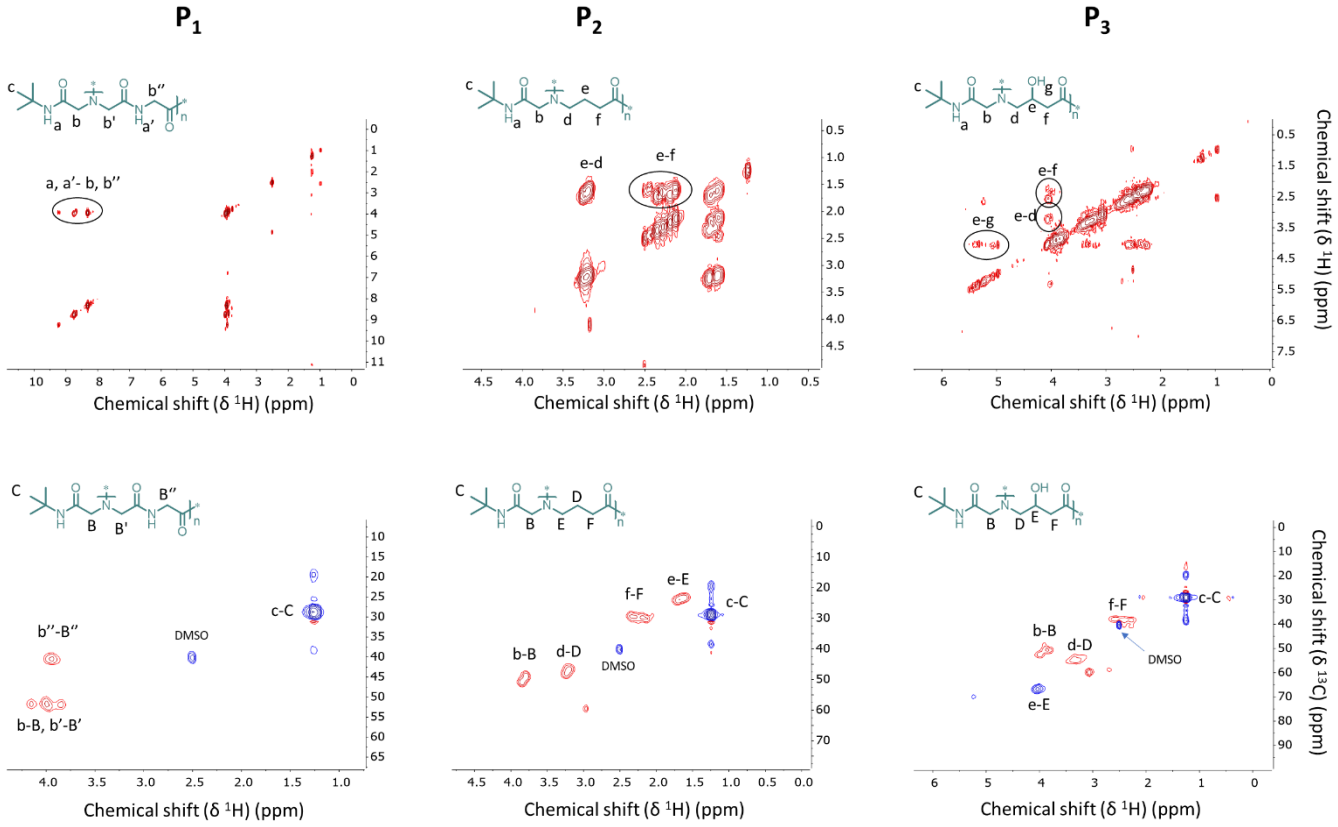

Figure S5. COSY and HSQC NMR spectra of P_1, P_2 and P_3 presented in Table S1. The lowercase letters and capital letters design protons and carbon respectively.

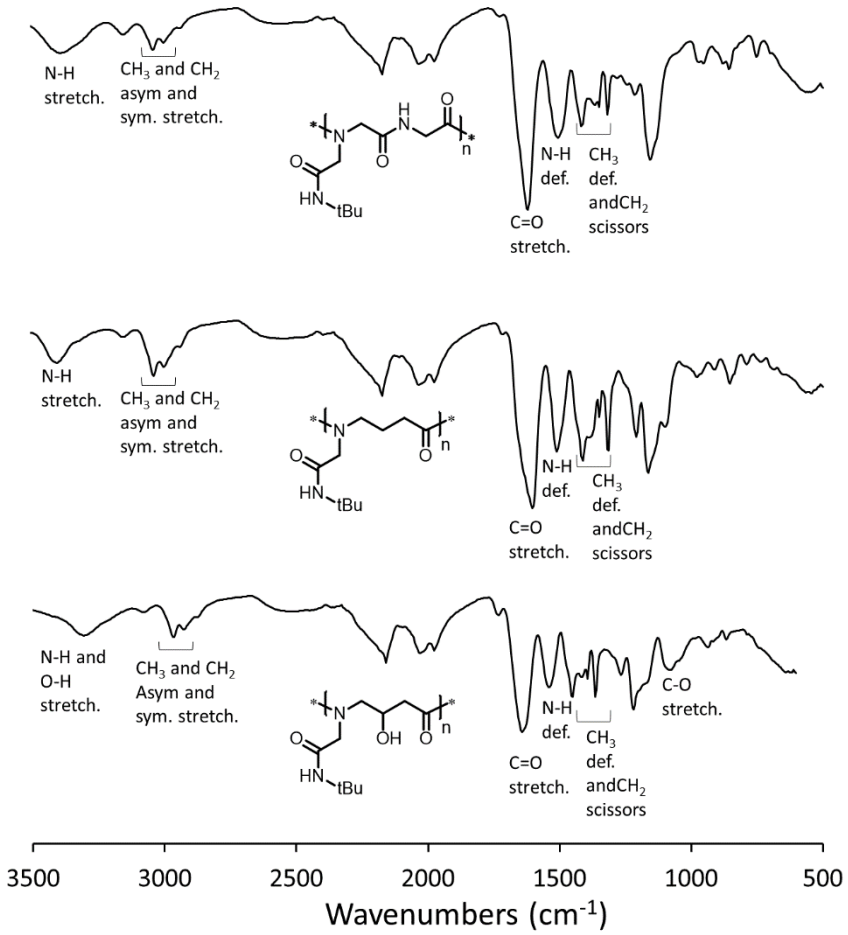

Figure S6. ATR spectra of P_1, P_2 and P_3 presented in Table S1. Peaks between 1900 and 2500 cm^{-1} corresponds to the signal of diamond phonon band.

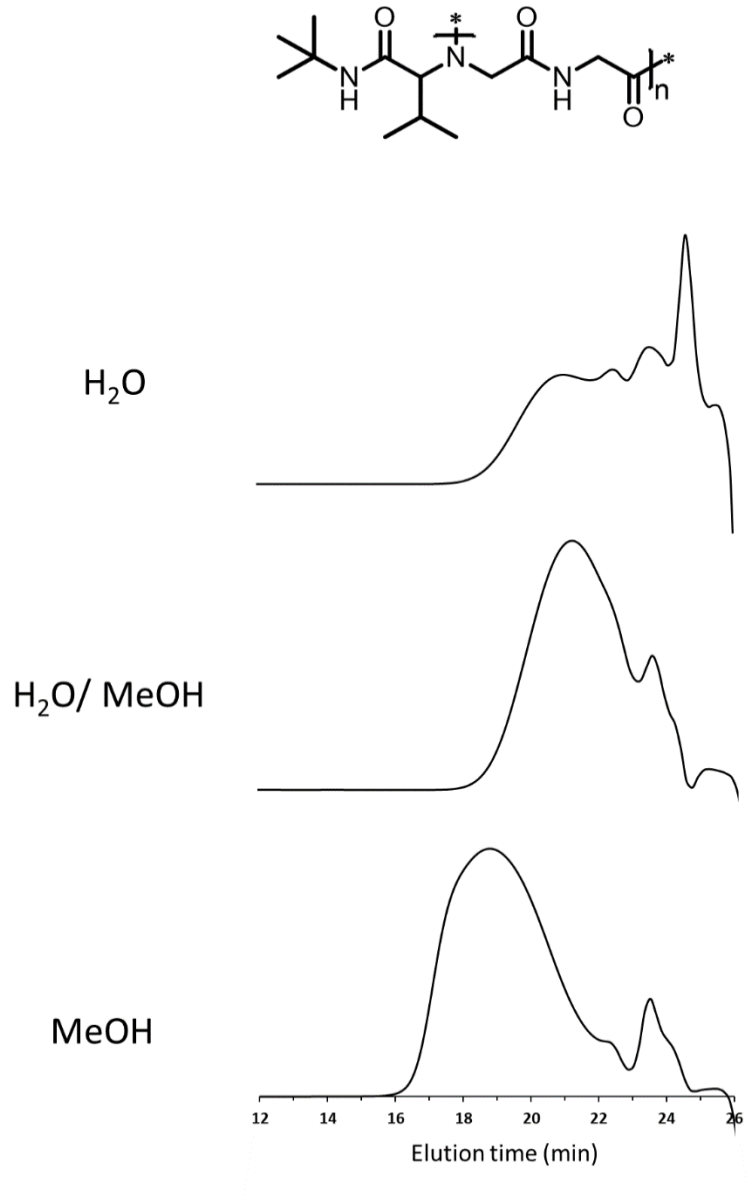

Figure S7. SEC chromatograms for the polymerizations of Gly-Gly with isobutyraldehyde and *tert*-butyl isocyanide in different solvents. Macromolecular parameters (M_n, M_w and $Đ$) are presented in Table 2.

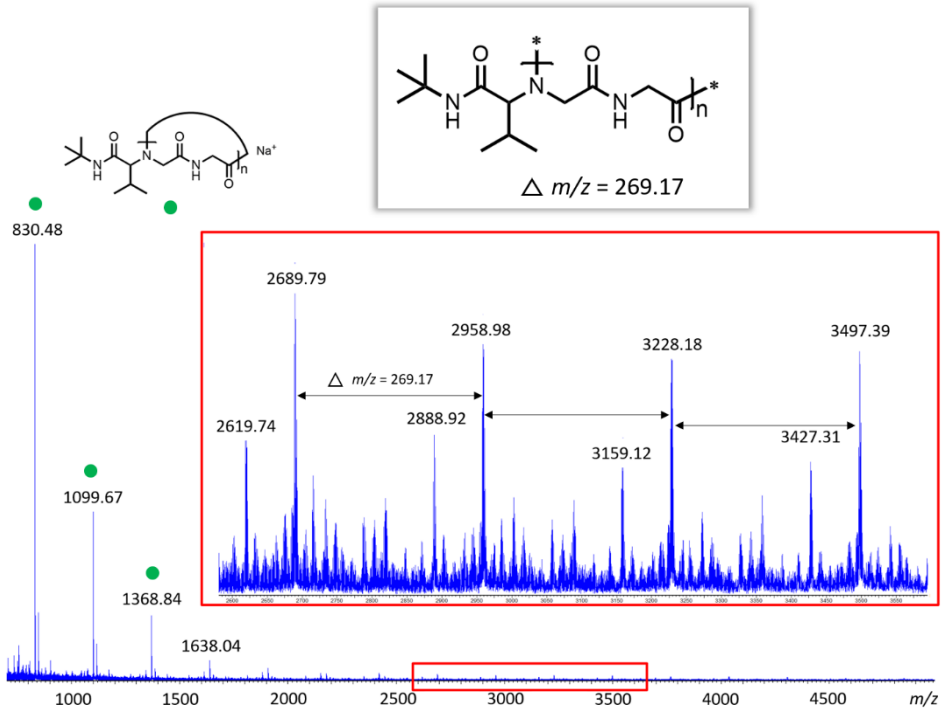

Figure S8. MALDI-ToF spectrum and magnification between *m/z* 2600 – 3600 of the polypeptoid obtained from glygly/tBuNC/isobutyraldehyde (entry 3, Table 2).

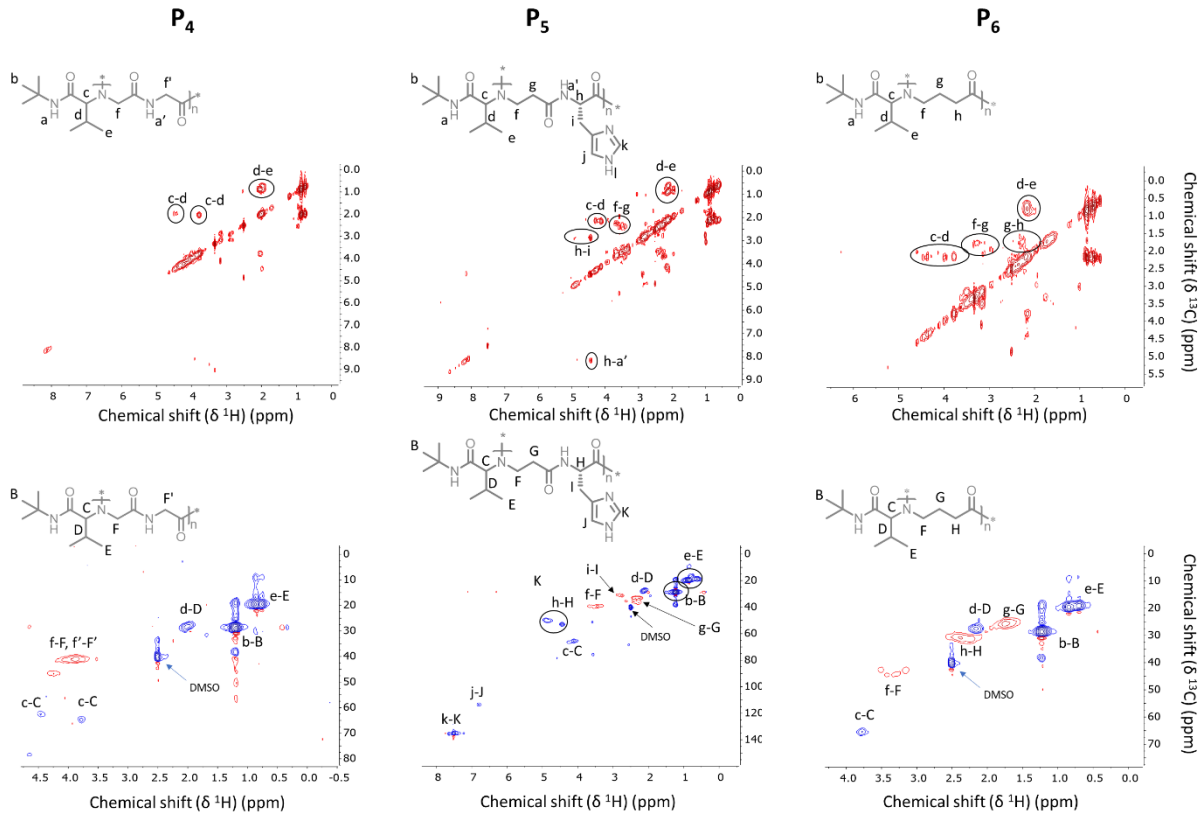

Figure S9. COSY and HSQC NMR spectra of P_4, P_5 and P_6 presented in Table S1. The lowercase letters and capital letters design protons and carbon respectively.

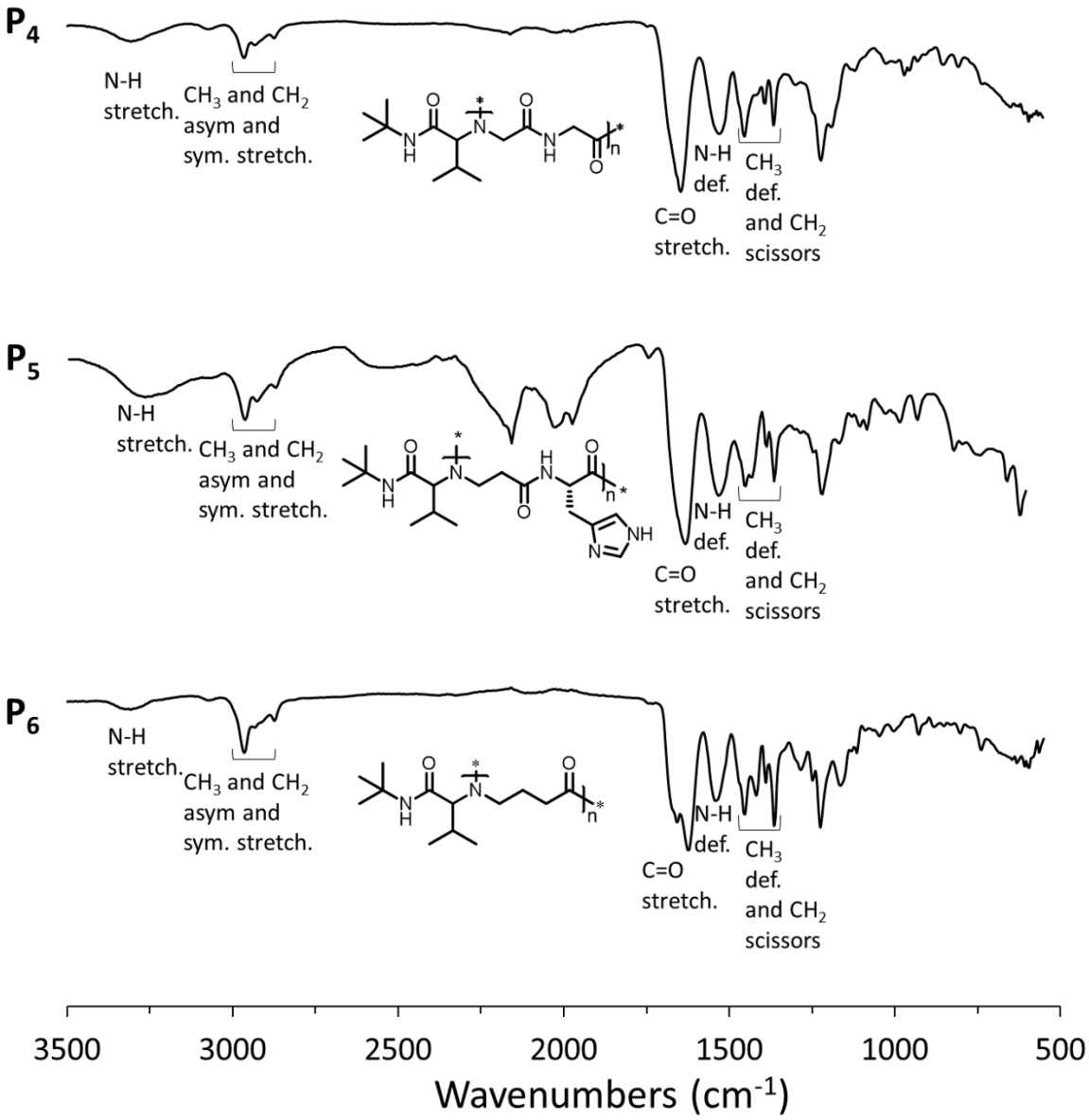

Figure S10. ATR spectra of P_4, P_5 and P_6 presented in table S1. Peaks between 1900 and 2500 cm^{-1} corresponds to the signal of diamond phonon band.

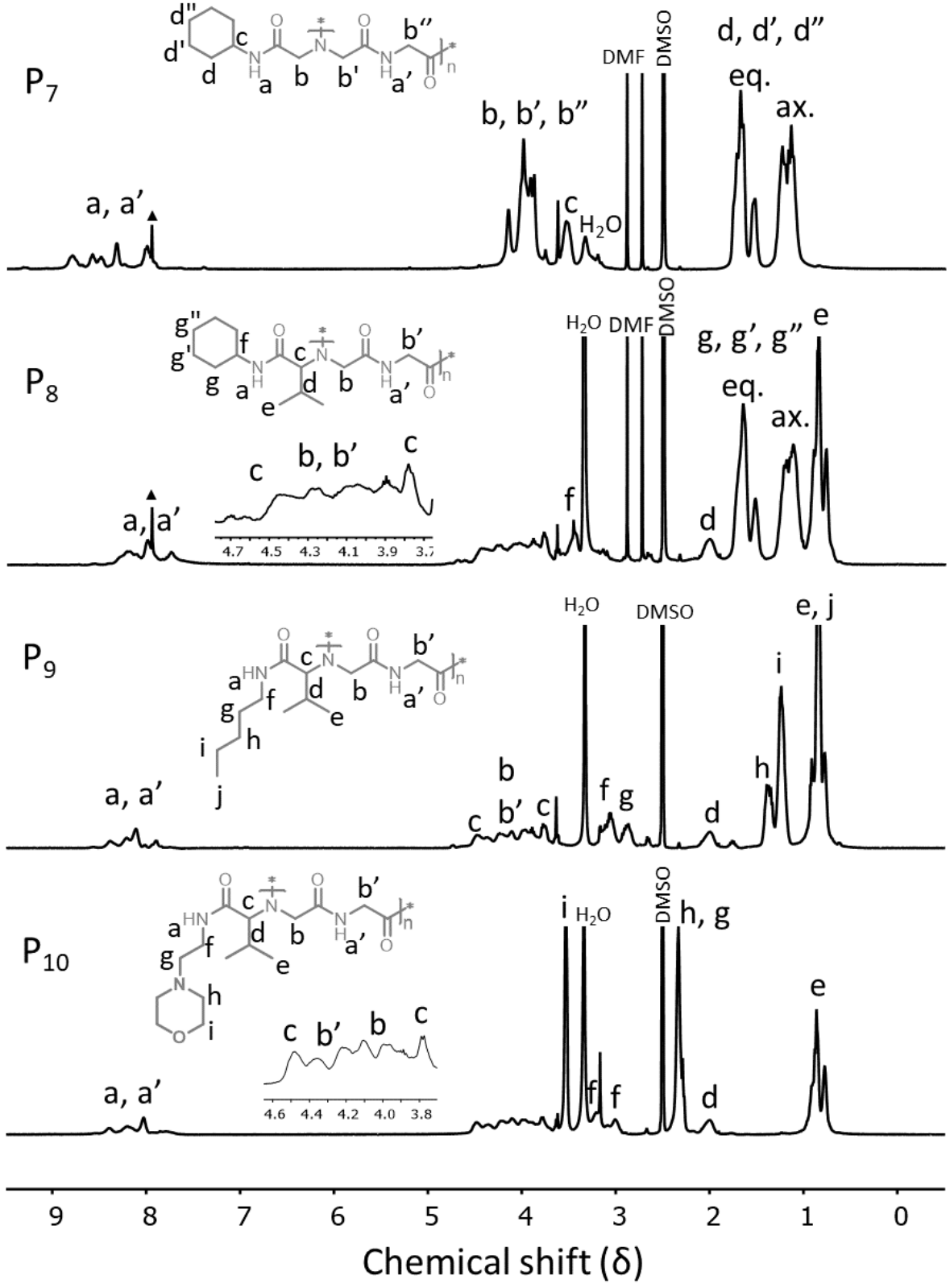

Figure S11. ^{1}H NMR spectra of P_7, P_8, P_9 and P_{10} presented in Table S1 in deuterated DMSO.

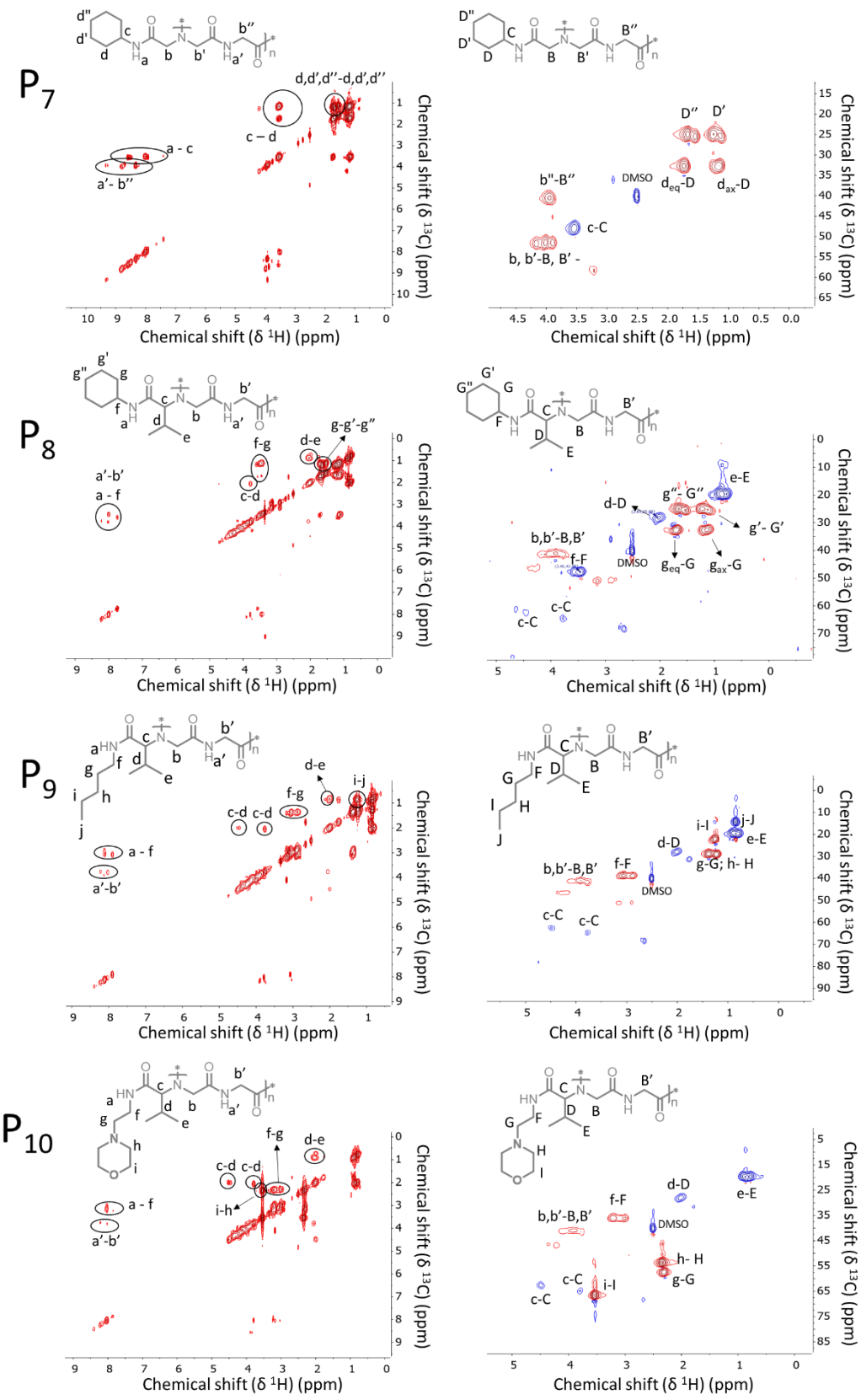

Figure S12. COSY and HSQC NMR spectra of P_7, P_8, P_9 and P_{10} presented in Table S1 in deuterated DMSO. The lowercase letters and capital letters design protons and carbon respectively.

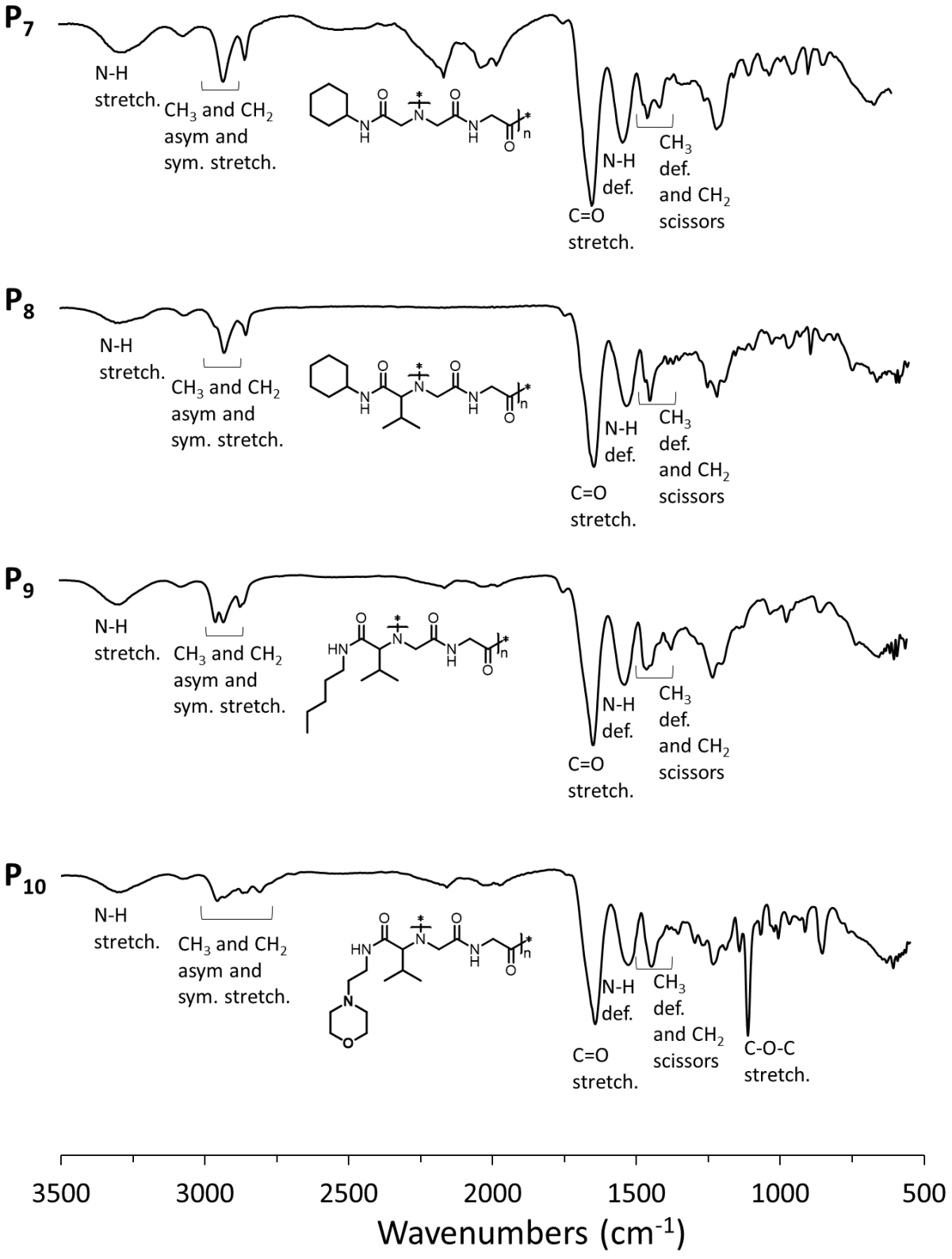

Figure S13. ATR spectra of P_4, P_5 and P_6 presented in Table S1. The Peaks between 1900 and 2500 cm^{-1} corresponds to the signal of diamond phonon band.

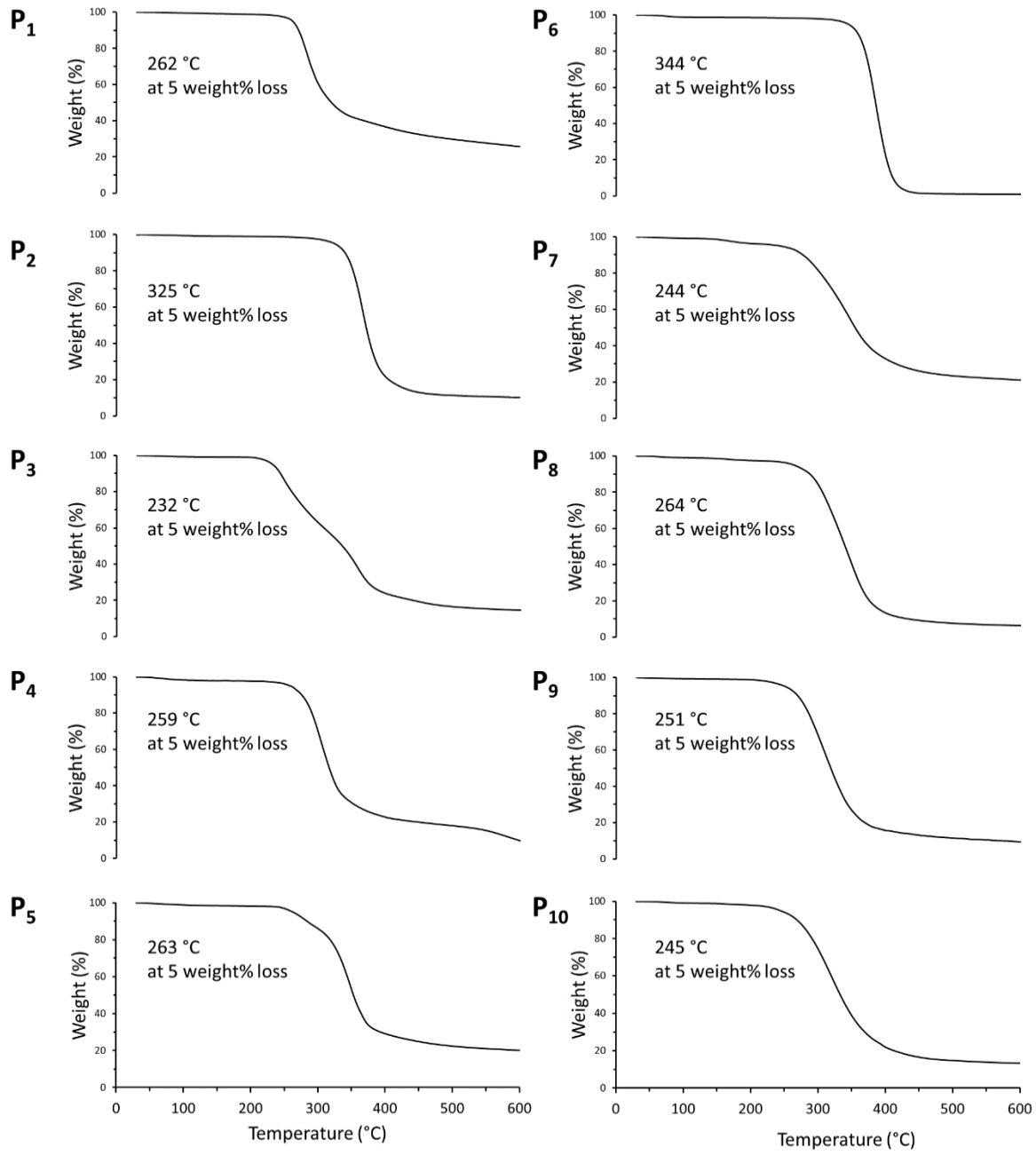

Figure S14. Thermogravimetric analysis of polymers P_1-P_{10} presented in Table S1 recorded with a temperature ramp of 20 °C min^{-1} from 30 to 600 °C.

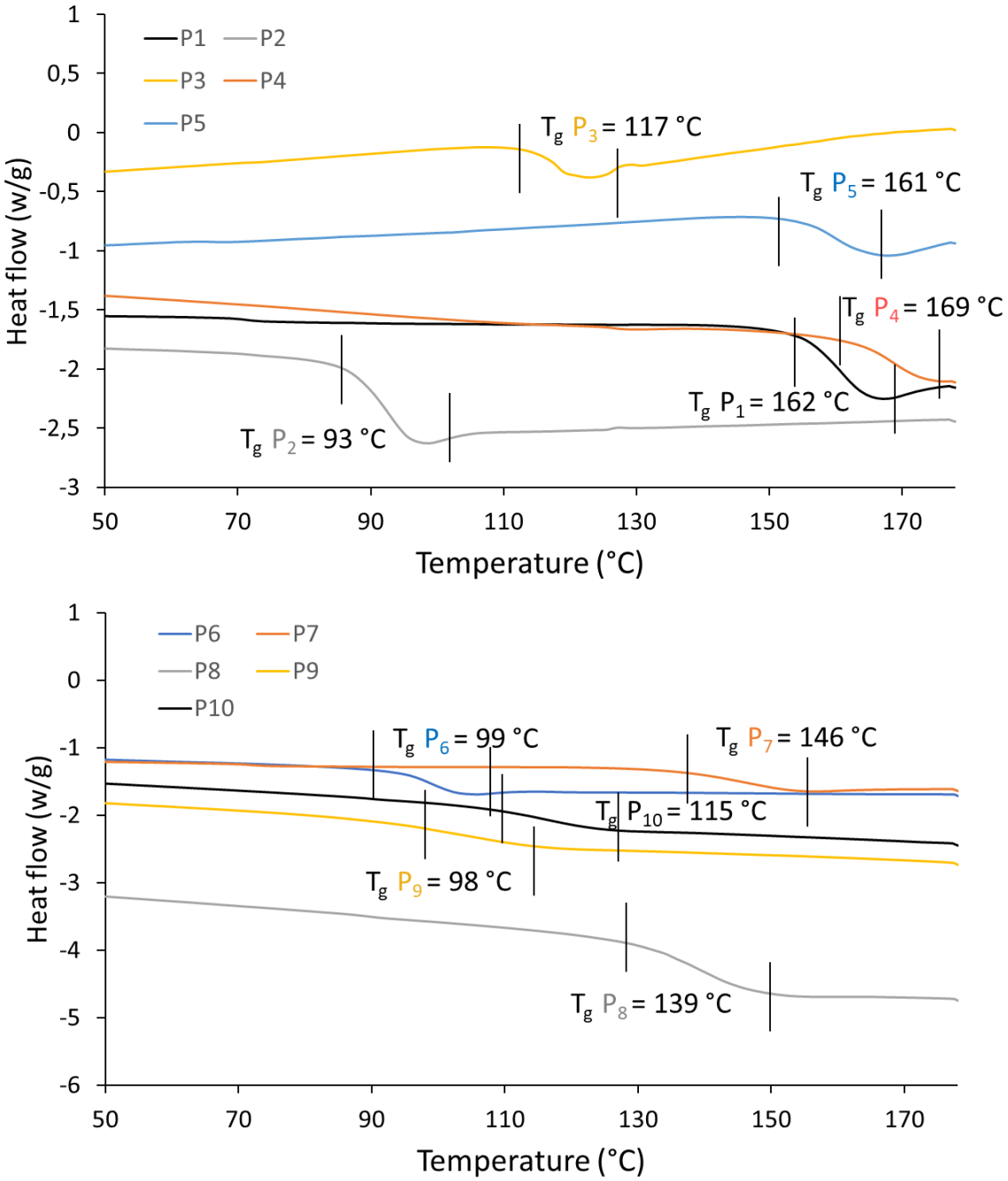

Figure S15. Differential scanning calorimetry analysis of polymers P_1-P_{10} presented in Table S1.

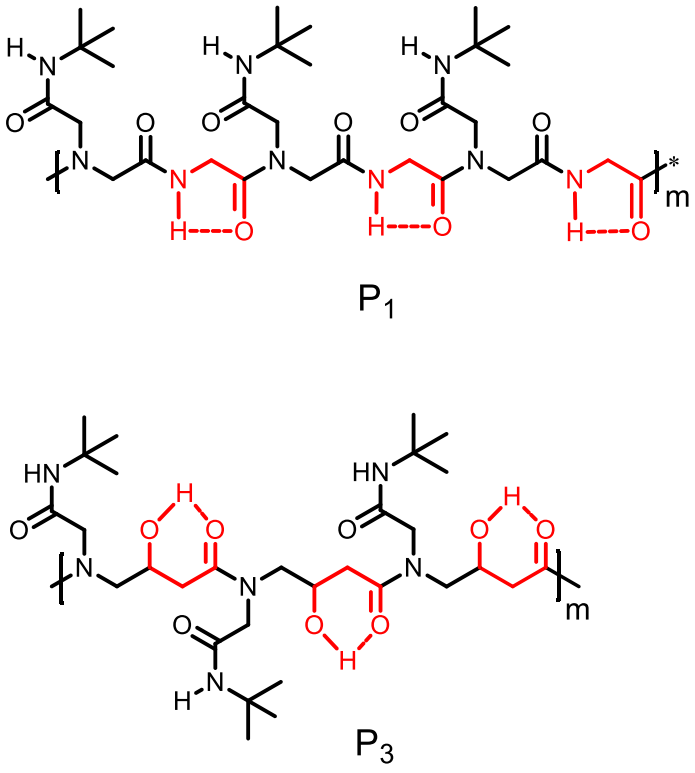

Figure S16. Possible intramolecular hydrogen bonds in P_1 and P_3 leading to 6-membered and 5-membered rings, respectively.

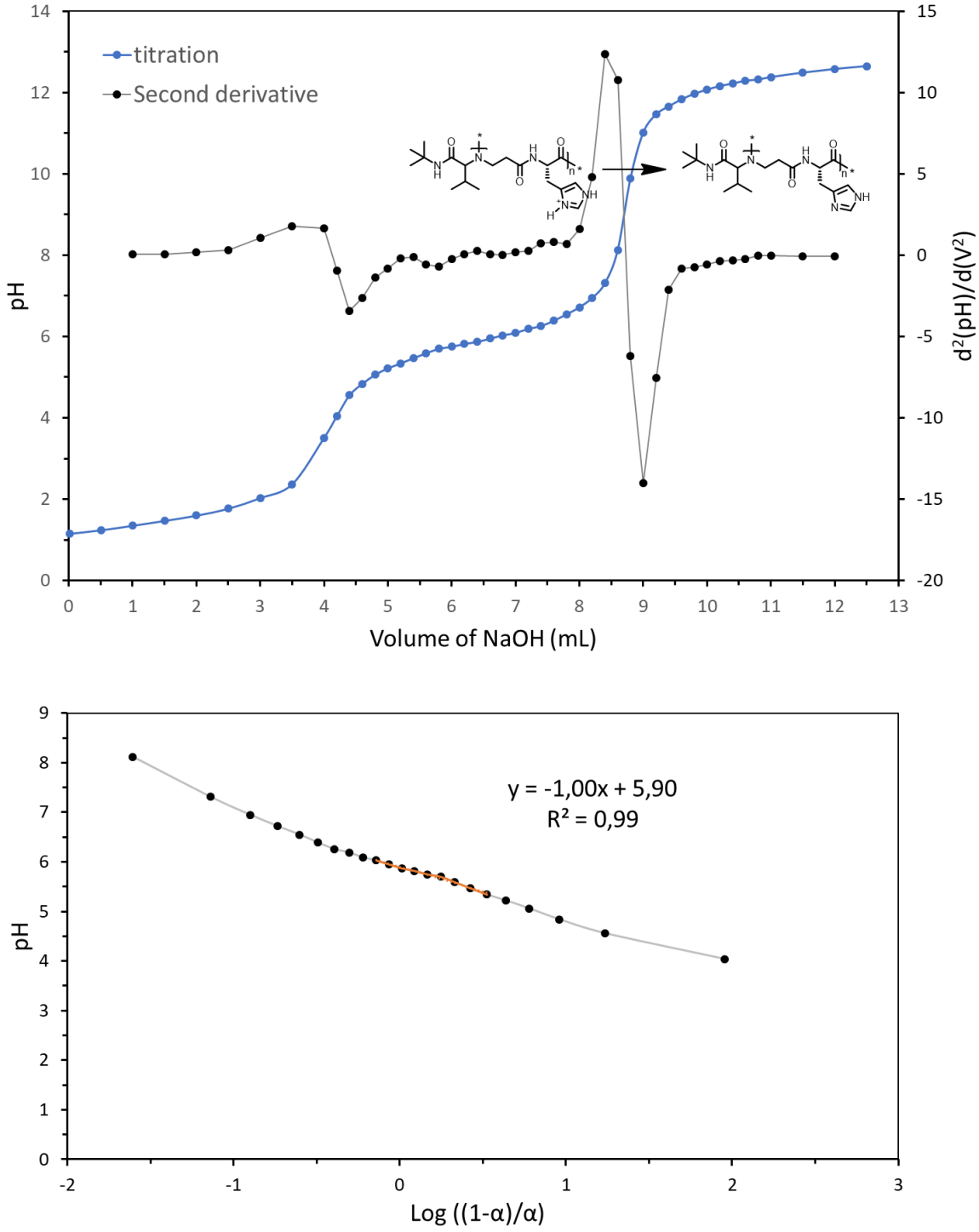

Figure S17. Upper plot: Titration curve of a solution 0.05 M of P_5 acidified with HCl, by NaOH 0.1 M. The second discrete derivative are represented on the curve and are obtained *via* the finite difference method. Lower plot: Henderson-Hasselbalch plot and linear regression on the region where α value ranges between 0.2 and 0.6.

Calculation:

The first and second derivatives were calculated *via* the finite difference method.

Second derivative: $\frac{\Delta(\frac{\Delta pH_n}{\Delta V_n})}{\Delta V_n} = \frac{(\frac{\Delta pH_n}{\Delta V_n})_{n+1} - (\frac{\Delta pH_n}{\Delta V_n})_{n-1}}{V_{n+1} - V_{n-1}}$

The second derivative allows to found the inflection point that are located at f'(x) = 0. The equivalence points and the half-equivalence correspond to inflection points. They are located at 4.15, 6.1 and 8.71 mL of NaOH.

The Henderson-Hasselbalch plot is calculated from the data from the titration. The degree of neutralization is fixed at 0 and 1 for volumes of NaOH of 4.15 and 8.71 mL respectively. It corresponds to the titration of the histidine moiety of P_5. Before 4.15 mL, it was the excess of HCl which was titrated.

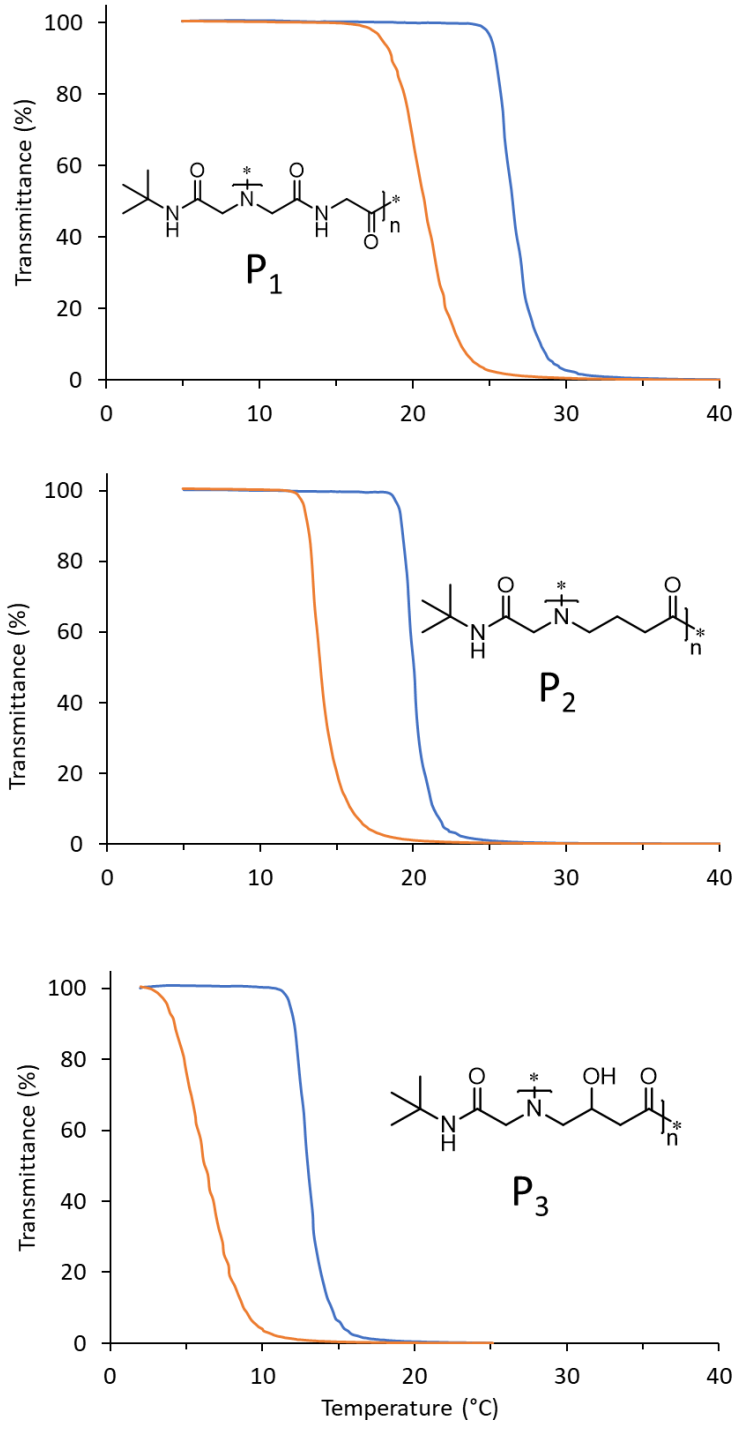

Figure S18. Turbidimetry measurements of aqueous solution of P_1, P_2 and P_3 at a concentration of 2 mg mL^{-1} subjected to heating-cooling cycle at a constant rate of 2 °C min^{-1}. The blue and orange curves represent the heating and cooling steps, respectively.

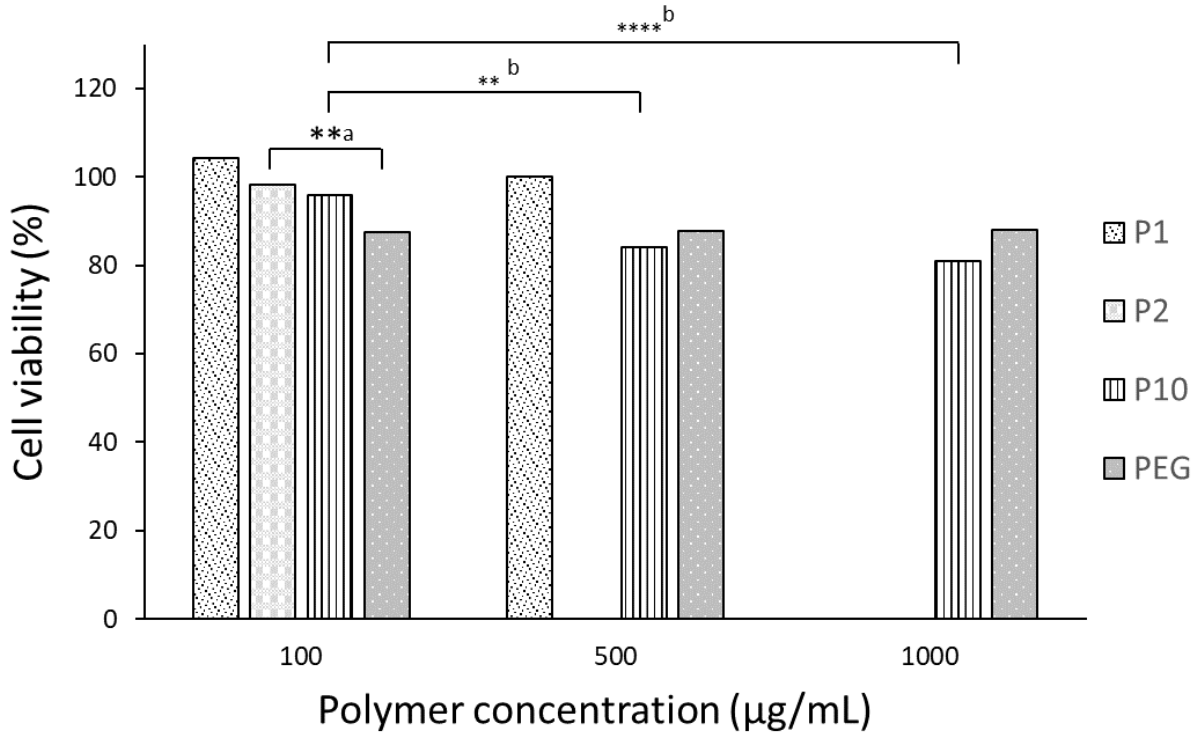

Figure S19. Cell viability of P_1, P_2 and P_{10} compared with PEG_{5K} evaluated by MTS method after 72 h of incubation with HeLa cells at 37 °C. The stars represent the summary of the statistical difference (* = p value < 0.05, ** = p value <0.01, *** = p value < 0.001 ****p value < 0.0001). [a] Unpaired t test. [b] Ordinary One-way ANOVA test followed by Tukey's multiple comparisons test.

Chapter III.

Ugi Three-Component Polymerization Toward Poly(α-amino amide)s.

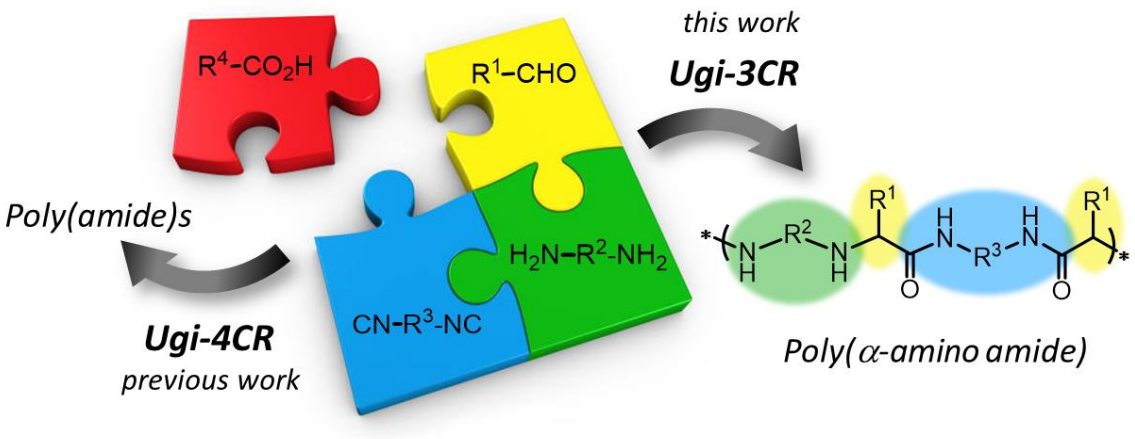

Abstract: Due to their great modularity, ease of implementation and atom economy, multicomponent reactions (MCRs) are becoming increasingly popular macromolecular engineering tools. In this context, MCRs suitable in polymer synthesis are eagerly searched for. This work demonstrates the potential of the Ugi-three component reaction (Ugi-3CR) for the design of polymers and, in particular, of poly(α-amino amide)s. A series of polymers containing amino and amido groups within their backbone was obtained through a one-pot process by reacting aliphatic or aromatic diamines, diisocyanides, and aldehydes. The impact of temperature, concentration, catalyst loading and substrates on polymerization efficiency is discussed. A preliminary study on the thermal properties and the solution behaviour of these poly(α-amino amide)s was carried out. An aliphatic-rich derivative notably showed some pH-responsiveness in water *via* protonation−deprotonation of its amino groups.

Inspired from:

Stiernet, P.; Lecomte, P.; De Winter, J.; Debuigne, A.; *ACS Macro Lett.* **2019**, 8, 4, 427–434

Chapter III. Ugi Three-Component Polymerization Toward Poly(α-amino amide)s.

III.1. Introduction

The demand for diversely substituted multifunctional polymers able to sustain cutting-edge applications is steadily increasing these days. In this context, the development of simple and efficient macromolecular engineering tools becomes essential, and the emergence of multicomponent reactions (MCR) in polymer science takes on its full meaning.[1–4] By definition, MCRs are highly efficient reactions involving more than two compounds that react and form one molecule containing essentially all atoms of the starting reagents.[5–7] Such straightforward and atom economic approach is highly valuable when considering the design of structurally complex macromolecules. MCRs have notably been used for monomer synthesis,[8–12] polymer postmodification,[13–19] in one-pot processes with radical polymerization[19–22] or click chemistry,[23,24] but also as polymerization tools in step-growth processes.[1–4] Only a few MCRs have been adapted for direct polymerization, which requires very high efficiency, including Biginelli,[25–29] Hantzsch,[29,30] Kabachnick-fields,[31] Radziszewski[32–34] and the transition metal-catalysed MCR,[35–37] but the most popular ones consist of isocyanide-based MCRs,[38] namely the Passerini [39–44] and the Ugi four-component (Ugi-4CR) [45–52] reactions.

The Ugi-4CR is based on the concomitant reaction of primary amine, aldehyde, isocyanide and carboxylic acid. The mechanism relies on the formation of a nitrilium ion intermediate resulting from the addition of the isocyanide onto the iminium generated through amine-aldehyde condensation. This intermediate then undergoes a nucleophilic addition of the carboxylate, followed by an acyl migration leading to α-amido amides, with water as the sole byproduct (Figure 1a).[53] Since the pioneering work of Meier *et al.* on the synthesis of polyamides by Ugi-4CR polymerization (Figure 1b),[45] this MCR was exploited for the synthesis of several polymers bearing α-amido amide moieties in their repeating units,[45–52] including polypeptoids[48,49,54] and alternating poly(peptide-peptoid)s copolymers. [50–52,54] A variant of the Ugi-4CR, *i.e.* the Ugi five-component reaction (Ugi-5CR),[55] was also investigated in step-growth polymerization.[56] Typically, a carbonate, formed *in situ* by a reaction between an alcohol and carbon dioxide, plays the role of the nucleophile, leading to poly(urethane-amide)s (Figure 1a).[56]

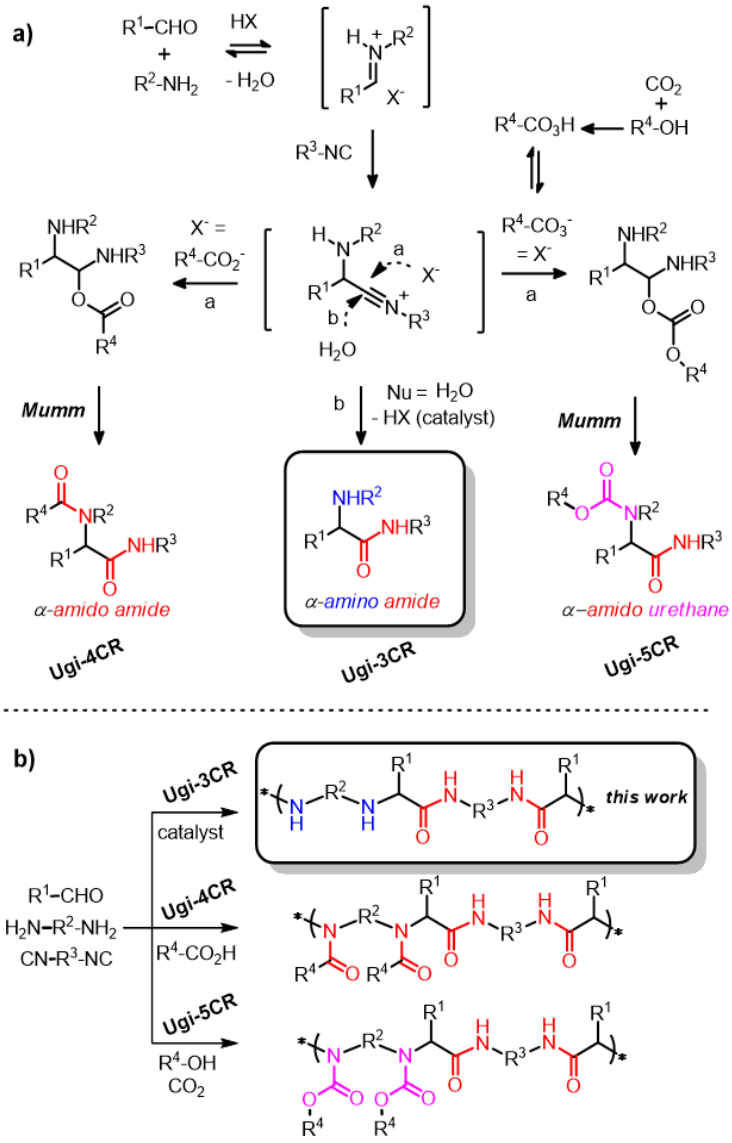

Figure 1. a) General mechanisms of Ugi three-, four- and five-component reactions. b) Examples of polymers produced *via* Ugi-type polymerizations.

A few years ago, Ugi-type reactions involving only three components (Ugi-3CR), *i.e.* amine/aldehyde/isocyanide, were also reported.[57–62] In these cases, water released during the imine formation plays the role of the nucleophile and traps the nitrilium key intermediate.[57–62] Such a reaction requires the presence of a catalyst and paves the way to α-amino amide derivatives.[57–62] Up to now, the Ugi-3CR has been disregarded in polymer chemistry in spite of the increasing interest for macromolecules bearing α-amino amide motifs in their repeating unit. For example, poly(ε-lysine) is currently receiving much attention due to its wide application in pharmaceutical, food, medical and biotechnology areas.[63] Recently, polymers bearing α-tertiary amino amide and phenol groups were produced *via* octylphosphonic acid (OPA)-catalysed MCR between diisocyanides and dibenzoxazines.[64]

In this work, we explored for the first time the potential of the Ugi-3CR in polymer synthesis and prepared unique macromolecules containing α-amino amide moieties in their repeating units (Figure 1b). In particular, we focused on the reaction of diamine/diisocyanide/aldhehyde which should lead to polymers with α-amino amide groups in their backbone. The step-growth polymerization conditions were optimized, and the nature of the building blocks was varied in order to evaluate the versatility of the approach and to modulate the structure of the polymers.

III.2 Results and discussions

III.2.1 Synthesis of poly(α-amino amide)s

So far, best yields in Ugi-3CR (95 %) were achieved by reacting aromatic aldehydes and amines with aliphatic isocyanides at 80 °C in toluene using phenylphosphinic acid (PPA) as a catalyst.[60] Because we anticipated a poor solubility of the poly(α-amino amide)s prepared from aromatic monomers in this solvent, we first studied a model Ugi-3CR in DMF, a common solvent for aromatic polyamides. In practice, aniline (1 equiv.), benzaldehyde (1 equiv.), and PPA (0.1 equiv.) were dissolved in DMF, followed by the addition of *t*BuNC (1 equiv.) and heating at 80 °C (Table S1). After 24 h, the targeted α-amino amide was isolated by silica gel chromatography in 50 % yield. The ^{1}H NMR analysis confirmed the product structure as indicated by characteristic signals of the methine group **a** in α position at 4.6 ppm, the amine **b** at 4.5 ppm, and the amide hydrogen **c** at 6.5 ppm (Figure 2a). The structure of the model compound was further supported by ^{13}C NMR (Figure S1). In order to have a clear insight into the efficiency of the reaction, we evaluated the conversion of the reactants into the α-amino amide derivative by ^{1}H NMR of the crude mixture (Figure S2b-d). At 80 °C, the formation of α-amino amide reached 76 % and 91 % after 1 and 3 days, respectively (Table S1, entries 1 and 2). A similar trend was observed when carrying out the reaction at 25 °C (92 % after 3 days, Table S1, entries 3 and 4). Overall, conversions superior to 90 % were obtained in DMF, which was a strong incentive to test these conditions for the Ugi-3CR step-growth polymerization.

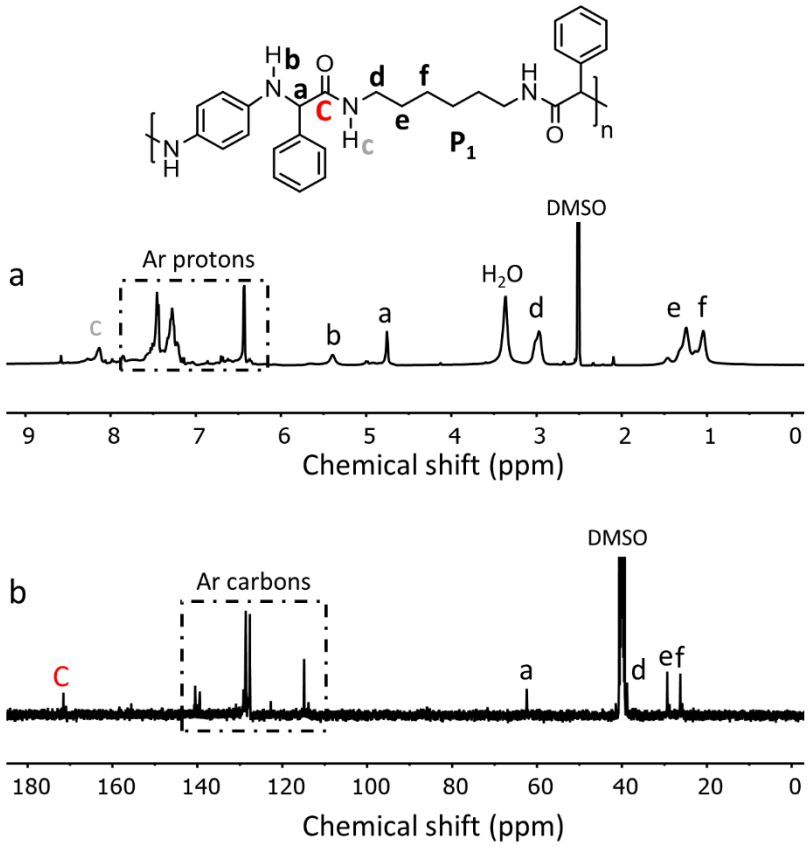

Figure 2. ^{1}H NMR analysis of the model α-amino amide (a) as well as ^{1}H NMR (b) and ^{13}C NMR spectra of polymer P_1 in deuterated dimethyl sulfoxide after purification by dialysis (cut off 1kD) against DMF, followed by precipitation in Et_2O.

The first Ugi-3CR polymerizations were performed in DMF at 80 °C using similar reactants compared to the model reaction, *i.e. para*-phenylenediamine (1 equiv.), freshly synthesized 1,6-diisocyanohexane (1 equiv.), benzaldehyde (2.2 equiv.) and 10 mol% of PPA (Table 1, entry 1). In line with previous studies on Ugi-polymerization,[45,50] the monofunctional component was used in slight excess to guarantee its availability even at high conversion. After 3 days under these conditions, the medium was homogeneous and the SEC analysis of the reaction mixture revealed the formation of polymer chains characterized by an M_n of 1400 g mol^{-1} and a dispersity of 1.6 (Table 1, entry 1 and Figure S3a). The Ugi-3CR polymerization was also carried out at lower temperatures, *i.e.* 50 and 25 °C (Table 1, entries 2-3 and Figure S3). As a result, polymers with higher molar mass were obtained, *i.e.* 5900 and 6300 g mol^{-1} at 50 and 25 °C, respectively. These M_n values correspond to a DP of about 13. According to the Carother's equation (DP_n = 1/(1-p)), where *p* designates conversion, a reaction efficiency of 92 % is necessary to reach a DP of 13, which is perfectly in line with the conversion observed in our model reaction (Table S1, entry 4). The polymerization temperature was further decreased to 6 °C but M_n no greater than 1700 g mol^{-1} was observed after 3 days (Table 1, entry 4).

Nonetheless, this value almost doubled when prolonging the polymerization time to 8 days at the same temperature (Table 1, entry 5). Overall, performing polymerizations at 6 or 80 °C was clearly not optimal. In contrast, a polymer with M_n of 4300 g mol^{-1} could be produced at intermediate temperature, *i.e.* 50 °C, even when shortening the polymerization time to 1 day (Table 1, entry 6). In order to optimize the Ugi-3CR polymerization, catalyst loading and concentration were varied. We notably doubled the concentration of the medium while keeping all other parameters constant but the molar mass dropped to 350 g mol^{-1} (Table 1, entry 7). Moreover, higher catalyst loading did not further increase the molar masses. Polymers with quite similar M_n were obtained with 10, 20 or 50 mol% of PPA (Table 1, entries 6, 8 and 9, respectively). Obviously, the temperature, the catalyst loading and the concentration affect the course of the polymerization and so the molar mass of the final polymer. Nevertheless, considering the complexity of this polymerization system and the competition of possible side reactions, it is very difficult to rationalize the effect of each parameter based on the M_n and dispersity.

Table 1. Ugi-3 CR polymerization involving *p*-phenylenediamine, benzaldehyde and 1,6-diisocyanohexane.

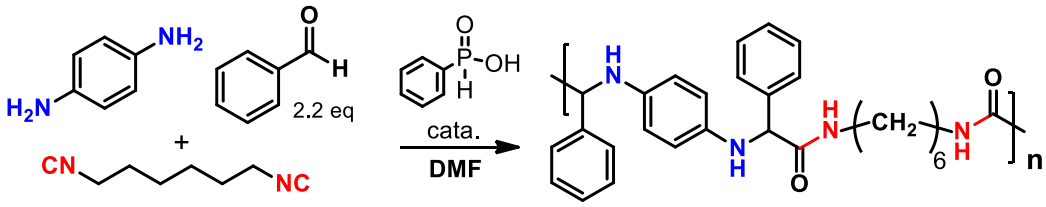

Entry	Temp. (°C)	Catalyst (mol%)	Time (days)	difunctional (mmol) /DMF (mL)	M_w (g mol^{-1})[a]	M_n (g mol^{-1})[a]	$Đ$[a]
1	80	10	3	1.5/3	2300	1400	1.6
2	50	10	3	1.5/3	10300	5900	1.7
3	25	10	3	1.5/3	14900	6300	2.4
4	6	10	3	1.5/3	2100	1700	1.2
5	6	10	8	1.5/3	5100	3100	1.7
6	50	10	1	1.5/3	6800	4300	1.6
7	50	10	1	1.5/1.5	400	350	1.1
8	50	20	1	1.5/3	8300	4300	1.9
9	50	50	1	1.5/3	7200	3900	1.9

Reaction conditions: PPA, p-phenylenediamine (1.5 mmol), benzaldehyde (3.3 mmol) and 1,6-diisocyanohexane (1.5 mmol) in DMF. [a] Determined by SEC in DMF.

Note that a precipitate appeared in the reaction mixture when the polymerization was carried out at 50 °C or below. This precipitate was dissolved in DMF/LiBr upon heating prior SEC analysis (Figure S3b-d). Besides the signal corresponding to the polymer chains, very low molar mass products were detected on the SEC chromatograms. To examine this, the precipitate was isolated by centrifugation (13 wt%) and the supernatant was dialysed against fresh DMF. Both samples were then submitted to SEC (Figure S4). These analyses demonstrated that the precipitate consists of low molar mass compounds whereas the polymer chains P_1 are fully soluble in DMF. NMR and IR analyses of P_1 confirmed the expected structure of the poly(α-amino amide). The ^{1}H NMR spectrum carried out in DMSO-d_6 showed characteristic signals of the amine **b** at 5.4 ppm, the methine hydrogen **a** in α position of the amide at 4.8 ppm and the amide hydrogen **c** at 8.2 ppm (Figure 2b). Typical signals of the aliphatic hydrogens **d-f**, initially contained in the 1,6-diisocyanohexane, as well as aromatic hydrogens were also assigned on Figure 2b. ^{13}C NMR (Figure 2c), COSY and HSQC analyses (Figure S5) provided additional evidence of the structure. As an illustration, the COSY spectrum showed cross peaks between hydrogen **a** in the α position of the amide and hydrogen **b** of the amine or between hydrogens **c** of the amido group and hydrogen **d** of the aliphatic chain. The presence of amides was also confirmed by infrared spectroscopy with specific peaks at 1650 cm^{-1} and at 1510 cm^{-1} corresponding respectively to C=O and N−H stretch for secondary amides (Figure S6a). P_1 was tentatively analysed by MALDI-ToF but no signals corresponding to the polymer could be detected due to its low ability to be desorbed and/or ionized (Figure S7a). In contrast, the structure of the precipitate was elucidated by electrospray ionization (ESI) mass spectrometry (Figure 3). The latter consists of a cyclic unimer generated from one molecule of diamine, one molecule of diisocyanide and two molecules of aldehyde. Indeed, peaks corresponding to the protonated, sodiated and potassiated cyclic derivative were detected at *m/z* 457.2, 479.2 and 495.2, respectively (Figure 3a). The signal at *m/z* 913.5 was attributed to a protonated aggregate of two cyclic unimers rather than a twice larger cyclic molecule thanks to a collision-induced dissociation (CID) experiment (Figure 3c). Indeed, this ion dissociated at low collisional energy (5 eV), consistent with noncovalent interactions, and gave rise to one main fragment at *m/z* 457.2 corresponding to the protonated cyclic unimer. IR as well as ^{1}H, ^{13}C and 2D NMR analyses confirmed the nature of the cyclic unimer (Figures S8 and S9). Ultimately, the desired poly(α-amino amide)s could be collected free of this side product.

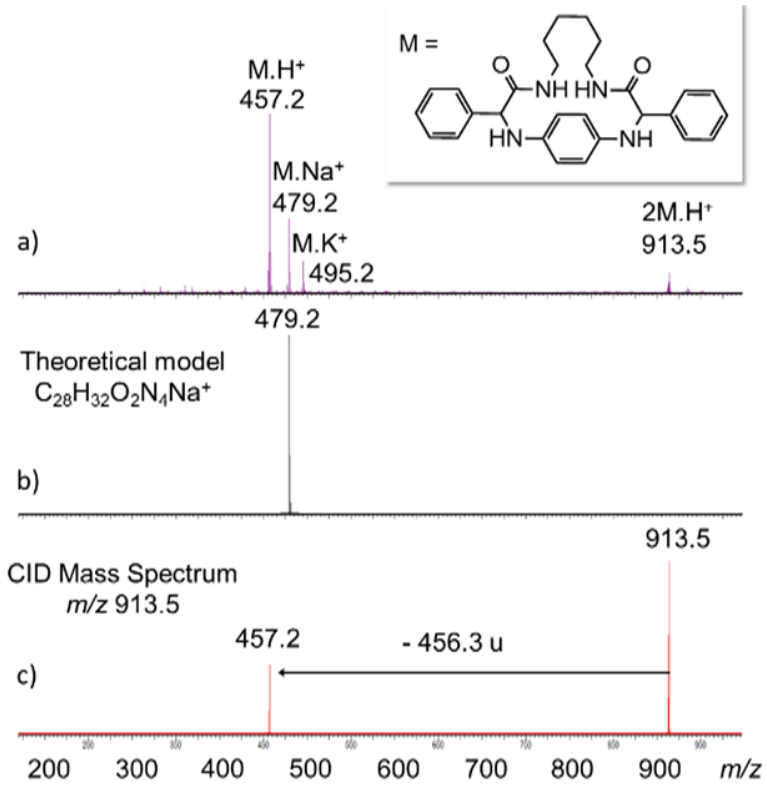

Figure 3. (a) ESI/MS spectrum of the cyclic unimer, (b) isotopic distribution for the sodiated cyclic unimer and (c) collision-induced dissociation (CID) analysis carried out at low collisional energy (5 eV) on the *m/z* 913.5 ions.

The optimized polymerization conditions were then applied to various aromatic and aliphatic compounds in order to synthesize a series of poly(α-amino amide)s with tunable structures (Table 2). Instead of the *para*-phenylenediamine, the *ortho*- and the *meta*-phenylenediamine were reacted with benzaldehyde and 1,6-diisocyanohexane in DMF at 50 °C in the presence of 10 mol% of PPA (Table 2, entries 3 and 4). When using the *ortho*-phenylenediamine, only oligomers P_3 (M_n ~ 900 g mol^{-1}) were produced most probably as a result of steric hindrance induced by the proximity of the amine functions on the aromatic ring. However, a polymer P_4 characterized by an M_n of 7100 g mol^{-1} and a dispersity of 1.7 was obtained with the *meta*-phenylenediamine, which is almost twice higher in M_n compared to P_1 and P_2 obtained from the *para* derivative. Contrary to the reactions performed with the *para*-phenylenediamine, we did not observe the precipitation of low molar mass cyclic compound when using *meta*-phenylenediamine, even at 50 °C. Although electronic and steric effect must be at the origin of these differences, the latter are difficult to rationalize due to the complexity of Ugi-3CR mechanism. The structure of P_4 was fully characterized by ^{1}H NMR (Figure 4a), HSQC (Figure S11a), solid-state NMR (SSNMR) (Figure S12) and IR (Figure S6b). Attempts to analyse P_4, and all poly(α-amino amide)s produced in this study, by MALDI-TOF failed as a result of its

low ability to be desorbed and/or ionized (Figure S7). Signals typical of P_4 were identified on the ^{1}H NMR spectrum in DMF-d_7 (Figure 4a) including aromatic protons between 5.5 and 7.8 ppm, methylene protons **e** and **f** ranging from 0.5 and 1.5 ppm and hydrogens **d** showing two peaks, at 3.0 and 3.5 pm, as a result of the different possible configurations of the amide function. We also distinguished a low intensity signal at 8.3 ppm assigned to the amide hydrogen **c** and a peak corresponding to the methine hydrogen **a** around 5 ppm. The latter assignments were confirmed by HSQC (Figure S11a). The presence of amide was further evidenced by a characteristic signal at 172 ppm in solid-state ^{13}C NMR (Figure S12) assigned to the ipso carbon of the amido group and by ATR analysis showing peaks at 1660 and 1510 cm^{-1} typical of the C=O and N−H stretching, respectively (Figure S6b).

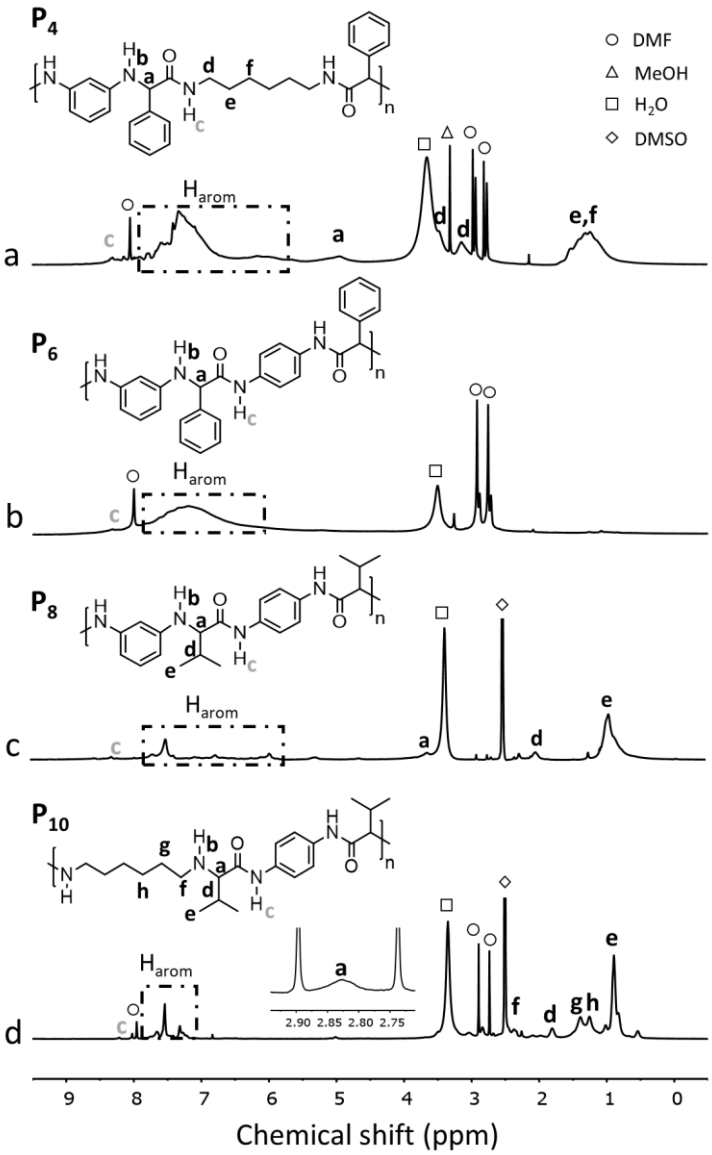

Figure 4. a) ^{1}H NMR spectra of polymer (a) P_4 ,(b) P_6, (c) P_8 and (d) P_{10} in DMF-d_7 or DMSO-d_6 after purification

Table 2. Synthesis of a series of poly(α-amino amide)s by Ugi-3CR.

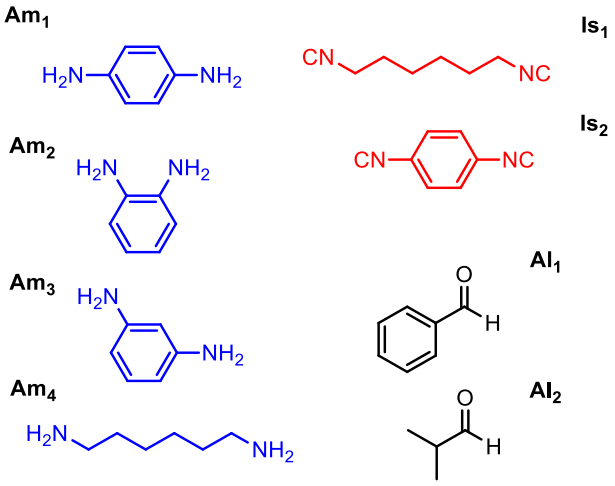

Entry	Polymer	Monomers	Catalyst (mol%)	$M_{w,SEC}$ [a] (g mol^{-1})	$M_{n,SEC}$ [a] (g mol^{-1})	$Đ$ [a]
1	P_1	$Am_1 + Is_1 + Al_1$	10	6800	4300	1.6
2	P_2	$Am_1 + Is_1 + Al_1$	20	8300	4300	1.9
3	P_3	$Am_2 + Is_1 + Al_1$	10	1100	900	1.2
4	P_4	$Am_3 + Is_1 + Al_1$	10	12100[b]	7100[b]	1.7 [b]
5	P_5	$Am_3 + Is_1 + Al_2$	10	2400	1200	2.0
6	P_6	$Am_3 + Is_2 + Al_1$	10	12400[b, c]	7300[b, c]	1.7 [b, c]
7	P_7	$Am_3 + Is_2 + Al_2$	10	6900	3000	2.3
8	P_8	$Am_3 + Is_2 + Al_2$	20	40300[b]	12600[b]	3.2[b]
9	P_9	$Am_4 + Is_2 + Al_2$	10	3200	1700	1.9
10	P_{10}	$Am_4 + Is_2 + Al_2$	20	6400	2900	2.2

Conditions: Diamine (1.5 mmol), diisocyanide (1.5 mmol), aldehyde (3.3 mmol), PPA (10 or 20 mol%), DMF, 50 °C, 24 h. Analyses performed after dialysis against DMF except for P3 and P5 having low M_n. [a] SEC in DMF/LiBr with PS calibration. [b] Polymers treated with trichloroacetyl isocyanate before SEC to avoid aggregation (Figure S10).[c] 72 h reaction.

An aliphatic aldehyde, *i.e.* isobutyraldehyde, was also reacted with the *meta*-phenylenediamine and 1,6-diisocyanohexane under the same experimental conditions (Table 2, entry 5). Nevertheless, we only collected oligomers P_5 (M_n ~ 1200 g mol^{-1}) suggesting a lower efficiency of the Ugi-3CR with aliphatic aldehyde, in line with the observations made by List *et al.*[60] The structure of the diisocyanide was also varied. An aromatic isocyanide, namely 1,4-

phenylenediisocyanide, was first reacted with *meta*-phenylenediamine (1 equiv.) and benzaldehyde (2.2 equiv.) for 72h leading to P_6 with an M_n of 7300 g mol^{-1} (Table 2, entry 6). When the reaction time was shortened to 24 h, the M_n of this polymer only slightly decreased (M_n = 6400 g mol^{-1}, $Đ$ = 2.76). Moreover, similar molar mass (M_n = 6700 g mol^{-1}, $Đ$ = 3.00) was observed when using a stoichiometric amount of aldehyde, amine and isocyanide functions. The structure of the poly(α-amino amide) P_6 was proved by ^{1}H NMR, HSQC and IR (Figures 4b, S11b and S6c, respectively). The *meta*-phenylenediamine and 1,4-phenylendiisocyanide were also reacted with the isobutyraldehyde (Table 2, entry 7). The resulting polymer P_7 exhibited a lower M_n (3000 g mol^{-1}, DP = 8) compared to P_6 (M_n = 6400 g mol^{-1}, DP = 14) confirming the lower efficiency of the aliphatic aldehyde for the Ugi-3CP. To overcome this issue, we repeated the same reaction with 20 mol% of PPA (Table 2, entry 8) and obtained P_8 with a much higher M_n, *i.e.* 12600 g mol^{-1}. ^{1}H NMR, HSQC and IR analyses of P_8 are provided in Figures 4c, S11c and S5d, respectively. Finally, phenylenediamine was substituted for hexamethylenediamine in order to further increase the aliphatic content in the polymer structure (Table 2, entries 9 and 10). This Ugi-3CR polymerization was tested with two catalyst loadings, *i.e.* 10 mol% and 20 mol% (Table 2, entries 9 and 10). Better results were obtained with 20 mol% of catalyst leading to P_{10} with a molar mass of 2900 g mol^{-1} compared to P_9 (1700 g mol^{-1}) produced in the presence of 10 mol% of PPA. Nevertheless, these molecular masses are lower than those obtained with the aromatic phenylenediamine as it was the case for aliphatic aldehydes. Again, a confirmation of the polymer structure was obtained by NMR, HSQC and IR (Figure 4d, S11d and S6e, respectively). To summarize, the Ugi-3CPs were generally performed at 50 °C for 1 day with a concentration of 0.5 M in monomers, a slight excess (2.2 equiv.) in monofunctional reagent and a catalyst loading of 10 mol%. Note that, prolonging the reaction time to 3 days slightly increased the M_n. Concerning the different components, aromatic amines and aldehydes led to higher molar masses than aliphatic ones. This trend was not observed for the isocyanide. Eventually, the effect of the catalyst loading on the molar mass of the polymer strongly varied from case to case.

III.2.2 Thermal properties and solution behaviour

Finally, a preliminary study of the thermal and solution properties of these poly(α-amino amide)s was conducted. All poly(α-amino amide)s showed a decomposition onset temperature (T_{DO}) between 289 and 327 °C (Figure S13). Expectedly, P_{10}, having the lowest amount of aromatic groups in its repeating unit, was the least stable (T_{DO} = 289 °C) whereas P_6 and P_8, containing two aromatic groups per repeating units in their backbone, were the most thermally

stable and showed a broad degradation profile. In general, these poly(α-amino amide)s appear less thermally stable than conventional aromatic and semiaromatic polyamides, *e.g.* poly(*m*-phenylene isophtalamide)[65] and poly(hexamethylene isophtalamide),[66] that are stable at least up to 400 °C. It is thus reasonable to assume that the amino groups accelerate the thermal decomposition of the poly(α-amino amide)s. Nevertheless, the latter possess a rather large temperature window for processing. The thermal transitions of the polymers were then analysed by DSC (Figure S14). No glass transition temperature (T_g) was detected below 250 °C, except for P_{10} and P_1 showing a T_g at 78 °C and 117 °C, respectively. The rather low T_g recorded for these two polymers probably results from their higher flexibility due to the lower aromatic content in their backbone. The same trend was observed for conventional polyamides. For example, the T_g of semiaromatic polyamides like poly(hexamethylene isophtalamide) (T_g = 124 °C)[67] is lower compared to their corresponding aromatic polyamide such as poly(*m*-phenylene isophtalamide) (T_g = 285 °C).[68] Regarding their solubility, all polymers were soluble in DMF, sometimes after heating. Interestingly, the aliphatic-rich poly(α-amino amide) P_{10} is also soluble in methanol and exhibits a pH responsive behaviour in water (Figure S15). Although insoluble when placed in water at pH 7 at 5 mg/mL, P_{10} becomes fully soluble at pH 1 upon addition of HCl as a result of the protonation of the amino group. A gradual return to pH 6 by addition of NaOH, triggered the precipitation of the polymer which increased the turbidity of the solution. The transition was observed around pH 5.5. Note that the other polymers containing more aromatic groups in their structure, especially in their backbone, remained insoluble in water even at low pH. This preliminary experiment emphasizes the potential of such an aliphatic-rich poly(α-amino amide) as a novel pH-responsive sequence.

III.3 Conclusions

In conclusion, we investigated for the very first time the Ugi-three component reaction in polymer synthesis. This straightforward and highly atom economic strategy paved the way to unprecedented poly(α-amino amide)s. After a preliminary study of a model reaction, the experimental Ugi-3CR polymerization conditions were optimized and most of the polymers exhibited a molar mass between 3000 and 12600 g mol^{-1}. These values could be improved in the future in parallel with progress in the optimization and mechanistic understanding of the catalytic Ugi-3CR reaction. As an illustration of the versatility of the Ugi-3CR polymerization, various aromatic and aliphatic components were used as starting materials leading to a series of poly(α-amino amide)s. In this work, diamines, diisocyanides and aldehydes were combined in order to incorporate the amino and amido groups within the polymer backbone. Nevertheless,

dialdehydes could also be associated with diamines or diisocyanides in the presence of the third monofunctional component giving access to macromolecules with lateral amino and amido groups. While further investigation is necessary to establish their full potential, we carried out preliminary studies of the thermal and solution properties of these poly(α-amino amide)s. The aliphatic-rich derivative notably showed some pH-responsiveness in water *via* protonation−deprotonation of its amine functions. Overall, the present study represents a significant step forward in the design of poly(α-amino amide)s and adds a new string to the bow of the increasingly popular macromolecular engineering based on multicomponent reactions.

III.4 References

(1) Rudick, J. G. *J. Polym. Sci. Part A* **2013**, No. 51, 3985–3991.

(2) Kakuchi, R. *Angew. Chem., Int. Ed.* **2014**, *53*, 46–48.

(3) Sehlinger, A.; Michael A.R. Meier. *Adv. Polym. Sci.* **2015**, *269*, 61–86.

(4) Yang, B.; Zhao, Y.; Wei, Y.; Fu, C.; Tao, L. *Polym. Chem.* **2015**, *6* (48), 8233–8239.

(5) Domling, A.; Wang, W.; Wang, K. *Chem Rev* **2012**, No. 112, 3083–3135.

(6) Ruijter, E.; Scheffelaar, R.; Orru, R. V. A. *Angew. Chem., Int. Ed.* **2011**, *50* (28), 6234–6246.

(7) Dömling, A.; Ugi, I. *Angew. Chem., Int. Ed.* **2000**, *39*, 3168–3210.

(8) Kreye, O.; Türünç, O.; Sehlinger, A.; Rackwitz, J.; Meier, M. A. R. *Chem. - A Eur. J.* **2012**, *18* (18), 5767–5776.

(9) Robotham, C. V.; Baker, C.; Cuevas, B.; Abboud, K.; Wright, D. L. *Mol. Divers.* **2003**, *6* (3–4), 237–244.

(10) Kreye, O.; Tóth, T.; Meier, M. A. R. *J. Am. Chem. Soc.* **2011**, *133* (6), 1790–1792.

(11) Sehlinger, A.; Kreye, O.; Meier, M. A. R. *Macromolecules* **2013**, *46* (15), 6031–6037.

(12) Zhang, Q.; Zhang, Y.; Zhao, Y.; Yang, B.; Fu, C.; Wei, Y.; Tao, L. *ACS Macro Lett* **2015**, *4*, 128–132.

(13) Shen, H.; Ma, H.; Liu, P.; Huang, W.; Han, L.; Li, C.; Li, Y. *Macromol. Rapid Commun.* **2017**, *37*, 1700353.

(14) Sirvio, J. A.; Visanko, M.; Liimatainen, H. *RSC Adv.* **2016**, 56544–56548.

(15) Kreye, O.; Trefzger, C.; Sehlinger, A.; Meier, M. A. R. *Macromol. Chem. Phys* **2014**, 2207–2220.

(16) Kakuchi, R.; Theato, P. *ACS Macro Lett.* **2014**, *3* (4), 329–332.

(17) Bachler, P. R.; Schulz, M. D.; Sparks, C. A.; Wagener, K. B.; Sumerlin, B. S.

Macromol. Rapid Commun. **2015**, *36* (9), 828–833.

(18) Wu, H.; Yang, L.; Tao, L. *Polym. Chem.* **2017**, *8* (37), 5679–5687.

(19) Zhu, C.; Yang, B.; Zhao, Y.; Fu, C.; Tao, L.; Wei, Y. *Polym. Chem.* **2013**, *4* (21), 5395–5400.

(20) Zhang, Y.; Zhao, Y.; Yang, B.; Zhu, C.; Wei, Y.; Tao, L. *Polym. Chem.* **2014**, *5* (6), 1857–1862.

(21) Huang, Z.; Chen, Q.; Wan, Q.; Wang, K.; Yuan, J.; Zhang, X.; Tao, L.; Wei, Y. *Polym. Chem.* **2017**, *8* (33), 4805–4810.

(22) Sun, Q.; Liu, G.; Wu, H.; Xue, H.; Zhao, Y.; Wang, Z.; Wei, Y.; Wang, Z.; Tao, L. *ACS Macro Lett.* **2017**, *6* (5), 550–555.

(23) Tunca, U. *Macromol. Chem. Phys.* **2018**, *219* (16), 1800163.

(24) Yang, B.; Zhao, Y.; Fu, C.; Zhu, C.; Zhang, Y.; Wang, S.; Wei, Y.; Tao, L. *Polym. Chem.* **2014**, *5* (8), 2704–2708.

(25) Zhao, Y.; Wu, H.; Wang, Z.; Wei, Y.; Wang, Z.; Tao, L. *Sci. China Chem.* **2016**, *59* (12), 1541–1547.

(26) Zhao, Y.; Yu, Y.; Zhang, Y.; Wang, X.; Yang, B.; Zhang, Y.; Zhang, Q.; Fu, C.; Wei, Y.; Tao, L. *Polym. Chem.* **2015**, *6* (27), 4940–4945.

(27) Boukis, A. C.; Llevot, A.; Meier, M. A. R. *Macromol. Rapid Commun.* **2016**, *37* (7), 643–649.

(28) Zhao, Y.; Wu, H.; Zhang, Y.; Wang, X.; Yang, B.; Zhang, Q.; Ren, X.; Fu, C.; Wei, Y.; Wang, Z.; Wang, Y.; Tao, L. *ACS Macro Lett.* **2015**, *4* (8), 843–847.

(29) Wu, H.; Fu, C.; Zhao, Y.; Yang, B.; Wei, Y.; Wang, Z.; Tao, L. *ACS Macro Lett.* **2015**, *4* (11), 1189–1193.

(30) Wu, H.; Wang, Z.; Tao, L. *Polym Chem* **2017**, *8*, 7290–7296.

(31) Moldenhauer, F.; Kakuchi, R.; Theato, P. *ACS Macro Lett.* **2016**, *5* (1), 10–13.

(32) Lindner, J.-P. *Macromolecules* **2016**, *49* (6), 2046–2053.

(33) Grygiel, K.; Kirchhecker, S.; Gong, J.; Antonietti, M.; Esposito, D.; Yuan, J. *Macromole chem phys* **2017**, *218*, 1600586.

(34) Castro-grijalba, A.; Reyes-gallardo, E. M.; Wuilloud, R. G. *RSC Adv.* **2017**, *7*, 42979–42985.

(35) Lee, I.-H.; Kim, H.; Choi, T.-L. *J. Am. Chem. Soc.* **2013**, *135* (10), 3760–3763.

(36) Siamaki, A. R.; Sakalauskas, M.; Arndtsen, B. A. *Angew. Chemie Int. Ed.* **2011**, *50* (29), 6552–6556.

(37) Chan, C. Y. K.; Tseng, N.-W.; Lam, J. W. Y.; Liu, J.; Kwok, R. T. K.; Tang, B. Z.

Macromolecules **2013**, *46* (9), 3246–3256.

(38) Llevot, A.; Boukis, A. C.; Oelmann, S.; Wetzel, K.; Meier, M. A. R. *Top Curr Chem* **2017**, *375*, 66.

(39) Sehlinger, A.; Schneider, R.; Meier, M. A. R. *Eur. Polym. J.* **2014**, *50*, 150–157.

(40) Wang, Y.-Z.; Deng, X.-X.; Li, L.; Li, Z.-L.; Du, F.-S.; Li, Z.-C. *Polym. Chem.* **2013**, *4* (3), 444–448.

(41) Deng, X.-X.; Li, L.; Li, Z.-L.; Lv, A.; Du, F.-S.; Li, Z.-C. *ACS Macro Lett.* **2012**, *1* (11), 1300–1303.

(42) Zhang, J.; Wu, Y.; Wang, J.; Du, F.; Li, Z. *Macromolecules* **2018**, *51*, 5842–5851.

(43) Cui, Y.; Zhang, M.; Du, F.; Li, Z. *ACS Macro Lett.* **2017**, *6*, 11–15.

(44) Zhang, J.; Zhang, M.; Du, F.-S.; Li, Z.-C. *Macromolecules* **2016**, *49* (7), 2592–2600.

(45) Sehlinger, A.; Dannecker, P.; Kreye, O.; Meier, M. A. R. *Macromolecules* **2014**, *47*, 2774–2783.

(46) Gangloff, N.; Nahm, D.; Döring, L.; Kuckling, D.; Luxenhofer, R. *J. Polym. Sci. Part A Polym. Chem.* **2015**, *53* (14), 1680–1686.

(47) Hartweg, M.; Becer, C. R. *Green Chem.* **2016**, *18* (11), 3272–3277.

(48) Zhang, X.; Wang, S.; Liu, J.; Xie, Z.; Luan, S.; Xiao, C.; Tao, Y.; Wang, X. *ACS Macro Lett.* **2016**, *5*, 1049–1054.

(49) Tao, Y.; Wang, S.; Zhang, X.; Wang, Z.; Tao, Y.; Wang, X. *Biomacromolecules* **2018**, *19* (3), 936–942.

(50) Al Samad, A.; De Winter, J.; Gerbaux, P.; Jérôme, C.; Debuigne, A. *Chem Comm* **2017**, No. 53, 12240--12243.

(51) Koyama, Y.; Gudeangadi, P. G. *Chem. Commun.* **2017**, *53* (27), 3846–3849.

(52) Koyama, Y.; Ihsan, A. B.; Taira, T.; Imura, T. *RSC Adv.* **2018**, *8*, 7509–7513.

(53) Medeiros, G. a; da Silva, W. a; Bataglion, G. a; Ferreira, D. a C.; de Oliveira, H. C. B.; Eberlin, M. N.; Neto, B. a D. *Chem. Commun. (Camb).* **2014**, *50* (3), 338–340.

(54) Hartweg, M.; Edwards-gayle, C. J. C.; Radvar, E.; Collis, D.; Reza, M.; Kaupp, M.; Steinkoenig, J.; Ruokolainen, J.; Rambo, R.; Barner-kowollik, C.; Hamley, I. W.; Azevedo, H. S.; Becer, C. R. *Polym Chem* **2018**, *9*, 482–489.

(55) Keating, T. A.; Armstrong, R. W. *J. Org. Chem.* **1998**, *63* (3), 867–871.

(56) Sehlinger, A.; Schneider, R.; Meier, M. A. R. *Macromol. Rapid Commun.* **2014**, *35* (21), 1866–1871.

(57) Kłossowski, S.; Wiraszka, B.; Berłozecki, S.; Ostaszewski, R. *Org. Lett.* **2013**, *15* (3), 566–569.

(58) Tanaka, Y.; Hasui, T.; Suginome, M. **2007**, Org. Lett. 2007, 9, 4407–4410.

(59) Neochoritis, C. G.; Livadiotou, D.; Tsiaras, V.; Zarganes-tzitzikas, T.; Samatidou, E. *Tetrahedron* **2016**, *72* (33), 5149–5156.

(60) Pan, S. C.; List, B. *Angew. Chem., Int. Ed.* **2008**, *47*, 3622–3625.

(61) Shaabani, A.; Keshipour, S.; Shaabani, S.; Mahyari, M. *Tetrahedron Lett.* **2012**, *53* (13), 1641–1644.

(62) Kumar, A.; Saxena, D.; Maneesh Kumar Gupta. *RSC Adv.* **2013**, 4610–4612.

(63) Bankar, S. B.; Singhal, R. S. *RSC Adv.* **2013**, *3* (23), 8586.

(64) Zhang, J.; Shi, W.; Liu, Q.; Chen, T.; Zhou, X.; Yang, C.; Zhang, K.; Xie, Z. *Polym. Chem.* **2018**, *9*, 5566–5571.

(65) Chatfield, D. A.; Einhorn, I. N.; Mickelson, R. W. *J. Polym. Sci.* **1979**, *17*, 1367–1381.

(66) Cousin, T. *PhD thesis;* INSA de Lyon, **2013**, NNT: 2013ISAL0019.

(67) Cousin, T.; Galy, J.; Dupuy, J. *Polymer.* **2012**, *53* (15), 3203–3210.

(68) Keating, M. Y. *Thermochim. Acta* **1998**, *319*, 201–212.

III.5 Experimental Section

Materials. Aniline (99.5 %), *tert*-butyl isocyanide (*t*BuNC) (98 %), hexamethylenediamine (98 %), ethyl formate (98 %), phosphoryl chloride ($POCl_3$) (%), p-phenylenediamine (98 %), m-phenylenediamine (99 %), 1,4-phenylene diisocyanide (97 %), isobutyraldehyde (99 %) were purchased from sigma-aldrich (Belgium). Benzaldehyde (99 %) was purchased from Alfa Aesar. *O*-phenylenediamine (99 %) was purchased from Fluka. Diisopropylamine (99 %) was purchased from Janssen Chimica. Phenylphosphinic acid (99 %) was purchased from abcr and methanol (MeOH), dimethylformamide (DMF), dichloromethane and diethylether (Et_2O) were purchased from VWR. All chemicals and solvents were used without purification except for DMF which was dried on molecular sieves. Spectra/por® dialysis tubings (cut-off, 1 kDa) were purchased from SpectrumLabs.

Characterizations. Molar masses (*M*n, *M*w) and dispersity (*Đ*) of the copolymers were characterized by size exclusion chromatography (SEC) at 55 °C in dimethylformamide (DMF) containing LiBr (0.025 M) using a flow rate of 1 mL min with a polystyrene calibration. SEC curves were recorded with a Waters chromatograph equipped with three columns (Waters Styragel pss gram 1000 Å (×2), 30 Å), a dual λ absorbance detector (Waters 2487) and a refractive index detector (Waters 2414). ^{1}H NMR, HSQC and COSY spectra were recorded at 298 K with a Bruker Avance III HD spectrometer (B_0=9.04 T) (400 MHz) and treated with MestReNova software. ^{13}C CP MAS NMR spectra were recorded with 4-mm zirconia rotors spinning at 10 kHz on a Bruker Avance III HD spectrometer (B_0=9.04 T) working at the Larmor frequency of 100.62 MHz. Cross polarization experiments were performed with a delay time of 2 s and a contact time of 2 ms. IR spectra were recorded on ThermoFischer Sientic Nicolet IS5 equipped with an ATR ID5 module using a diamond crystal (650 cm^{-1} - 4000 cm^{-1}). Differential scanning calorimetry (DSC) was performed on a TA Instruments Q1000 DSC, using hermetic aluminium pans, indium standard for calibration, nitrogen as the purge gas, a sample weight of ~5 mg. The sample was cooled down to -80 °C at 40 °C min^{-1} cooling rate, followed by an isotherm at −80°C for 2 min and heating up to 250 °C at 10 °C min^{-1} heating rate. These cycles were repeated twice. The fourth cycle (last heating from -80 to 50 °C) is analysed and showed in figure S13. TGA analyses were carried out with a Hi-Res TGA Q500 from TA Instruments under nitrogen at a heating rate of 20°C min^{-1} from ambient temperature to 100 °C, followed by an isotherm of 20 min and heated up to 650 °C at a heating rate of 20 °C min^{-1} with a sample weight of ~10 mg. ElectroSpray Ionization (ESI) mass spectra were recorded using Waters Synapt G2-S*i* mass spectrometer. The solution (1 µg.mL^{-1}) is directly

infused in the ESI source with a typical flow rate of 5 µl min^{-1} with a capillary voltage of 3.1 kV, a source temperature of 80 °C and a desolvation temperature of 120 °C. The quadrupole was set to pass ions from 100 to 1500Th and all ions were transmitted into the pusher region of the time-of-flight analyser (Resolution~20,000) for mass-analysis with 1 s integration time. Concerning the Collision Induced Dissociation (CID) experiment, *m/z* 913.5 ions were selected by the quadrupole and accelerated into the Trap region of the Tri-Wave® (filled with Ar), survival parent ions and fragment ions are finally analysed in the ToF region. For all mass spectra, data were acquired in continuum mode until acceptable average data were obtained (~1min acquisition). Matrix Assisted Laser Desoption/Ionization (MALDI) mass spectra were recorded using a Waters QToF Premier mass spectrometer equipped with a Nd:YAG (third harmonic) operating at 355 nm with a maximum output of 65 µJ delivered to the sample in 2.2 ns pulses at 50 Hz repeating rate. Time-of-flight mass analyses were performed in the reflectron mode at a resolution of about 10,000. All the samples were analysed using trans-2-[3-(4-tert-butylphenyl)-2-methylprop-2-enylidene]malononitrile (DCTB) as matrix. That matrix was prepared as 40 $mg.mL^{-1}$ solution in $CHCl_3$. The matrix solution (1 µL) was applied to a stainless-steel target and air-dried. Polymer samples were dissolved in DMF to obtain 1 $mg.mL^{-1}$ solutions. Therefore, 1 µL of this solution was applied onto the target area already bearing the matrix crystals, and air-dried. Additionally, 1µL of 2 $mg.mL^{-1}$ NaI solution in acetonitrile has been spotted as well onto some spots in order to eventually promote cationization. For the recording of the single-stage MS spectra, the quadrupole (rf-only mode) was set to pass all the ions of the distribution, and they were transmitted into the pusher region of the time-of-flight analyser where they were mass analysed with 1s integration time.

Model Ugi-3CR reaction.

In a 25 mL flask, benzaldehyde (318 mg, 3.0 mmol) was dissolved in dry DMF (3.0 mL) followed by addition of aniline (280 mg, 3.0 mmol), and *tert*-butyl isocyanide (249 mg, 3.0 mmol) and phenylphosphinic acid (43 mg, 0.3 mmol). The reaction mixture was then stirred at 80 °C for 24 hours. The mixture was then cooled to room temperature, concentrated under reduced pressure and purified on silica gel column eluted with 25/75 ethylacetate/*n*-hexane (rf = 0.67). The targeted α-amino amide was collected as a white powder in 50 % yield. ^1H NMR (400 MHz; $CDCl_3$) $\delta 1_H$: 1.31 (s, 9H), 4.50 (s, ^1H, NH) 4.60 (s, 1H, CH), 6.51 (s, 1H, NH), 6.63

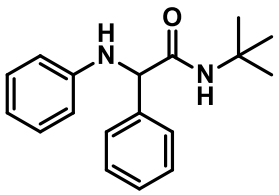

(d, 2H), 6.80 (t, 1H), 7.19 (t, 2H), 7.30-7.45 (m, 5H). ^{13}C NMR (400 MHz; $CDCl_3$) δ_{C13}: 28.6, 51.2, 64.9, 113.9, 119.1, 127.3, 128.5, 129.2, 129.3, 139.3, 146.8,170.2. IR (ATR): ν = 3406, 3278, 3084, 2965, 1647, 1600, 1556, 1507, 1451, 1435, 1391, 1360, 1315, 1282, 1252, 1226, 1192,1155, 1135, 1075, 1030, 991, 954, 919, 872, 799, 758, 744, 702, 692, 621, 573, 558 cm^{-1}.

This reaction was reproduced in order to determine the conversion of the reactants into α-amino amide *via* ^{1}H NMR analysis of the crude mixture. Typically, a solution of benzaldehyde in dry DMF (3.15 g of a 1.0 M stock solution, 3.0 mmol) was introduced in a 25 mL flask followed by addition of aniline (280 mg, 3.0 mmol), and *tert*-butyl isocyanide (249 mg, 3.0 mmol) and phenylphosphinic acid (43 mg, 0.3 mmol). The reaction mixture was then stirred at 80 °C for 24 hours. A sample was withdrawn from the reaction mixture, diluted in deuterated chloroform and added with one drop of trichloroacetyl isocyanate before ^{1}H NMR analysis. The conversion of the reactants into α-amino amide (76 %) was evaluated by integrating the peak at 6 ppm corresponding to the methine in the α position of the amide function using the ^{1}H NMR spectrum of the initial benzaldehyde/DMF stock solution as a reference. The same procedure was repeated with different temperatures and reaction times as detailed in table 1.

Synthesis of 1,6-diisocyanohexane: Inspired by a procedure reported by Meier *et al.* (Macromol. Rapid Commun. 2014, 35, 1866), hexamethylenediamine (10.2 g, 88 mmol) was dispersed in ethyl formate (152 g, 165 mL, 2.02 mol) and refluxed overnight. The mixture was concentrated *in vacuo* then directly dissolved in 175 mL dichloromethane followed by the addition of diisopropylamine (52.6 g, 73 mL, 519 mmol). The mixture was cooled below 0 °C and phosphoryl chloride (36.3 g, 22 mL, 237 mmol) was added dropwise to keep the temperature below 0 °C. The solution was stirred for 2 hours prior to be poured into 500 mL of a solution potassium carbonate (1.5 M). The resulting emulsion was stirred for 1 hour maintaining the temperature below 25 °C. The organic layer was separated and the aqueous layer extracted three times with 50 mL dichloromethane. The combined organic layers were dried with anhydrous potassium carbonate. Purification by column chromatography (hexane/ethyl acetate 5:1) and concentration under *vacuum* yielded 1,6-diisocyanohexane (5.2 g, 38 mmol) as a yellow oil with 43 % yield. The product was stored at -20 °C in dark room under argon.

Synthesis poly(α-amino amide) P_1 *via* Ugi-3CR polymerization. In a 25 mL flask, phenylphosphinic acid (44 mg, 0.3 mmol), benzaldehyde (350 mg, 0.34 mL, 3.3 mmol), p-phenylenediamine (166 mg, 1.5 mmol) and 1,6-diisocyanohexane (204 mg, 1.5 mmol) were

dissolved sequentially in dry DMF (3 mL) at 50 °C. The mixture was stirred at the same temperature for 24 h. Under these conditions, the formation of a precipitate was observed. A sample was withdrawn from the reaction medium for SEC analysis in DMF showing a bimodal signal. The crude mixture was then centrifuged (10k rpm, 5 °C, 15 min) in order to remove the precipitate. The supernatant was dialyzed (1 kD pore size) against DMF p.a. during 24 h and poured into diethyl ether in order to recover the polymer by precipitation. The solid was dried under vacuum at 80 °C (20 % recovered yield). The poly(α-amino amide) P_1 was analysed by SEC ($M_{n\ SEC\ DMF\ cal\ PS}$ = 4300 g mol^{-1}, $Đ$ = 1.6), ^{1}H NMR, HSQC, COSY, ATR, TGA and DSC. Similar experiments were carried out with different temperature, time, concentration, amount of catalyst, as detailed in Table 2.

Synthesis poly(α-amino amide) $P_{3\text{-}10}$ *via* Ugi-3CR polymerization. In a 25 mL flask, phenylphosphinic acid (0.3 mmol), aldehyde (3.3 mmol), diamine (1.5 mmol), and diisocyanide (1.5 mmol) were dissolved sequentially in dry DMF (3 mL) at 50 °C. The mixture was stirred at the same temperature for 24 h. The crude mixture was dialyzed (1 kD pore size) against DMF p.a. during 24 h and poured into diethyl ether in order to recover the polymer by precipitation. The solid was dried under vacuum at 80 °C (recovered yield ~ 20-50 %). The poly(α-amino amide)s $P_{3\text{-}10}$ were analysed by SEC in DMF. Note that P_4, P_6 and P_8 were treated with trichloroacetyl isocyanate before SEC analysis in order to limit aggregation and/or interaction with the columns. All polymers were also analysed by ^{1}H NMR, HSQC, ATR, TGA and DSC. P_4 was also analysed by solid state ^{13}C NMR. Experimental conditions and macromolecular characteristics are detailed in Table 3.

III.6 Supporting information

Table S1. Model Ugi-3 CR between aniline, benzaldehyde and *tert*-butyl isocyanide.

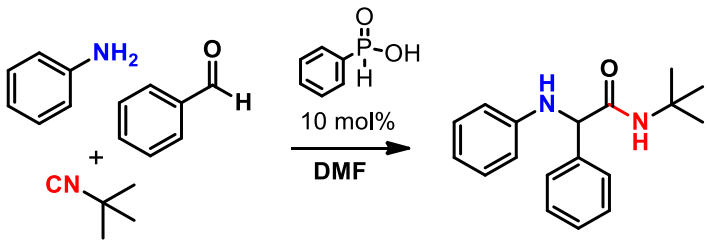

Entry	Temperature (°C)	Time (days)	Conv (%)[a]
1	80	1	76
2	80	3	91
3	25	1	84
4	25	3	92

Reaction conditions: phenylphosphinic acid (0.3 mmol), aniline (3 mmol), benzaldehyde (3 mmol) and *t*BuNC (3 mmol) in dry DMF (3 mL). [a] Conversion of reactants into α-amino amide determined by ^{1}H NMR (400 MHz) of the reaction mixture in deuterated chloroform.

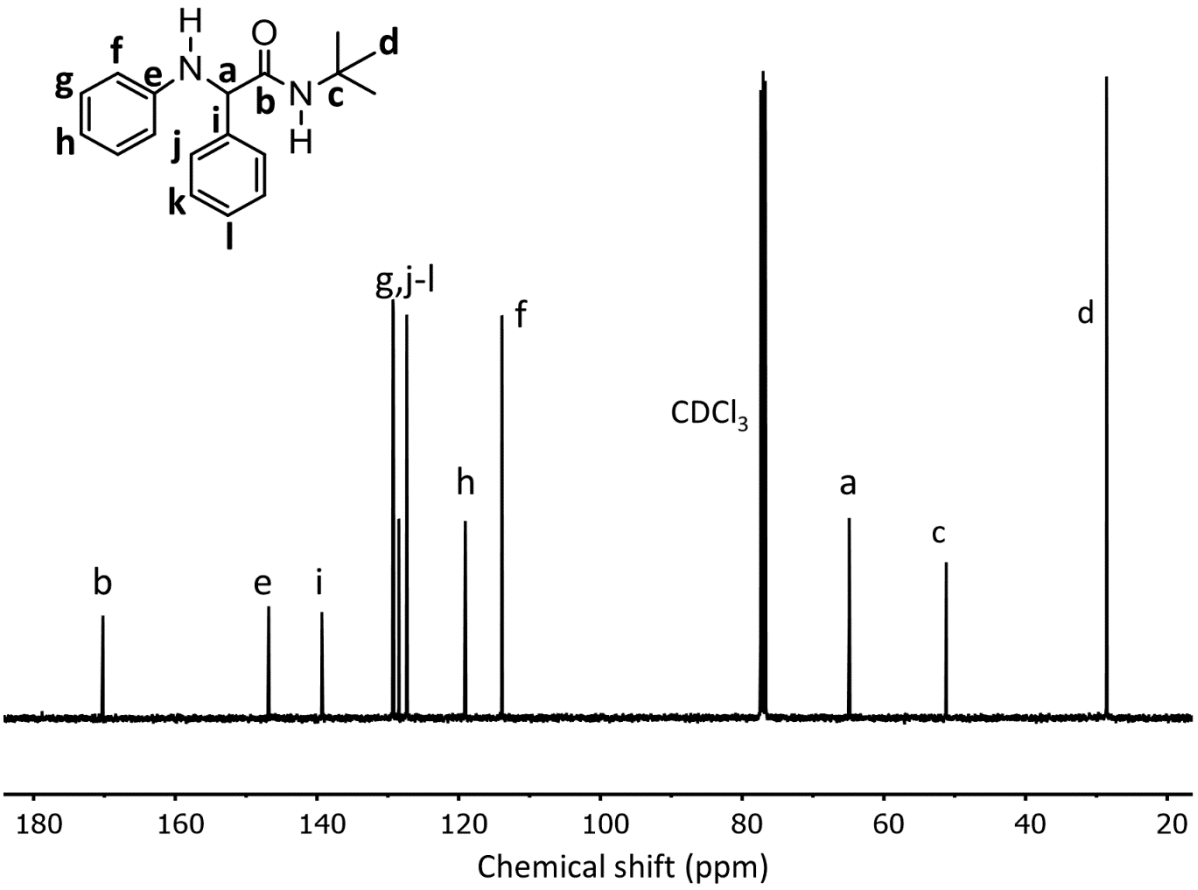

Figure S1. ^{13}C NMR spectrum of the model α-amino amide formed by the Ugi-3CR model reaction between aniline (3 mmol), benzaldehyde (3 mmol) and tert-butyl isocyanide (3 mmol), in the presence of phenylphosphinic acid (0.3 mmol), in dry DMF (3 mL) at 80 °C after 24 h and isolated by column chromatography.

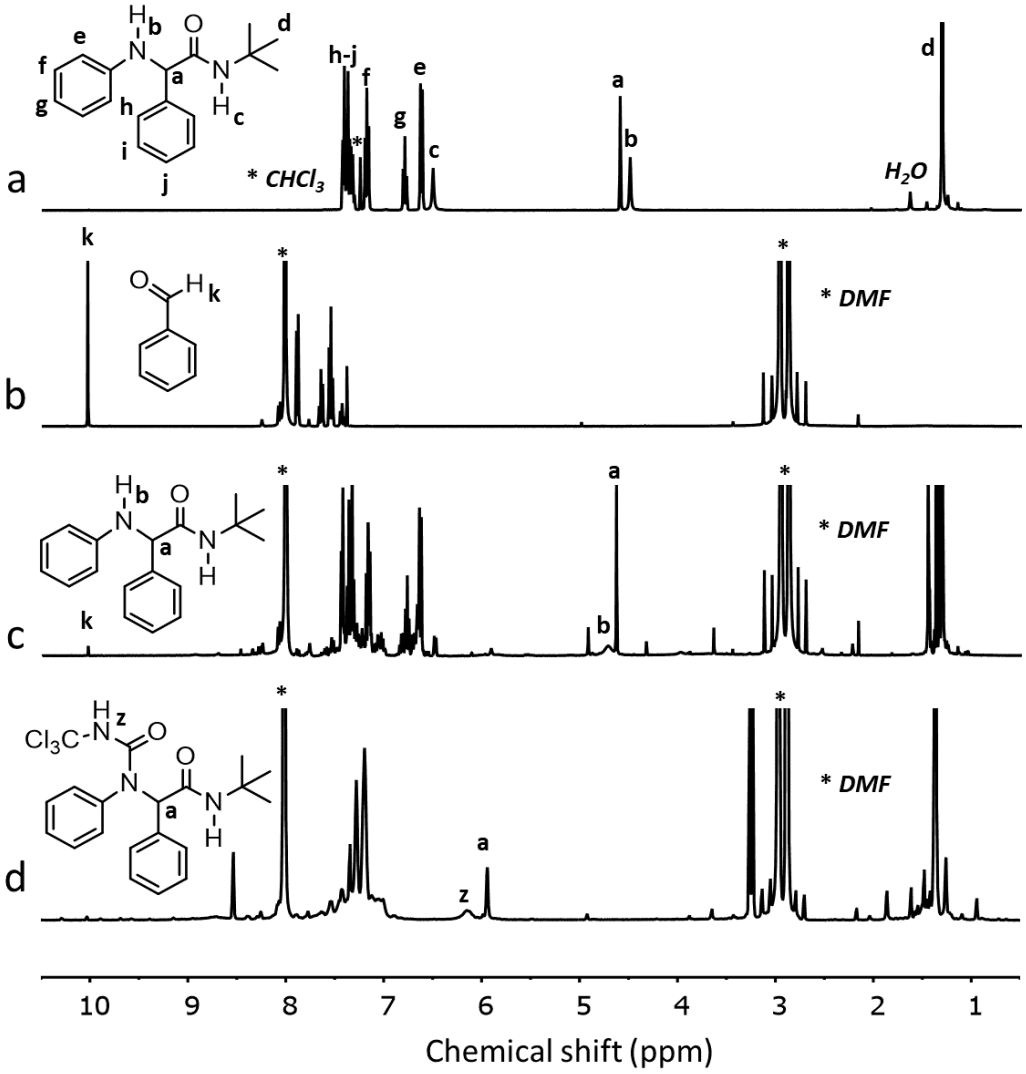

Figure S2. ^{1}H NMR spectrum in $CDCl_3$ of the isolated α-amino amide (a) produced *via* Ugi-3CR and of the crude reaction at 24 h and 80 °C before (c) and after addition of trichloroacetyl isocyanate (d). The ^{1}H NMR spectrum of benzaldehyde (3 mmol) in 3 mL of dry DMF (b) was used as a standard.

Additional comment on the determination of conversion: The initial solution of benzaldehyde in DMF (Figure S1b) was used as a standard to quantify the formation of the desired α-amino amide in the crude reaction mixture. The drastic decrease of the intensity of the aldehyde signal k in Figure S1c confirmed the occurrence of the reaction but the overlay of signals a and b hampered the proper determination of the reaction yield. This issue was tackled by reacting the crude mixture with trichoroacetyl isocyanate which quantitatively transformed the amino group into urea, as reported elsewhere (a) A. K. Bose *et al.*, Tetrahedron, 1975, 31, 3025–3029. b) V. W. Goodlett, Anal. Chem., 1965, 37, 431–432. c) A. Postma *et al.*, 2006, 47,

1899–1911). This treatment generated a new signal z fully dissociated from a (Figure S1d) allowing proper quantification of the yield of α-amino amide.

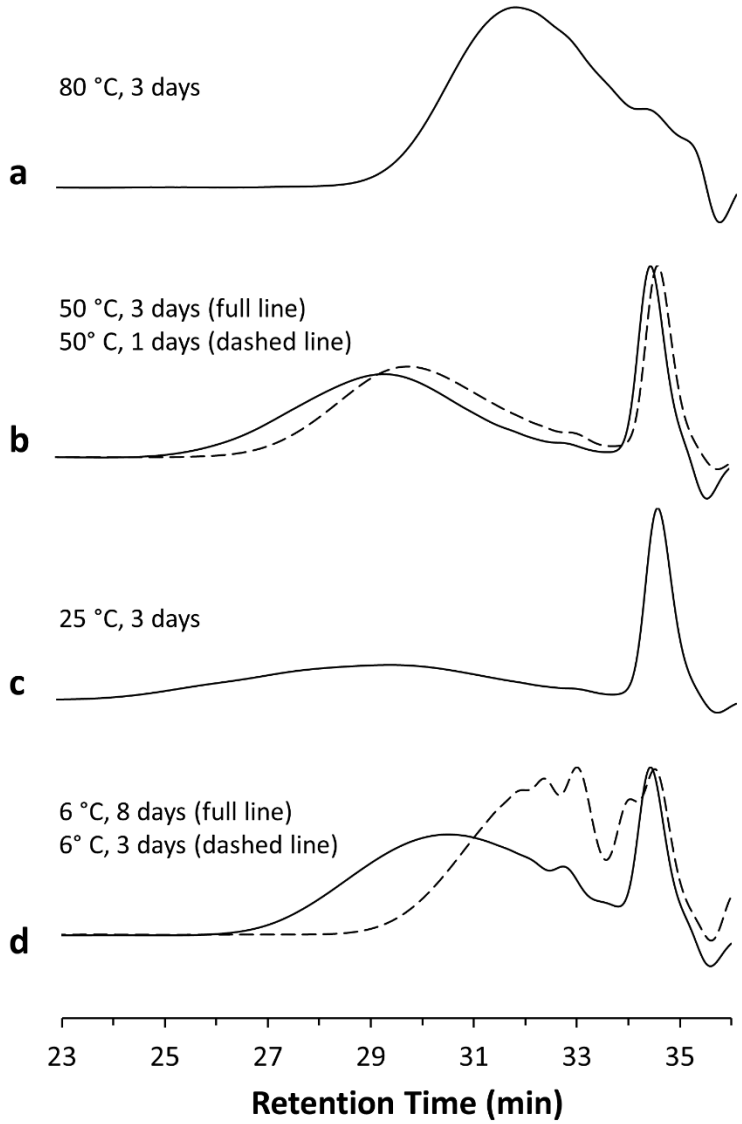

Figure S3. SEC chromatograms for the polymerization of p-phenylenediamine, benzaldehyde and 1,6-diisocyanohexane under different conditions. Reaction conditions and macromolecular characteristics (M_n, M_w and $Đ$) are presented in Table 2.

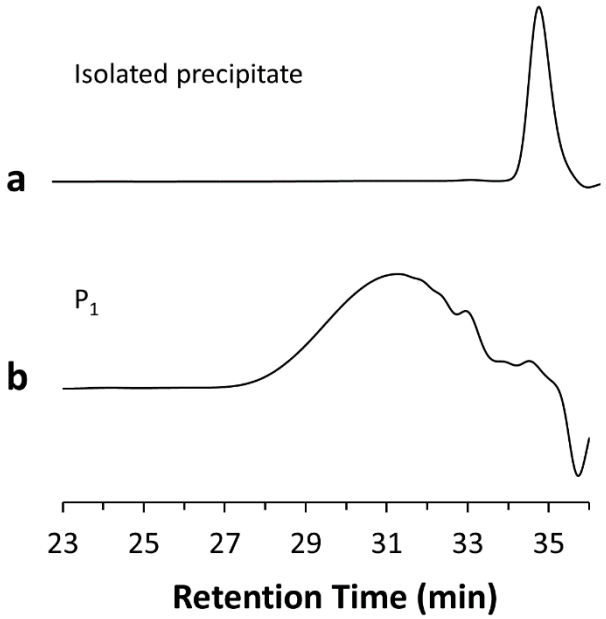

Figure S4. a) Size exclusion chromatogram of the isolated precipitate formed during the polymerization of p-phenylenediamine, benzaldehyde and 1,6-diisocyanohexane carried out at 50 °C for 1 day. b) Size exclusion chromatogram of P_1 contained in the dialyzed supernatant for the same polymerization.

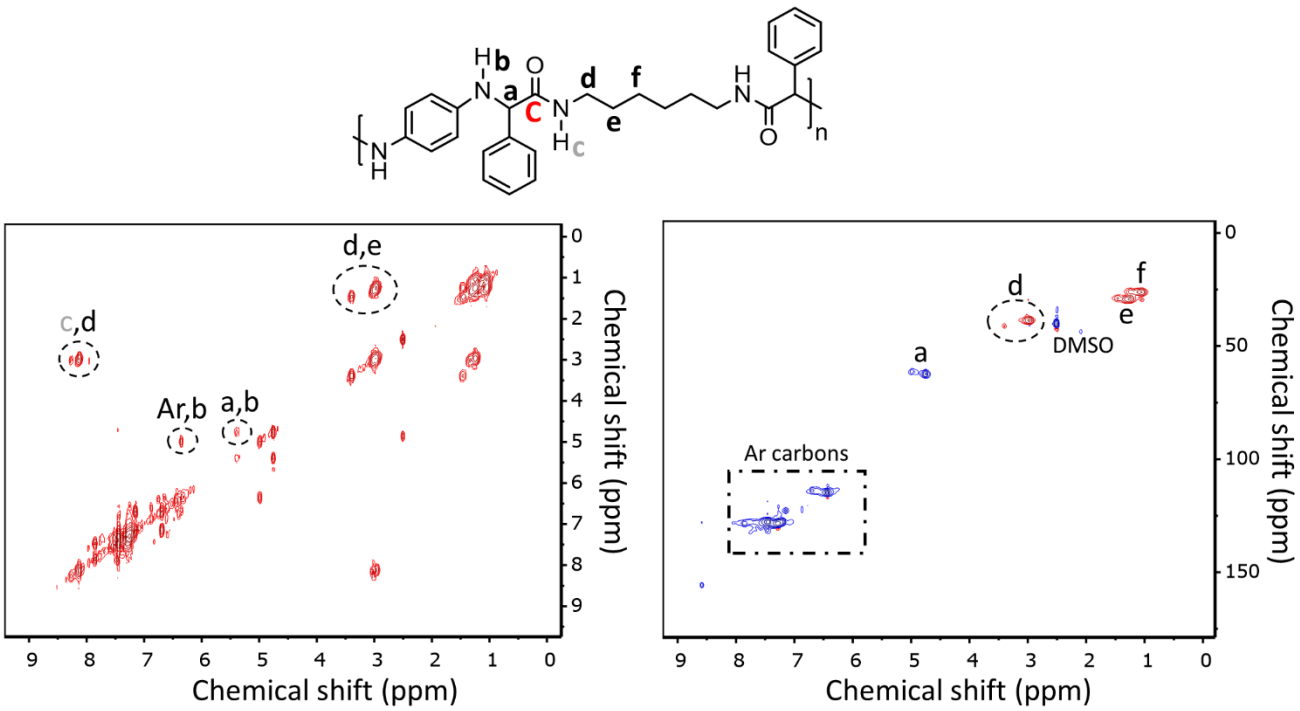

Figure S5. COSY (left) and HSQC (right) spectra of P_1 (Table 3, entry 1) in DMSO-d_6.

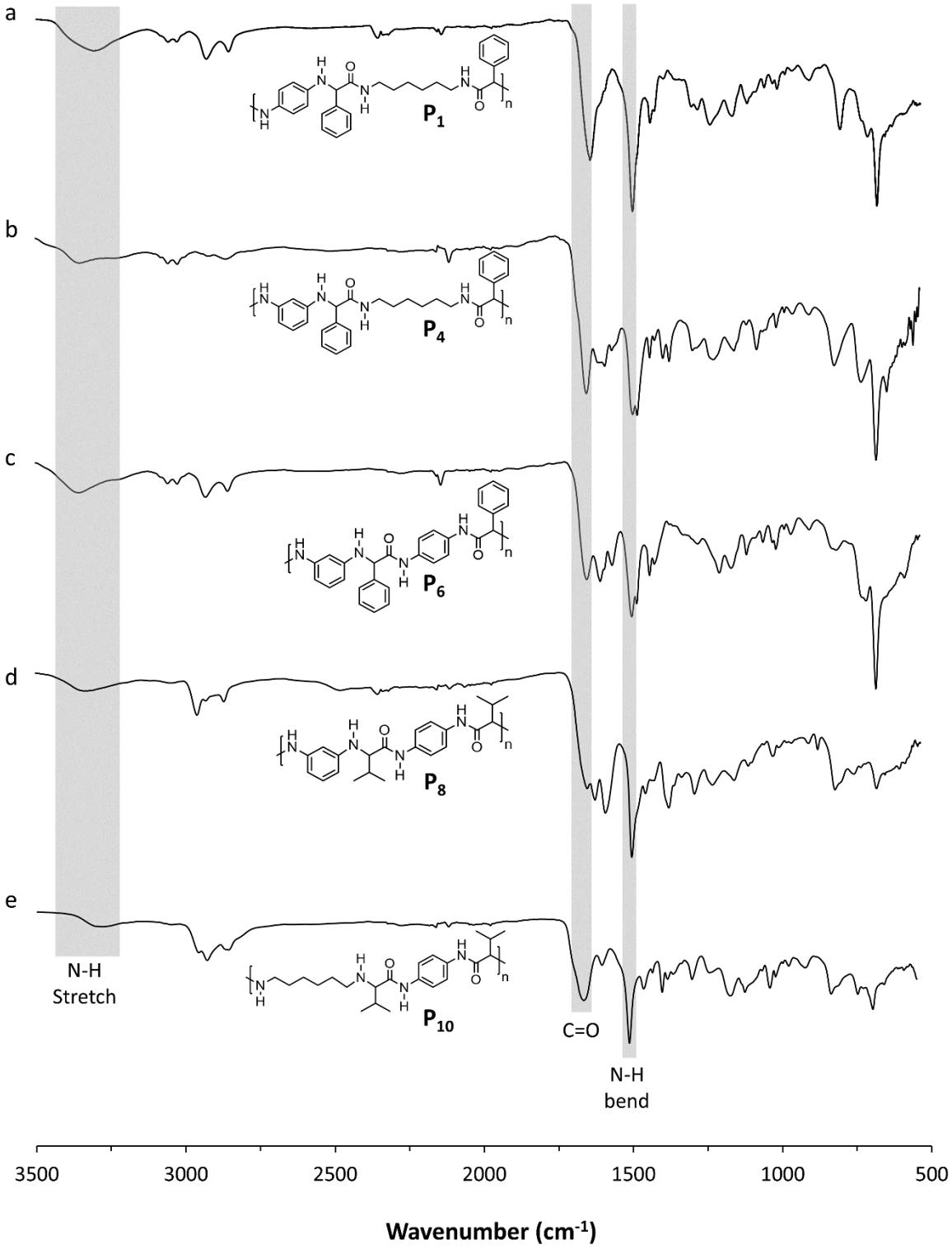

Figure S6. ATR analysis of a) P_1 (entry 1 in table 3), b) P_4 (entry 4 in table 3), c) P_6 (entry 4 in table 3), d) P_8 (entry 1 in table 3) and e) P_{10} (entry 4 in table 3).

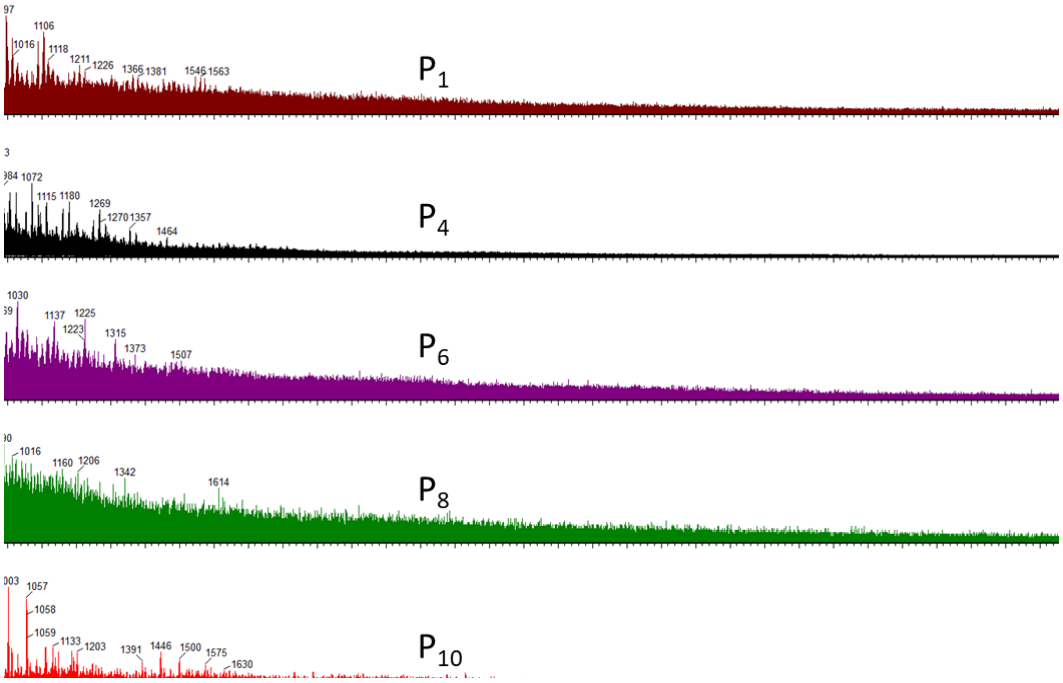

Figure S7. MALDI-TOF spectra of P1, P4, P6, P8, P10 recorded with trans-2-[3-(4-tert-butylphenyl)-2-methylprop-2-enylidene]malononitrile (DCTB) as matrix and NaI as for cationization.

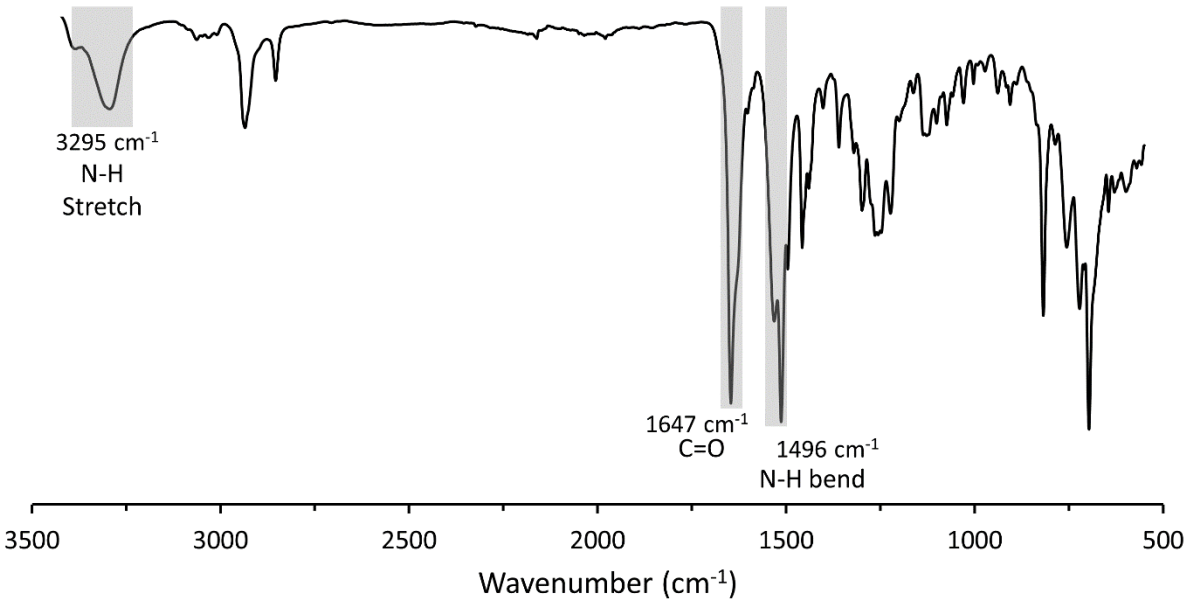

Figure S8. ATR analysis of the cyclic unimer which precipitates during the polymerization of p-phenylenediamine, benzaldehyde and 1,6 diisocyanohexane carried out at 50°C for 1 days (Figure S4a)

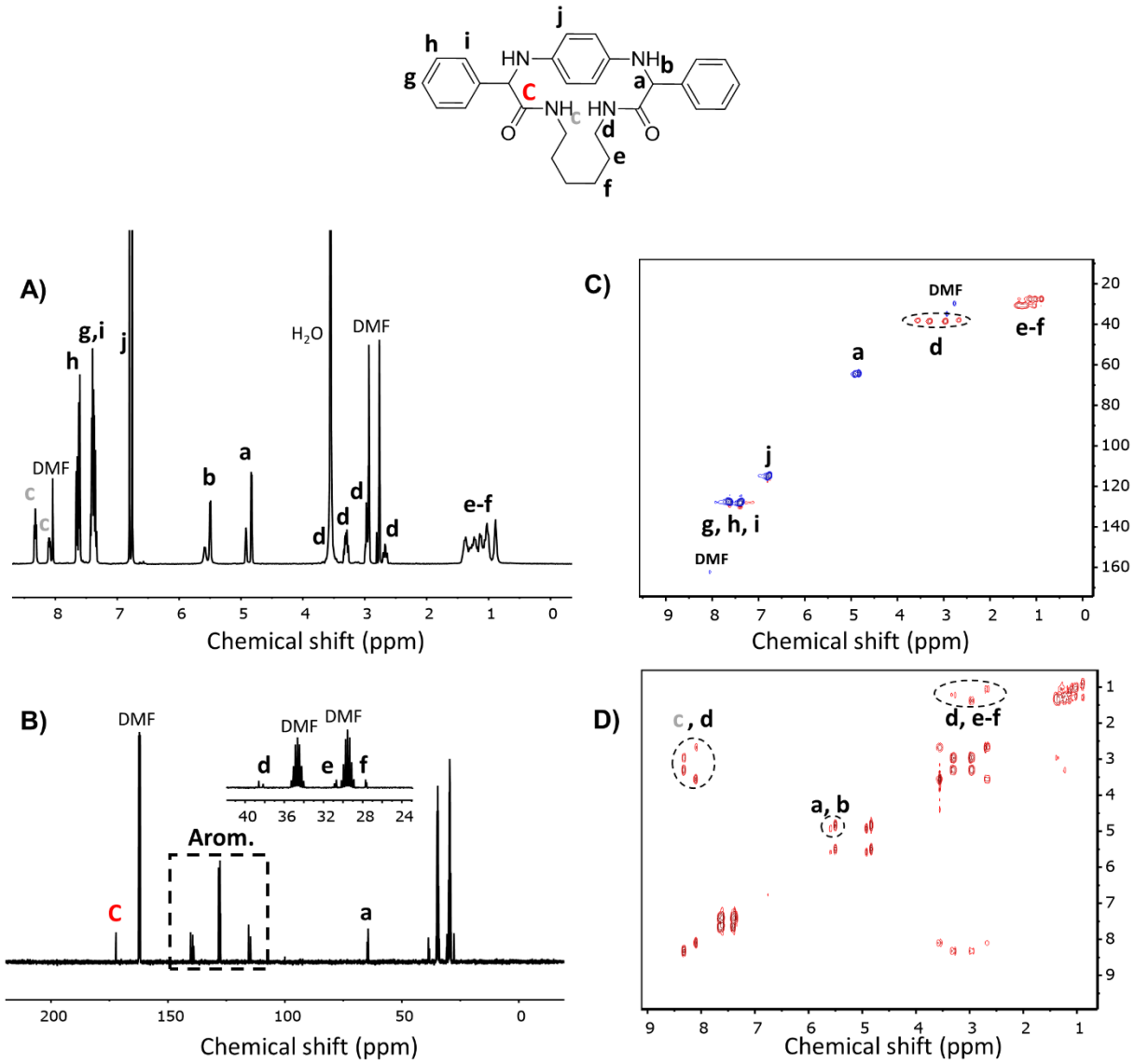

Figure S9. ^{1}H (A), ^{13}C (B), HSQC (C) and COSY (D) NMR spectra of the cyclic unimer which precipitates during the polymerization of p-phenylenediamine, benzaldehyde and 1,6 diisocyanohexane carried out at 50 °C for 1 days (Figure S4a).

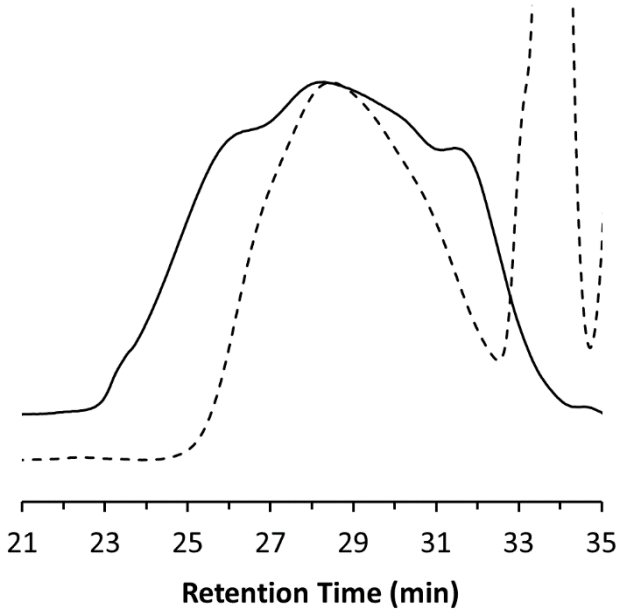

Figure S10. Size exclusion chromatograms of P_4 (entry 4 in table 3) before (full line) and after (dashed line) treatment with trichloroacetyl isocyanate. This treatment with trichloroacetyl isocyanate allows to transform the amine into urea and to prevent aggregation of the chains *via* hydrogen bonds or interaction with the column. Indeed, in the absence of such a treatment, a multimodal peak with unusually high dispersity (Đ = 3.9) was recorded (full line).

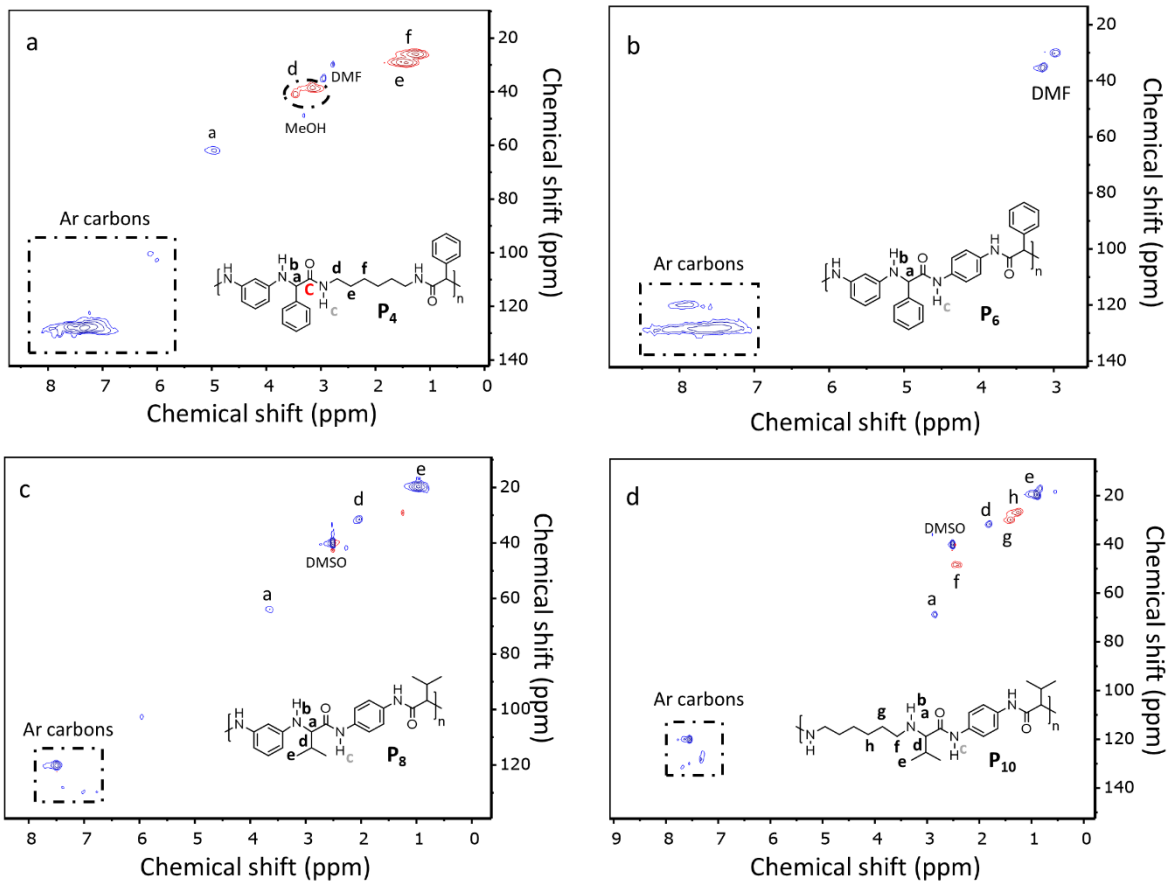

Figure S11. HSQC spectra of A) P_4, B) P_6 and C) P_8 (entry 4, 6 and 8, Table 3) in deuterated DMF for P_4 and P_6 and DMSO for P_8 and P_{10}.

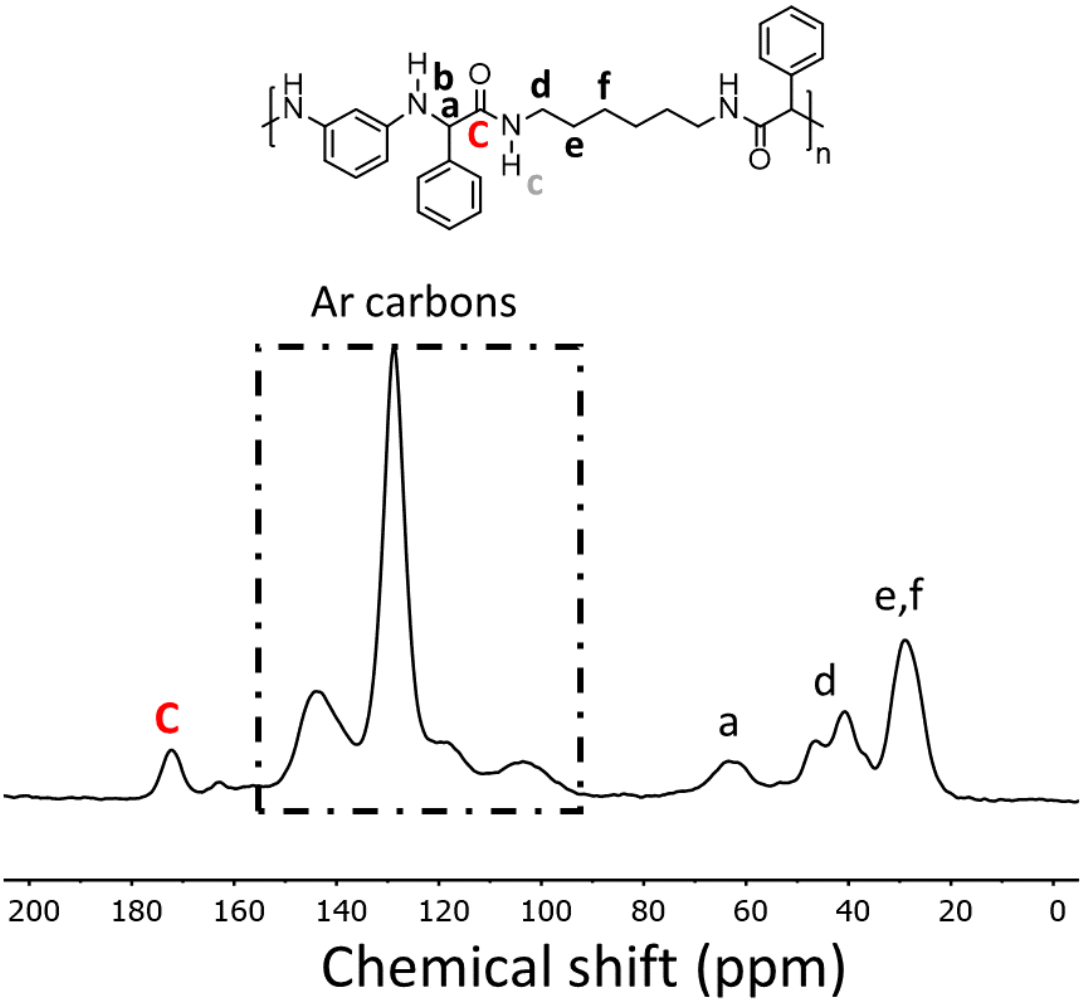

Figure S12. ^{13}C solid-state MAS NMR of P_4 recorded with 4-mm zirconia rotors spinning at 10 kHz on a Bruker Avance III HD spectrometer (B_0=9.04 T) working at the Larmor frequency of 100.62 MHz. Cross polarization experiments were performed with a delay time of 2 s and a contact time of 2 ms.

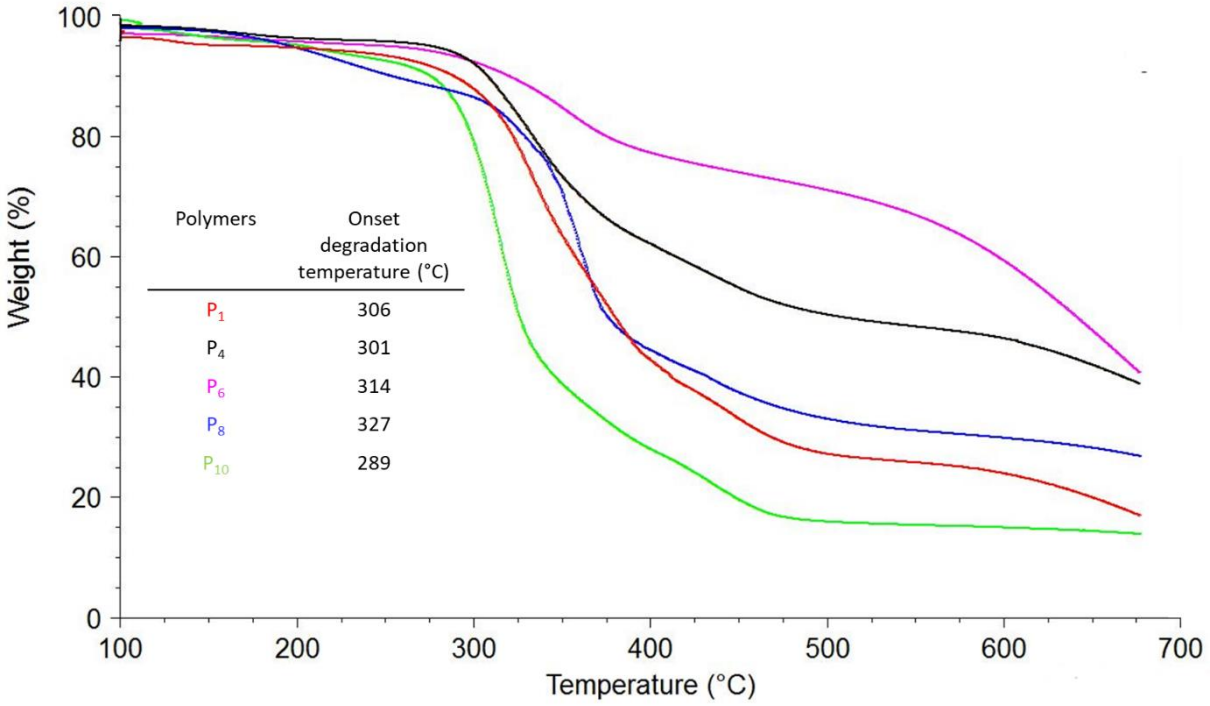

Figure S13. Thermogravimetric analysis of poly(α-amino amide)s (see Table 3 for detailed synthesis and structures) recorded with a temperature ramp of 20 °C min^{-1}.

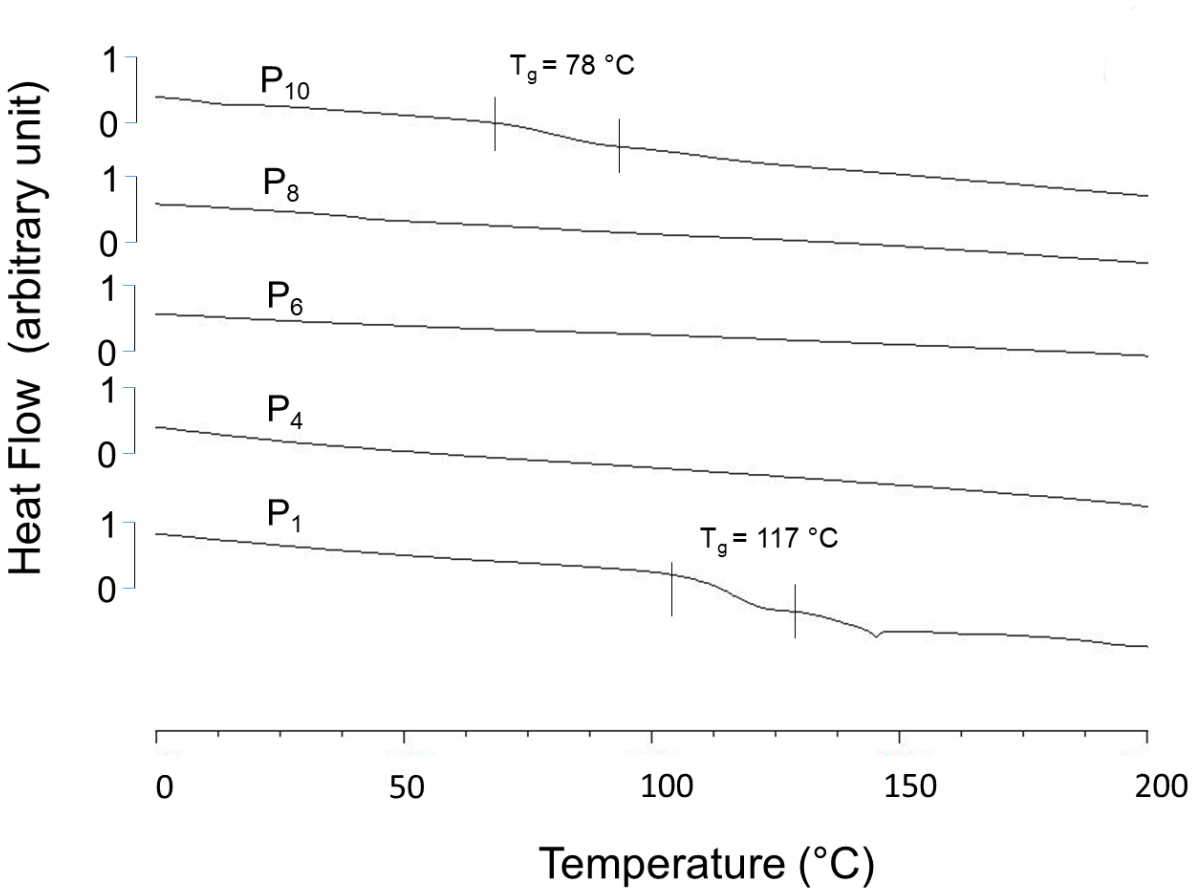

Figure S14. Differential scanning calorimetry analysis of poly(α-amino amide)s (see Table 3 for detailed synthesis and structures) recorded with a temperature ramp of 20 °C min^{-1}.

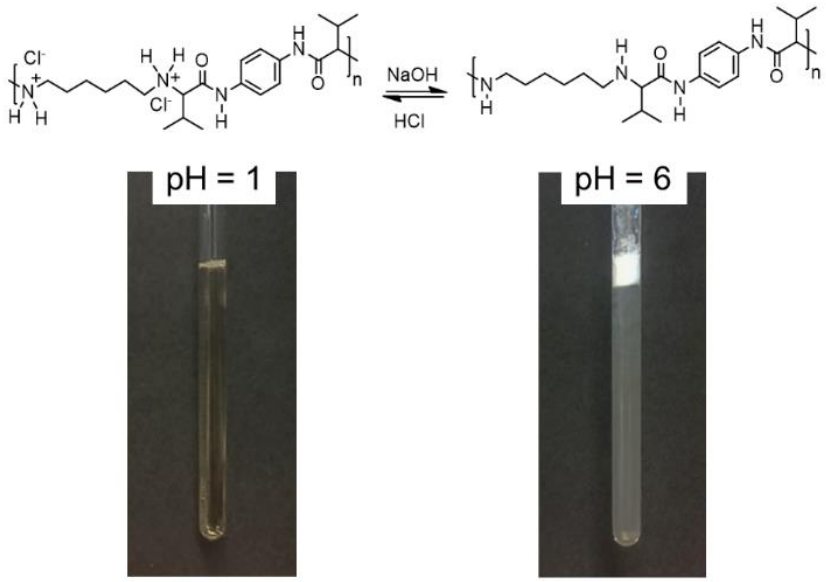

Figure S15. Illustration of the pH-responsive behaviour of the poly(α-amino amide) P_{10} in water at 5 mg mL^{-1}.

Chapter IV.

Multicomponent Radziszewski Emulsion Polymerization toward Macroporous Poly(ionic liquid) Catalysts

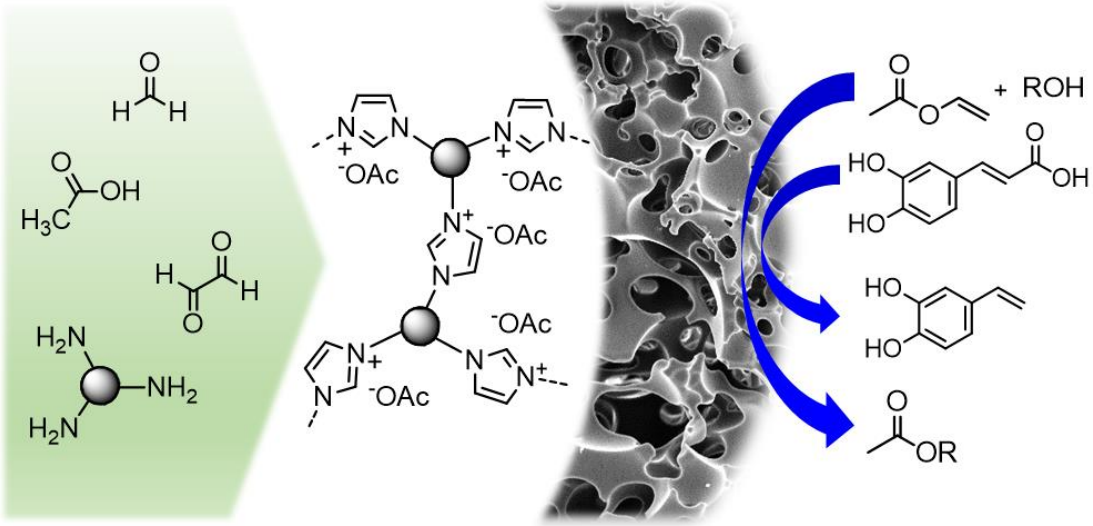

Abstract: Interconnected macroporous imidazolium-based monoliths are produced *via* the modified Radziszewski multicomponent reaction (MCR) applied to triamines under high internal phase emulsion (HIPE) conditions. This straightforward one-pot synthesis combines the efficiency and versatility of MCRs with the ease of implementation of the emulsion templating polymerization process. The characterization of the chemical structure and morphology of the resulting materials confirms the formation of the expected macroporous poly(ionic liquid)s (PILs) networks. The promising catalytic activity and recyclability of these porous PIL monoliths are illustrated for transesterification reaction and decarboxylation of caffeic acid. In these cases, almost complete conversion is reached while benefitting from the advantages associated to a heterogeneous catalyst.

Inspired from:

Stiernet, P.; Aqil, A.; Zhu, X.; Debuigne, A.; *ACS Macro Lett.* 2020, 9, 1, 134–139

Chapter IV. Multicomponent Radziszewski Emulsion Polymerization Towards Macroporous Poly(ionic liquid) Catalysts.

IV.1. Introduction

In the last years, multicomponent reactions (MCRs) have attracted a growing interest in the field of polymer chemistry and emerged as powerful macromolecular engineering methods due to their high efficiency, robustness, ease of implementation, atom economy as well as substrate versatility.[1–4] In these reactions, more than two compounds react in one-pot and form a product featuring almost all atoms of the starting materials.[5] Some famous MCRs have already been exploited for designing functional polymers such as the Passerini,[6–11] Ugi,[12–1920–24] Biginelli,[25–29] Kabachnick-fields[30–32] and Hantzsch[29,33] reactions, to name a few. The modified Debus-Radziszewski MCR, which converts primary amines, aldehyde and dicarbonyl compound into imidazolium derivatives under mild conditions, also proved its relevance in polymer synthesis, especially for the preparation of imidazolium-based poly(ionic liquid)s (PILs).[34] This reaction was used for the synthesis of ionic liquid building blocks,[35] as post-polymerization modification and crosslinking[36–40] but also for the preparation of linear PILs containing imidazolium moieties in their backbone. [41–43]

The development of PILs is also a fast-growing research area because these materials combine some valuable features of ionic liquids (ILs) with the intrinsic characteristics of polymers. In particular, porous PILs[44,45] raise tremendous interest in gas capture,[37,46–48] separation,[48–54] and catalysis,[55–59] due to their enlarged surface area, high ionic density, spatial structuration and tunability of their properties through counterions exchange. Structuring PILs into porous materials was achieved by hard templating based on inorganic particles,[47,53,54,60] by soft templating involving self-assembled copolymers[57] but also *via* template-free methods relying on porogenic solvents[59,61] or ionic complexations.[51,52,62,63] Some emulsion-templated radical polymerization methods also led to macroporous PILs.[64–66] Note that the porous PILs mentioned above were obtained using multistep approaches based on the polymerization of preformed ILs monomers and cross-linkers or by post-modification of porous organic networks. Therefore, the search for a simpler and straightforward synthesis of interconnected porous PILs is highly relevant.

In the present work, we applied the modified Radziszewski multicomponent polymerization under high internal phase emulsion (HIPE) for the first time and produced interconnected macroporous imidazolium-based networks in one-pot. To the best of our knowledge, it is the

first example of emulsion multicomponent polymerization. This practical and straightforward approach combines the great availability of the starting reagents, the efficiency of one-pot MCRs and the ease of implementation of emulsion templating polymerization.[67] The great potential of these interconnected macroporous PILs polyHIPEs as heterogeneous catalysts is highlighted for a model transesterification reaction and for the decarboxylation of renewable hydroxycinnamic acid derivatives.

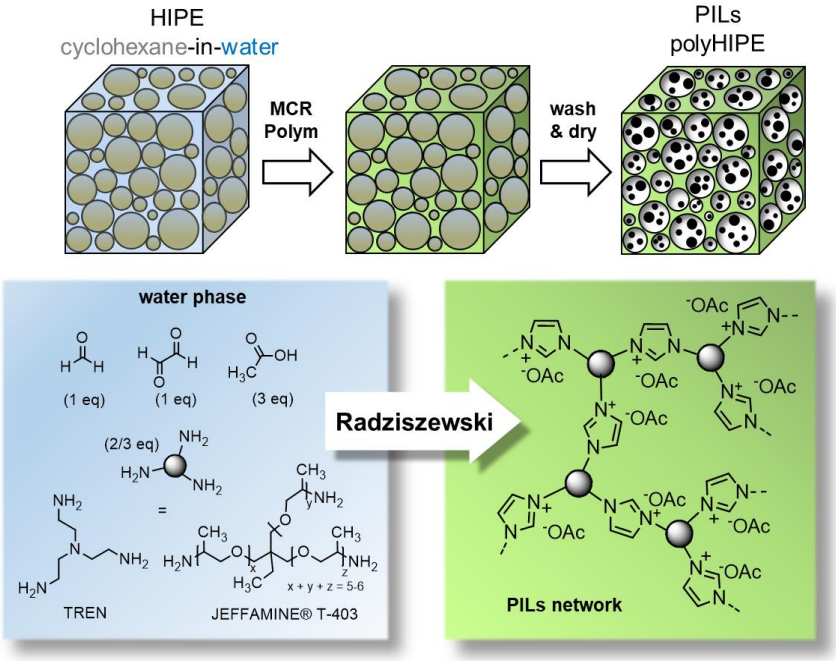

Scheme 1. General strategy for the synthesis of interconnected macroporous PILs via emulsion templating Radziszewski polymerization.

IV.2 Results and discussions

IV.2.1 Synthesis of polyHIPEs and their characterizations

The imidazolium units of our PIL networks were formed *via* Radziszewski reaction, which consists of coupling two amino groups with glyoxal and formaldehyde in the presence of acetic acid. Two commercially available triamines, namely tris(2-aminoethyl)amine (TREN) and Jeffamine-T403® (JEFF) composed of short poly(propylene oxide) (PPO) sequences, were considered as reactants to ensure the crosslinking of the final materials (Scheme 1). In order to create an interconnected porosity within these PILs, the polymerization was carried out in the external aqueous phase of a cyclohexane-in-water HIPE emulsion whose organic dispersed phase represents more than 74% of the emulsion volume. After the curing step, cyclohexane was removed leading to a typical polyHIPE structure composed of cavities connected to each other by pores. In practice, cyclohexane (75 v%) was added dropwise under stirring to an aqueous solution (25 v%) containing formaldehyde (1 equiv.), glyoxal (1 equiv.), triamine

(TREN or JEFF, 2/3 equiv.), acetic acid (3 equiv.) and PEO-PPO-PEO Pluronic® F-68 (4 wt% of the aqueous phase) used as a surfactant. The resulting mixtures were simply casted in a mould and cured at room temperature for 3 days. No demixing of the emulsions was observed during the polymerization and monoliths were collected accordingly. The latter are designated as P_{TREN} and P_{JEFF} throughout the text in reference to the triamines that compose them. After washing and drying under vacuum, P_{TREN} and P_{JEFF} were characterized by ^{13}C solid state NMR to ascertain their chemical structure (Figure 1). The formation of the imidazolium moieties is evidenced by peaks (**a** and **b**) at 125 and 140 ppm corresponding to the carbons of the heterocycles. The acetate counterions also feature peaks at 177 and 26 ppm assigned to the carbonyl **c** and the methyl group **d**, respectively. Expectedly, the ^{13}C spectra of $P_{TREN\text{-}OAc}$ and $P_{JEFF\text{-}OAc}$ only differ by signals corresponding to the spacers between the imidazolium ring (**e-k**). IR analyses further confirmed the formation of the PIL materials based on peaks at 1573 and 1381 cm^{-1} attributed to the C=O stretching of the acetate group and signals at 1150 and 1060 cm^{-1} assigned to the stretching vibrations of the imidazolium ring (Figures S1 and S2).[68]

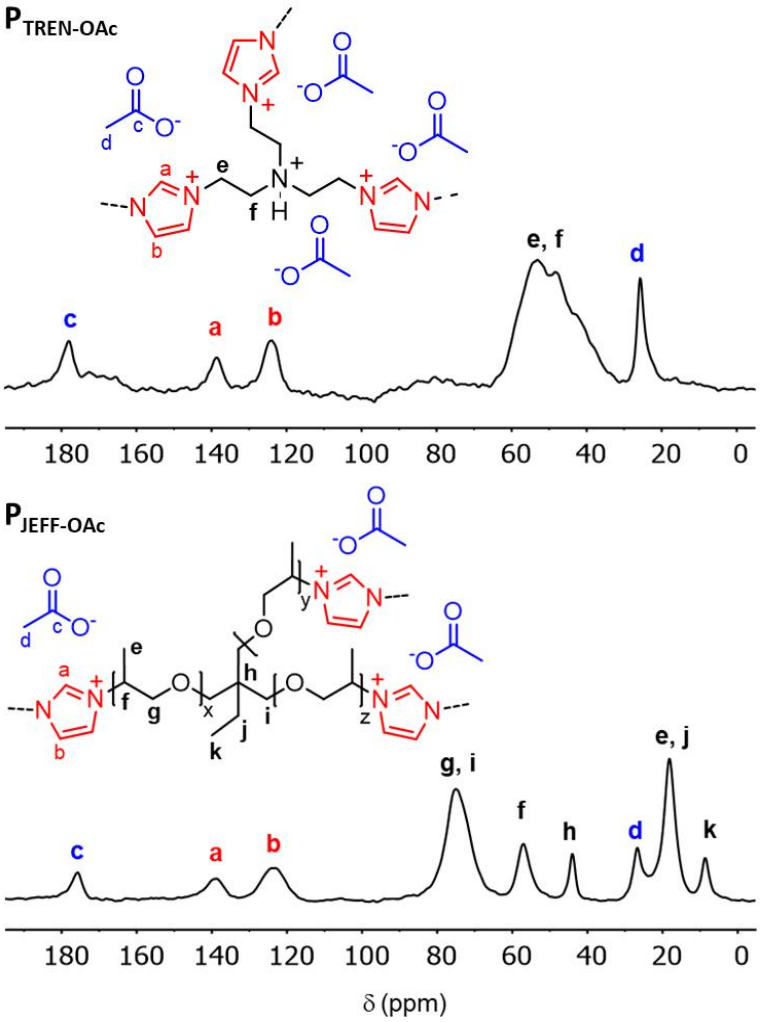

Figure 1. ^{13}C solid state NMR spectra of $P_{TREN\text{-}OAc}$ and $P_{JEFF\text{-}OAc}$.

After confirming the chemical structures of the PIL materials, we addressed their macroscopic behaviours and porous architectures. The morphology of $P_{TREN\text{-}OAc}$ and $P_{JEFF\text{-}OAc}$ was tentatively investigated by conventional scanning electron microscopy (SEM). However, significant shrinkage of the samples occurred upon drying, especially for $P_{JEFF\text{-}OAc}$. The volume of $P_{TREN\text{-}OAc}$ and $P_{JEFF\text{-}OAc}$ are reduced by a factor 2 and 10, respectively, compared to the crude materials, as displayed in Figures S3A-F. In spite of this phenomenon, SEM images of $P_{TREN\text{-}OAc}$ show the typical open-porous structure of polyHIPEs (Figure S3G). Although some remnants of the cavities of $P_{JEFF\text{-}OAc}$ seem to appear on the SEM pictures, no conclusion can be drawn on their porosity which collapsed upon drying (Figure S3H). Such a discrepancy between these materials might be due to the lower intrinsic crosslinking density of $P_{JEFF\text{-}OAc}$ produced from a triamine with longer arms. In order to overcome the shrinkage issue, the polyHIPEs were dried using a procedure based on the critical point drying and analysed by FESEM (Figure 2). First, the crude $P_{TREN\text{-}OAc}$ and $P_{JEFF\text{-}OAc}$ (Figures 2A-B) were washed by prolonged immersion in DMSO (Figures 2C-D). The comparison of Figures 2C and 2D clearly suggests a higher solvent uptake (SU) in DMSO for P_{JEFF} compared to P_{TREN} (SU $P_{TREN\text{-}OAc}$ = 2000 wt% and $P_{JEFF\text{-}OAc}$ = 4200 wt%). The higher swelling of the latter can be ascribed to the affinity of its PPO sequences for DMSO and to its lower ^{crosslinking} density previously mentioned. Then, DMSO contained in the polyHIPEs was exchanged for water prior to drying *via* the critical point method. As expected, the FESEM images clearly highlight the open structure of both polyHIPEs (Figures 2E-J). In the case of $P_{TREN\text{-}OAc}$, the cavities vary in size from 5 to 30 μm with an average diameter of 9 μm, whereas the pores size is around 2-5 μm (Figures 2E-H). Because FESEM pictures do not display defined spherical voids for $P_{JEFF\text{-}OAc}$, it is difficult to evaluate properly the average size of its cavities. Nevertheless, the presence of an interconnected porosity is undeniable, especially at the highest magnification (Figure 2J), and the pores of $P_{JEFF\text{-}OAc}$ and $P_{TREN\text{-}OAc}$ seem to be in the same range, *i.e.* 2-5 µm (compare Figures 2I and 2J).

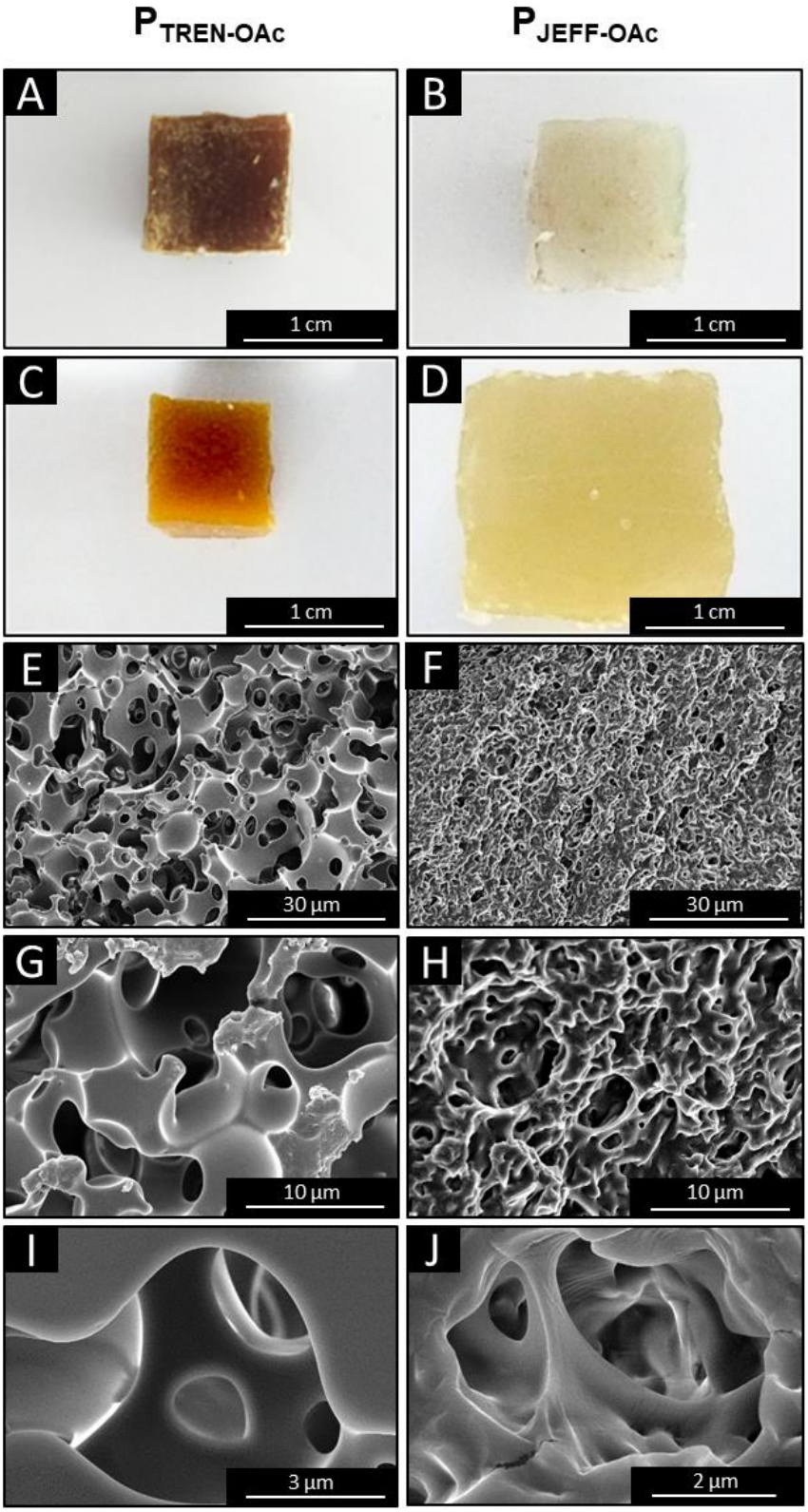

Figure 2. Pictures of $P_{TREN\text{-}OAc}$ (A, C) and $P_{JEFF\text{-}OAc}$ (B, D) before (A, B) and after (C, D) immersion in DMSO. FESEM pictures of $P_{TREN\text{-}OAc}$ (E, G, I) and $P_{JEFF\text{-}OAc}$ (F, H, J).

Before considering any application of these macroporous PILs, we studied their thermal properties and swelling in order to identify their potential operating conditions and also their ability to undergo counterion exchange reactions, because the properties of PILs highly depend on this parameter.[69] Such ion exchange reactions were thus applied to the imidazolium-based polyHIPEs composed of acetate anions originating from the acetic acid used in the Radziszewski reaction. As illustrated above, such a polar anion favors the swelling of the porous PILs in polar solvents like water, DMSO and MeOH. The acetate anions of $P_{TREN\text{-}OAc}$ and $P_{JEFF\text{-}OAc}$ were then exchanged for bromide (Br^-) and bis(trifluoromethanesulfonyl)imide (TFSI) in MeOH using an excess of NaBr and LiTFSI salts. Note that the macroporosity of the polyHIPEs facilitates the diffusion of the anions in the heart of the monoliths. IR (Figures S1 and S2) and solid-state NMR (Figures S4 and S5) analyses confirmed the successful ion-exchange *via* the disappearance of signals characteristic of the carbonyl of the acetate. As anticipated, changing the counterion of the polyHIPEs significantly affected their swelling. Indeed, when immersed in the NaBr or LiTFSI solutions, P_{TREN} and P_{JEFF} gradually shrank until there was a complete exchange (Figure S6). Like linear PILs,[69] the thermal properties of the PIL polyHIPEs, in particular, P_{JEFF}, are also influenced by the nature of anions (Table S1). For example, Jeffamine-based polyHIPEs with different anions are ranked in the following order of increasing glass transition temperature (T_g): $P_{JEFF\text{-}TFSI}$ (−5 °C) < $P_{JEFF\text{-}OAc}$ (27 °C) < $P_{JEFF\text{-}Br}$ (61 °C). The onset degradation temperatures (T_{OD}) followed a different order, that is, $P_{JEFF\text{-}OAc}$ (172 °C) < $P_{JEFF\text{-}Br}$ (300 °C) < $P_{JEFF\text{-}TFSI}$ (347 °C). The same trend was observed for the T_{OD} of the P_{TREN} derivatives, which exhibit lower thermal stabilities compared to their P_{JEFF} counterparts (151 °C < T_{OD} < 274 °C, Table S1). Overall, these ion-properties dependences emphasize that the imidazolium-based polyHIPEs possess the intrinsic characteristics of PIL materials.

IV.2.3 Catalysis application

Finally, we explored the potential of P_{TREN} and P_{JEFF} macroporous PILs in catalysis especially for transesterification and decarboxylation reactions known to be catalysed in the presence of imidazolium derivatives.[70,71] For example, Taton et al. catalysed transesterifications with styrene/vinyl imidazolium acetate-based copolymers.[72] In this case, transesterification yields as high as 97% were reached after 2 h at 80 °C in THF. Recently, Singh et al. described the use of 1-ethyl-3-methyl imidazolium acetate for catalysing the decarboxylation of hydroxycinnamic acid derivatives, which are naturally abundant in plants, leading to vinyl catechol.[71] In this case, the self-deprotonation of the imidazolium moieties produced *in situ N*-

heterocyclic carbenes (NHCs), which catalysed the decarboxylation of the hydroxycinnamic acid compounds.[71] The organocatalyst was recycled *via* extraction using a biphasic reaction system. Considering the excellent flow through properties and the substantial surface area associated to macroporous materials, the imidazolium-based polyHIPEs developed in this work appear as very promising supports for catalysis notably in terms of accessibility to the catalytic site and recyclability. For this reason, we tested $P_{TREN\text{-}OAc}$ and $P_{JEFF\text{-}OAc}$ as catalysts for the decarboxylation of cinnamic acid derivatives and transesterification of vinyl esters (Scheme 2 and Table 1).

The catalytic efficiencies of $P_{TREN\text{-}OAC}$ and $P_{JEFF\text{-}OAc}$ were first assessed for the transformation

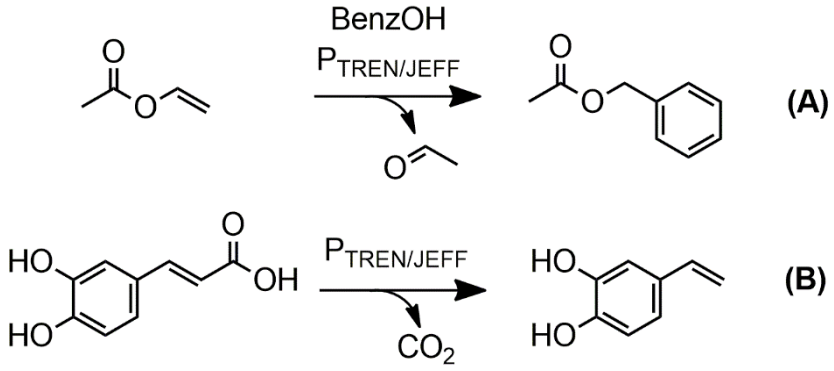

Scheme 2. Porous PILs-catalysed transesterification and decarboxylation.

of vinyl acetate (VAc) into benzyl acetate (BenzOAc) in the presence of benzyl alcohol (Table 1, part A). This model transesterification reaction was performed in THF at 80 °C using 10 mol% of imidazolium moieties, as described elsewhere,[72] and the conversion was monitored by ^{1}H NMR (Figure S7). After 4 h, the conversion reached 58 % for P_{JEFF} and only 4 % for P_{TREN}. Such a discrepancy most probably accounts for the lower swelling of P_{TREN} in THF compared to P_{JEFF}, which limits the access of the substrates to the catalytic moieties located in the polyHIPE walls. Longer reaction time, for example 24 h, improved the conversion (15 and 83 % for P_{TREN} and P_{JEFF}, respectively). Finally, a conversion as high as 92 % was achieved when doubling the catalyst load for P_{JEFF}.

Inspired by Singh *et al.* who reported the complete decarboxylation of caffeic acid into 4-vinyl catechol after 1 h at 120 °C in the presence of 100 mol% of 1-ethyl-3-methyl imidazolium acetate,[71] we tested $P_{TREN\text{-}OAc}$ and $P_{JEFF\text{-}OAc}$ as catalysts of this reaction under similar conditions (115 °C, 100 mol% of imidazolium functions; Table 1, part B). Note that the temperature was lowered to 115 °C in order to prevent any degradation of $P_{TREN\text{-}OAc}$ which exhibits the lowest T_{OD}, as mentioned earlier. Under these conditions, near quantitative formation of vinyl catechol

(determined by ^{1}H NMR, Figure S8) was achieved after 90 min with both polyHIPEs, which is quite similar to the performances reported for the free imidazolium acetate catalysts.[71] Hence, lower catalyst loadings were considered. These experiments underlined the higher catalytic efficiency of $P_{JEFF\text{-}OAc}$. The conversion reached 100 % and 54 % in the presence of 50 mol% of P_{JEFF} and P_{TREN}, respectively. High conversion (95 %) can also be achieved after 8 h with 10 mol % of P_{JEFF}, which represents a 10-fold decrease of the catalyst loading compared to the initial report involving free ILs.[71] Decreasing the temperature to 80 °C almost inhibits the decarboxylation reaction (Table 1). Overall, P_{JEFF} appears as the most promising catalyst for both types of reactions.

Table 1. Transesterification and decarboxylation reactions catalysed by $P_{JEFF\text{-}OAc}$ and $P_{TREN\text{-}OAc}$.

Reaction	Solvent	Temp. (°C)	Cata. [a] (mol %)	Time (h)	Conv. [b] (%) P_{TREN} / P_{JEFF}
(A) Transester.	THF	80	10	4	4 / 58
	THF	80	10	8	7 / 69
	THF	80	10	24	15 / 83
	THF	80	20	24	17 / 92
	THF	80	0	24	0
(B) Decarbox.	DMSO	115	100	1.5	98/100
	DMSO	115	50	1.5	54 / 100
	DMSO	115	10	1.5	19 / 32
	DMSO	115	10	8	65 / 95
	DMSO	80	50	1.5	2 / 11
	DMSO	115	0	4	0

[a] Mol % of imidazolium moieties compared to BenzOH or caffeic acid. [b] Determined by ^{1}H NMR. Cond. transester.: BenzOH (5 mmol, 1 M), VAc (6 mmol, 1.2 M). Cond. decarbox.: Caffeic acid (0.5 mmol, 0.1 M).

Finally, the excellent recyclability of the macroporous PIL catalysts was demonstrated for the decarboxylation reaction. P_{JEFF} and P_{TREN} were used five times without drastic deactivation or formation of side products (Figure S9). Note that the recycling procedure is very easy to implement. For the sake of the accuracy of the study, polyHIPEs were immersed in DMSO between each recycling, but in practice, this step is not mandatory: new portions of reactants can be added to the porous PILs after simple removal of the reaction supernatant.

IV.3 Conclusions

In conclusion, we implemented a multicomponent polymerization under emulsion conditions for the first time and developed a unique and straightforward platform for the synthesis of macroporous imidazolium-based networks. This one-pot approach combining the Radziszewski MCR and the emulsion templating polymerization process satisfies several criteria for widespread use in practical applications, including great availability of the reactants, high atom economy, metal-free, room temperature, and non-sensitivity to moisture or air. The resulting

porous PIL monoliths were shown to be very efficient catalysts for transesterification and decarboxylation reactions. They were also easily recycled, and no loss of activity was detected after several recycling steps. Given the excellent flow-through properties associated to macroporous polyHIPEs, their use as supported catalysts in continuous flow chemistry is promising and is under current investigation. In this study, the imidazolium acetate-based polyHIPEs were selected to illustrate the potential of such materials, but we also demonstrated the possibility of exchanging their counterions and tuning their properties. This feature allows to consider numerous other catalytic reactions and to considerably broaden the scope of their use, especially for separation and gas capture applications.

IV.4 References

(1) Kakuchi, R. *Angew. Chemie Int. Ed.* **2014**, *53* (1), 46–48.

(2) Yang, B.; Zhao, Y.; Wei, Y.; Fu, C.; Tao, L. *Polym. Chem.* **2015**, *6* (48), 8233–8239.

(3) Rudick, J. G. *J. Polym. Sci. Part A* **2013**, No. 51, 3985–3991.

(4) Meier, M. A. R.; Sehlinger, A. Theato, P., Ed.; Springer, Cham, 2015.

(5) Dömling, A.; Wang, W.; Wang, K. *Chem. Rev.* **2012**, *112* (6), 3083–3135.

(6) Zhang, J.; Wu, Y.; Wang, J.; Du, F.; Li, Z. *Macromolecules* **2018**, *51*, 5842–5851.

(7) Cui, Y.; Zhang, M.; Du, F.-S.; Li, Z.-C. *ACS Macro Lett.* **2017**, *6* (1), 11–15.

(8) Zhang, J.; Zhang, M.; Du, F.-S.; Li, Z.-C. *Macromolecules* **2016**, *49* (7), 2592–2600.

(9) Sehlinger, A.; Schneider, R.; Meier, M. A. R. *Eur. Polym. J.* **2014**, *50*, 150–157.

(10) Wang, Y.-Z.; Deng, X.-X.; Li, L.; Li, Z.-L.; Du, F.-S.; Li, Z.-C. *Polym. Chem.* **2013**, *4* (3), 444–448.

(11) Deng, X.-X.; Li, L.; Li, Z.-L.; Lv, A.; Du, F.-S.; Li, Z.-C. *ACS Macro Lett.* **2012**, *1* (11), 1300–1303.

(12) Stiernet, P.; Lecomte, P.; De Winter, J.; Debuigne, A. *ACS Macro Lett.* **2019**, *8* (4), 427–434.

(13) Tao, Y.; Wang, Z.; Tao, Y. *Biopolymers* **2019**, *110* (6), e23288.

(14) Schade, O. R.; Dannecker, P.-K.; Kalz, K. F.; Steinbach, D.; Meier, M. A. R.; Grunwaldt, J.-D. *ACS Omega* **2019**, *4* (16), 16972–16979.

(15) Hartweg, M.; Edwards-Gayle, C. J. C.; Radvar, E.; Collis, D.; Reza, M.; Kaupp, M.; Steinkoenig, J.; Ruokolainen, J.; Rambo, R.; Barner-Kowollik, C.; Hamley, I. W.; Azevedo, H. S.; Becer, C. R. *Polym. Chem.* **2018**, *9* (4), 482–489.

(16) Koyama, Y.; Ihsan, A. B.; Taira, T.; Imura, T. *RSC Adv.* **2018**, *8* (14), 7509–7513.

(17) Tao, Y.; Wang, S.; Zhang, X.; Wang, Z.; Tao, Y.; Wang, X. *Biomacromolecules* **2018**,

19 (3), 936–942.

(18) Al Samad, A.; De Winter, J.; Gerbaux, P.; Jérôme, C.; Debuigne, A. *Chem. Commun.* **2017**, *53* (90), 12240–12243.

(19) Koyama, Y.; Gudeangadi, P. G. *Chem. Commun.* **2017**, *53* (27), 3846–3849.

(20) Hartweg, M.; Becer, C. R. *Green Chem.* **2016**, *18* (11), 3272–3277.

(21) Zhang, X.; Wang, S.; Liu, J.; Xie, Z.; Luan, S.; Xiao, C.; Tao, Y.; Wang, X. *ACS Macro Lett.* **2016**, *5* (9), 1049–1054.

(22) Gangloff, N.; Nahm, D.; Döring, L.; Kuckling, D.; Luxenhofer, R. *J. Polym. Sci. Part A Polym. Chem.* **2015**, *53* (14), 1680–1686.

(23) Sehlinger, A.; Dannecker, P. K.; Kreye, O.; Meier, M. A. R. A. R. *Macromolecules* **2014**, *47* (9), 2774–2783.

(24) Sehlinger, A.; Schneider, R.; Meier, M. A. R. *Macromol. Rapid Commun.* **2014**, *35* (21), 1866–1871.

(25) Boukis, A. C.; Llevot, A.; Meier, M. A. R. *Macromol. Rapid Commun.* **2016**, *37* (7), 643–649.

(26) Zhao, Y.; Wu, H.; Wang, Z.; Wei, Y.; Wang, Z.; Tao, L. *Sci. China Chem.* **2016**, *59* (12), 1541–1547.

(27) Zhao, Y.; Yu, Y.; Zhang, Y.; Wang, X.; Yang, B.; Zhang, Y.; Zhang, Q.; Fu, C.; Wei, Y.; Tao, L. *Polym. Chem.* **2015**, *6* (27), 4940–4945.

(28) Zhao, Y.; Wu, H.; Zhang, Y.; Wang, X.; Yang, B.; Zhang, Q.; Ren, X.; Fu, C.; Wei, Y.; Wang, Z.; Wang, Y.; Tao, L. *ACS Macro Lett.* **2015**, *4* (8), 843–847.

(29) Wu, H.; Fu, C.; Zhao, Y.; Yang, B.; Wei, Y.; Wang, Z.; Tao, L. *ACS Macro Lett.* **2015**, *4* (11), 1189–1193.

(30) Moldenhauer, F.; Kakuchi, R.; Theato, P. *ACS Macro Lett.* **2016**, *5* (1), 10–13.

(31) Bachler, P. R.; Schulz, M. D.; Sparks, C. A.; Wagener, K. B.; Sumerlin, B. S. *Macromol. Rapid Commun.* **2015**, *36* (9), 828–833.

(32) Zhang, Y.; Zhao, Y.; Yang, B.; Zhu, C.; Wei, Y.; Tao, L. *Polym. Chem.* **2014**, *5* (6), 1857–1862.

(33) Wu, H.; Wang, Z.; Tao, L. *Polym Chem* **2017**, *8*, 7290–7296.

(34) Saxer, S.; Marestin, C.; Mercier, R.; Dupuy, J. *Polym. Chem.* **2018**, *9* (15), 1927–1933.

(35) Esposito, D.; Kirchhecker, S.; Antonietti, M. *Chem. – A Eur. J.* **2013**, *19* (45), 15097–15100.

(36) Zhao, X.; Guo, S.; Li, H.; Liu, J.; Liu, X.; Song, H. *Macromol. Rapid Commun.* **2017**, *38* (21), 1700415.

(37) Dani, A.; Crocellà, V.; Magistris, C.; Santoro, V.; Yuan, J.; Bordiga, S. *J. Mater. Chem. A* **2017**, *5* (1), 372–383.

(38) Sirviö, J. A.; Visanko, M.; Liimatainen, H. *RSC Adv.* **2016**, *6* (61), 56544–56548.

(39) Talapaneni, S. N.; Buyukcakir, O.; Je, S. H.; Srinivasan, S.; Seo, Y.; Polychronopoulou, K.; Coskun, A. *Chem. Mater.* **2015**, *27* (19), 6818–6826.

(40) Krannig, K.-S.; Esposito, D.; Antonietti, M. *Macromolecules* **2014**, *47* (7), 2350–2353.

(41) Grygiel, K.; Kirchhecker, S.; Gong, J.; Antonietti, M.; Esposito, D.; Yuan, J. *Macromol. Chem. Phys.* **2017**, *218* (18), 1600586.

(42) Lindner, J.-P. *Macromolecules* **2016**, *49* (6), 2046–2053.

(43) Castro-grijalba, A.; Reyes-gallardo, E. M.; Wuilloud, R. G. *RSC Adv.* **2017**, *7*, 42979–42985.

(44) Zhang, W.; Zhao, Q.; Yuan, J. *Angew. Chemie Int. Ed.* **2018**, *57* (23), 6754–6773.

(45) Zhang, S.; Dokko, K.; Watanabe, M. *Chem. Sci.* **2015**, *6* (7), 3684–3691.

(46) Soll, S.; Zhao, Q.; Weber, J.; Yuan, J. *Chem. Mater.* **2013**, *25* (15), 3003–3010.

(47) Wilke, A.; Yuan, J.; Antonietti, M.; Weber, J. *ACS Macro Lett.* **2012**, *1* (8), 1028–1031.

(48) Zulfiqar, S.; Sarwar, M. I.; Mecerreyes, D. *Polym. Chem.* **2015**, *6* (36), 6435–6451.

(49) Li, Y.; Qi, L.; Shen, Y.; Zhang, H.; Ma, H. *Chinese J. Chem.* **2014**, *32* (7), 619–625.

(50) Yin, M.-J.; Zhao, Q.; Wu, J.; Seefeldt, K.; Yuan, J. *ACS Nano* **2018**, *12* (12), 12551–12557.

(51) Lin, H.; Gong, J.; Miao, H.; Guterman, R.; Song, H.; Zhao, Q.; Dunlop, J. W. C.; Yuan, J. *ACS Appl. Mater. Interfaces* **2017**, *9* (17), 15148–15155.

(52) Zhao, Q.; Yin, M.; Zhang, A. P.; Prescher, S.; Antonietti, M.; Yuan, J. *J. Am. Chem. Soc.* **2013**, *135* (15), 5549–5552.

(53) Huang, J.; Tao, C.; An, Q.; Lin, C.; Li, X.; Xu, D.; Wu, Y.; Li, X.; Shen, D.; Li, G. *Chem. Commun.* **2010**, *46* (23), 4103–4105.

(54) Hu, X.; Huang, J.; Zhang, W.; Li, M.; Tao, C.; Li, G. *Adv. Mater.* **2008**, *20* (21), 4074–4078.

(55) Guo, Z.; Jiang, Q.; Shi, Y.; Li, J.; Yang, X.; Hou, W.; Zhou, Y.; Wang, J. *ACS Catal.* **2017**, *7* (10), 6770–6780.

(56) Wang, Q.; Hou, W.; Li, S.; Xie, J.; Li, J.; Zhou, Y.; Wang, J. *Green Chem.* **2017**, *19* (16), 3820–3830.

(57) Gao, C.; Chen, G.; Wang, X.; Li, J.; Zhou, Y.; Wang, J. *Chem. Commun.* **2015**, *51* (24), 4969–4972.

(58) Wang, X.; Zhou, Y.; Guo, Z.; Chen, G.; Li, J.; Shi, Y.; Liu, Y.; Wang, J. *Chem. Sci.* **2015**, *6* (12), 6916–6924.

(59) Kuzmicz, D.; Coupillaud, P.; Men, Y.; Vignolle, J.; Vendraminetto, G.; Ambrogi, M.; Taton, D.; Yuan, J. *Polymer.* **2014**, *55* (16), 3423–3430.

(60) Huang, J.; Tao, C.; An, Q.; Zhang, W.; Wu, Y.; Li, X.; Shen, D.; Li, G. *Chem. Commun.* **2010**, *46* (6), 967–969.

(61) Zhang, H.; Bai, L.; Wei, Z.; Liu, S.; Liu, H.; Yan, H. *Talanta* **2016**, *149*, 62–68.

(62) Täuber, K.; Zhao, Q.; Antonietti, M.; Yuan, J. *ACS Macro Lett.* **2015**, *4* (1), 39–42.

(63) Zhao, Q.; Zhang, P.; Antonietti, M.; Yuan, J. *J. Am. Chem. Soc.* **2012**, *134* (29), 11852–11855.

(64) Mathieu, K.; Jérôme, C.; Debuigne, A. *Polym. Chem.* **2018**, *9* (4), 428–437.

(65) Boyère, C.; Favrelle, A.; Léonard, A. F.; Boury, F.; Jérôme, C.; Debuigne, A. *J. Mater. Chem. A* **2013**, *1* (29), 8479–8487.

(66) Yan, F.; Texter, J. *Chem. Commun.* **2006**, No. 25, 2696–2698.

(67) Zhang, T.; Sanguramath, R. A.; Israel, S.; Silverstein, M. S. *Macromolecules* **2019**, *52* (15), 5445–5479.

(68) Kiefer, J.; Fries, J.; Leipertz, A. *Appl. Spectrosc.* **2007**, *61* (12), 1306–1311.

(69) Qian, W.; Texter, J.; Yan, F. *Chem. Soc. Rev.* **2017**, *46*, 1124–1159.

(70) Lai, C.-L.; Lee, H. M.; Hu, C.-H. *Tetrahedron Lett.* **2005**, *46* (37), 6265–6270.

(71) Liu, D.; Sun, J.; Simmons, B. A.; Singh, S. *ACS Sustain. Chem. Eng.* **2018**, *6* (6), 7232–7238.

(72) Lambert, R.; Coupillaud, P.; Wirotius, A.-L.; Vignolle, J.; Taton, D. *Macromol. Rapid Commun.* **2016**, *37* (14), 1143–1149.

IV.5 Experimental Section

Materials. Formaldehyde (aqueous solution 37 w%), glyoxal (aqueous solution 40 w%), vinyl acetate (VAc) (> 99 %), caffeic acid (98 %) and tris(2-aminoethyl)amine (TREN) (96 %) were purchased from sigma-aldrich (Belgium). Acetic acid glacial (> 99 %), Methanol (MeOH, > 99.9 %), cyclohexane (> 99.9 %), dimethylsulfoxide (DMSO, 99.5 %)) and tetrahydrofuran (THF, 99.9 %) were purchased from VWR. Benzyl alcohol (99 %) was purchased from TCI Europe and deuterated solvents from Eurisotop. Jeffamine-T403® was kindly provided by HUNTSMAN. PluronicMR PEF68 was purchased from ICI Surfactants. All chemicals and solvents were used without purification with a few exceptions. DMSO and THF used in the transesterification and decarboxylation reactions were dried on molecular sieves and stored under inert atmosphere (Argon). Benzyl alcohol and VAc which were dried under calcium hydride, purified by distillation under reduced pressure and degassed by freeze-drying cycle under vacuum.

Characterizations. ^{13}C CP MAS NMR spectra were recorded with 4-mm zirconia rotors spinning at 10 kHz on a Bruker Avance III HD spectrometer (B0=9.04 T) working at the Larmor frequency of 100.62 MHz. Cross polarization experiments were performed with a delay time of 2 s and a contact time of 2 ms. ^{1}H NMR spectra were recorded at 298 K with a Bruker Avance III HD spectrometer (B0=9.04 T) (400 MHz) and treated with MestReNova software. IR spectra were recorded on ThermoFischer Sientic Nicolet IS5 equipped with an ATR ID5 module using a diamond crystal (650 cm^{-1} - 4000 cm^{-1}). Differential scanning calorimetry (DSC) was performed on a TA Instruments Q1000 DSC, using hermetic aluminium pans, indium standard for calibration, nitrogen as the purge gas, a sample weight of ~5 mg. The sample was dried at 90 °C during 20 minutes under flux of nitrogen. Then, the sample was cooled down to -80 °C at 20 °C min-1 cooling rate, followed by an isotherm at −80 °C for 2 min and heating up to 120 °C at 10 °C min-1 heating rate. These cycles were repeated twice. The fourth cycle (last heating from -80 to 120 °C) were analysed and reported in table S1. TGA analyses were carried out with a TGA 2 from Metler Toledo under nitrogen at a heating rate of 20°C min-1 from 30 °C to 600 °C with a sample weight between 5 and 10 mg. The solvent uptake (SU) values were determined by gravimetry and calculated as follows: SU (%) = ([Ww - Wd] / Wd) * 100, Ww and Wd correspond to the weight of the polymer wet and dry, respectively. The SU represents the entire solvent quantity in the materials which includes the swellability and the filling of the macropores. The SEM images of the polyHIPEs were collected with a Jeol JSM 804-A

apparatus after metallization of the sample with Pt (30 nm) in order to estimate the size of cavities and pores. To analyse the porous structure of the materials, a critical point drying method was used to prepare the samples for electron microscopy. The polyHIPEs were fixed in a 3% glutaraldehyde solution (1h at room temperature), and were then washed in 0.1 M Soerensen's Phosphate Buffer for 15 min. Afterwards, they were dehydrated first through acetone solutions of 30%, 50%, 70% and 90%, with 10 min in each, and then through pure acetone 3 times for 10 min. The samples were transferred to a small wire-basket holder in a Balzers Critical Point Dryer and flooded with liquid CO_2. After 20 min CO_2 was slowly vented. Flooding and venting as above were repeated to purge all acetone. The samples were then fixed onto a silicon wafer substrate using a carbon glue and coated with a 6 nm AuPd conducting layer. FESEM measurements were performed on a Hitachi S4800 field emission scanning electron microscope.

Typical procedure for the synthesis of macroporous PILs. In a beaker, formaldehyde (37 wt% in water, 0.983 g, 12 mmol), glyoxal (40 wt% in water, 1.741 g, 12 mmol), acetic acid (2.160 g, 36 mmol), water (1.000 g) and the surfactant PEF68 (0.285 g, 4 w% of the total aqueous phase) were mixed together at 6 °C. At this temperature, tris(2-aminoethyl)amine (TREN) (1.168 g, 8 mmol) was added slowly under mechanical stirring (500 rpm) followed by dropwise addition of cyclohexane (15.94 g, 20.46 mL, 75 v% of the total emulsion). The resulting HIPE emulsion was casted into a polyethylene mould and cured at room temperature for 3 days. Finally, the $P_{TREN\text{-}OAc}$ monoliths produced accordingly were immersed in DMSO for washing and stored in this solvent.

In order to carry out the SEM analyses of the polyHIPEs in the dry state, DMSO was first exchanged for MeOH before drying under vacuum.

A similar procedure was repeated using Jeffamine-T403 (3.520 g, 8 mmol) instead of TREN, cyclohexane (21.86 g, 28.06 mL, 75 v% of the total emulsion) and PEF68 (0.410 g, 4 w% of the total aqueous phase).

Typical procedure for anions exchange. In a 100 mL Erlenmeyer, the acetate-based polyHIPE (approximately 1 cm^3 of $P_{TREN\text{-}OAc}$ or $P_{JEFF\text{-}OAc}$) was immersed for three days under gentle stirring in a methanol solution (50 mL) containing the counterion salt in excess, i.e. NaBr (2.0 g, 19 mmol) or LiTFSI (2.0 g, 7 mmol). The samples were then immersed in pure MeOH for washing.

Typical procedure for transesterification. The acetate-based polyHIPE swollen by THF ($P_{TREN\text{-}OAc}$ or $P_{JEFF\text{-}OAc}$, 0.5 mmol of imidazolium, 10 mol% of imidazolium moieties compared to the BenzOH was placed under inert argon in a Schlenk tube followed by addition of dry and degassed reagents, namely THF (5 mL), VAc (0.6 mL, 534 mg, 6.2 mmol) and BenzOH (0.5 mL, 541 mg, 4.8 mmol). The reaction mixture was heated at 80 °C and stirred under inert atmosphere. The conversion was determined by ^{1}H NMR in deuterated chloroform by comparing the relative intensities of the methylene signals of benzyl acetate and benzyl alcohol at 5.1 ppm and 4.7 ppm, respectively.

$$Conversion = \frac{\int 5.1\ ppm}{\int 4.7\ ppm + \int 5.1\ \ ppm}$$

Typical procedure for caffeic acid decarboxylation. The acetate-based polyHIPE swollen by DMSO ($P_{TREN\text{-}OAc}$ or $P_{JEFF\text{-}OAc}$, 0.25 mmol of imidazolium, 50 mol% of imidazolium moieties compared to caffeic acid) was placed under inert argon in a Schlenk tube followed by addition of a degassed solution of caffeic acid in dry DMSO (5 mL, 0.1 M, 0.5 mmol). The reaction mixture was heated at 115 °C and stirred for 1 hour under inert atmosphere. The conversion was determined *via* ^{1}H NMR in deuterated DMSO by comparing the relative intensities of the olefinic methine hydrogen of vinyl catechol and caffeic acid at 6.2 ppm and 6.5 ppm, respectively.

$$Conversion = \frac{\int\ 6.20\ ppm}{\int\ 6.20\ ppm + \int 6.50\ ppm}$$

Recycling experiments. At the term of the decarboxylation reaction described above (115 °C, 50 mol% of imidazolium compared to caffeic acid), the reaction mixture was removed from the reaction vessel and the polyHIPE was washed with a fresh portion of DMSO under inert atmosphere before being reused as catalyst for the same decarboxylation reaction (same conditions). Four recycling steps were performed accordingly.

IV.6 Supporting information

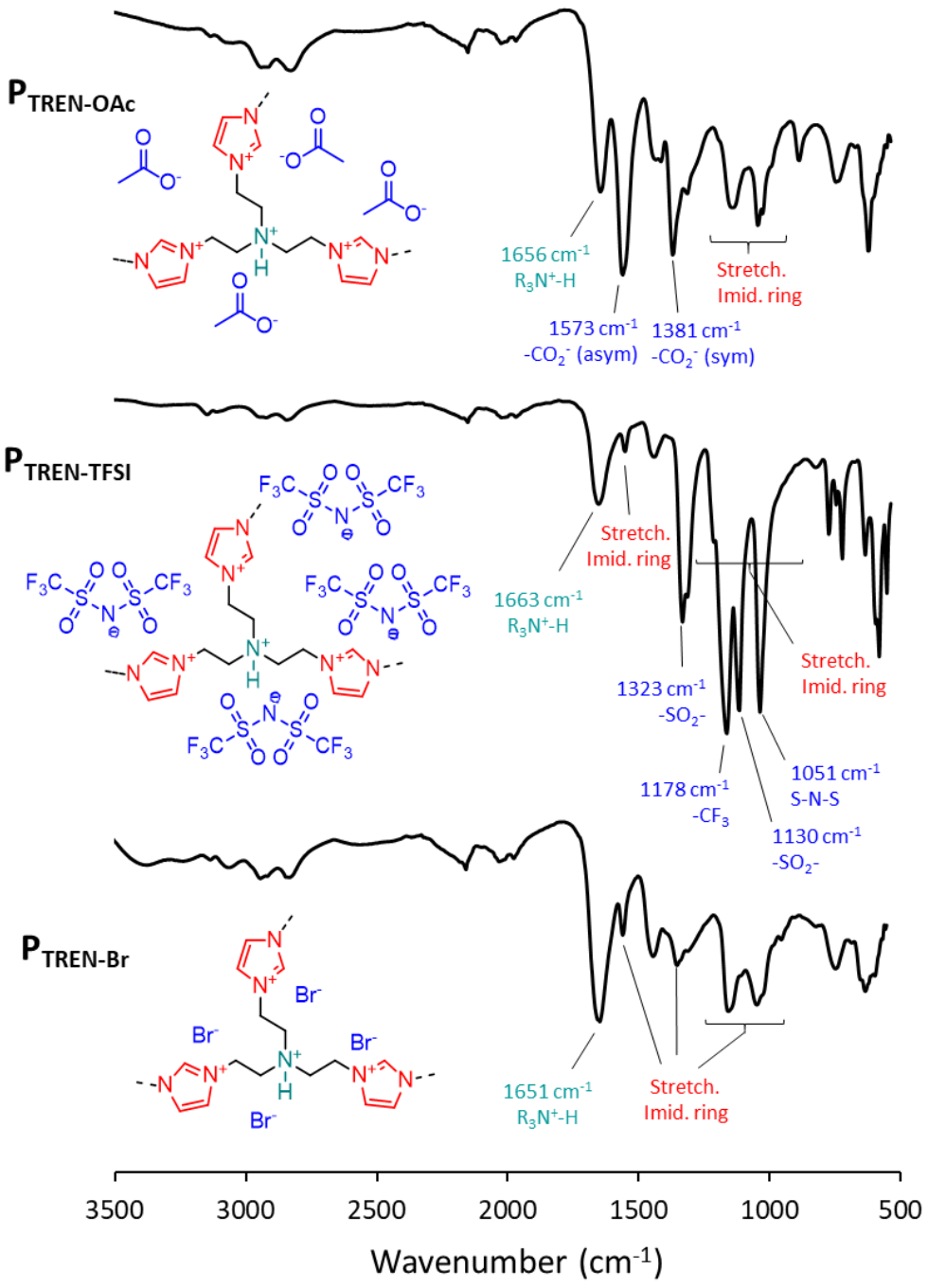

Figure S1. Infrared spectra (ATR) of P_{TREN} with acetate, TFSI and bromide as counterions.

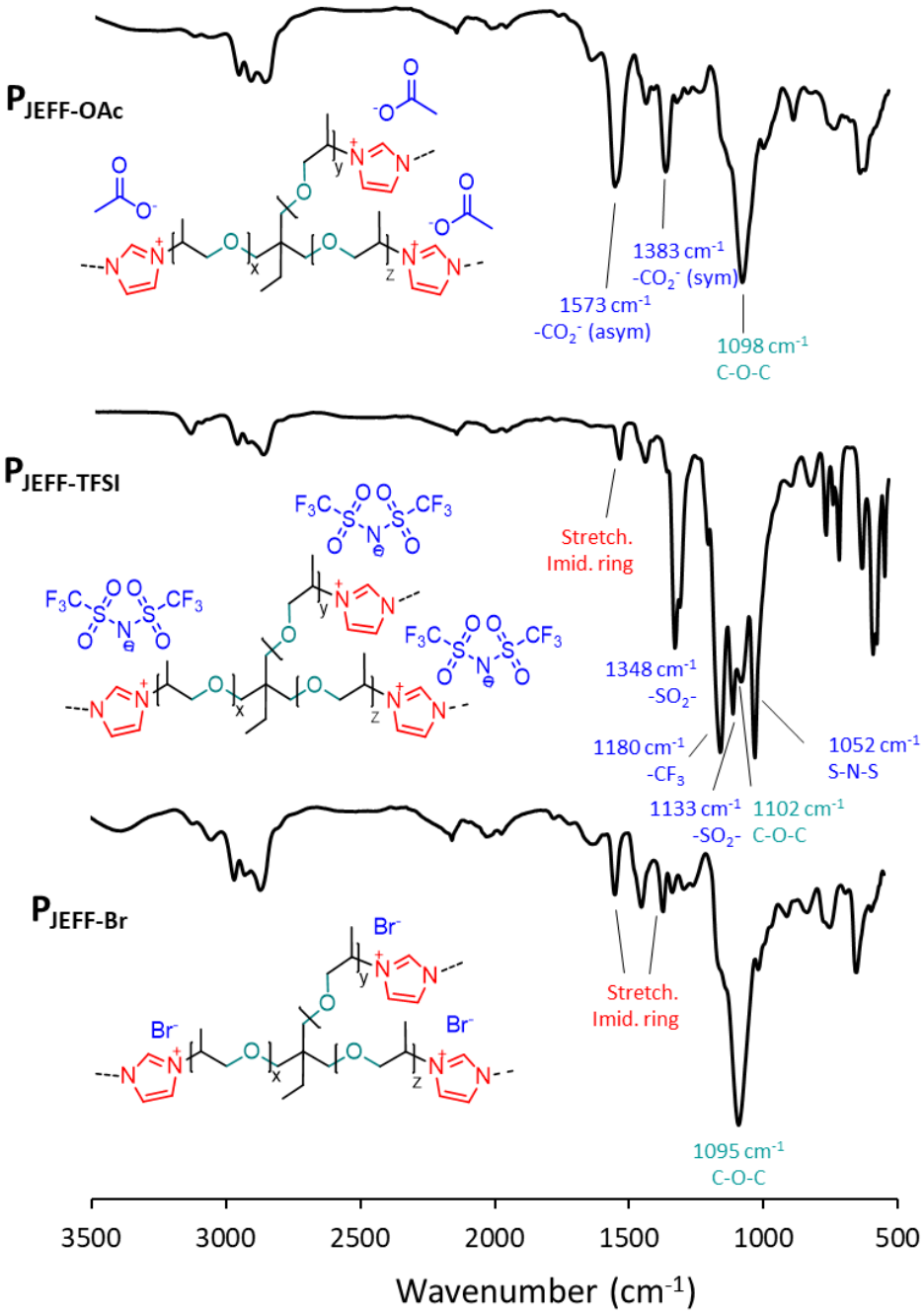

Figure S2. Infrared spectra (ATR) of P_{JEFF} with acetate, TFSI and bromide as counterions.

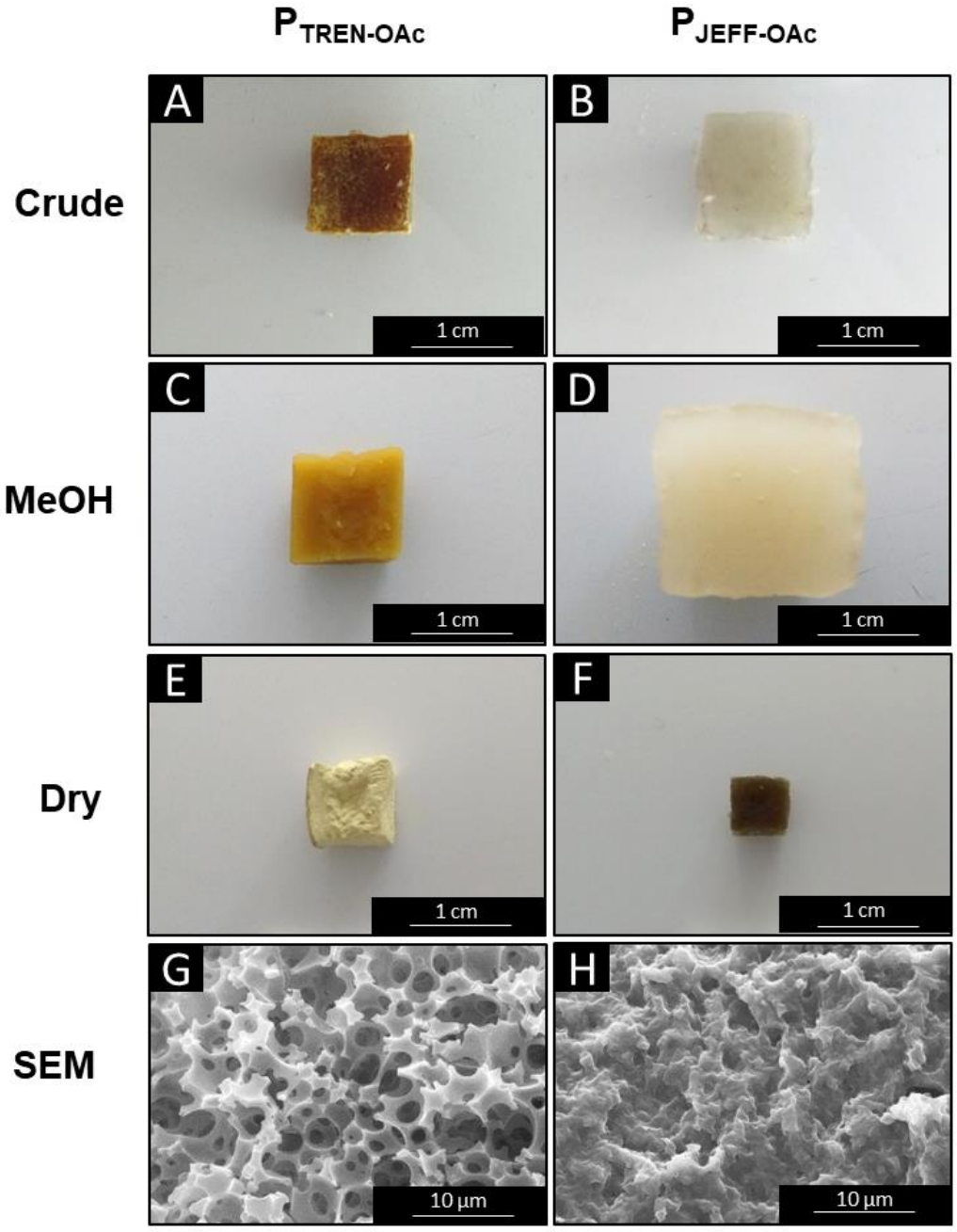

Figure S3. Pictures of the crude $P_{TREN\text{-}OAc}$ (A) and $P_{JEFF\text{-}OAc}$ (B) samples after curing. Images of the same $P_{TREN\text{-}OAc}$ (C) and $P_{JEFF\text{-}OAc}$ (D) samples swollen in MeOH. Pictures of the same $P_{TREN\text{-}OAc}$ (E) and $P_{JEFF\text{-}OAc}$ (F) samples dried under vacuum at 50 °C as well as the corresponding SEM images ($P_{TREN\text{-}OAc}$ (G) and $P_{JEFF\text{-}OAc}$ (H)).

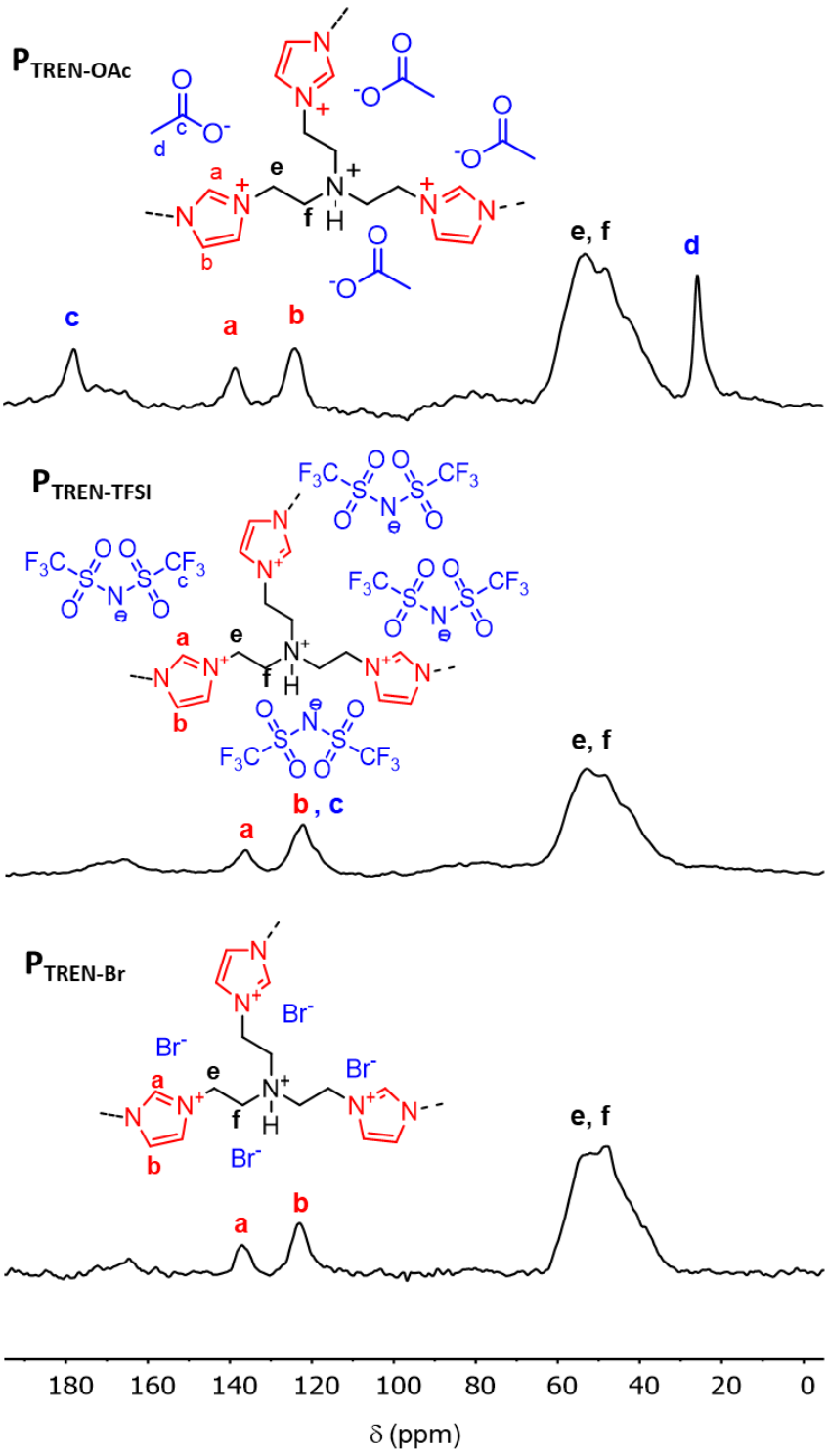

Figure S4. ^{13}C solid state NMR spectra of P_{TREN} with acetate, TFSI and bromide as counterions.

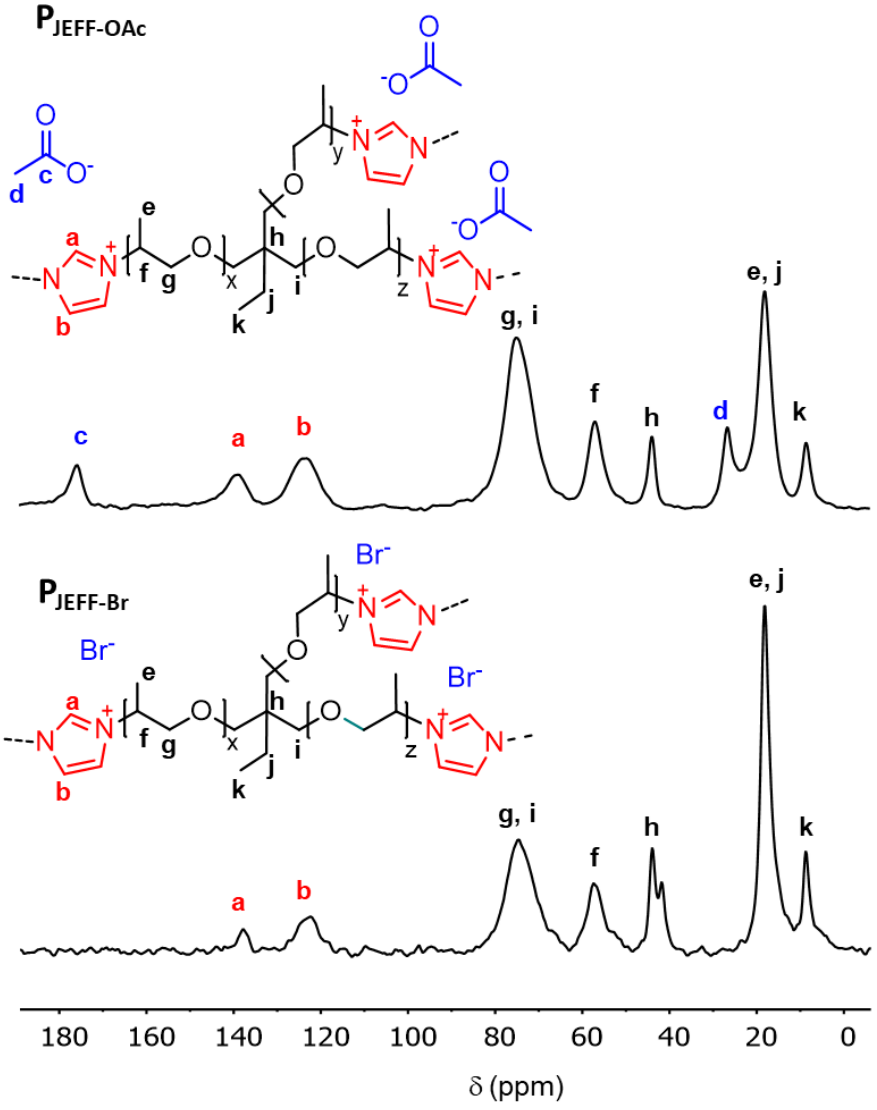

Figure S5. ^{13}C solid state NMR spectra of P_{JEFF} with acetate and bromide as counterions.

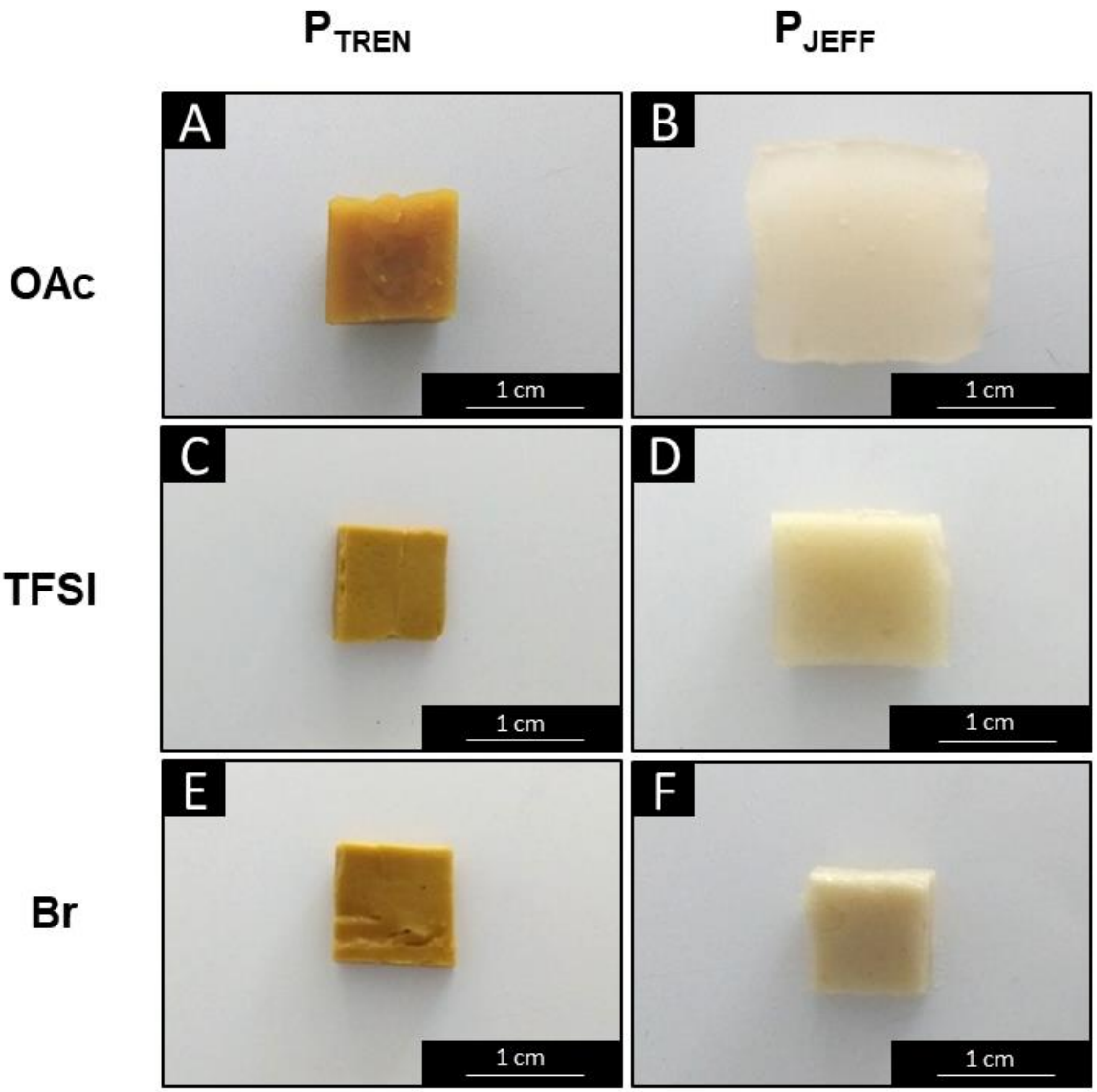

Figure S6. Pictures of polyHIPEs swollen in MeOH. $P_{TREN\text{-}OAc}$ (A), $P_{TREN\text{-}TFSI}$ (C), $P_{TREN\text{-}Br}$ (E) and $P_{JEFF\text{-}OAc}$ (B), $P_{JEFF\text{-}TFSI}$ (D), $P_{JEFF\text{-}Br}$ (F).

Table S1. Thermal properties of P_{TREN} and P_{JEFF} with different counterions.

Cation	Anion	T_{OD} [a] (°C)	T_g (°C)
P_{TREN}	Acetate	151	NA
	TFSI	274	NA
	Bromide	203	NA
P_{JEFF}	Acetate	172	27
	TFSI	347	-5
	Bromide	300	61

[a] Onset degradation temperature (T_{OD}) corresponding to a loss of 5 wt%.

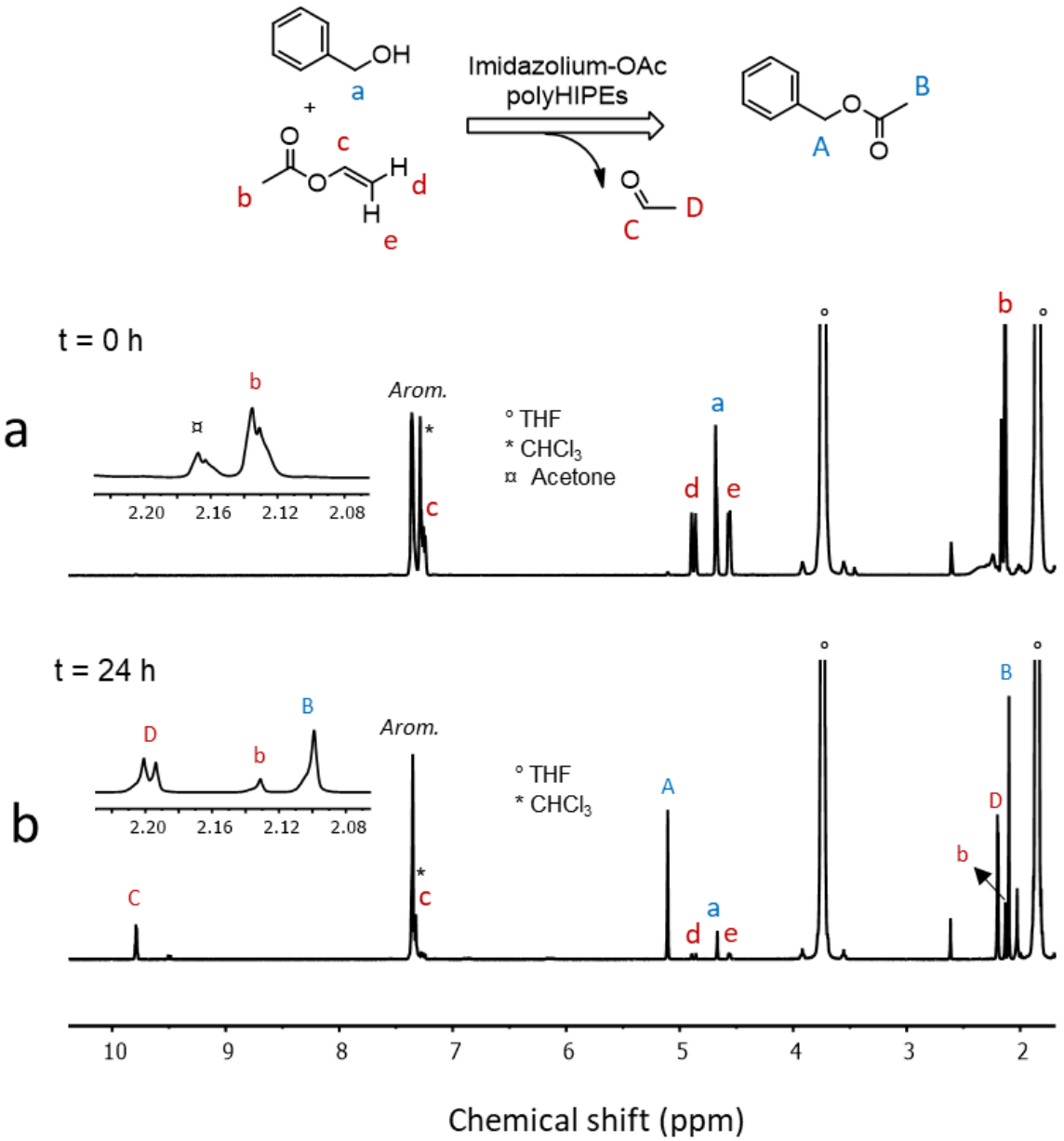

Figure S7. ^{1}H NMR spectra (in $CDCl_3$) for the transesterification reaction between of benzylic alcohol (0.5 mL) and vinyl acetate (0.6 mL) in dry THF (5 mL) in the presence of the $P_{JEFF-OAC}$ catalyst (193 mg, 10 mol%). a) spectrum of the initial reaction mixture at room temperature. b) Spectrum of the reaction mixture after 24 hours at 80 °C. (conversion = 83 %). For details, see Table 1.

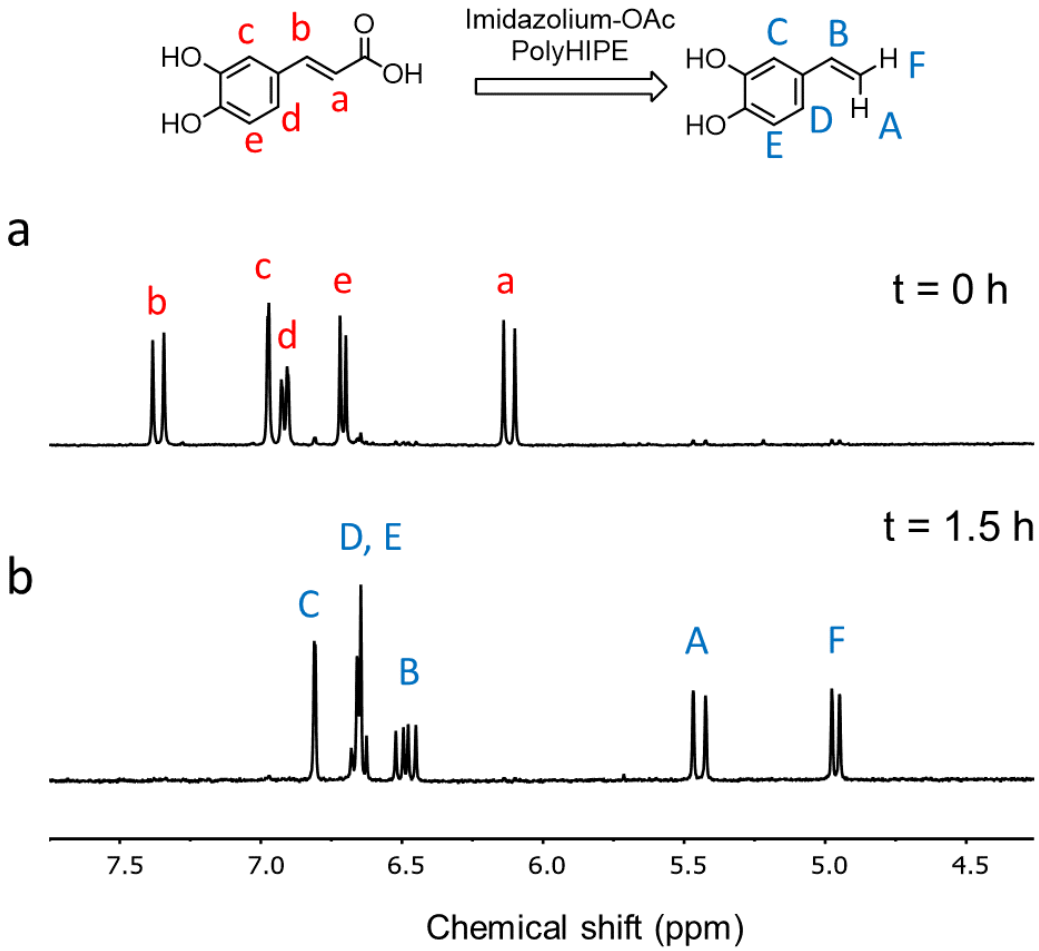

Figure S8. ^{1}H NMR spectra (in deuterated DMSO) for the decarboxylation reaction of caffeic acid (90 mg) in dry DMSO (5 mL) in presence of the $P_{JEFF\text{-}OAc}$ catalyst (97 mg, 50 mol%). a) Spectrum of the initial reaction mixture at room temperature. b) Spectrum of the reaction mixture after 90 minutes at 115 °C (conversion = 100 %). For details, see Table 1.

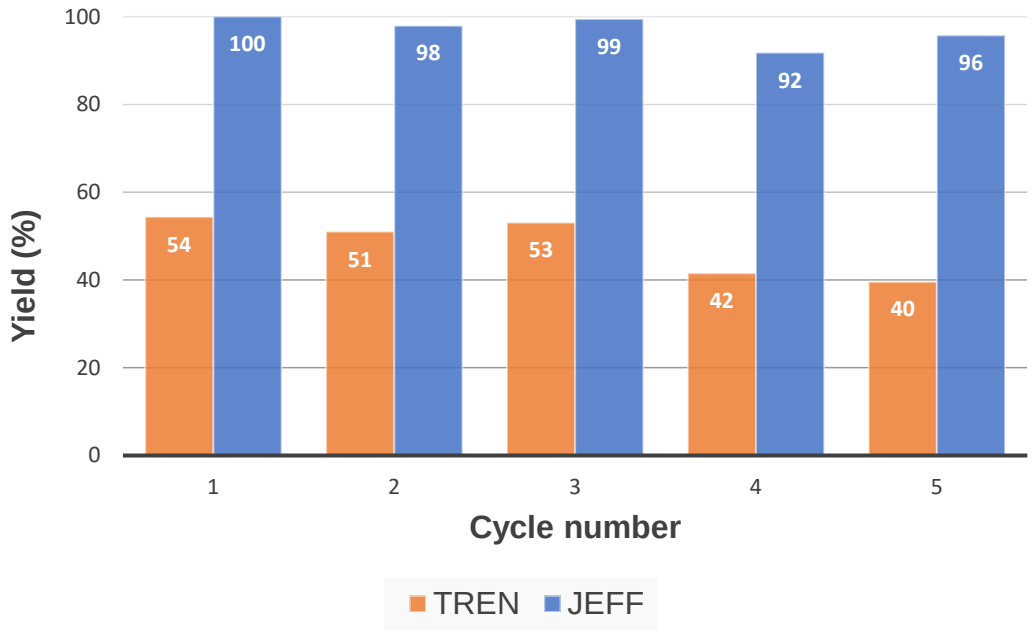

Figure S9. Recycling experiments carried out on the decarboxylation reaction catalysed by PJEFF-OAc and PTREN-OAc. The cycle was repeated five times for each catalyst.

IV.7 Annexe

IV.7.1 Heterogenous catalysis of the cycloaddition of CO_2 and epoxide by imidazolium- and carbene-based macroporous materials.

The capture and utilisation of CO_2 is of paramount importance in the current context of global-warming. A route to value CO_2 is the cycloaddition of the latter and epoxides towards the synthesis of cyclic carbonates. Nevertheless, this reaction requires a catalyst to occur in mild conditions. Imidazolium salts were reported as efficient catalysts[1,2] although the purification of the final product from the salt could be difficult. In this respect, immobilized[3] or polymerized[4,5] imidazoliums allow an easier retrieval and a better recyclability of the catalyst. In this work, we evaluated the potential of a series of macroporous imidazolium- and carbene-based networks as catalysts for the CO_2/epoxide cycloaddition reaction. A first porous network containing imidazolium acetate moieties was prepared in one-pot by combination of the Radziszewski multicomponent reaction and the high internal phase emulsion (HIPE) polymerization, as described in Chapter IV ($P_{TREN\text{-}OAc}$, Scheme 1). This polyHIPE showed a macroporosity with cavities interconnected to each other by pores (Figure 1). $P_{TREN\text{-}OAc}$ was further derivatized in its imidazolium bromide counterpart ($P_{TREN\text{-}Br}$) *via* anion metathesis (Scheme 1, path a) while a carbene-based porous network ($P_{carbene}$) was obtained by treating $P_{TREN\text{-}OAc}$ with a strong base, namely potassium *tert*-butoxide, according to a reported procedure (Scheme 1, path b).[6]

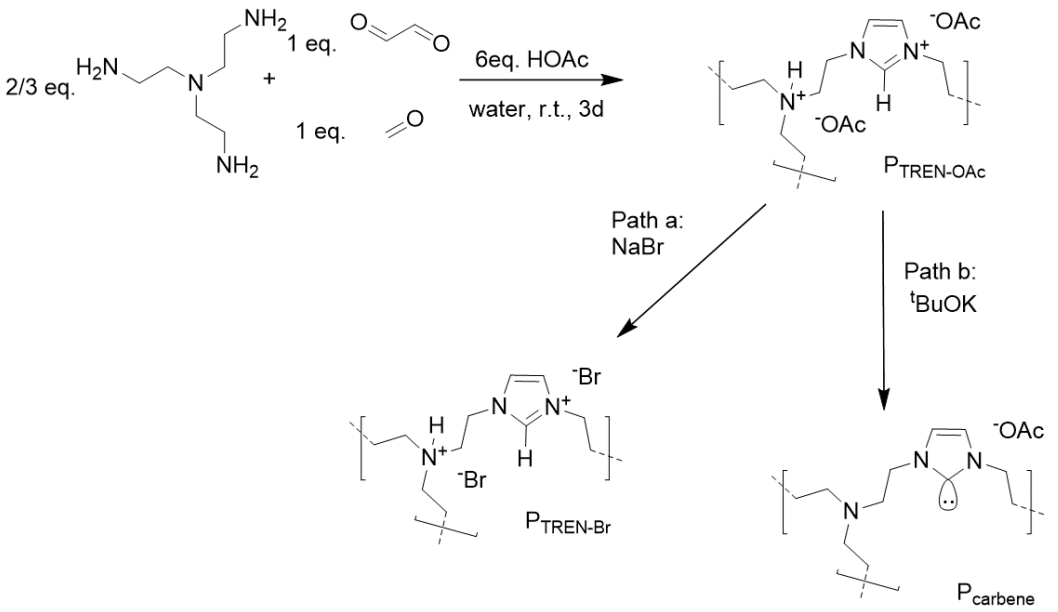

Scheme 1. Synthetic routes toward the preparation of porous imidazolium acetate network, path a) imidazolium bromide porous network and path b) carbene-based porous network.

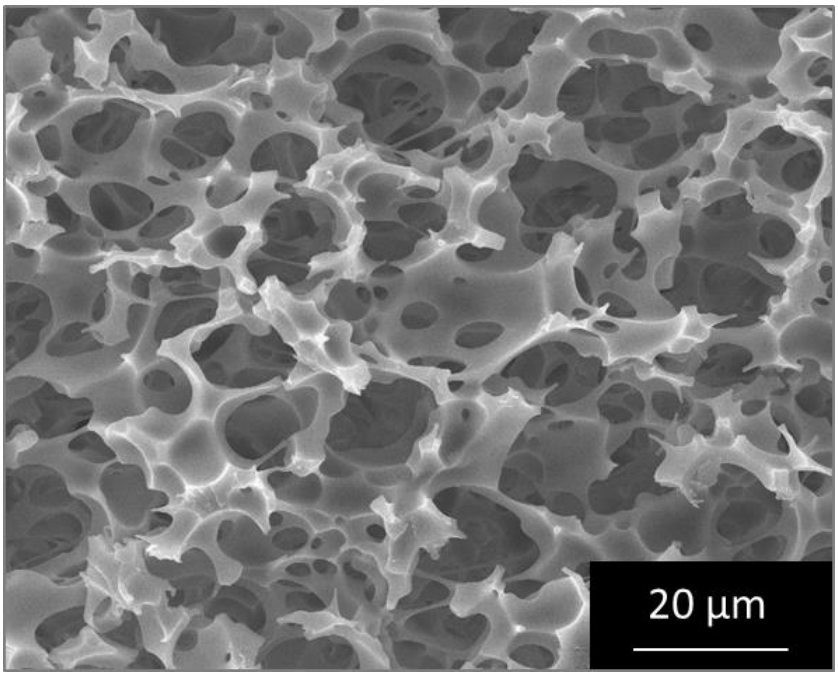

Figure 1. SEM image of $P_{TREN\text{-}OAc}$

These porous supports were then tested as catalysts for the cycloaddition of CO_2 and an epoxide, *i.e.* the allyl glycidyl ether, to form the corresponding cyclic carbonate. The reaction was carried out at 115 °C and under a CO_2 pressure of 15 bar and a catalyst load of 1.1 wt%. To get insight of the reaction rates with the different catalysts, the reaction was probed by operando FT-ATR. We followed the appearance of the carbonyl signals at 1792 cm^{-1} typical from the cyclic carbonates and monitored the change in absorbance of this peak as a function of the time (Figure 2a). At the end of the reaction (48 hours max), the conversion was determined by ^{1}H NMR (Figure 3). In these conditions, the reaction catalysed by $P_{TREN\text{-}OAc}$ allows a conversion of 82 % after 48 hours (Figure 1 b). Although a plateau was not yet reached, the reaction seemed to drastically slow down. Changing the acetate counterion for bromide, accelerated the reaction kinetic and enabled to achieve complete conversion (>99%) after only 20 hours (Figure 1 b). At the end of the reaction, $P_{TREN\text{-}Br}$ was retrieved as a single piece. Finally, the $P_{carbene}$ showed an intermediate reaction rate with a complete conversion (>99%) after 31 hours (Figure 1b).

This highlight the impact of the nature of the imidazolium counterion and of the conversion of imidazolium into carbene on the catalytic activity. Moreover, the deprotonation of the imidazolium in C2 position to afford the carbene changes the catalytic activity probably by altering the mechanism of the catalysis. Overall, these porous materials offer promising preliminary performances in CO_2 conversion and certainly deserve to be further investigated in

the frame of this application. Given the known affinity of imidazolium and carbene functionalities for CO_2, it would be interesting to determine the CO_2 uptake of each catalyst to see if it is correlated with the kinetic and efficiency of the reaction.

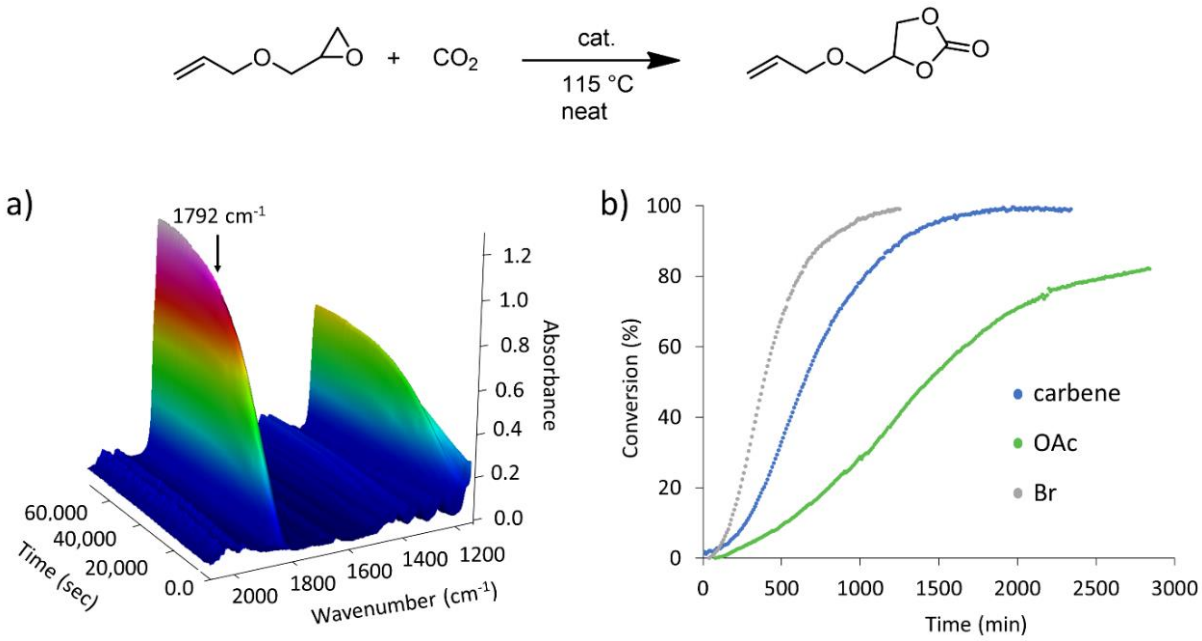

Figure 2. Cycloaddition of CO_2 and allyl glycidyl ether. a) 3D profile showing the evolution of the C=O absorption region of cyclic carbonate obtained by operando FT-ATR spectroscopy for the reaction catalysed by $P_{TREN\text{-}Br}$. b) Conversion of the reaction as a function of time. Conditions: the reactions were carried out at 115 °C under a CO_2 pressure of 15 bar and a catalyst load of 1.1 wt%.

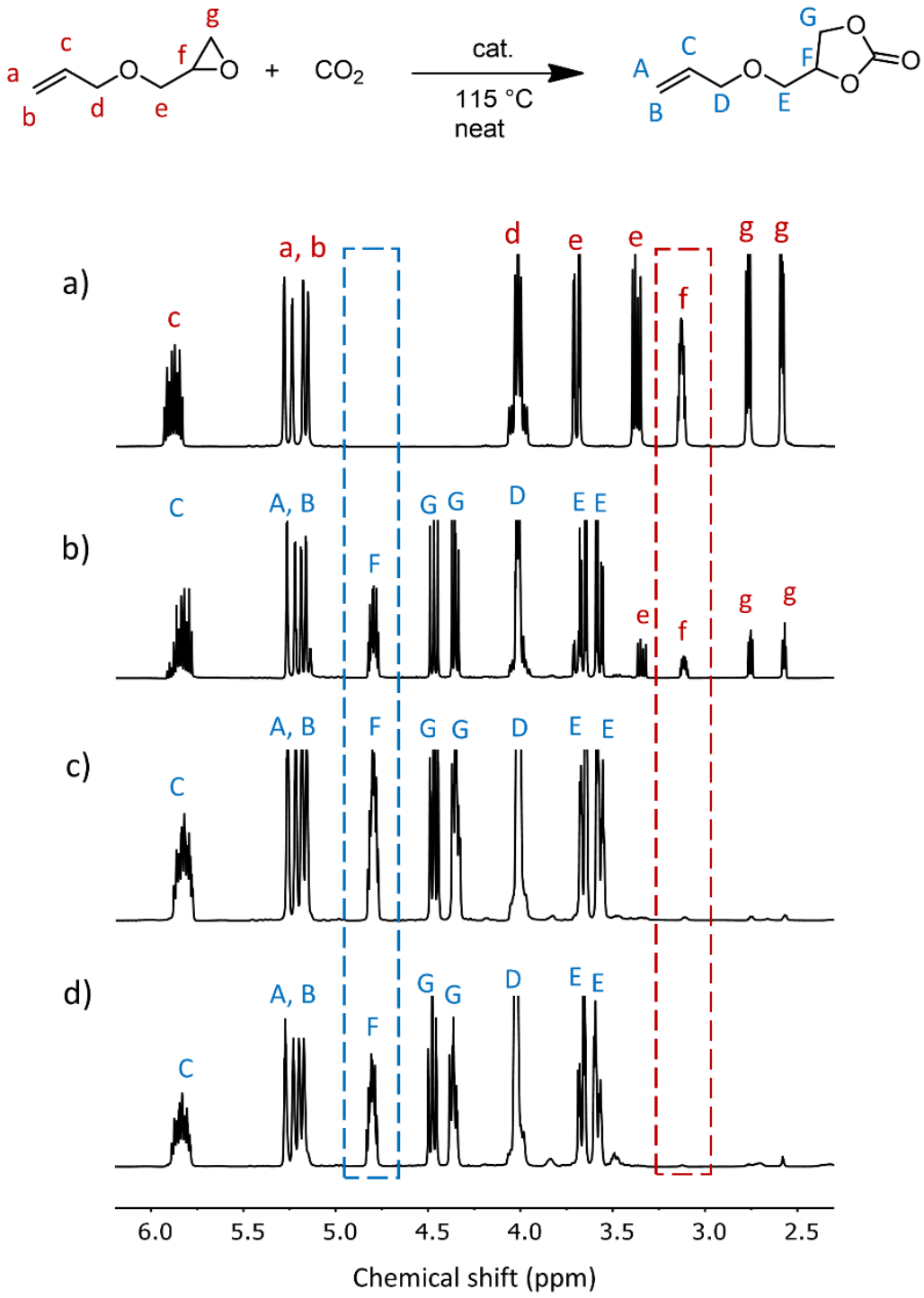

Figure 3. ^{1}H NMR spectra of carbonatation reaction between allyl glycidyl ether and CO_2 (15 bar). a) Spectrum of allyl glycidyl ether and spectra of the crude product after reaction in presence of catalyst b) $P_{TREN\text{-}OAc}$ (135 mg, 1.1 wt%), c) $P_{TREN\text{-}Br}$ (135 mg, 1.1 wt% mol%) and d) $P_{carbene}$ with respective yields of 82, 99 and 99 % in $CDCl_3$.

IV.7.2 References.

(1) Yue, C.; Su, D.; Zhang, X.; Wu, W.; Xiao, L. *Catal. Letters* **2014**, *144* (7), 1313–1321.

(2) Yue, S.; Wang, P.; Hao, X. *Fuel* **2019**, *251*, 233–241.

(3) Udayakumar, S.; Lee, M.-K.; Shim, H.-L.; Park, S.-W.; Park, D.-W. *Catal. Commun.* **2009**, *10* (5), 659–664.

(4) Wang, X.; Zhou, Y.; Guo, Z.; Chen, G.; Li, J.; Shi, Y.; Liu, Y.; Wang, J. *Chem. Sci.* **2015**, *6* (12), 6916–6924.

(5) Ziaee, M. A.; Tang, Y.; Zhong, H.; Tian, D.; Wang, R. *ACS Sustain. Chem. Eng.* **2019**, *7* (2), 2380–2387.

(6) Dani, A.; Crocellà, V.; Magistris, C.; Santoro, V.; Yuan, J.; Bordiga, S. *J. Mater. Chem. A* **2017**, *5* (1), 372–383.

IV.7.3 Experimental section.

Material. Formaldehyde (aqueous solution 37 w%), glyoxal (aqueous solution 40 w%), potassium tert-butoxide (97 %), allyl glycidyl ether (99%) and tris(2-aminoethyl)amine (TREN) (96 %) were purchased from sigma-aldrich (Belgium). Acetic acid glacial (> 99 %), Methanol (MeOH, > 99.9 %), cyclohexane (> 99.9 %), dimethylsulfoxide (DMSO, 99.5 %) and tetrahydrofuran (THF, 99.9 %) were purchased from VWR. Deuterated chloroform was purchased from Eurisotop. Pluronics PEF68 was purchased from ICI Surfactants. All chemicals and solvents were used without purification.

Characterization. 1H NMR spectra were recorded at 298 K with a Bruker Avance III HD spectrometer (B_0 = 9.04 T) (400 MHz) and treated with MestReNova software. The SEM image of the polyHIPE was collected with a Jeol JSM 804-A apparatus after metallization of the sample with Pt (30 nm) in order to estimate the size of cavities and pores. *In situ* IR spectroscopy experiments were conducted using a stainless-steel reactor suitable for high-pressure measurements (up to 400 bar) and high temperature (up to 150 °C) coupled with a FT-ATR spectrometer from Brucker, equipped with an air-cooled globar source (12V), a KBr beamsplitter, a mechanical rocksolid interferometer, permanently aligned, a diamond ATR fibre probe IN350-T (Ø 6 mm) and a liquid nitrogen cooled mercury cadmium telluride (MCT) detector. Single beam spectra recorded in the spectral range (750-3500 cm-1) with a 4 cm^{-1} resolution were obtained after the Fourier transformation of 32 accumulated interferograms until the end of reaction time. A spectrum was recorded every ten minutes.

Procedure for the synthesis of macroporous PILs. In a beaker, formaldehyde (37 wt% in water, 0.983 g, 12 mmol), glyoxal (40 wt% in water, 1.741 g, 12 mmol), acetic acid (2.160 g, 36 mmol), water (1.000 g) and the surfactant PEF68 (0.285 g, 4 w% of the total aqueous phase) were mixed together at 6 °C. At this temperature, tris(2- aminoethyl)amine (TREN) (1.168 g, 8 mmol) was added slowly under mechanical stirring (500 rpm) followed by dropwise addition of cyclohexane (15.94 g, 20.46 mL, 75 v% of the total emulsion). The resulting HIPE emulsion was casted into a polyethylene mould and cured at room temperature for 3 days. Finally, the $P_{TREN\text{-}OAc}$ monoliths produced accordingly were immersed in DMSO for washing and stored in this solvent. The chemical structure and the morphology of the polyHIPE was assessed in chapter IV.

Procedure for anions exchange. In a 100 mL Erlenmeyer, the acetate-based polyHIPE (approximately 1 cm3 of $P_{TREN\text{-}OAc}$) was immersed for three days under gentle stirring in a methanol solution (50 mL) containing the counter-ion salt in excess, i.e. NaBr (2.0 g, 19 mmol). The sample were then immersed in pure MeOH for washing. The chemical structure and the morphology of the polyHIPE was assessed in chapter IV.

Procedure for conversion of imidazolium into carbene. In a reaction tube, $P_{TREN\text{-}OAc}$ (239 mg, 1 mmol) was immersed in 15 mL of THF followed by the addition of potassium tert-butoxide (^{t}BuOK, 1.12 g, 10 mmol). The reaction was carried out for 72 hours at r.t. The monolith was washed and store in THF.

Typical procedure for the cycloaddition of CO_2 and allyl glycidyl ether. The dried polyHIPE catalyst (135 mg, 1.1 wt%) was placed in the reactor followed by addition of allyl glycidyl ether (12 mL, 11, 64 g, 102 mmol). The reactor was hermetically sealed and put under pressure of CO_2 (15 bar). The reaction mixture was heated at 115 °C and stirred at 100 rpm. The reaction was monitored by operando infrared spectroscopy *via* an ATR device inside the reactor. The final conversion was determined by ^{1}H NMR in deuterated chloroform by comparing the relative intensities of the methine hydrogen next the epoxide (f) and the cyclic carbonate (F) at 3.15 ppm and 4.81 ppm, respectively (Figure 2).

$$Conversion = \frac{\int 4.81\ ppm}{\int 4.81\ ppm + \int 3.15\ ppm}$$

The absorbance was converted into a conversion by using the Beer-Lambert equation.

$$\text{Absorbance} = \varepsilon(\omega)\, l\, C$$

where ε (ω) is the molar extinction coefficient that is a function of the wavelength, l is the pathlength of the light and C is the molar concentration. In the case of FT-ATR, the pathlength should be replaced with the effective pathlength as follow:

$$l_{eff} = d_p\, N_R$$

where d_p is the penetration depth and N_R the total number of internal reflections.

Note that the validity of Beer-Lambert's law could be affected by the use of highly concentrated media and a large oscillator strength. In this respect, only qualitative information is taken from the operando FT-ATR.

Chapter V.

One-Pot Synthesis of Imidazolium/Amine Bi-functional Porous Materials for Highly Selective CO_2 Capture.

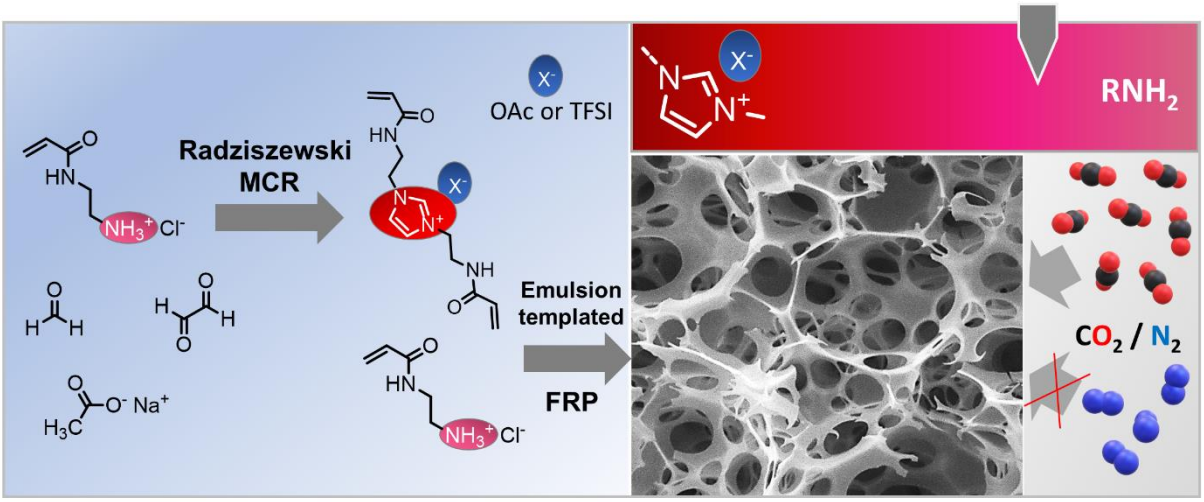

Abstract. While amine and imidazolium functionalities are well-known for CO_2 capture, their combination in porous materials and the possible synergistic effect for this application have not been considered yet. This work reports a straightforward strategy to synthesize bi-functional imidazolium/amine macroporous networks with tunable ratio of these functions through the combination of Radziszewski MCR, free radical polymerization and emulsion-templating polymerization. The resulting materials exhibit fast CO_2 sorption with good capacities up to 2 mmol g^{-1} as well as high CO_2/N_2 selectivity. Moreover, the incorporation of imidazolium in amine-based matrices deeply impacts their properties as highlighted by the drastic change of CO_2 sorption upon anion metathesis from acetate to bis(trifluoromethane)sulfonimide. Overall, these materials are promising candidates for post-combustion or even direct-air CO_2 capture applications.

Stiernet, P.; Mazaj, M.; Kovačič, S.; Debuigne, A.; *to be submitted.*

Chapter V. One-Pot Synthesis of Imidazolium/Amine Bi-functional Porous Materials for Highly Selective CO_2 Capture.

V.1. Introduction

Polymerized high internal phase emulsions (polyHIPEs or PHs) are a class of highly porous, usually monolithic, polymeric foams often with three-dimensional (3D) interconnected microcellular morphology.[1–3] The key design factors of PH foams lie in their modulable morphology (pore sizes and interconnectivity), mechanical properties or chemical functionality. The applicative performance of PH foams can be well influenced especially by adapting the chemical functionality. Therefore, many different ways to tune the functional groups of PH have been developed, such as the addition of monomers carrying functional moieties for possible post-polymerization functionalization (PPF),[4] by incorporation of comonomers carrying the desired functionality,[5–7] or by surfactant-assisted functionalization.[8–12] Recently, nitrogen-containing PH foams, such as those based on amino or imidazolium functional groups, have become very attractive for a variety of applications, especially in gas capture.[13]

Driven by the capacity of organic amines to interact with CO_2,[14] numerous amine-functionalized PHs were prepared and used as solid sorbents to capture CO_2.[15–27] Series of amino-functional PHs were produced by PPF of vinylbenzyl chloride (VBC)-based precursors using various amine derivatives such as ethylenediamine, imidazole and piperazine as well as piperidine derivatives.[15,16] The best CO_2 uptake was recorded in case of ethylenediamine-derivatized PHs. Further, quaternary ammonium hydroxide-PPF PHs were also tested and revealed good reversible CO_2 capture performances.[20,21] Triazole functionalized glycidyl methacrylate (GMA)-based PHs exhibited CO_2 sorption capacity of 3.6 mmol g^{-1} and good CO_2/N_2 selectivity.[22] Other organic amine compounds widely used for chemical functionalization of PHs for CO_2 capture are poly(ethylenimine)s (PEIs).[23,25–27] Some PEI-grafted TiO_2[17,18] and metal-organic framework (MOF)[19,24] PHs composites were also developed and proved efficiency as CO_2 sorbents.

In the past few years, porous polymerized ionic liquids (PILs) have also proven to be promising sorbents for CO_2 capture.[28–37] In addition, some PILs have been structured into highly interconnected porous PHs but, to the best of our knowledge, the latter have never been considered for CO_2 capture. PILs-based PHs were synthesized through radical polymerization of various HIPE systems such as carbon dioxide-in-water (CO_2/W),[38] carbon dioxide-in-ionic liquid (CO_2/IL)[39] or water-in-oil (W/O) HIPEs.[7] Very recently, another chemistry has been used

to cure HIPE, such as the Radziszewski multicomponent reaction (MCR), in which imidazolium-based PH monoliths were obtained in a one-pot manner.[40] The excellent atom- and step-economy of MCRs offer an efficient and environmentally friendly synthetic approach for macromolecular design with good substrate diversity and has therefore attracted growing interest in the field of polymer synthesis.[41–44]

Despite the obvious advantages of the amine- and PIL-based materials for CO_2 capture applications, the combination of both functional domains in a single PH monolith and the possible synergistic effect have not been considered so far. Moreover, the use of imidazolium-based PH monoliths remains underdeveloped as support for CO_2-capture and warrant exploration. The present work reports an innovative and straightforward one-pot synthesis route to create bi-functional amino/imidazolium-based PH foams relevant to capture CO_2. For this purpose, we combined the Radziszewski MCR and radical polymerization in a two-phase HIPE system for the first time. In the resulting bi-functional PH monoliths, amines and imidazolium crosslinks were combined in tunable proportions going from full PIL-based to amino-rich PHs (Scheme 1). Given the notorious affinity of the amine and imidazolium moieties for CO_2, we explored the CO_2-sorption performance of these bi-functional PHs and studied the effect of the amine/imidazolium ratio and imidazolium counterion on the CO_2 capture capacity and selectivity.

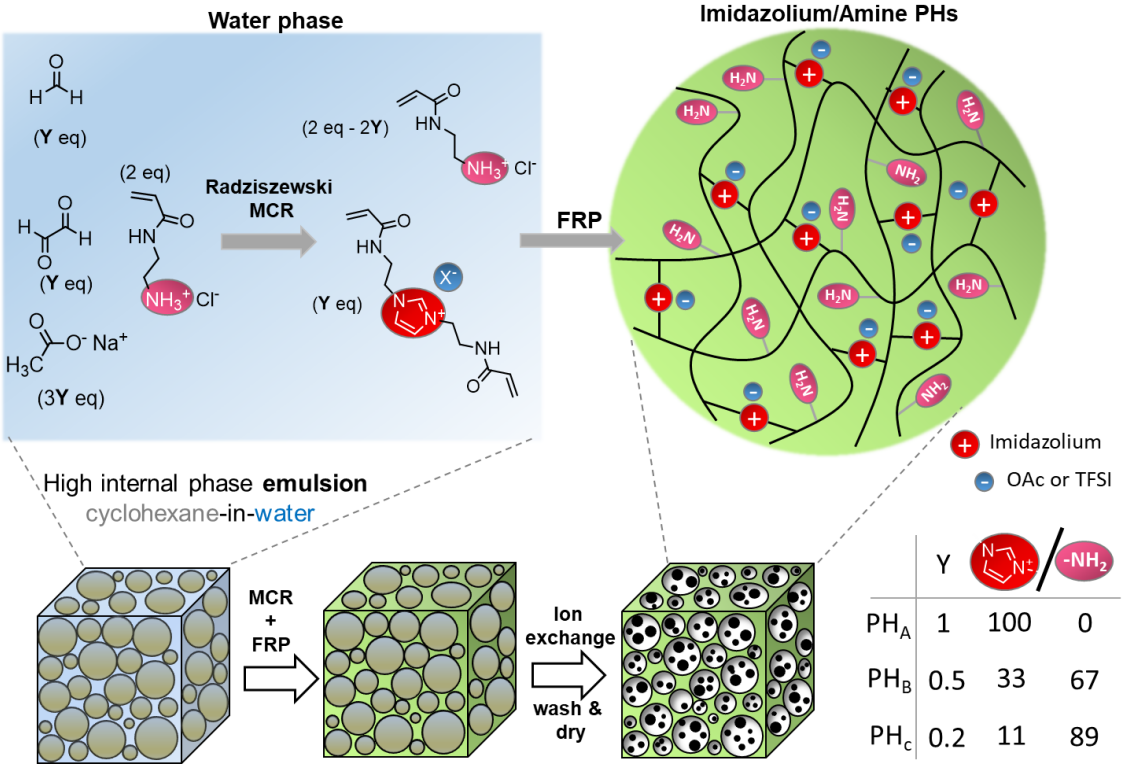

Scheme 2. General strategy for the synthesis of PHs *via* emulsion templating combination of Radziszewski MCR and free radical polymerization.

V.2 Results and discussions

V.2.1 Synthesis of the imidazolium-based crosslinker by MCR.

The general strategy of this work relies on the conversion by Radziszewski MCR of a vinyl monomer bearing a primary amine, namely the aminoethyl acrylamide (AEAm), into an imidazolium bis-acrylamide (IBAm) crosslinker that is further used in HIPE polymerization. The synthesis of the starting AEAm was adapted from a previously reported procedure.[45] Briefly, *N*-Boc-ethylenediamine was reacted with acryloyl chloride and the resulting *N*-Boc-aminoethyl acrylamide was deprotected with hydrochloric acid leading to aminoethyl acrylamide hydrochloride (AEAm-HCl) (Figure S1 and S2). Next, the conversion of AEAm-HCl into the imidazolium crosslinker was studied through a series of experiments in order to define optimal reaction conditions for curing the HIPE system. The classical conditions reported in literature for synthesis of imidazoliums by Radziszewski MCR using acetic acid (HOAc) as catalyst were tested first.[46] In this case, AEAm-HCl (2 eq) was dissolved in Milli-Q water containing an excess HOAc (6 eq) before the addition of an aqueous solution of formaldehyde and glyoxal (1 eq of each) (Table 1, entry 1). Surprisingly, after one hour at room temperature, no imidazolium was detected by ^{1}H NMR analysis in the reaction mixture (Figure S4, spectrum A). This absence of reaction suggests that the HOAc alone may not catalyse the reaction and that the MCR might be promoted by the acetate formed *in situ via* the neutralization of the amine by the HOAc, which did not occur in the case of the protonated AEAm-HCl. To further confirm this assumption, the reaction was repeated but one equivalent of HOAc was replaced by sodium acetate (NaOAc) (Table 1, entry 2). The ^{1}H NMR spectrum (Figure S4, spectrum B) recorded after one hour revealed some typical imidazolium aromatic protons **g** and **f** at 7.56 and 8.89 ppm, respectively, as well as the methylene **e'** close to the imidazolium at 4.39 ppm. In this case, approximately half of the amines were converted into imidazoliums. Increasing the amount of NaOAc (3 equiv.) and omitting HOAc (Table 1, entry 3) resulted in complete conversion after 1 hour (Figure S4, spectrum C). Overall, the Radziszewski MCR seems to occur with acetate playing the role of catalyst and a slight excess of the latter compared to the amine functions (1.5 fold) is enough to achieve complete reaction within one hour in mild condition. Eventually, the concentration was increased from 0.5 to 1.67 mol/L (compared to formaldehyde) in order to meet the conditions required for subsequent HIPE radical polymerizations (Table 1, entry 4). Complete conversion of the amine was also achieved

accordingly (Figure S4, spectrum D) and the product was fully characterized by NMR without further purification (Figure S5).

Table 2. Optimization of the Radziszewski reaction applied to AEAm-HCl

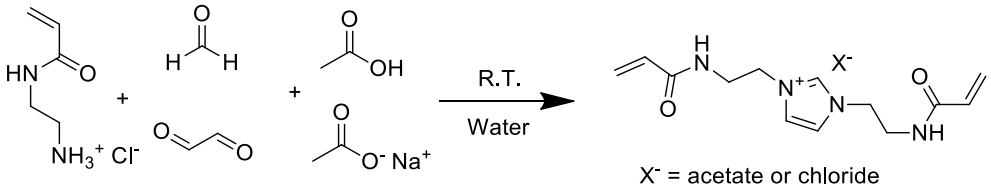

Entry	code	Conc. (mol/L)[a]	HOAc/NaOAc (eq/eq)[a]	Conv.[b] (%)
1	A	0.5	6/0	0
2	B	0.5	5/1	51
3	C	0.5	0/3	> 99
4	D	1.67	0/3	> 99

Conditions: room temperature, reaction time of 1 hour, water, [AEAm-HCl]/[formaldehyde]/[Glyoxal] = 2/1/1. [a] compared to formaldehyde. [b] determined by NMR.

V.2.2 One-pot emulsion-templated synthesis.

A one-pot procedure was developed to combine the Radziszewski MCR and radical polymerization in a O/W HIPE system for the design of imidazolium-based PHs and bi-functional amine/imidazolium PHs with tunable compositions. The preparation of imidazolium-based PHs was considered first. For this purpose, IBAm was synthesize in water by Radziszewski MCR and, without any purification, an emulsifier and a water-soluble azo initiator, *i.e.* the PPO-PPO-PEO Pluronic F-68 (5 wt% of the aqueous phase) and VA-044 (vinyl/initiator = 50) were added. The resulting aqueous solution served as external phase of an O/W HIPE obtained by dropwise addition of cyclohexane (internal phase 75 v%) under stirring. The obtained emulsion was cured for 5 hours at 60 °C *via* radical polymerization which proceeded without demixing and led to the targeted macroporous poly(imidazolium) networks. At this stage, however, uncertainty existed about the nature of the counterion of the imidazolium since both acetate and chloride were present during the *in situ* formation of the imidazolium crosslinker and its emulsion templated polymerization. The PH was therefore treated with NaOAc/MeOH or LiTFSI/MeOH solutions to obtain poly(imidazolium)-based PHs containing

either acetate (OAc) or bis(trifluoromethane)sulfonimide (TFSI) anions. The resulting materials were then washed from the excess of salts in water and freeze-dried. For simplicity, these samples will be referred to as $PH_{A\text{-}OAc}$ and $PH_{A\text{-}TFSI}$ throughout the document. Their chemical structures were assessed by ^{13}C CP/MAS ssNMR and FTIR (Figure 1). The aromatic carbons from imidazolium are evidenced by peaks **a** and **b** at 139 and 124 ppm, the aliphatic carbons are gathered between 30 and 55 ppm (**c-f**) and the amide signal **g** appears at 177 ppm. Incorporation of acetate counter anion is confirmed by the characteristic methyl (**i**) signal at 26 ppm, whereas the carbon (**j**) from TFSI is barely distinguishable from the imidazolium carbon (**b**). FTIR analyses further confirmed the nature of the counterions with the C=O stretching at 1549 and 1396 cm^{-1} for acetate and multiple signals around 1150 cm^{-1} for TFSI (Figure 1).

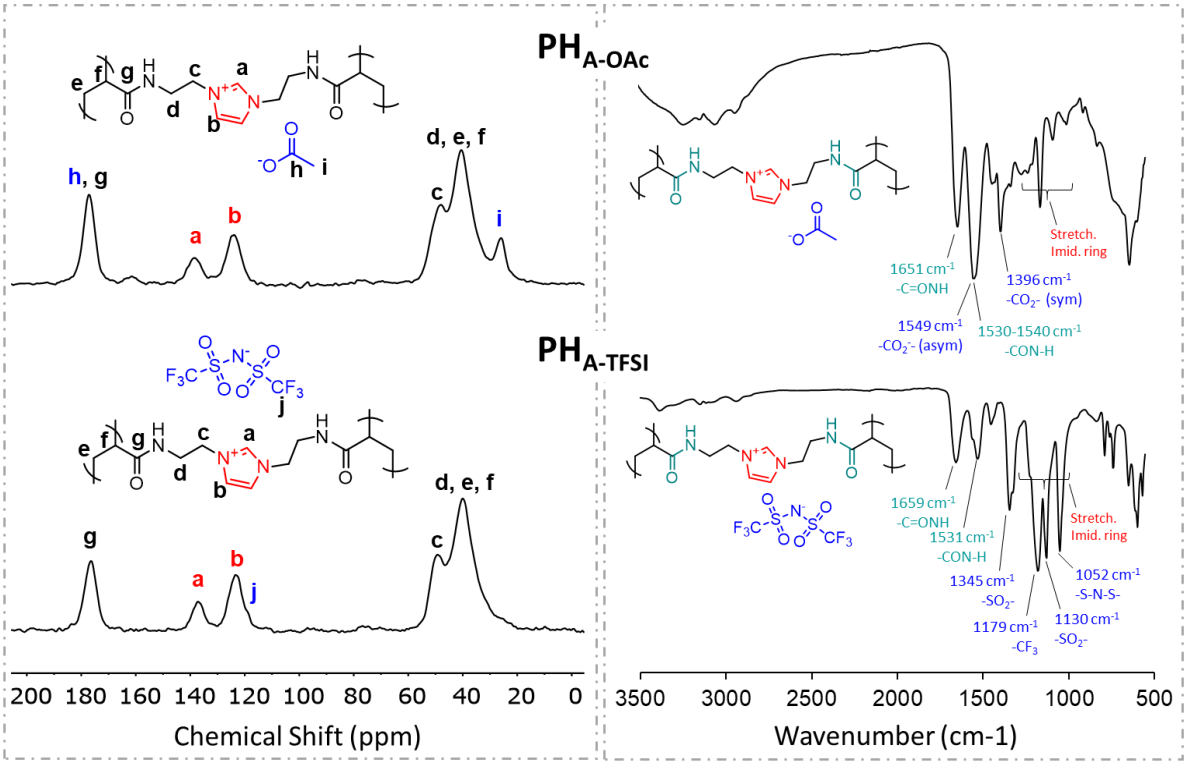

Figure 1. ^{13}C solid state NMR and infrared spectra of $PH_{A\text{-}OAc}$ and $PH_{A\text{-}TFSI}$.

Eventually, the porous architecture was addressed by scanning electron microscopy (SEM) (Figure 2). Both samples show the typical interconnected porosity of PHs but the nature of the counterion induces significant variance in their morphology. $PH_{A\text{-}OAc}$ exhibits bigger voids (cavities) with an average diameter of 20 µm compared to $PH_{A\text{-}TFSI}$ whose voids diameter is around 12 µm (Table 2, entries 1 and 4). The pores size follows the same trend, with average diameters of 7 and 3 µm for $PH_{A\text{-}OAc}$ and $PH_{A\text{-}TFSI}$, respectively. Such a discrepancy is believed to arise from the swelling properties of the materials. Indeed, both PHs were immersed in water

prior to freeze-drying and the acetate-based PH exhibited a water uptake (WU) of 29.3 g g^{-1} against only 4.4 g g^{-1} for the more hydrophobic $PH_{A\text{-}TFSI}$ (Table 2, entries 1 and 4). This behaviour induced a macroscopic change in volume of the porous material prior to freeze-drying which might account for the difference in the diameters of the voids.

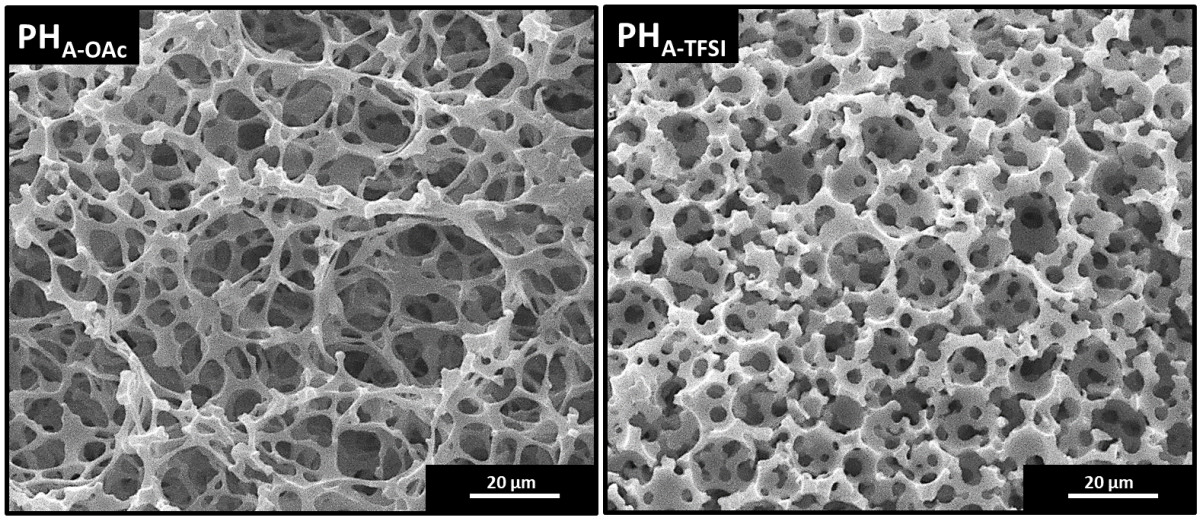

Figure 2. SEM pictures of $PH_{A\text{-}OAc}$ and $PH_{A\text{-}TFSI}$.

Table 2. Summary of the PHs characteristics.

Entry	Sample name	Anion	Imidazolium content (%)[a]	Sulfur content (%)[b]	Voids / Pores diameter (µm)[c]	WU (g g^{-1})[d]	T_{OD} (°C)
1	$PH_{A\text{-}OAc}$		100	0	20 / 7	29.3	220
2	$PH_{B\text{-}OAc}$	Acetate	33	0	32 / 7	28.3	221
3	$PH_{C\text{-}OAc}$		11 (16) [f]	0	27 / 7	44.4	114
4	$PH_{A\text{-}TFSI}$		100	11.7	12 / 3	4.4	338
5	$PH_{B\text{-}TFSI}$	TFSI	33	7.7	21 / 5	10.4	269
6	$PH_{C\text{-}TFSI}$		11 (16) [f]	5.6	27 / 8	29.8	222

[a] Theoretical value based on the reagents engaged in the reaction. [b] Determined by elemental analyses of the PHs-TFSI. [c] Determined by SEM. [d] Determined by gravimetry. [e] Calculated value based on the sulfur content.

This one-pot strategy combining MCR with emulsion templating radical polymerization then served as a platform for the preparation of bi-functional PHs with tunable amounts of imidazolium and amine moieties. Instead of transforming all the aminoethyl acrylamide monomer into the crosslinker, here, only 50 or 20 % of the AEAm-HCl was engaged in the Radziszewski reaction leading to imidazolium crosslinker/amine monomer ratios of 33/67 and 11/89. In practice, after one hour of MCR, the surfactant, the initiator and the rest of the amine monomer were added to the *in situ* formed IBAm and the O/W HIPEs were obtained by the addition of the internal phase (cyclohexane). After polymerization and purification, PHs were neutralized in order to deprotonate amino groups and treated with NaOAc/MeOH or LiTFSI/MeOH solutions to decorate the imidazolium groups with either acetate or TFSI counter anion. $PH_{B\text{-}OAc}$ and $PH_{B\text{-}TFSI}$ containing 33% of imidazolium groups as well as $PH_{C\text{-}OAc}$ and $PH_{C\text{-}TFSI}$ with an imidazolium content of 11% were produced accordingly. Their chemical structures were examined by solid state NMR and FTIR (Figure 3, S6, S7, S8 and S9), confirming the successful anion metathesis. Even for PH_c with the lowest imidazolium content, the nature of counterion is easily identifiable with specific peaks corresponding to acetate or TFSI, especially on the IR spectra (Figure 3 and S8 and S9). As anticipated, NMR signals of the aromatic carbons (**a** and **b**) become less pronounced as the imidazolium content of the PHs decreases (Figures S6 and S7). Note, however, that such observation needs to be considered with care since the ^{13}C solid state NMR done with cross polarization is not quantitative. In order to get a more accurate insight into the composition of the materials, elemental analyses (EA) were performed on the TFSI-based PHs which contain sulfur (Table 2 and S1). The sulfur level should be directly proportional to the imidazolium content of the PHs. The percentage measured for $PH_{A\text{-}TFSI}$ (11.7 %) matched the theoretical value (11.8 %). The sulfur content of $PH_{B\text{-}TFSI}$ (7.7 %) was also close to the theoretical prediction (8.3 %) whereas $PH_{C\text{-}TFSI}$ had a higher sulfur percentage than expected (5.6 % instead of 4.1 %). This discrepancy is probably due to unreacted AEAm during polymerization, which coincides with the lower polymerization yield in the case of PHc (~ 55%). Finally, based on the sulfur percentage measured by EA, it is possible to estimate the effective imidazolium content of PH_c which is 16 mol % rather than the targeted 11 mol %. When considering this composition (16%, imidazolium), the experimental and recalculated theoretical percentages of the other atoms (C, H and N) are in better agreement (Table S1, entry 4).

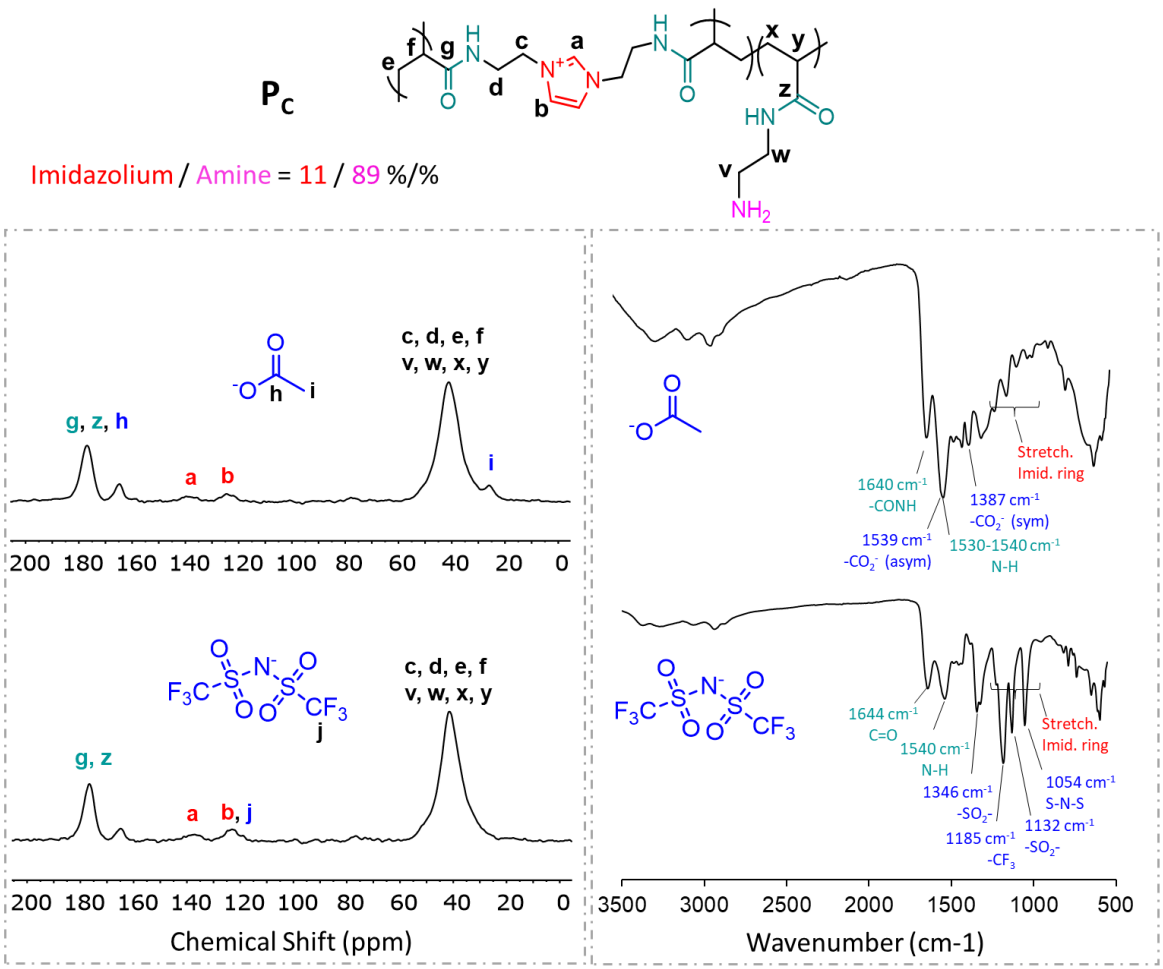

Figure 3. ^{13}C solid state NMR and infrared spectra of $PH_{C\text{-}OAc}$ and $PH_{C\text{-}TFSI}$.

SEM analysis confirmed the open-porous morphology of the bi-functional amino/imidazolium PHs (Figure 4). The PH_B samples (33% of Im) show different voids sizes depending on the nature of the counterions with average diameters of 32 µm and 21 µm for acetate and TFSI, respectively (Table 2). Pore diameters of $PH_{B\text{-}OAc}$ and $PH_{B\text{-}TFSI}$ also slightly differ (7 and 5 µm). Again, these variations might be explained by the higher water uptake of the acetate-based PH_B (28.3 g g^{-1}) compared its TFSI counterparts (10.4 g g^{-1}). In contrast, void and pore diameters of the imidazolium-poor PH_Cs do not vary with the nature of the counterions ($diam_{voids}$ ~ 27 µm and $diam_{pores}$ ~ 7 µm, Table 2). Their water uptakes are also closer, *i.e.* 44.4 g g^{-1} for acetate and 29.8 g g^{-1} for TFSI. As a general trend, the morphological disparities between PHs with different counterions are more pronounced for imidazolium-rich materials highlighting the great impact of the anion on their structure and properties.

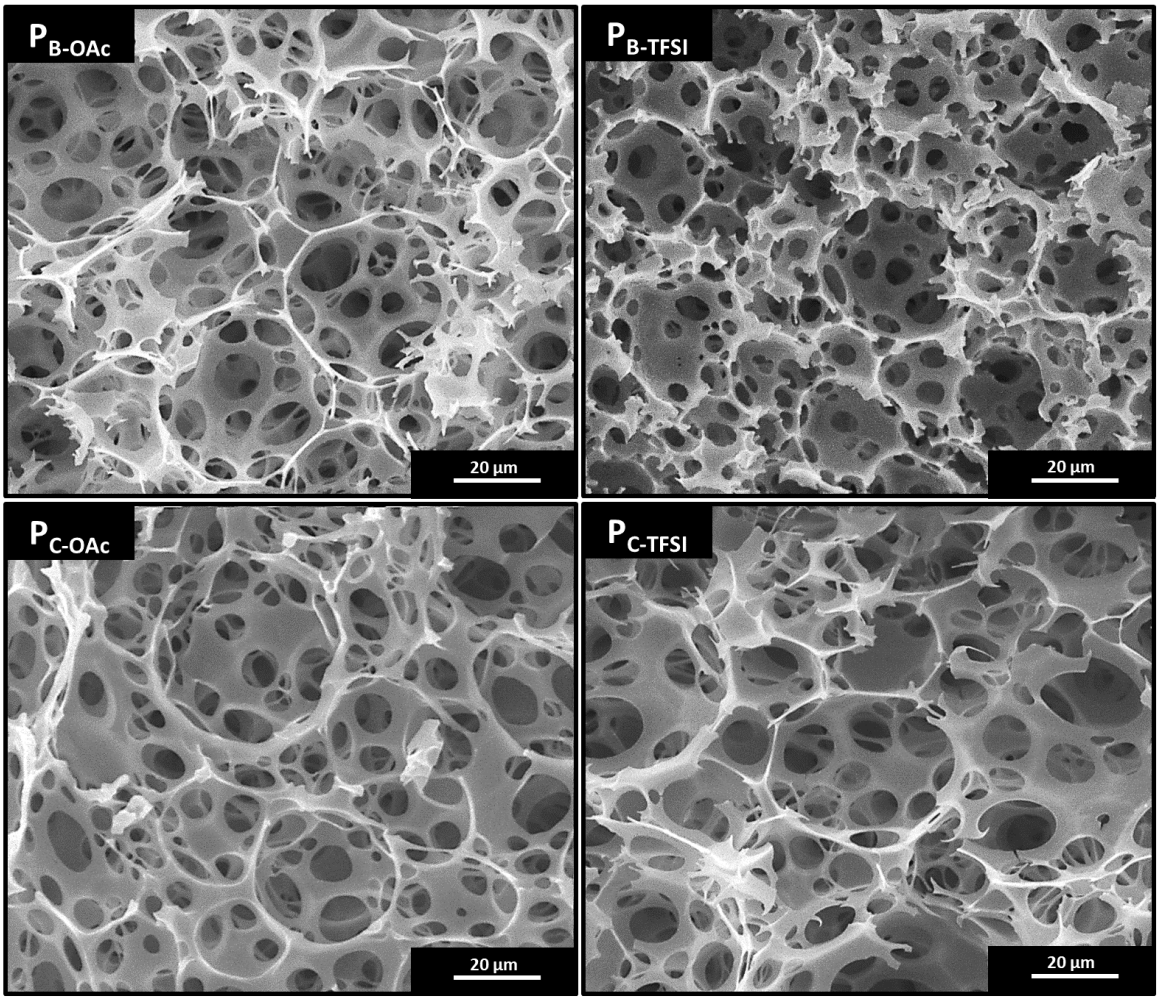

Figure 4. SEM pictures of P_B and P_C with both acetate and TFSI as counterions.

If water uptake of the PHs varies with the nature of the counterion ($WU_{OAc} > WU_{TFSI}$), this property also follows some trends when considering their amine/imidazolium ratio. In this respect, it is important to keep in mind that a higher content of imidazolium, and so of counterions, goes hand in hand with a higher nominal crosslinking ratio which also deeply impacts water uptake. When considering the PH_{TFSI} series, the water uptake systematically decreases with the increase of the imidazolium content ($PH_{A\text{-}TFSI} < PH_{B\text{-}TFSI} < PH_{C\text{-}TFSI}$) (Table 2). This trend is logical since a higher level of imidazolium in the PH implies more hydrophobic TFSI in the material as well as a higher crosslinking density, two factors unfavourable to WU. The situation is more complex in the PH_{OAc} series. Indeed, increasing the content of imidazolium-acetate, which is more hydrophilic than the neutral amine, also increases the crosslinking density; two parameters with antagonist effects on WU. As a result, the water uptake of $PH_{A\text{-}OAc}$ (100% of ImOAc) and $PH_{B\text{-}OAc}$ (33% of ImOAc) exhibits quite similar WU values (29.3 and 28.3 g g^{-1}) because the higher crosslinking density of $PH_{A\text{-}OAc}$ is compensated

by its higher amount of ImOAc groups. In the case of $PH_{C\text{-}OAc}$, the low crosslinking ratio (11%) prevails on the low content of hydrophilic imidazolium affording the highest water uptake (44.4 g g^{-1}).

Finally, the thermogravimetric analyses (TGA) of PH_{TFSI} and PH_{OAc} were investigated in the temperature range of 30–600 °C and demonstrate that PH_{TFSI} are thermally stable up to 338 °C (Figure S10). As previously observed in literature,[40] PHs with acetate counterions have significantly lower degradation temperatures (T_{OD}s) compared to their TFSI counterparts (Table 2). As an example, the T_{OD} of $PH_{A\text{-}OAc}$ (220 °C) is 118 °C lower than $PH_{A\text{-}TFSI}$ (338 °C). Moreover, the T_{OD} tends to decrease together with the imidazolium content, especially in the PH_{TFSI} series ($PH_{A\text{-}TFSI}$: 338 > $PH_{B\text{-}TFSI}$: 269 > $PH_{C\text{-}TFSI}$: 222 °C).

V.2.3 CO_2 uptake capacity, selectivity and kinetics.

The CO_2 uptakes were measured for all materials by recording the equilibrium isotherms at 25 °C and different pressures up to 1 bar (Figure 5a). In the PH_{TFSI} series, $PH_{C\text{-}TFSI}$ reached the maximum CO_2 uptake of 2.0 mmol·g^{-1} and the uptake capacity decreased with the increase in the imidazolium content, down to 0.1 mmol·g^{-1} for $PH_{A\text{-}TFSI}$. The opposite trend was observed in the PH_{OAc} series; the highest CO_2 uptake (0.5 mmol·g^{-1}) was recorded for the sample with the highest imidazolium content. All isotherms reach about 50 % of the total sorption capacities at low pressure (200 mbar). This indicates a strong binding affinity of CO_2 molecules for the sorption sites of PHs, which is further evidenced in the case of the $PH_{C\text{-}TFSI}$ sample where about 75 % of the total amount of gas captured is retained when lowering the pressure (Figure 5a). In order to compare the kinetics of CO_2 sorption for each sample, the relative average sorbate concentrations at 25°C and 1 bar were plotted as a function of time and fitted with a linear driving force adsorption (LDF) model (Figure 5b). The relatively fast equilibrium times correlate closely with CO_2 sorption capacities, suggesting that the 3D-interconnected microcellular morphology of PHs provides low resistant pathways for the diffusion of CO_2 molecules and that the sorption process is mainly determined by the available sorption sites.

Sorption selectivity is another key characteristic of solid sorbents in view of their practical application. N_2 isotherms recorded at 25 °C and 1 bar showed very small amount of adsorbed nitrogen (Figure 5c and S11). Based on these measurements, the CO_2/N_2 selectivity was predicted by the ideal adsorption solution theory (IAST) and plotted as a function of the partial pressure of CO_2 in binary mixtures of CO_2 in N_2 gas at 25 °C (Figure 5d). Very high CO_2/N_2 selectivity of 176 was found at CO_2 partial pressure of 0.15 MPa in the case of $PH_{B\text{-}TFSI}$ while

$PH_{C\text{-}TFSI}$ showed a lower selectivity of 50 in spite of its higher CO_2 uptake. Due to its very low CO_2 sorption capacity, $PH_{A\text{-}TFSI}$ exhibited a lower selectivity (20). PHs from the OAc series showed CO_2/N_2 selectivity between 68 and 13.

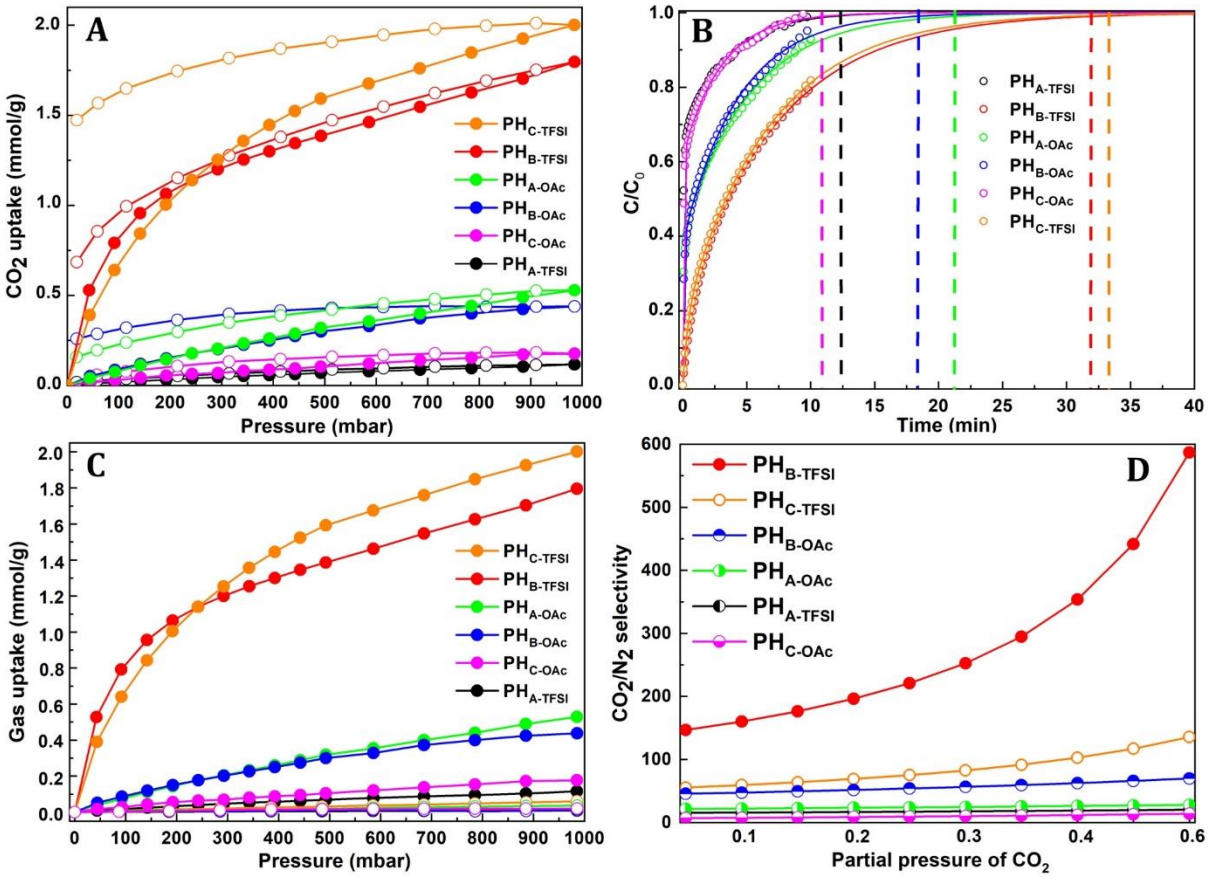

Figure 5. **(A)** Equilibrium CO_2 isotherms of the indicated materials measured at 25 °C up to 1 bar. Full circles – sorption, empty circles – desorption; **(B)** Kinetics of CO_2 sorption of the indicated materials loaded up to 1 bar. Circles – experimental data, line – LDF model fit, vertical dashed lines indicate the time required to reach 99% of the equilibrium values; **(C)** comparison of CO_2 (full circles) and N_2 (empty circles) isothermal data measured at 25 °C up to 1 bar; **(D)** CO_2/N_2 selectivity as a function of CO_2 partial pressure in CO_2/N_2 mixture for a total pressure of 1 bar.

In spite of their negligible N_2-detectable surface areas, some PHs from this study show CO_2-capture performances competitive to those reported for porous poly(imidazolium)s and amine-based PHs, including organic-inorganic hybrid materials, with larger specific surface areas (Table S2), which indicates that the chemistry rather than the microcellular structure dictates the CO_2 capture capacity of our materials.

First, the counter anion (TFSI vs OAc) significantly impacts the CO_2 uptake capacity of these PHs. In the case of pure imidazolium PHs, the lower CO_2 uptake of $PH_{A\text{-}TFSI}$ compared to $PH_{A\text{-}}$

$_{OAc}$ (0.1 and 0.5 mmol g^{-1}, respectively) can be attributed to the bulkiness of the TFSI anion, which prevents access of CO_2 to the cationic imidazolium sites by steric hindrance. This behaviour is well documented for PILs and supported ILs.[47,48] Note that the CO_2 sorption of $PH_{A\text{-}OAc}$ is partially irreversible (30 % retained) at 25 °C under reduced pressure as previously observed for poly(imidazolium acetate).[47] This reveals strong interactions with CO_2 that might be attributed to the carboxylation of imidazolium as evidenced for ILs.[49]

Regarding the bi-functional amine/imidazolium PHs, different trends are observed depending on the counterion. First, the bi-functional TFSI-based PHs afford much higher CO_2 sorption capacities than their pure imidazolium counterpart ($PH_{C\text{-}TFSI} > PH_{B\text{-}TFSI} >> PH_{A\text{-}TFSI}$). The CO_2 uptake also increases with respect to the amine content indicating that the amine functions are mainly responsible for the sorption. As a confirmation, the amount of CO_2 absorbed largely exceeds the amount of imidazolium especially for $PH_{C\text{-}TFSI}$ (Table S3). In addition, $PH_{C\text{-}TFSI}$ retains almost 75 % of the CO_2 in desorption experiment (Figure 5A) probably due to chemisorption *via* the formation of carbamic acid by reaction between an amine and CO_2.[50] $PH_{B\text{-}TFSI}$ that contains a lower amount of amine only retains about 40 % of CO_2 upon depressurization.

Eventually, in contrast to pure imidazolium materials, the CO_2 sorption of bi-functional PHs is much higher with TFSI than OAc ($PH_{C\text{-}TFSI} > PH_{C\text{-}OAc}$ and $PH_{B\text{-}TFSI} > PH_{B\text{-}OAc}$). One reason might be that the fluorinated TFSI improves the CO_2-philicity of these PHs facilitating access of CO_2 to amines. As these bi-functional PHs_{TFSI} materials possess low to moderate crosslinking density and TFSI content, this occurs without the detrimental steric hindrance of the anion encountered for $PH_{A\text{-}TFSI}$. This highlights the key role of the imidazolium counterion as well as the synergy of amine and imidazolium functions in the CO_2 sorption process.

Overall, the best performing materials in CO_2 capture are the bi-functional TFSI-based PHs. $PH_{C\text{-}TFSI}$ affords the highest CO_2 sorption capacity (2 mmol g^{-1}), *i.e.* slightly higher than $PH_{B\text{-}TFSI}$ (1.8 mmol g^{-1}). However, $PH_{B\text{-}TFSI}$ presents better CO_2 uptake efficiency (0.46 mol mol^{-1}) and selectivity in realistic conditions (1 bar, 15 vol% of CO_2 in N_2). In addition, the CO_2 sorption of the latter is more reversible in the tested conditions allowing its repeated use for post-combustion or even direct-air CO_2 capture applications, both currently under the investigation in our laboratories.

V.3 Conclusions

In summary, we developed a straightforward platform to synthesize imidazolium and bi-functional imidazolium/amine macroporous materials in one-pot *via* the combination of Radziszewski MCR with emulsion-templating radical polymerization. For the first time, both imidazolium and amine are structured in a single polyHIPE and tested in CO_2 capture application. The interconnected macroporous structure provides low resistant pathways for the diffusion of CO_2 molecules affording short sorption equilibrium times. Moreover, the incorporation of imidazolium in amine-based materials allows a fine tuning of their thermal and swelling properties as well as CO_2 capture ability by exchanging the counterion of the imidazolium groups. Even at low imidazolium content (16 mol %), exchanging the acetate anion for TFSI drastically improves the CO_2 sorption capacities from 0.2 to 2 mmol g^{-1}. Eventually, a higher imidazolium content (33 mol %), with TFSI anion, exhibits the highest CO_2 uptake efficiency (0.46 mol mol^{-1} in pure CO_2) as well as a very high CO_2/N_2 selectivity of 176 in realistic conditions (15 vol% of CO_2 in N_2, 1 bar). This make the latter, a promising candidate for post-combustion or even direct-air CO_2 capture applications. Besides, such innovative bi-functional amine/imidazolium materials could be real assets for other environmental applications notably as catalysts for the conversion of CO_2 into valued chemicals or for the removal of pollutants (heavy metals and charged dyes) from wasted water.

V.4 References

(1) Kimmins, S. D.; Cameron, N. R. *Adv. Funct. Mater.* **2011**, *21* (2), 211–225.

(2) Silverstein, M. S. *Polymer.* **2014**, *55* (1), 304–320.

(3) Silverstein, M. S. *Progress in Polymer Science*. Elsevier Ltd 2014, pp 199–234.

(4) Jurjevec, S.; Debuigne, A.; Žagar, E.; Kovačič, S. *Polym. Chem.* **2021**, *12* (8), 1155–1164.

(5) Nikjoo, D.; Akhtar, F. *J. CO2 Util.* **2017**, *21*, 473–479.

(6) Jurjevec, S.; Žagar, E.; Kovačič, S. *J. Colloid Interface Sci.* **2020**, *575*, 480–488.

(7) Wang, R.; Li, W.; Lu, R.; Peng, J.; Liu, X.; Liu, K.; Peng, H. *Colloids Surfaces A Physicochem. Eng. Asp.* **2020**, *605* (July), 125334.

(8) Kovačič, S.; Preishuber-Pflügl, F.; Pahovnik, D.; Žagar, E.; Slugovc, C. *Chem. Commun.* **2015**, *51* (36), 7725–7728.

(9) Mathieu, K.; Jérôme, C.; Debuigne, A. *Macromolecules* **2015**, *48* (18), 6489–6498.

(10) Khodabandeh, A.; Arrua, R. D.; Coad, B. R.; Rodemann, T.; Ohigashi, T.; Kosugi, N.; Thickett, S. C.; Hilder, E. F. *Polym. Chem.* **2018**, *9* (2), 213–220.

(11) Mathieu, K.; Jérôme, C.; Debuigne, A. *Polymer.* **2016**, *99*, 157–165.
(12) Mathieu, K.; De Winter, J.; Jérôme, C.; Debuigne, A. *Polym. Chem.* **2017**, *8* (11), 1850–1861.
(13) Zhang, T.; Sanguramath, R. A.; Israel, S.; Silverstein, M. S. *Macromolecules* **2019**, *52* (15), 5445–5479.
(14) Nugent, P.; Giannopoulou, E. G.; Burd, S. D.; Elemento, O.; Giannopoulou, E. G.; Forrest, K.; Pham, T.; Ma, S.; Space, B.; Wojtas, L.; Eddaoudi, M.; Zaworotko, M. J. *Nature* **2013**, *495* (7439), 80–84.
(15) Saiwan, C.; Muchan, P.; De Montigny, D.; Tontiwachwutikul, P. *Energy Procedia* **2014**, *63*, 2317–2322.
(16) Muchan, P.; Saiwan, C.; DeMontigny, D.; Tontiwachwuthikul, P. *Chem. Eng. Trans.* **2013**, *35*, 391–396.
(17) Wang, Q.; Ma, H.; Chen, J.; Du, Z.; Mi, J. *J. Environ. Chem. Eng.* **2017**, *5* (3), 2807–2814.
(18) Wang, Q.; Ma, H.; Chen, J.; Du, Z.; Mi, J. *Polym. Sci. - Ser. B* **2018**, *60* (3), 380–386.
(19) Zhu, J.; Wu, L.; Bu, Z.; Jie, S.; Li, B. G. *Ind. Eng. Chem. Res.* **2019**, *58* (10), 4257–4266.
(20) He, H.; Li, W.; Zhong, M.; Konkolewicz, D.; Wu, D.; Yaccato, K.; Rappold, T.; Sugar, G.; David, N. E.; Matyjaszewski, K. *Energy Environ. Sci.* **2013**, *6* (2), 488–493.
(21) He, H.; Li, W.; Lamson, M.; Zhong, M.; Konkolewicz, D.; Hui, C. M.; Yaccato, K.; Rappold, T.; Sugar, G.; David, N. E.; Damodaran, K.; Natesakhawat, S.; Nulwala, H.; Matyjaszewski, K. *Polymer.* **2014**, *55* (1), 385–394.
(22) Zhu, J.; Wu, L.; Bu, Z.; Jie, S.; Li, B. G. *Ind. Eng. Chem. Res.* **2017**, *56* (36), 10155–10163.
(23) Dejburum, P.; Saiwan, C.; Tontiwachwuthikul, P. *Chem. Eng. Trans.* **2012**, *29*, 193–198.
(24) Yin, J.; Zhang, T.; Schulman, E.; Liu, D.; Meng, J. *J. Mater. Chem. A* **2018**, *6* (18), 8441–8448.
(25) Han, J.; Du, Z.; Zou, W.; Li, H.; Zhang, C. *Ind. Eng. Chem. Res.* **2015**, *54* (31), 7623–7631.
(26) Wang, Q.; Liu, Y.; Chen, J.; Du, Z.; Mi, J. *Environ. Sci. Technol.* **2016**, *50* (14), 7879–7888.
(27) Irani, M.; Jacobson, A. T.; Gasem, K. A. M.; Fan, M. *Energy* **2018**, *157*, 1–9.
(28) Qian, W.; Texter, J.; Yan, F. *Chem. Soc. Rev.* **2017**, *46*, 1124–1159.
(29) Zhang, S.; Dokko, K.; Watanabe, M. *Chem. Sci.* **2015**, *6*, 3684–3691.
(30) Zulfiqar, S.; Sarwar, M. I.; Mecerreyes, D. *Polym. Chem.* **2015**, *6*, 6435–6451.

(31) Wang, X.; Zhou, Y.; Guo, Z.; Chen, G.; Li, J.; Shi, Y.; Liu, Y.; Wang, J. *Chem. Sci.* **2015**, *6* (12), 6916–6924.
(32) Sun, J.-K.; Antonietti, M.; Yuan, J. *Chem. Soc. Rev.* **2016**, *45* (23), 6627–6656.
(33) Guo, Z.; Jiang, Q.; Shi, Y.; Li, J.; Yang, X.; Hou, W.; Zhou, Y.; Wang, J. *ACS Catal.* **2017**, *7* (10), 6770–6780.
(34) Soll, S.; Zhao, Q.; Weber, J.; Yuan, J. *Chem. Mater.* **2013**, *25* (15), 3003–3010.
(35) Wilke, A.; Yuan, J.; Antonietti, M.; Weber, J. *ACS Macro Lett.* **2012**, *1* (8), 1028–1031.
(36) Feng, X.; Gao, C.; Guo, Z.; Zhou, Y.; Wang, J. *RSC Adv.* **2014**, *4*, 23389–23395.
(37) Dani, A.; Crocellà, V.; Magistris, C.; Santoro, V.; Yuan, J.; Bordiga, S. *J. Mater. Chem. A* **2017**, *5* (1), 372–383.
(38) Boyère, C.; Favrelle, A.; Léonard, A. F.; Boury, F.; Jérôme, C.; Debuigne, A. *J. Mater. Chem. A* **2013**, *1* (29), 8479–8487.
(39) Mathieu, K.; Jérôme, C.; Debuigne, A. *Polym. Chem.* **2018**, *9* (4), 428–437.
(40) Stiernet, P.; Aqil, A.; Zhu, X.; Debuigne, A. *ACS Macro Lett.* **2020**, *9* (1), 134–139.
(41) Saxer, S.; Marestin, C.; Mercier, R.; Dupuy, J. *Polym. Chem.* **2018**, *9* (15), 1927–1933.
(42) Llevot, A.; Boukis, A. C.; Oelmann, S.; Wetzel, K.; Meier, M. A. R. *Top. Curr. Chem.* **2017**, *375* (66), 1–29.
(43) Yang, B.; Zhao, Y.; Wei, Y.; Fu, C.; Tao, L. *Polym. Chem.* **2015**, *6* (48), 8233–8239.
(44) Kakuchi, R. *Angew. Chemie - Int. Ed.* **2014**, *53* (1), 46–48.
(45) Ma, Y.; Yung, L.-Y. L. *Anal. Chem.* **2014**, *86* (5), 2429–2435.
(46) Esposito, D.; Kirchhecker, S.; Antonietti, M. *Chem. – A Eur. J.* **2013**, *19* (45), 15097–15100.
(47) Privalova, E. I.; Karjalainen, E.; Nurmi, M.; Mäki-Arvela, P.; Eränen, K.; Tenhu, H.; Murzin, D. Y.; Mikkola, J.-P. *ChemSusChem* **2013**, *6* (8), 1500–1509.
(48) Aquino, A. S.; Bernard, F. L.; Borges, J. V; Mafra, L.; Vecchia, F. D.; Vieira, M. O.; Ligabue, R.; Seferin, M.; Chaban, V. V; Cabrita, E. J.; Einloft, S. *RSC Adv.* **2015**, *5* (79), 64220–64227.
(49) Besnard, M.; Cabaço, M. I.; Chávez, F. V.; Pinaud, N.; Sebastião, P. J.; Coutinho, J. A. P.; Danten, Y. *Chem. Commun.* **2012**, *48* (9), 1245–1247.
(50) McCann, N.; Phan, D.; Wang, X.; Conway, W.; Burns, R.; Attalla, M.; Puxty, G.; Maeder, M. *J. Phys. Chem. A* **2009**, *113* (17), 5022–5029.

V.5 Experimental Section

Materials. Glyoxal (40 wt% in H_2O), formaldehyde (37 wt % in H_2O), calcium hydride (95 %, +4 mesh), sodium sulfate anhydrous (>99 %), sodium citrate dihydrate (>99 %), sodium bicarbonate ($NaHCO_3$, >99.7 %) citric acid (99 %) and acryloyl chloride (>96 %) were purchased from Sigma Aldrich. 2,2'-Azobis[2-(2-imidazolin-2-yl)propane]dihydrochloride (VA-044) (>98 %) was purchased from TCI. *Tert*-butyl *N*-(2-aminoethyl)carbamate (98%) and HCl (4M) in dioxane were purchased from Fluorochem. Diethyl ether (Et_2O, technical grade), tetrahydrofuran (HPLC) and cyclohexane (> 99%) and sodium chloride (NaCl, >99 %) were purchased from VWR. Triethylamine (TEA, 99%) was purchased from Acros. Sodium acetate anhydrous (p.a.) was purchased from Vel. Chloroform ($CHCl_3$, >99.8 %) and methanol (MeOH, >99.9 %) were purchased from Fisher Scientific. Deuterated solvents were purchased from Eurisotop. Pluronics PEF68 was purchased from ICI Surfactants. All chemicals and solvents were used without purification except for THF that was dried onto molecular sieves and TEA which was dried under calcium hydride, purified by distillation under reduced pressure and kept under Ar.

Characterization. ^{13}C Cross Polarization (CP) and Magic Angle Spinning (MAS) ssNMR spectra were recorded with 4-mm zirconia rotors spinning at 10 kHz on a Bruker Avance III HD spectrometer (B_0 = 9.04 T) working at the Larmor frequency of 100.62 MHz. Cross polarization experiments were performed with a delay time of 2 s and a contact time of 2 ms. ^1H NMR, HSQC, HMBC and COSY spectra were recorded at 298 K with a Bruker Avance III HD spectrometer (B_0 = 9.04 T) (400 MHz) and treated with MestReNova software. IR spectra were recorded on ThermoFischer Sientific Nicolet IS5 equipped with an ATR ID5 module using a diamond crystal (650 cm^{-1} - 4000 cm^{-1}). Differential scanning calorimetry (DSC) was performed on a DSC 250 TA Instruments, using hermetic aluminium pans, indium standard for calibration, nitrogen as the purge gas, a sample weight of ~5 mg. The sample was cooled down to -20 °C at 20 °C/min cooling rate, followed by an isotherm at −20°C for 2 min and heating up to 100 °C with acetate as counterion (or 120 °C with TFSI) at 10 °C/min heating rate. These cycles were done twice. The fourth cycle (last heating from -20 to 100 °C or 120 °C) was analysed. Thermogravimetric analysis (TGA) analyses were carried out with a TGA 2 large furnace from Mettler Toledo under nitrogen at a heating rate of 20°C /min from 30°C to 600 °C with a sample weight of ~6 mg. Elemental analysis was used to determine the percent weight of specific atoms of carbon (C), hydrogen (H), nitrogen (N) and sulfur (S) in the PHs and therefore enabling to verify their empirical formula (CxHyNjSk). Elemental analysis was

realized on a Thermo Electron Corporation Flash EA 1112 CHNS Elemental Analyzer (Interscience sprl, Louvain-la-Neuve, Belgium) equipped with a dry sample auto-sampler on the top of furnace, and under Eager 300 dedicated software control for organic elemental analysis in the following analytical conditions: 900℃ for sample combustion, 130 mL/min of the Carrier Flow, 100 mL/min for Reference Flow, 250 mL/min for Oxygen Flow, 5 sec for Oxygen Injection End (0 sec for Oxygen analysis), 12 sec for Sample Delay Time, 10 min for Run time, and 1.3 – 1.8 mg for sample weight. Electrospray ionization mass spectrometry (ESI-MS) were performed on a SYNAPT G2-Si from Waters. The sample was solubilized in a mixture of Milli-Q water-acetonitrile (1:1 v:v) in presence of 0.1 v% of formic acid prior to ionization. N_2 and argon isothermal measurements were carried out on an iQ3 gas analyzer (Quantachrome Instruments) at 77 K and 87 K, respectively. CO_2 and N_2 isothermal sorption IMI-HTP manometric gas analyser (Hiden Isochema Inc.).

Synthesis of *N*-boc-aminoethyl acrylamide (Boc-AEAm). Acryloyl chloride (8.1459 g, 90 mmol) in 120 ml THF was added dropwise into an ice cooled dried THF (180 ml) containing Boc-ethylenediamine (12.0158 g, 75 mmol), dried triethylamine (9.1071 g, 90 mmol) and 3A molecular sieve in 1 h under stirring. The mixture was stirred for another 2 h in ice water, and then at room temperature overnight. After removal of white precipitate by filtration, THF was removed by rotary evaporator. The residual powder was dissolved into 300 ml chloroform and washed subsequently with citrate buffer solution (citric acid and trisodium citrate dihydrate, 500 mM buffer strength, 300 ml, pH 5.0), saturated brine (300 ml), saturated $NaHCO_3$ (300 ml), finally saturated brine (300 ml). The organic layer was collected and dried by anhydrous Na_2SO_4. After removal of the chloroform, yellowish powder was obtained. Isolated yield: 91.7 %. ^{1}H NMR ($CDCl_3$): δ 1.43 (s, 9H, $(CH_3)_3C$), 3.31 (m, 2H, CH2-amide), 3.43 (m, 2H, CH_2-carbamate), 5 (s, ^{1}H, NH carbamate), 5.63 (m, 1H, =CH), 6.06-6.28 (m, 2H, CH2=CH), 6.49 (s, 1H, NH amide) (Figure S1)

Synthesis of aminoethyl acrylamide (AEAm). 60 ml 4 M HCl in dioxane was injected onto Boc-AA (10 g, 47 mmol) in a 100 ml flask. After 4 h reaction, the yellowish powder (AEAm) was collected and washed thoroughly with cold diethyl ether. The powder was poured into 100 mL of cold diethyl ether under stirring for 1 hour then filtered and dried for 48 hours under vacuum at 30 °C. The highly hygroscopic product was stored at -20 °C with caution to avoid water absorption. Isolated yield: 96.6 %. ^{1}H NMR (D_2O): δ 3.18 (m, 2H, CH_2-protonated amine), 3.58 (m, 2H, CH_2-amide), 5.75-5.84 (m, 1H, =CH), 6.17-6.33 (m, 2H, CH_2=) (Figure S2). ESI-MS: 115.08 m/z and 229.16 m/z corresponding to the desired product and the Michael

addition adduct respectively (Figure S3). NMR calculation for purity: 94 % of AEAm and 6% of the side-product (Figure S2).

Optimization of the synthesis of imidazolium bis-acrylamide crosslinker (IBAm). In reaction tube, 5 mmol of AEAm (753 mg) was dissolved in 5 or 1.5 ml of Milli-Q water. Depending on the trial, acetic acid (15, 12.5 or 0 mmol) and/or sodium acetate (0,2, 5 or 7.5 mmol) were added. Solutions of formaldehyde (37 wt% in water, 2.5 mmol, 203 mg) and glyoxal (40 wt% in water, 2.5 mmol, 363 mg) were put in the reaction mixture. The reactions were carried out at room temperature under air. After for 1 hour, the solutions were drawn under reduced pressure at 30 °C to remove the volatile residual compounds and concentrate the solution. Sample were analyzed by ^{1}H NMR in D_2O (Figure S4). The conversions were calculated based on NMR integrals, according to the following equation:

$$Conv. = \frac{2 * \int g}{\int b', c' + \int b, c}$$

were the signal **g** corresponds to the aromatic protons, **b'** and **c'** correspond to the vinylic protons of IDA while **b** and **c** correspond to the vinylic protons of AEAm. The vinylic protons of both AEAm and IDA being indistinguishable, they were integrated together. The results of the different reactions are presented in Table 1.

Synthesis of imidazolium-based PHs. In a reaction tube, AEAm (1.506 g, 10 mmol), formaldehyde (37 wt% in water, 0.410 g, 5 mmol), glyoxal (40 wt% in water, 0.726 g, 5 mmol), sodium acetate (1.231 g, 15 mmol) were dissolved in water (3 g). After 1 hour at room temperature, the surfactant PEF68 (0.346 g, 5 w% of the total aqueous phase) and VA-044 (65 mg, 0.2 mmol) were added to the reaction mixture, followed by dropwise addition of cyclohexane (15.59 g, 20.026 mL, 75 v% of the total emulsion) under mechanical stirring (500 rpm). The resulting HIPE emulsions were put under argon after brief flushing to remove oxygen and cured at 60 °C for 5 hours. Finally, the materials produced accordingly were immersed in MeOH/THF (1:1 v:v) followed by a short immersion in water for washing (2 hours). The samples were then freeze-dried.

Synthesis of bi-functional amine/imidazolium-based PHs. In a reaction tube, AEAm (5 or 2 mmol), formaldehyde (2.5 or 1 mmol), glyoxal (2.5 or 1 mmol) and sodium acetate (7.5 or 3 mmol) were dissolved in water (1.5 or 0.6 mL). After 1 hour at room temperature, fresh AEAm (5 or 8 mmol), water (1.5 or 2.4 mL), PEF68 (0.288 or 0.252 g, 5 w% of the total aqueous phase) and VA-044 (65 mg, 0.2 mmol) were added to the reaction mixture before emulsification by dropwise addition of cyclohexane (13.40 or 12.09, 75 v% of the total emulsion) under mechanical stirring (500 rpm). The resulting HIPE emulsions were put under argon after brief

flushing to remove oxygen and cured at 60 °C for 5 hours. Finally, the materials produced accordingly were immersed in MeOH/THF (1:1 v:v) followed by a short immersion in water for washing (2 hours). The samples were then freeze-dried.

Typical procedure for anions exchange. In an Erlenmeyer, the dried PHs were immersed for 24 hours in 100 mL of aqueous solution $NaHCO_3$ (0.2 M) at +6 °C under gentle stirring. The samples were splitted into two equal part and immersed in a methanol solution (100 mL) containing the counterion salt in excess, i.e. NaOAc (3.3 g, 40 mmol) and LiTFSI (12 g, 40 mmol). The samples were then immersed in Milli-Q water for washing the excess of salt. Eventually the samples were freeze-dried.

Water uptake (WU). The samples are weighted before and after the freeze-drying last step of their synthesis. The water uptake is calculated based on the following formula:

$$WU\ (g\ g^{-1}) = \frac{m_{wet} - m_{dried}}{m_{dried}}$$

CO_2 capture measurement. CO_2 (and N_2) isothermal sorption measurements along with the kinetic studies were performed on an IMI-HTP manometric gas analyser (Hiden Isochema Inc.). Prior the measurements the samples were outgassed at 130 °C for 2 hours. The kinetic measurements were fitted using the linear driving force (LDF) adsorption model. This is a simplified model used to predict dynamic behaviour of sorption and desorption processes defining mass transfer resistance as a linear function of concentration. The LDF model of the relaxation $q(t)$ is,

$$q(t) = q_o + \Delta q(1 - e^{-\frac{t-t_o}{k}})$$

where q_o is the uptake at the time origin t_o, k is the exponential time constant and Δq is the uptake change.

The prediction of the selectivity of CO_2/N_2 mixtures was made by using the ideal adsorption solution theory (IAST) which is a widely used method to predict binary mixture adsorption from the experimental results of pure-gas isotherms. Firstly, the pure-gas isotherms should be well fitted by a proper adsorption model. Here, we used the following adsorption model to fit the isotherms of CO_2 and N_2.

Single-site Langmuir equation (SSL)

$$q = \frac{q_m * b * p}{1 + bp}$$

where p is the pressure of the bulk gas at equilibrium (MPa), q is the adsorbed amount per mass of adsorbent (mmol/g), q_m is the saturation capacity of adsorbent and b is the affinity coefficient.

The selectivity of mixtures is defined as:

$$S_{A/B} = \frac{X_A}{P_A} * \frac{P_B}{X_B}$$

where X and P are the mole fractions of the components in the adsorbed and the partial pressure in the gas phases, respectively. The subscript A and B represent the components of the mixtures, which stand for CO_2 and N_2 here.

V.6 Supporting information

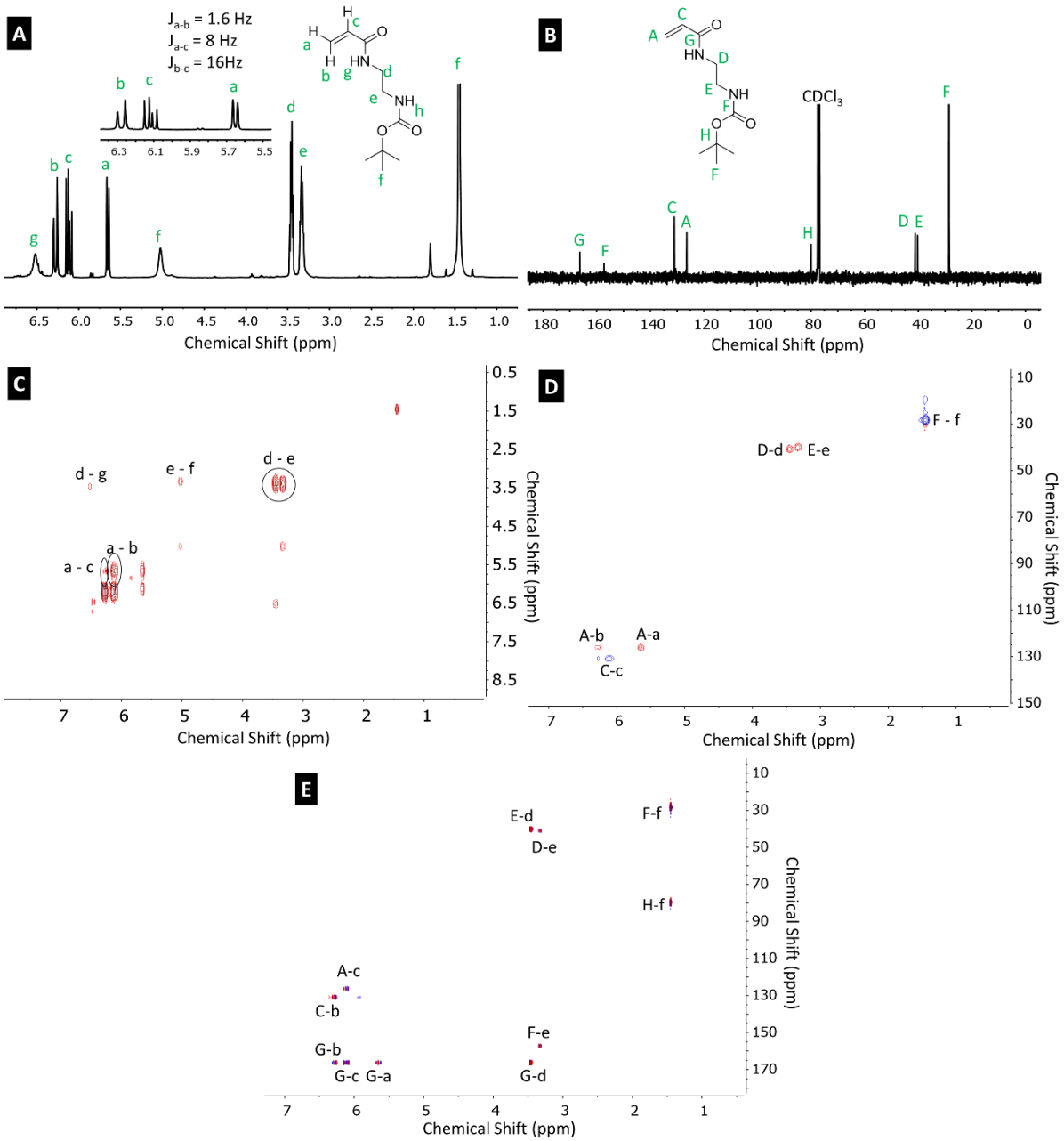

Figure S1. NMR spectra of *N*-boc-aminoethyl acrylamide (Boc-AEAm) in deuterated chloroform. A) ^{1}H, B) ^{13}C, C) COSY, D) HSQC and E) HMBC analyses.

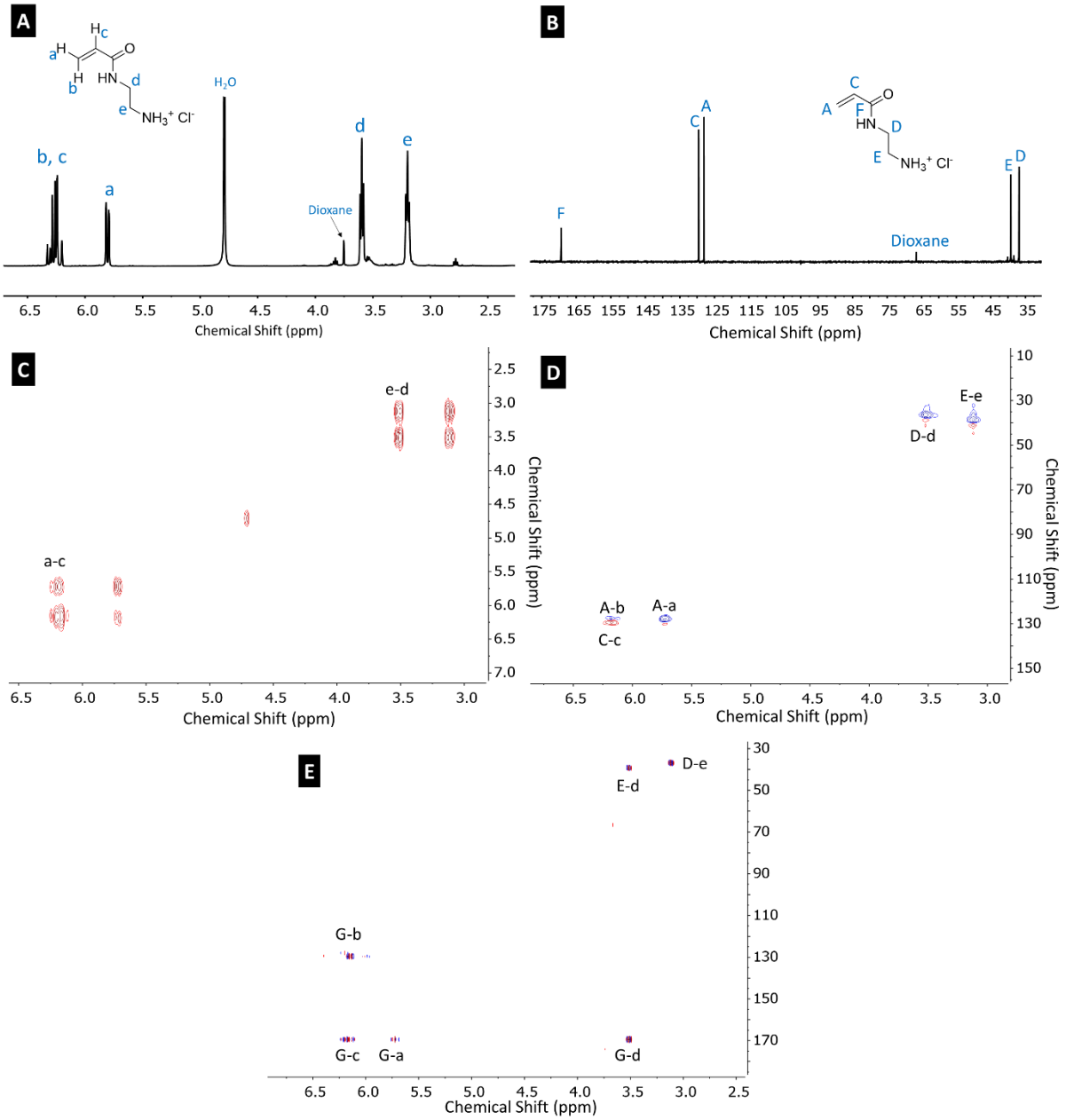

Figure S2. NMR spectra of aminoethyl acrylamide (AEAm-HCl) in deuterium oxide. A) ^{1}H, B) ^{13}C, C) COSY, D) HSQC and E) HMBC analyses.

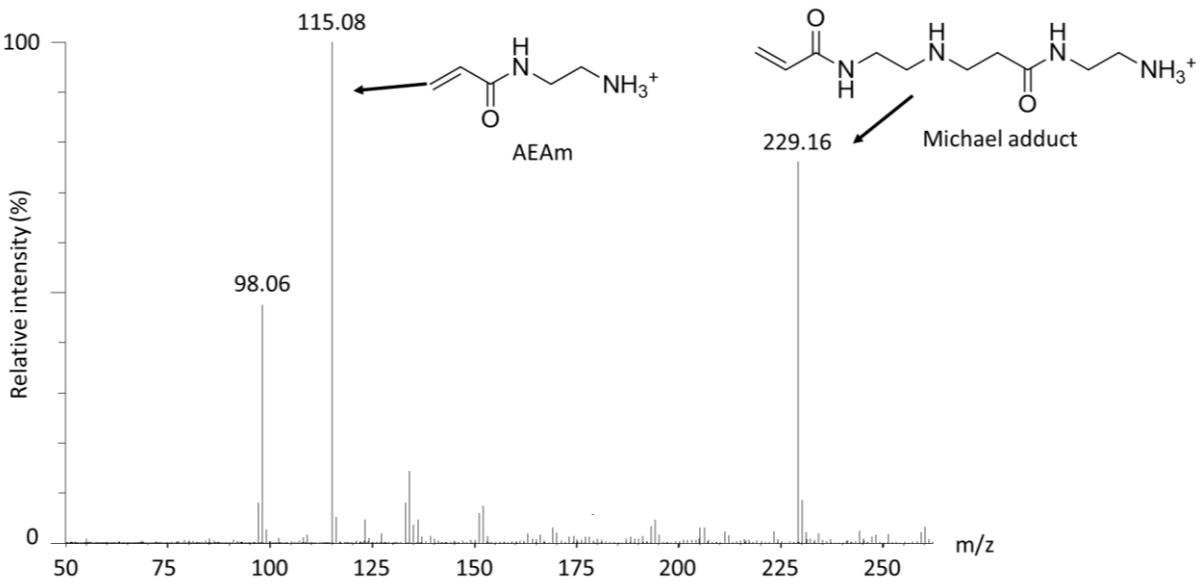

Figure S3. ESI-MS of AEAm (115.08 m/z) contaminated with the Michael adduct (229.16 m/z).

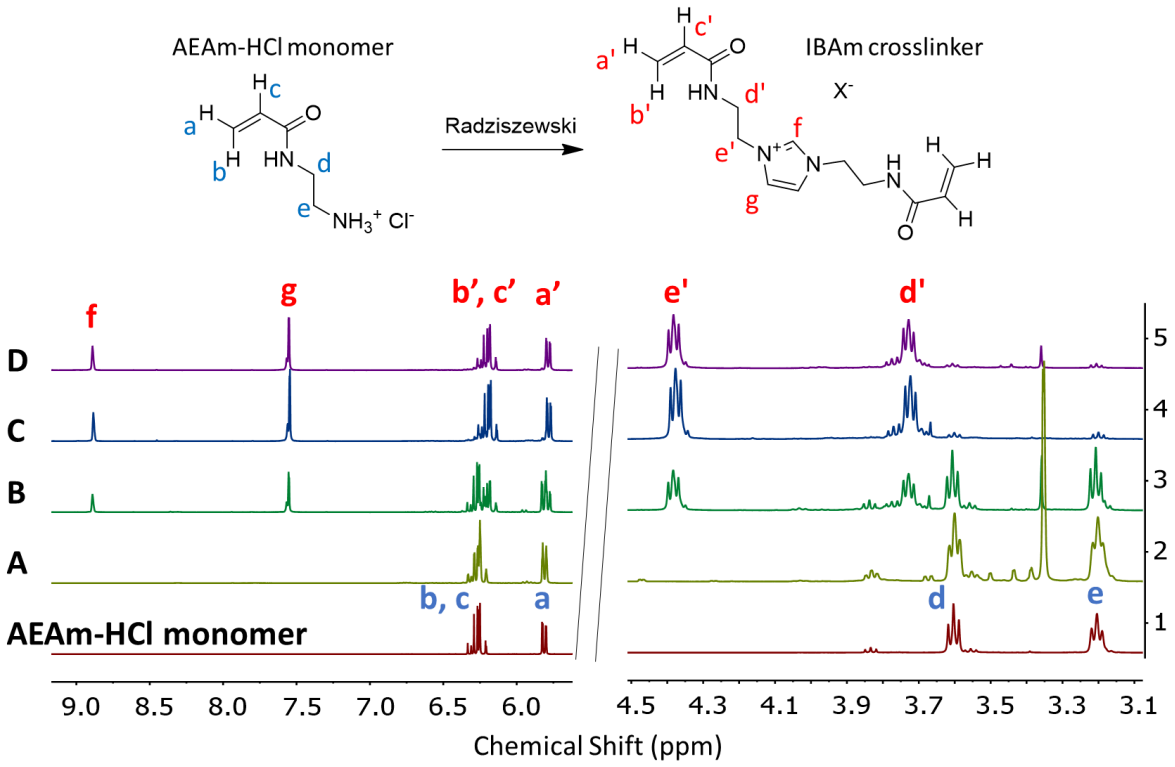

Figure S4. NMR spectra of AEAm-HCl monomer before and after Radziszewski reactions with glyoxal and formaldehyde under different conditions listed in Table 1.

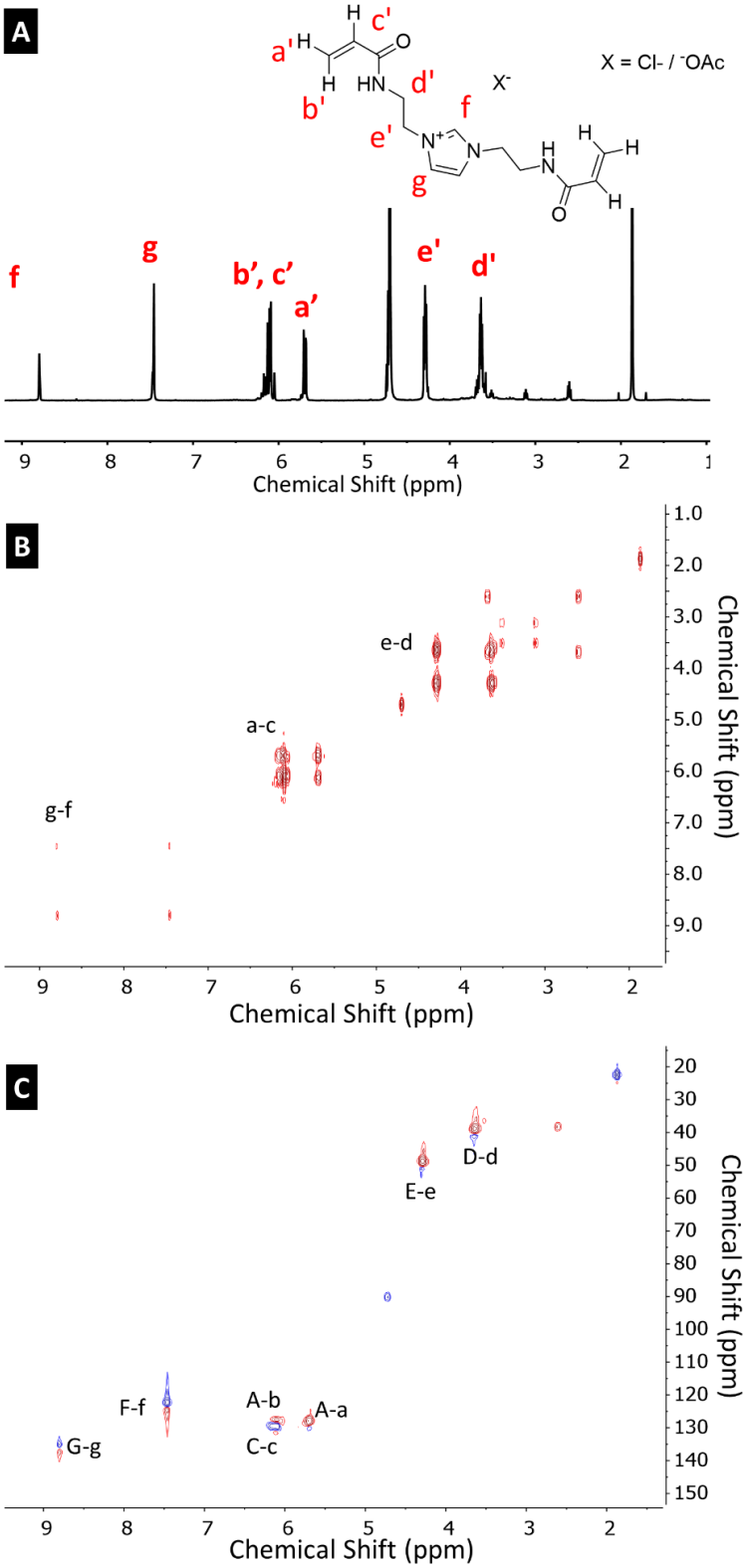

Figure S5. NMR spectra of the imidazolium bis-acrylamide (IBAm) crosslinker in deuterium oxide. A) ^{1}H, B) COSY and C) HSQC analyses. The analyses were done on the unpurified product after the reaction (Table 1, entry 3, code C).

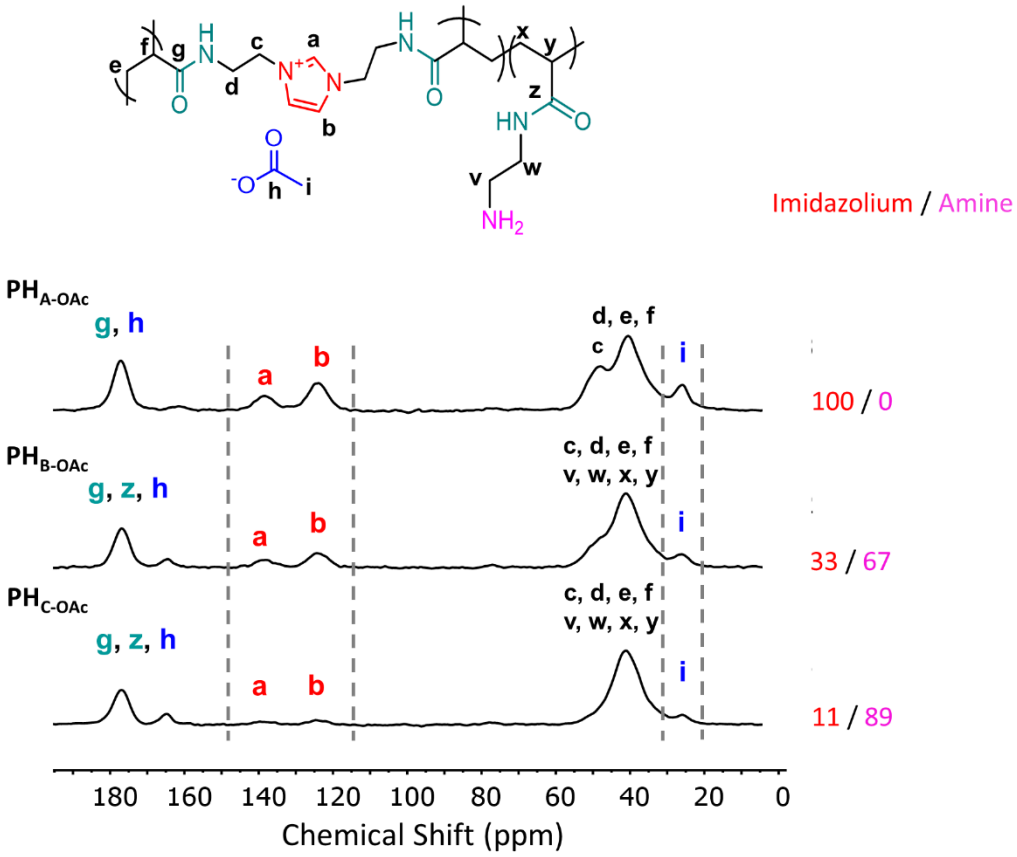

Figure S6. ^{13}C solid state NMR spectra of $PH_{A\text{-}OAc}$, $PH_{B\text{-}OAc}$ and $PH_{C\text{-}OAc}$.

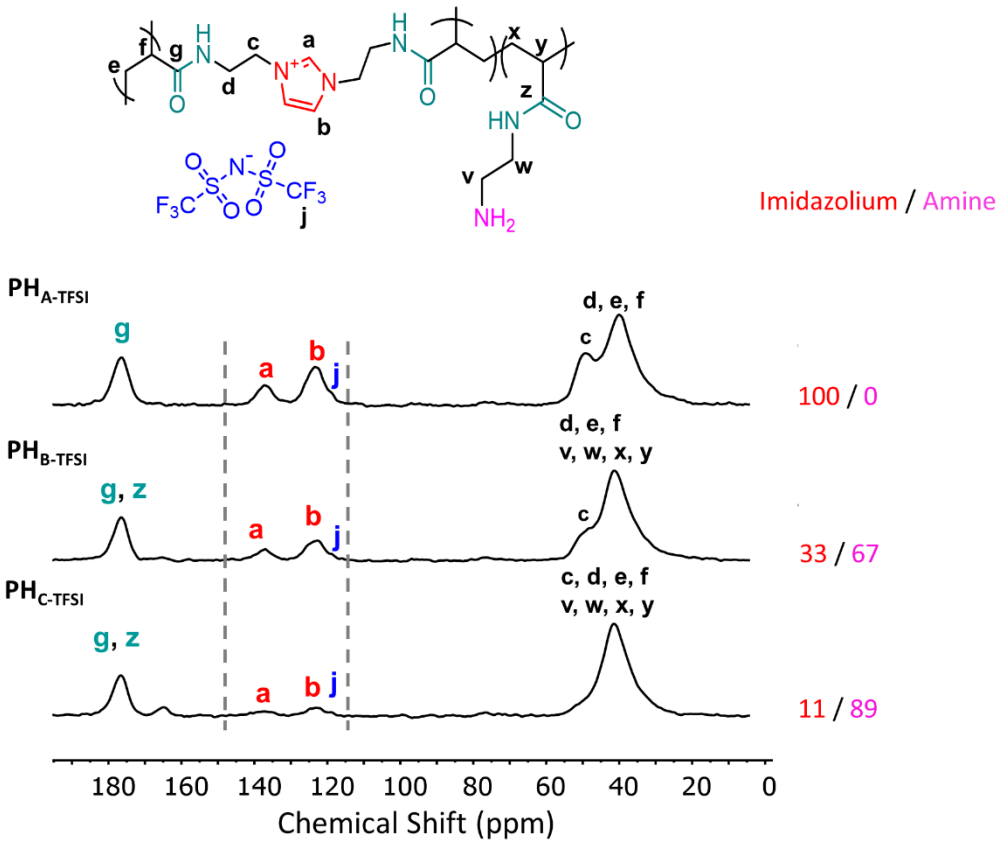

Figure S7. ^{13}C solid state NMR spectra of $PH_{A\text{-}TFSI}$, $PH_{B\text{-}TFSI}$ and $PH_{C\text{-}TFSI}$.

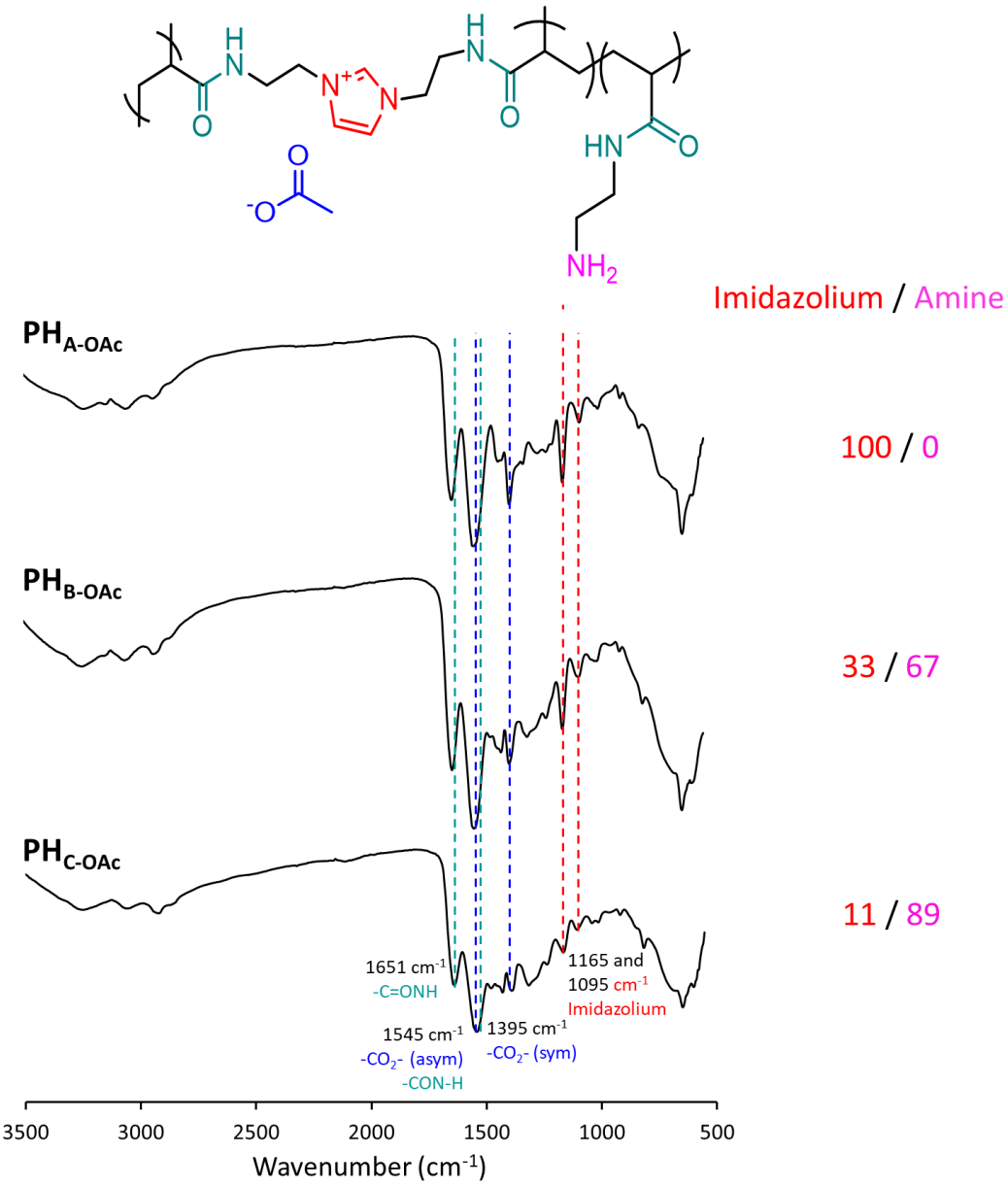

Figure S8. Infrared spectra of $PH_{A\text{-}TFSI}$, $PH_{B\text{-}TFSI}$ and $PH_{C\text{-}TFSI}$.

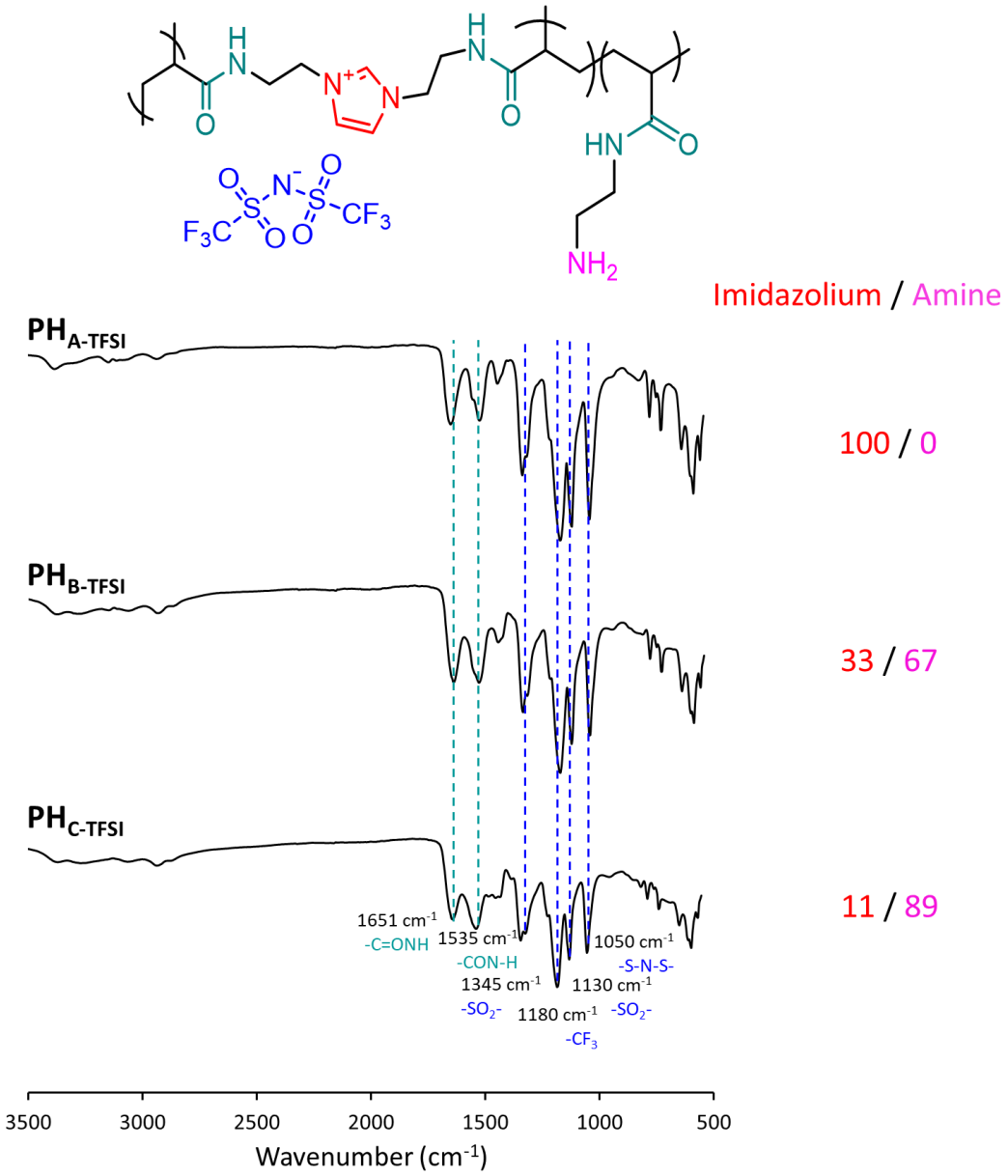

Figure S9. Infrared spectra of $PH_{A\text{-}TFSI}$, $PH_{B\text{-}TFSI}$ and $PH_{C\text{-}TFSI}$.

Table S1. Elemental analyses of the PHs with TFSI as counterion.

Entry	Sample	Imidazolium content (mol %)	Molecular formula		Content % C	H	N	S
1	$PH_{A\text{-}TFSI}$	100	$C_{15}H_{19}N_5O_6F_6S_2$	Theo.	33.15	3.52	12.89	11.80
				Exp.	34.75	4.03	13.15	11.74
2	$PH_{B\text{-}TFSI}$	33	$C_{25}H_{39}N_9O_8F_6S_2$	Theo.	38.91	5.09	16.33	8.31
				Exp.	39.07	5.03	15.56	7.72
3	$PH_{C\text{-}TFSI}$	11	$C_{55}H_{99}N_{21}O_{14}F_6S_2$	Theo.	45.35	6.85	20.19	4.40
				Exp.	41.04	6.18	17.39	5.63
4		16 [a]	$C_{661}H_{1145}N_{248}O_{180}F_{96}S_{32}$	Theo.	43.33	6.30	18.98	5.63
				Exp.	41.04	6.18	17.39	5.63

[a] Recalculated based on the experimental sulfur content.

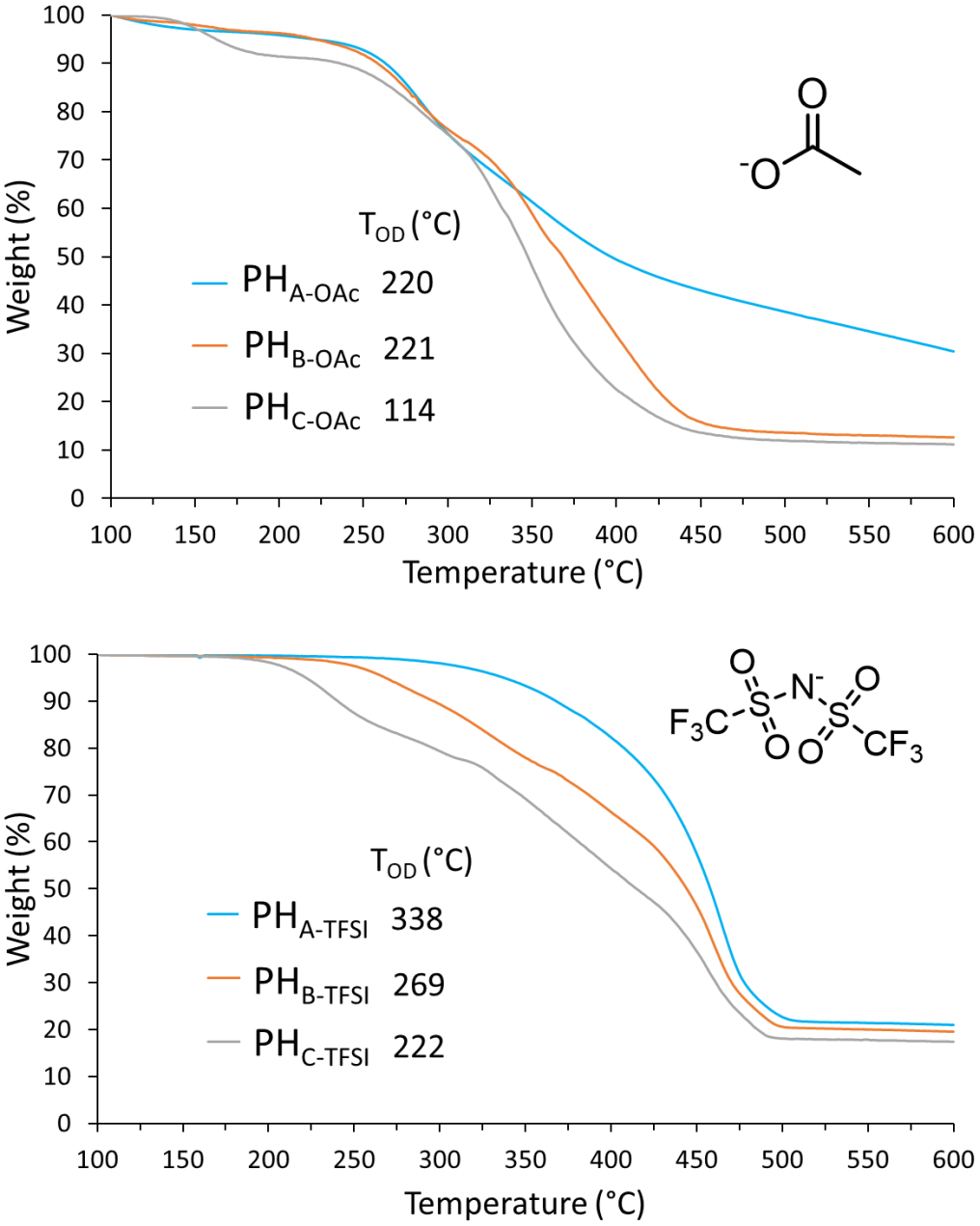

Figure S10. Thermogravimetric analyses of the PHs. The T_{OD}s are determined at 5 weight percent loss.

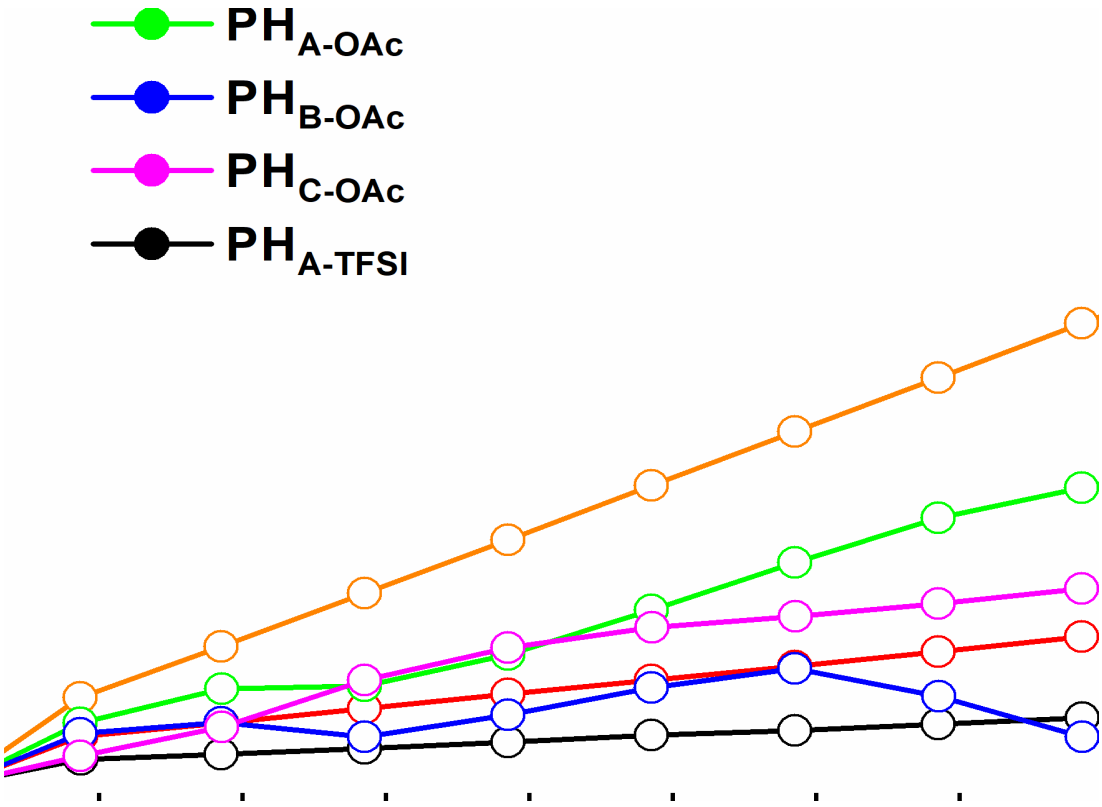

Figure S11. Equilibrium N_2 isotherms of the indicated materials measured at 25 °C up to 1 bar.

Table S2. CO_2 sorption capacity and selectivity of various sorbents.

Sorbent	Temp. (K)	CO_2 uptake (mmol g^{-1}) [a]	Specific surface area [b] (m^2 g^{-1})	Selectivity		Ref
				S_1 [c]	S_2 [d]	
PH from this work						
$PH_{B\text{-}TFSI}$	298	1.8	< 1	108	176	this work
$PH_{C\text{-}TFSI}$	298	2.0	<1	33	50	this work
Amine-based PHs						
PVBC-*grafted*-AEP	298	0.2 [e]	97	*nr*	*nr*	[16]
PGMA-*grafted*-TZL	298	3.6	20	30	*nr*	[22]
PGMA-*grafted*-PEI	313	4.9	12	41	*nr*	[25]
$Fe(OH)_3$ gel-*soaked*-PEI	348	5.6	154	*nr*	359 [g]	[26]
PEHMA-*soaked*-PEI	343	2.8 [f]	20	*nr*	*nr*	[27]
MOF of PS-TiO_2-PEI	348	5.3	18	*nr*	*nr*	[17]
MOF of PS-TiO_2-PEI	348	1.5	3	*nr*	*nr*	[18]
MOF of PGMA-CuO-HBTC-*grafted*-PEI	298	4.2	83	73	*nr*	[19]
MOF of PMF-Zn	273	0.9 [h]	497	*nr*	50 [h]	[24]
Porous poly(imidazolium)s						
PDVIm Br	273	1.0	205	*nr*	*nr*	[31]
PVImOH Br	273	1.0	239	*nr*	*nr*	[33]
PVIm-*co*-DAA	273	0.6	190	*nr*	*nr*	[34]
PDVIm TFSI	273	0.5	150-220	*nr*	200	[35]
PVIm Br	298	0.5	512	*nr*	*nr*	[36]
PIm OAc RMCP	298	1.2	419	*nr*	*nr*	[37]
PIm TFSI RMCP	298	1.1	176	*nr*	*nr*	[37]

PVBC, Poly(vinylbenzyl chloride); AEP, aminoethylpiperazine; PGMA, poly(glycidyl methacrylate); TZL, triazole; PEI, poly(ethylenimine); PEHMA, poly(2-Ethylhexyl methacrylate); MOF, metal-organic framework; PS, poly(styrene); CuO-HBTC, MOF of CuO reacted with 1,3,5-benzenetricarboxylic acid; PMF, poly(melamine-formaldehyde) resin. DVIm, divinyl imidazolium; VIm, vinyl imidazolium; DAA, deprotonated acrylic acid; Im RMCP, imidazolium synthesized by Radziszewski MCP. [a] Determined at 1 bar of pure CO_2 except if stated otherwise. [b] Determined by BET analysis using N_2 adsorption. [c] CO_2/N_2 selectivity: $S = n_{CO2}(1\ atm)/n_{N2}\ (1\ atm)$. [d] CO_2/N_2 selectivity predicted by ideal adsorption solution theory (IAST) model, $S = [n_{CO2}(0.15\ bar)/n_{N2}(0.85\ bar)] * (0.85/0.15)$ for a pressure of 1 bar. [e] Measured in a mixture of CO_2/N_2 with 4 vol% of CO_2. [f] Measured in a mixture of CO_2/N_2 with 10 vol% of CO_2. [g] Measured for partial pressure of CO2 of 0.10 bar. [h] Measured at a total pressure of 0.1 bar.

Table S3. CO_2 capture efficiency of PHs with different counterions.

Entry	Samples	Composition (%)		Chemical function density (mmol g^{-1})			CO_2 uptake (mmol g^{-1})	CO_2 uptake efficiency (mol mol^{-1}) [a]
		Imid.	*Am.*	*Imid.*	*Am.*	*Tot.*		
1	$PH_{A\text{-}OAc}$	100	0	3.1	0.0	3.1	0.53	0.17
2	$PH_{B\text{-}OAc}$	33	67	1.8	3.7	5.5	0.44	0.08
3	$PH_{C\text{-}OAc}$	16	84	1.1	5.7	6.8	0.18	0.03
4	$PH_{A\text{-}TFSI}$	100	0	1.8	0.0	1.8	0.12	0.06
5	$PH_{B\text{-}TFSI}$	33	67	1.3	2.6	3.9	1.96	0.50
6	$PH_{C\text{-}TFSI}$	16	84	0.9	4.6	5.5	2.00	0.37

[a] The CO_2 uptake efficiency correspond to the quantity CO_2 sorbed per chemical function (imidazolium + amine).

Chapter VI.

General conclusions and perspectives.

Chapter VI. General conclusions and perspectives

Although essential in organic chemistry, pharmacology and combinatorial chemistry, the multicomponent reactions (MCRs) were quite disregarded in polymer chemistry till recently. As highlighted in the introductory chapter I, MCRs have become a useful tool in polymer chemistry especially for step-growth polymerization (MCP). Nevertheless, these techniques are still in infancy and the full potential of MCRs has not been exploited yet. The main objective of this thesis was to take advantages of imine-based MCRs to synthesize novel functional polymers and structured materials as illustrated in scheme a. Further exploitation of existing MCPs and the introduction of a new one have been considered to enrich the available macromolecular engineering toolbox. The main achievements of this thesis are summarized hereafter.

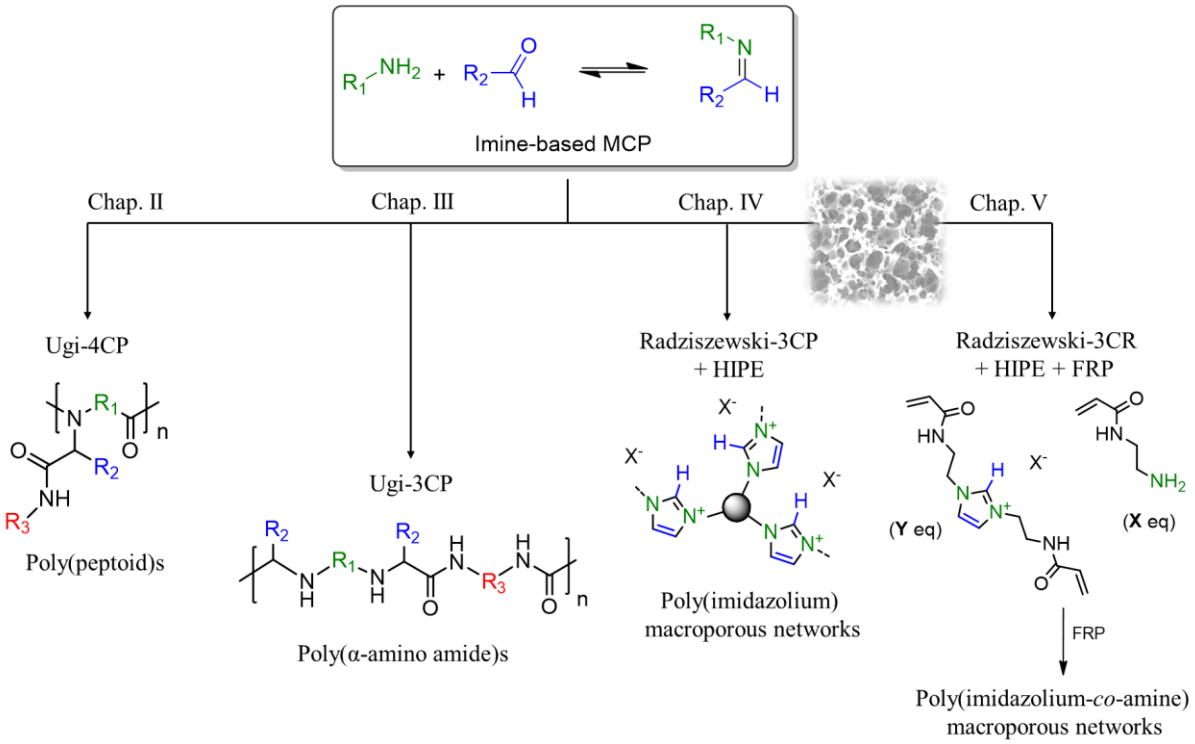

Scheme a. General strategies of this work taking advantages of MCRs to synthesize and structure polymer materials.

The first part of the thesis focused on the synthesis of linear polymers using Ugi-type MCPs. The chapter II explores the combinatorial character of the Ugi four-component polymerization of amino acid derivatives with different aldehydes and isocyanides for the synthesis of polypeptoids, consisting of nitrogen-substituted analogues of polypeptides. Overall, a library of structurally diverse polypeptoids was prepared and their thermal properties as well as their solution behaviours were characterized. The combinatorial method enables to establish a structure-property correlation. Some materials showed pH- and thermo-responsiveness with tunable transition temperatures depending on the nature of their backbone and side chains. For the most water-soluble polymers, the biocompatibility toward human cells was assessed making them potential candidates for stimuli-responsive biomaterials.

So far, few multicomponent reactions have been used as direct polymerization tools due to the high efficiency required to achieve polymers with decent molecular weights. In chapter III, the Ugi three-component reaction (Ugi-3CR) was adapted for step-growth polymerization allowing the introduction of an α-amino amide moiety in polymer materials. Special care was dedicated to find suitable polymerization conditions by playing with the different parameters (solvent, temperature, concentration and catalyst loading). The limitations of this approach for some substrates were also emphasized and discussed. Nevertheless, a series of poly(α-amino amide)s was obtained accordingly. A preliminary study of their thermal properties and solution behaviours was performed and notably revealed the pH-responsiveness of an aliphatic-rich derivative. Overall, this work represents a significant step forward in the synthesis of unprecedented poly(α-amino amide)s.

In the second part of the thesis, the structuration of imidazolium-based poly(ionic liquid)s (PILs) networks was investigated by combining for the first time multicomponent reactions and emulsion-templated polymerization. In the last years, porous PILs raised interest in gas capture, separation and catalysis, due to their enlarged surface area, high ionic density, spatial structuration and tunability of their properties by counterions exchange. Structuring PILs into porous materials was achieved by different methods but mainly *via* multistep approaches. In chapter IV, we described a straightforward one-pot one-step method to synthesize interconnected macroporous imidazolium acetate monoliths. They are produced *via* the modified Radziszewski three-component reaction (MR-3CR) applied to two different triamines and carried out under high internal phase emulsion (HIPE) conditions. The materials properties (thermal and swelling) were tuned by exchanging the acetate counterion for bromide or bistrifluorosulfonamide (TFSI). Excellent catalytic activity was observed for transesterification

reaction and decarboxylation of caffeic acid along with easy recyclability and purification associated with heterogeneous catalysis.

Eventually, in chapter V, the MR-3CR was combined with both HIPE and free radical polymerization (FRP). In a one-pot procedure, a bisacrylamide imidazolium crosslinker was generated *in situ* by MR-3CR from an acrylamide monomer bearing a primary amine followed by its free radical polymerization under emulsion condition. Depending on the amount of amino acrylamide monomers reacted in the first step, the resulting materials contained adjustable amounts of imidazolium and amine moieties. Three different materials were synthesized accordingly with 100, 33 and 11 mol% of imidazolium. Given the affinity of both functionalities for CO_2 and the interconnected porosity allowing easy diffusion of the gas in the core of the monoliths, these materials were tested in CO_2 capture revealing different behaviours (capacity and selectivity) as a function of the imidazolium content and nature of the counterion (acetate or TFSI).

The present work contributes to the quest for increasingly complex structures while respecting a simpler and more efficient chemistry. It also raises future prospects and sometimes interrogations as discussed below.

In chapter II dedicated to the synthesis of poly(peptoid)s *via* the Ugi-4CP, limitations in terms of molecular weight were encountered and attributed to termination through side-reactions. Preliminary attempts to identify these side-reactions *via* MALDI-ToF analysis of the polymer chain ends failed. A deeper investigation would be necessary to gain insight in these parasite reactions and ultimately limit them. Note however that a high molecular weight is not compulsory for biomedical applications. Moreover, one of the poly(peptoid)s was obtained from a pure enantiomer of amino acids (L-carnosine) and might exhibit interesting properties and peculiar folding behaviour like natural peptides. This aspect merits closer examination. In the same trend, a chiral Ugi-4CR catalyst was recently reported to confer chirality to the Ugi product (*Science*, 2018, **361**, eaas8707). Applied to polymers, this catalyst should paved the way to more realistic peptidomimetics.

Promising results were obtained for the synthesis of poly(α-amino amide)s by Ugi-3CP but the scope of polymers was restrained to aromatic and semiaromatic due to lack of reactivity of aliphatic monomers (chapter III). Expectedly, it limits the aqueous solubility of the polymers and the understanding of the amide-amine interactions. Considering the great potential of poly(ε-lysine), *i.e.* the sole example of fully aliphatic poly(α-amino amide), notably for biomedical applications, it is worth to try to unlock the synthesis of aliphatic poly(α-amino amide)s by the Ugi-3CP. The key parameter is believed to be the nature of the catalyst. Aside

from phenylphosphinic acid used in this work, there are other catalysts reported for the Ugi-3CR that might enable the use of aliphatic monomers. Preliminary results were obtained with boric acid in a model reaction carried out in water. Unexpectedly, the catalyst was so efficient that the secondary amine generated by a first Ugi-3CR is implied in a second one (Annexe A). This promising catalyst could therefore lead to aliphatic poly(α-amino amide)s providing the use of suitable secondary diamines monomers.

The MR-3CP was successfully combined with HIPE for two triamines leading to porous poly(imidazolium)s with different physical properties and catalytic activities (chapter IV). In the future, other triamines or polyamines could be considered notably to enhance the mechanical properties of the final porous supports and meet the requirements for heterogeneous catalysis under continuous-flow using a column reactor.

Additionally, only one counterion (acetate) was tested for catalysis applications but a screening with different counterions would be interesting to further enhance the catalytic activity of the porous PILs to target other applications. In addition, preliminary results showed that other reactions can be catalysed by these materials and notably the carbonatation of epoxide with CO_2 (Annexe B). Until recently, MR-3CR was restricted to few aldehydes such as glyoxal (or pyruvaldehyde) and formaldehyde preventing the substitution of the imidazolium aromatic carbons. This issue was recently tackled using a suitable catalyst, namely the proline (*J. Memb. Sci., 2020, 610, 118283*), which opens new perspectives in terms of polymer design and the applications resulting therefrom. As an example, the substitution of the C2 carbon increases the stability of the imidazolium toward ring opening in basic conditions and allows a longer life cycle for fuel-cells application.

Eventually, some of bi-functional imidazolium/amine porous materials obtained in the chapter V, in particular the TFSI-based materials, showed promising CO_2 sorption behaviours for post-combustion or even direct-air CO_2 capture applications. Although a synergy between both functions seems to occur, the sorption mechanism requires deeper investigation and to take full benefit of these materials for gas capture applications. Inspired by the successful combination of MR-3CR with HIPE but also with FRP, it would be interesting to apply this general approach to other MCRs for structuring a large range of innovative functional materials in a straightforward way.

Overall, there is still a lot of work ahead to extend the scope of MCPs and make them greener, notably by using renewable starting reagents, but we see a bright future for the use of MCRs in polymer synthesis and many applications could benefit of it in the coming years.